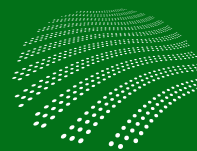


Cooperative Research Centre for **Contamination  
Assessment and Remediation of the Environment**

[www.crccare.com](http://www.crccare.com)



**CRCCARE**

*A safer, cleaner  
environmental future*



## TECHNICAL REPORT NO. 47

**Australian case studies of light non-aqueous  
phase liquid (LNAPL) natural source zone  
depletion rates compared with conventional  
active recovery efforts**

**Cooperative Research Centre for Contamination Assessment and Remediation of the Environment, Technical Report series, no. 47**

March 2020

Copyright © CRC CARE Pty Ltd, 2020

This book is copyright. Except as permitted under the Australian Copyright Act 1968 (Commonwealth) and subsequent amendments, no part of this publication may be reproduced, stored or transmitted in any form or by any means, electronic or otherwise, without the specific written permission of the copyright owner.

ISBN: 978-1-921431-68-5

**Enquiries and additional copies:**

CRC CARE, C/- Newcastle University LPO, PO Box 18, Callaghan NSW, Australia 2308

Tel: +61 (0) 2 4985 4941

Fax: +61 (0) 8 8302 3124

admin@crccare.com

www.crccare.com

**This report should be cited as:**

Rayner, JJ, Bekele, E, Donn, M, Bastow, T, Davis, GB, Woodbury, R, Furness, A & Geste, Y 2020, *Australian case studies of light non-aqueous phase liquid (LNAPL) natural source zone depletion rates compared with conventional active recovery efforts*, CRC CARE Technical Report no. 47, CRC for Contamination Assessment and Remediation of the Environment, Newcastle, Australia.

**Disclaimer:**

This publication is provided for the purpose of disseminating information relating to scientific and technical matters. Participating organisations of CRC CARE do not accept liability for any loss and/or damage, including financial loss, resulting from the reliance upon any information, advice or recommendations contained in this publication. The contents of this publication should not necessarily be taken to represent the views of the participating organisations.

**Cover image:**

Bill van Aken, CSIRO

CRC for Contamination Assessment and Remediation of the Environment

Technical Report No. 47

**Australian case studies of light non-aqueous phase liquid (LNAPL) natural source zone depletion rates compared with conventional active recovery efforts**

JL Rayner, E Bekele, M Donn, TP Bastow, GB Davis,  
R Woodbury, A Furness & Y Geste

CSIRO Land and Water, Floreat, Western Australia

March 2020

# Executive summary

---

## Overview

Natural rates of mass loss and biodegradation of light non-aqueous phase liquid (LNAPL) fuels and oils in soil and groundwater is termed natural source zone depletion (NSZD). The project 'Towards national guidance of natural source zone depletion (NSZD)' was initiated by the Cooperative Research Centre for Contamination Assessment and Remediation of the Environment (CRC CARE) to understand the role of NSZD in management of LNAPL contaminated sites. This report complements the LNAPL NSZD application guidance document *The role of natural source zone depletion in the management of light non-aqueous phase liquid (LNAPL) contaminated sites* (Technical report 46, CRC CARE 2020) and the LNAPL NSZD measurement guidance document *Technical measurement guidance for LNAPL natural source zone depletion* (Technical report 44, CRC CARE 2018).

Here we provide detailed, Australian-specific measurements and case studies for six Australian sites and multiple LNAPL product types. For these sites we estimate NSZD rates for a range of LNAPLs such as crude oil, diesel, jet fuel and gas condensate (predominantly gasoline range). The NSZD rates are compared to the most representative active product recovery rates from each of these sites to provide context to the scale of the NSZD rates.

NSZD in soils and groundwater, especially associated with natural biodegradation, results in oxygen consumption, carbon dioxide production, increases in temperature, consumption of other electron acceptors in groundwater, increased microbial populations, changes in the composition of the LNAPL itself and total LNAPL mass reduction. Typically, methods used to estimate LNAPL NSZD rates include the measurement of fluxes of carbon dioxide exiting at ground surface, major gas composition changes in the subsurface, methane production, biogenic heat production measured by temperature gradients, and electron acceptor depletion during natural attenuation in groundwater. Less used are LNAPL compositional changes, and microbial population numbers and activity.

## The six sites across Australia

The six sites investigated in this study had a range of aquifer and hydrogeological conditions: (site A) calcareous limestone system with strong tidal influences and depth to water table of 4–15 m; (site B) sandy soil and aquifer system with depth to water table of 2–4 m; (site C) fractured basalt with a water table between 3–7 mbgl; (site D) clay overlying fractured basalt; (site E) sand overlying conglomerate and sandstone; and (site F) clay overlying weathered and fractured phyllite. Additionally, two locations (and fuel types) were investigated at one site, and seasonal data are presented for two sites.

Table 1 and Figure 1, provide a summary of the measurement methodologies employed and outcomes from the investigation. Key data or measurements that were used to estimate NSZD rates at these sites were: (i) instantaneous measurement of surface fluxes of carbon dioxide by a chamber LI-COR technique; (ii) measurement of time averaged surface fluxes of carbon dioxide using E-Flux carbon dioxide sorption canisters that account for background organic carbon mineralisation via radiometric



means; (iii) temperature profiles in existing boreholes (manual thermistor and iButton) and buried thermistors; (iv) major gas composition in existing open boreholes and buried multiport profiles; and (v) LNAPL composition changes. A general description of these methods can be found in Technical report 44 (CRC CARE 2018).

Overall, at these sites remediation efforts to recover LNAPL mass ranged from less than 1 L day<sup>-1</sup> to >60 L day<sup>-1</sup> (effectively zero to 17.5 t yr<sup>-1</sup>). These LNAPL mass recovery operations range in timeframe from weeks to multiple decades.

## Results for sites A to F

At site A, LNAPL mass recovery was estimated as 3.7 t yr<sup>-1</sup>, averaged 13.2 L day<sup>-1</sup> over a three-year period (2015–2017) representing cumulative recovery from all remedial techniques employed. In the last year product recovery rates have started to plateau. Compositional changes in the LNAPL from the release period (~2012–2014) to 2018 suggest that estimated mass losses (due to volatilisation, dissolution and biodegradation) range between 26 and 64% of the initial LNAPL mass released. Further evidence from 2019 samples indicates that mass loss is still occurring (increasing to between 52 and 79%). Applying the 2018 composition-based mass losses to an initial mass estimate from 2018, this might equate to an average mass loss rate of 250–600 L day<sup>-1</sup> over the four-year period.

Estimated NSZD rates for site A ranged from zero or low values for some methods up to 34,000 L LNAPL ha<sup>-1</sup> yr<sup>-1</sup> based on E-Flux measurements and as high as 36,000 L LNAPL ha<sup>-1</sup> yr<sup>-1</sup> based on the gradient method for CO<sub>2</sub> flux using vapour multiport monitoring data. The upper estimates of the range of NSZD rates from temperature data (maximum of 4471 L LNAPL ha<sup>-1</sup> yr<sup>-1</sup>) were, in general, lower than those determined by other methods. Reasons for the discrepancies between temperature and other methods could be resolved in future by measuring the subsurface thermal conductivity of different strata in the profile.

Remedial mass recovery efforts at site B plateaued across a large area at less than 50 t yr<sup>-1</sup> (as at 2015). Mass losses (due to volatilisation, dissolution and biodegradation) up to 65–80% of the initial spill release was estimated for a spill that was perhaps greater than 50 years old (based on the extent of weathering, Johnston *et al* (2007)). NSZD rate estimates from temperature data were consistent across multiple thermistor strings and measurement periods, but with 3–4 times higher rate estimates for the diesel location (maximum of 7575 L LNAPL ha<sup>-1</sup> yr<sup>-1</sup>) compared to the crude oil location. LI-COR carbon dioxide fluxes gave NSZD rate estimates that supported temperature estimates. Gas-gradient based NSZD rate estimates were higher for both crude oil and diesel, with estimates up to 17,663 L LNAPL ha<sup>-1</sup> yr<sup>-1</sup>.

For site B, at the diesel location, overall NSZD rates were estimated between 120 and 280 t yr<sup>-1</sup> for an impacted area of 28 ha. When compared with the active diesel recovery rates of about 17.5 t yr<sup>-1</sup>, NSZD rates were around 7–15 times higher. For the crude oil location at site B, overall NSZD rates were estimated between 4.4 and 71 t yr<sup>-1</sup> for the impacted area of 6 ha. Very little recovery of crude has been possible at this location to compare with NSZD rates due to the limited mobility of LNAPL in this area.

For site C, compositional changes from 2011 to 2019 suggest estimated mass losses (due to volatilisation, dissolution and biodegradation) of between 3 and 21% over the eight-year period. Higher estimates of NSZD rates resulted from using temperature and

surface CO<sub>2</sub> flux methods. LI-COR surface CO<sub>2</sub> flux measurements were recorded at only one monitoring site, and the average NSZD rate was 866 L LNAPL ha<sup>-1</sup> yr<sup>-1</sup> in May and 12,700 L LNAPL ha<sup>-1</sup> yr<sup>-1</sup> in September of the same year. E-Flux estimates ranged from 1141 to 10,185 L LNAPL ha<sup>-1</sup> yr<sup>-1</sup>, with an average of 3599 L LNAPL ha<sup>-1</sup> yr<sup>-1</sup>. Temperature estimates were more than three times higher in May 2019 (maximum of 12,531 L LNAPL ha<sup>-1</sup> yr<sup>-1</sup>) compared to September 2019 and the reason for this has not yet been determined. Across the 18 ha of LNAPL impacted area, these rates provide overall NSZD rate estimates of 11–69 t yr<sup>-1</sup>. The maximum active LNAPL recovery rate from a range of remedial efforts was 3.8 t yr<sup>-1</sup>. Overall the NSZD rate is three to 20 times larger than this maximum active LNAPL recovery rate.

For site D, active remedial efforts recovered around 5.8 t yr<sup>-1</sup> over 6 months of operation, although these estimates can be variable due to the difficulty of measuring mass fluxes of volatile compounds at relatively high flow rates. LNAPL compositional changes (due to volatilisation, dissolution and biodegradation) from 2013 to 2018 suggest estimated relative mass losses of between -1 and 24% over that five-year period. NSZD rates were determined using temperature profiles, three E-Flux deployments of 4 traps, and in-well sampling of oxygen. In well oxygen data yielded the lowest NSZD rates (280 to 1110 L LNAPL ha<sup>-1</sup> yr<sup>-1</sup>) and an overall NSZD mass depletion of about 1.4 t yr<sup>-1</sup>. Temperature profiling gave the highest NSZD rates (2837 to 5140 L LNAPL ha<sup>-1</sup> yr<sup>-1</sup>) with an overall NSZD mass depletion of 6.9 t yr<sup>-1</sup> over the assumed impacted zone at the site. Overall the NSZD rate estimates were approximately 5 times lower than LNAPL recovery estimates if based on oxygen data alone, but NSZD rate estimates were similar or higher to LNAPL recovery rates if based on temperature profile data.

For site E, active remedial efforts removed approximately 0.2 t yr<sup>-1</sup> of LNAPL. Very high estimates of NSZD rates were determined at this site using the LI-COR and E-Flux carbon dioxide surface flux methods. The rates ranged from 47,339 to 164,634 L LNAPL ha<sup>-1</sup> yr<sup>-1</sup> and the ranges of LI-COR and E-Flux results are similar. Overall the NSZD mass loss estimate for a 175 m<sup>2</sup> area of the site was 1.1–1.2 t yr<sup>-1</sup> which is ~7 times the LNAPL recovery rate. If all of the surface flux data across the site within the plume boundary (0.48 ha) is considered, the mass flux estimates of NSZD are 14 t yr<sup>-1</sup> for LI-COR and 20 t yr<sup>-1</sup> for E-Flux.

For site F, recent remedial efforts had recovered approximately 1.7 t yr<sup>-1</sup> of LNAPL and may have resulted in large mass losses (due to volatilisation, dissolution and biodegradation) of between 28 and 99% (since release) based on LNAPL compositional changes. In well oxygen data yielded the lowest NSZD rates (0 to 1600 L LNAPL ha<sup>-1</sup> yr<sup>-1</sup>) giving an overall NSZD mass depletion rate of 0.40 to 0.68 t yr<sup>-1</sup>. Temperature profiling gave the highest NSZD rates (0 to 15,000 L LNAPL ha<sup>-1</sup> yr<sup>-1</sup>) with an overall NSZD mass depletion rate of 3.4 to 4.3 t yr<sup>-1</sup> over the assumed impacted zone at the site. Overall, NSZD rates from gas gradient analysis were 2.5 to four times lower than LNAPL recovery rates but estimates from temperature data suggest NSZD rates were 2.0–2.5 times higher than LNAPL recovery rates. There was good agreement between manual, short term (60 min) thermistor measurements and longer term deployed, monthly averaged iButton data.

## Synthesis of site data and rates

This study demonstrates different techniques for measuring rates of NSZD, were found to be variable both spatially and temporally. This is an expected outcome given the

non-uniform distribution of LNAPL across a source zone and seasonal impacts of variations in parameters affecting NSZD processes such as water table elevation and vadose zone moisture contents.

As all sites demonstrated some level of NSZD, zero or very low rates may be real but may also be the result of the application of an inappropriate method, such as using a surface flux approach over a heavy clay profile, or the selection of non-representative background locations for the temperature profiling method for example. For this reason, multiple approaches should be applied over seasonal cycles and corroborated against each other and then refined as the understanding of the representative NSZD processes for that site improves.

Mass loss estimates from changes in LNAPL composition proved very insightful as the technique involves direct measurement and interpretation of the LNAPL itself and is therefore more direct than other methods. In addition, it can distinguish different processes by the relative change in different compounds representing different properties and this can be correlated with the subsurface conditions encountered on site. In general, LNAPL composition changes are only reported as relative percent mass losses and more work is needed to fulfil the potential of this technique. This requires the coupling of the relative mass loss with the spill mass or a subsequently measured specific mass, to estimate the absolute mass loss. In this study absolute mass losses were not calculated as the mass of LNAPL in the subsurface relating to the relative mass loss period was not known.

The challenge of finding and applying suitable background sites for NSZD rate correction in all methods except E-Flux was evident across all five out of six sites and this can have a profound effect on estimated rates. Additionally, having site specific measurements of relevant parameters needed for NSZD rate calculation (e.g. thermal properties for temperature methods and diffusion coefficients for gases) increases confidence in estimates and allows for detailed comparisons to be made between methods. Additional studies will yield such data.

Despite spatial, temporal and method variability, sites A, B, C and E all measured NSZD rates that were considerably higher than LNAPL recovery rates (2–80 times higher). At site D, all in-well soil gas and E-Flux NSZD rates were below LNAPL recovery rates by two to three times. However, temperature methods were higher than LNAPL recovery rates. The primary uncertainties in determining these rates are the thermal conductivity and gas diffusion properties of the subsurface which were estimated from literature values. For site F, NSZD rates determined from temperature profiles were well above LNAPL recovery rates, while NSZD rates estimated from in-well oxygen data were well below LNAPL recovery rates.

Overall the case studies investigated here support the growing body of evidence that in many instances, especially at mature LNAPL sites, LNAPL mass removal through NSZD processes exceeds those achieved through active remediation efforts.

**Table 1. Summary of information for each site including NSZD rates for each measurement method. Different historical periods were used for the comparative analysis and may not refer to current conditions at all sites. NSZD rate estimation methods that were not implemented (grey-shaded cells) are indicated.**

Description			Site A	Site B (Two locations)		Site C (Two seasons)		Site D	Site E		Site F (Two seasons)	
Surface geology			Coastal limestone or lime-cemented sand	Coastal sand overlying limestone		Alluvial deposits overlying fractured, heavily weathered basalt		Clay overlying fractured, variably weathered basalt	Sand overlying conglomerate and sandstone		Clay overlying weathered and fractured phyllite	
Climate (average annual rainfall in mm)			Arid subtropical (280)	Mediterranean (630)		Tropical-arid (100–770)		Mild temperate (550)	Warm temperate (1033)		Cool temperate (600)	
Product type			Gas condensate	<i>Diesel (Location D6)</i>	<i>Crude oil (Location D10)</i>	Multiple (diesel and lube oil)		Multiple (gasoline, kerosene, diesel and lube oil)	Jet fuel		Gasoline	
Estimate of mass loss based on compositional changes (%)			52–79 (since release)	65–80 (since release)	—	3–21 (2011 to 2019)		-1–24 (2013 to 2018)	—		28–99 (since release)	
Estimate of NSZD area (ha)			5.5	28	6	18		2.7	0.018	0.48	1.1	
Estimate of LNAPL recovery (t yr <sup>-1</sup> )			1.7	Overall at site B: 50		3.8		5.8	~0.2		1.7	
				17.5	no data							
NSZD (t yr <sup>-1</sup> )*	Temperature gradient	iButton	3.7	—	—	66 <sup>†</sup> (May)	16 <sup>†</sup> (September)	3.9 <sup>†</sup>	—		3.3 <sup>†</sup> (May)	5.9 <sup>†</sup> (September)
		Thermistor	5.6	120–170 <sup>†</sup>	4.4–13 <sup>†</sup>	35 (May)	11 (September)	6.9	—		3.4 (May)	4.3 (September)
	Major gas concentration gradient	Soil vapour port	O <sub>2</sub> : 42–130 <sup>†</sup> CO <sub>2</sub> : 39–140 <sup>†</sup>	O <sub>2</sub> : 210 <sup>†</sup> CO <sub>2</sub> : 230 <sup>†</sup>	O <sub>2</sub> : 65 <sup>†</sup> CO <sub>2</sub> : 71 <sup>†</sup>	—		—	—		—	—
		In-well	O <sub>2</sub> : 19 CO <sub>2</sub> : 18	O <sub>2</sub> : 260 <sup>†</sup> CO <sub>2</sub> :280 <sup>†</sup>	O <sub>2</sub> : 29 <sup>†</sup> CO <sub>2</sub> : 31 <sup>†</sup>	—		1.4	—		0.40 (May)	0.68 (September)
	Surface CO <sub>2</sub> flux	E-Flux	16	—	—	—	69	1.9	1.2 <sup>†</sup>	20	—	—
		LI-COR flux chamber	33	120 <sup>†</sup>	24 <sup>†</sup>	##		—	1.1 <sup>†</sup>	14	#	—

\*Voronoi polygons used to compute a site-wide average, except where noted (†); mass in metric tonnes (t); # attempted historically but deemed not successful; ## attempted for this study but background corrected rates could not be obtained.



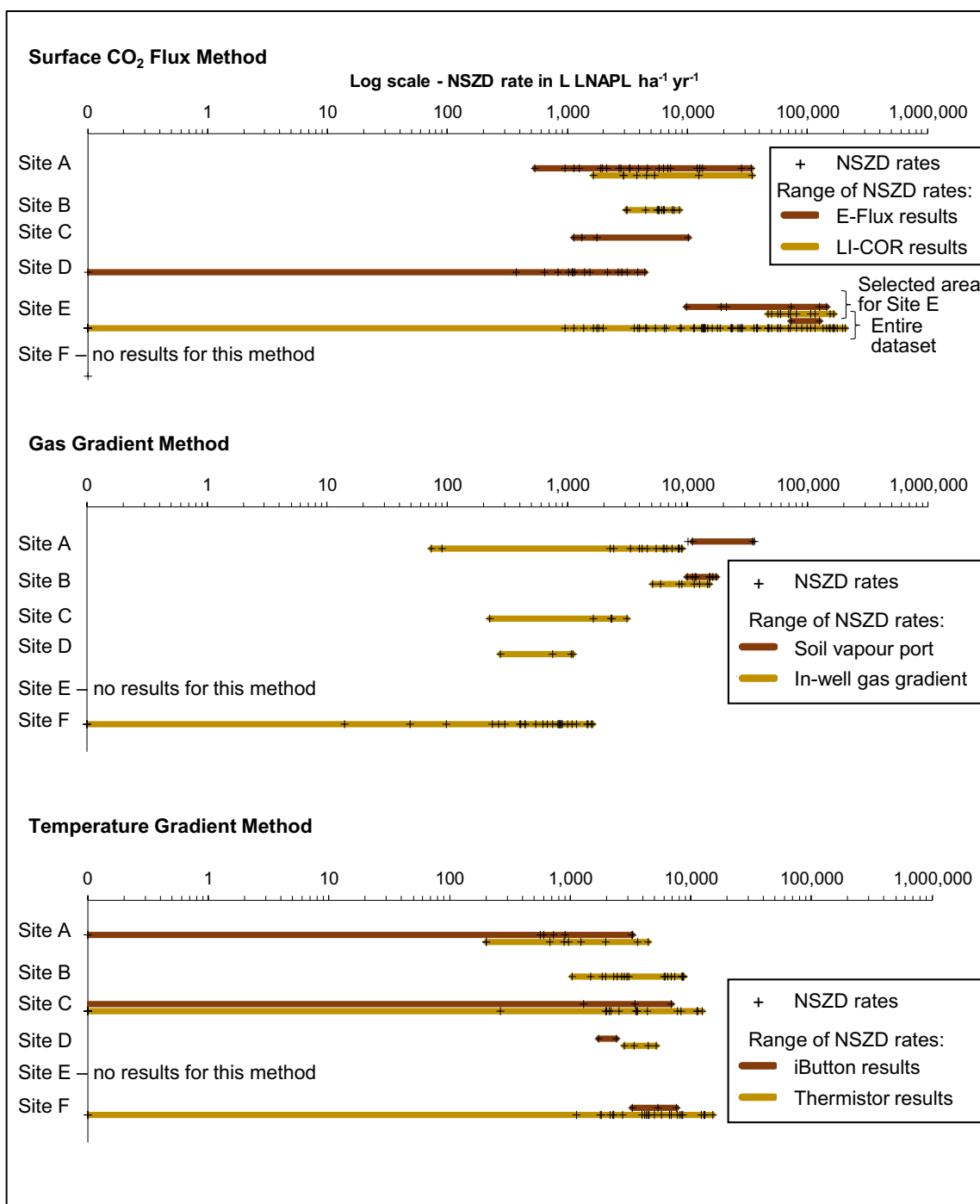


Figure 1. Comparison of NSZD rates in L LNAPL ha<sup>-1</sup> yr<sup>-1</sup> across the six sites by method

## Abbreviations

---

AST	Aboveground storage tank
C	Carbon
CO <sub>2</sub>	Carbon dioxide
CRC CARE	Cooperative Research Centre for Contamination Assessment and Remediation of the Environment
CSIRO	Commonwealth Scientific and Industrial Research Organisation
DPH	Dissolved phase hydrocarbon
GC-FID	Gas chromatography-flame ionisation detector
GC-MS	Gas chromatography-mass spectrometry
ha	Hectare
LNAPL	Light non-aqueous phase liquid
mAHD	meters, Australian height datum
mbg(l)	Metres below ground (level)
mBTC	Metres below top of casing
m	Metre
MPE	Multi-phase extraction
MW	Monitoring well
NAPL	Non-aqueous phase liquid
NSZD	Natural source zone depletion
O <sub>2</sub>	Oxygen
PFW	Process formation water
PSH	Phase separated hydrocarbons
SIP	Spectral induced polarization
SWL	Static water level
SVE	Soil vapour extraction
TFP	Total fluid pump/pumping
TPH	Total petroleum hydrocarbons
UST	Underground storage tank
VEP	Vacuum enhanced pumping
VER	Vacuum enhanced recovery
VOC	Volatile organic compound

# Table of contents

---

<b>Executive summary</b>	<b>i</b>
<b>1. Introduction</b>	<b>1</b>
<b>2. Key features, processes, and measurement of LNAPL behaviour and NSZD</b>	<b>3</b>
2.1 LNAPL contamination	3
2.2 Source zone depletion	4
2.3 LNAPL zone depletion processes	4
2.4 Estimating rates of NSZD	5
2.4.1 Gradient method for soil gas flux	6
2.4.2 Passive flux trap	6
2.4.3 Dynamic closed chamber (DCC) method	6
2.4.4 Biogenic heat method	7
2.4.5 LNAPL compositional change method	7
2.5 Total site-wide rate estimation for NSZD and active recovery	8
2.5.1 Area determination	9
2.5.2 Geospatial integration	11
<b>3. Site A</b>	<b>12</b>
3.1 Introduction	12
3.2 Site description	12
3.2.1 Distribution of wells and measurement methods	14
3.2.1 Profile stratigraphy	14
3.3 Data supplied by site owner	17
3.3.1 Hydrogeological parameters	18
3.3.2 Groundwater levels and flows	18
3.3.3 Product thicknesses in local wells on the site over time	19
3.3.4 Measurements of LNAPL transmissivity	22
3.3.5 LNAPL sampling and analysis (compositional analyses)	23
3.3.6 LNAPL recovery operations	23
3.4 Methods	23
3.4.1 Active recovery	23
3.4.2 NSZD rate estimation	25
3.4.3 NSZD: LNAPL sampling and analysis (compositional analyses to assess the extent of weathering)	29
3.5 Results	30

3.5.1 Estimation of total hydrocarbon mass removal by active recovery	30
3.5.2 NSZD results: measurements and total site-wide rate estimates	31
3.5.1 NSZD results: LNAPL composition	37
3.6 Overview of hydrocarbon mass removal – recovery and NSZD	40
3.7 Sources of uncertainty in hydrocarbon mass loss estimation	43
<b>4. Site B</b>	<b>44</b>
4.1 Introduction	44
4.2 Site description	45
4.2.1 Distribution of wells and measurement methods	45
4.2.1 Profile stratigraphy	45
4.3 Data supplied by site owner	47
4.3.1 Hydrogeological parameters	47
4.3.2 Well construction and mean groundwater levels	47
4.3.3 Product thicknesses in local wells	48
4.3.1 Measurements of LNAPL transmissivity	48
4.3.2 LNAPL recovery operations	49
4.4 Methods	49
4.4.1 Active recovery	49
4.4.2 NSZD rate estimation	50
4.4.3 NSZD: LNAPL sampling and analysis (compositional analyses to assess the extent of weathering)	52
4.5 Results	53
4.5.1 Estimation of total hydrocarbon mass removal by active recovery	53
4.5.2 NSZD rate results: measurements and total site-wide rate estimates	55
4.5.3 NSZD results: LNAPL composition	59
4.6 Overview of hydrocarbon mass removal – recovery and NSZD	69
4.7 Sources of uncertainty in hydrocarbon mass loss estimation	71
<b>5. Site C</b>	<b>72</b>
5.1 Introduction	72
5.2 Site description	72
5.2.1 Distribution of wells and measurement methods	72
5.2.2 Profile stratigraphy	74
5.3 Data supplied by site owner and other data	74
5.3.1 Hydrogeological parameters	74



5.3.2 Well construction and mean groundwater levels	77
5.3.1 Product thicknesses in local wells on the site over time	78
5.3.2 Measurements of LNAPL transmissivity	82
5.3.3 LNAPL sampling and analysis (compositional analysis and extent of weathering)	82
5.3.4 LNAPL recovery operations	82
5.4 Methods	82
5.4.1 Active recovery	82
5.4.2 NSZD rate estimation	84
5.4.3 NSZD: LNAPL compositional analyses to assess the extent of weathering	86
5.5 Results	87
5.5.1 Estimation of total hydrocarbon mass removal by active recovery	87
5.5.2 NSZD rate results: measurements and total site-wide rate estimates	88
5.5.3 NSZD results: LNAPL composition	93
5.6 Overview of hydrocarbon mass removal – recovery and NSZD	93
5.7 Sources of uncertainty in hydrocarbon mass loss estimation	94
<b>6. Site D</b>	<b>95</b>
6.1 Introduction	95
6.2 Site description	95
6.2.1 Distribution of wells and measurement methods	95
6.2.2 Profile stratigraphy	95
6.3 Data supplied by site owner and other data	99
6.3.1 Hydrogeological parameters	99
6.3.2 Well construction and mean groundwater levels	99
6.3.3 Product thicknesses in local wells on the site over time	100
6.3.4 Measurements of LNAPL transmissivity	101
6.3.5 LNAPL compositional analysis and extent of weathering	101
6.3.6 LNAPL recovery operations	101
6.4 Methods	102
6.4.1 Active recovery	102
6.4.2 NSZD rate estimation	103
6.4.3 NSZD: LNAPL compositional analyses to assess the extent of weathering	104
6.5 Results	105

6.5.1 Estimation of total hydrocarbon mass removal by active recovery	105
6.5.2 NSZD rate results: measurements and total site-wide rate estimates	105
6.5.3 NSZD results: LNAPL composition	108
6.6 Overview of hydrocarbon mass removal – recovery and NSZD	108
6.7 Sources of uncertainty in hydrocarbon mass loss estimation	109
<b>7. Site E</b>	<b>110</b>
7.1 Introduction	110
7.2 Site description	110
7.2.1 Distribution of wells and measurement methods	110
7.2.2 Profile stratigraphy	113
7.3 Data supplied by site owner and other data	113
7.3.1 Hydrogeological parameters	113
7.3.2 LNAPL recovery operations	114
7.4 Methods	114
7.4.1 Active recovery	114
7.4.2 NSZD rate estimation	114
7.5 Results	115
7.5.1 Estimation of total hydrocarbon mass removal by active recovery	115
7.5.1 NSZD rate results: measurements and total site-wide rate estimates	116
7.6 Overview of hydrocarbon mass removal – recovery and NSZD	119
7.7 Sources of uncertainty in hydrocarbon mass loss estimation	121
<b>8. Site F</b>	<b>122</b>
8.1 Introduction	122
8.2 Site description	124
8.2.1 Distribution of wells and measurement methods	124
8.2.2 Profile stratigraphy	124
8.3 Data supplied by site owner and other data	125
8.3.1 Hydrogeological parameters	125
8.3.2 Well construction and mean groundwater levels	125
8.3.3 Product thicknesses in local wells on the site over time	126
8.3.4 Measurements of LNAPL transmissivity	126
8.3.5 LNAPL sampling and analysis (compositional analyses)	127
8.3.6 LNAPL recovery operations	127

8.4 Methods	127
8.4.1 Active recovery	127
8.4.2 NSZD rate estimation	127
8.4.3 NSZD: LNAPL compositional analyses to assess the extent of weathering	129
8.5 Results	130
8.5.1 Estimation of total hydrocarbon mass removal by active recovery	130
8.5.2 NSZD results: measurements and total site-wide rate estimates	130
8.5.3 NSZD results: LNAPL composition	135
8.6 Overview of hydrocarbon mass removal – recovery and NSZD	135
8.7 Sources of uncertainty in hydrocarbon mass loss estimation	136
<b>9. Site-specific considerations for estimating rates of NSZD: observations from this study</b>	<b>138</b>
<b>10. Conclusion</b>	<b>141</b>
<b>11. References</b>	<b>143</b>
<b>12. Coded references to confidential reports and files</b>	<b>147</b>
12.1 Site A	147
12.2 Site B	147
12.3 Site C	148
12.4 Site D	148
12.5 Site E	149
12.6 Site F	149
 <b>Appendix</b>	
Appendix A.1 Site A methodology for E-Flux	153
Appendix A.2 Site A methodology for LI-COR	154
Appendix A.3 Site A well construction logs	155
Appendix A.4 Site A time series plots of LNAPL thickness (bn), corrected water table elevation (Zaw), and LNAPL elevation (Zan) for selected wells	167
Appendix A.5 Site A methodology for in-well temperature monitoring	173
Appendix A.6 Site A methodology for sampling soil vapour from soil vapour probes	174
Appendix A.7 Site A methodology for in-well gas sampling	176
Appendix A.8 Site A density and analytical results for condensate LNAPL samples	177

Appendix A.9	Site A LNAPL percentage loss relationships	180
Appendix B.1	Site B methodology for gas sampling and CSIRO analytical methods	181
Appendix C.1	Site C GC-MS analytical and density results	188
Appendix C.2	Site C logs from six wells drilled for a research program conducted by CSIRO (SiteC_Ref3 2014)	197
Appendix D.1	Site D GC-FID analytical and density results	204
Appendix D.2	Site D well logs	210
Appendix E.1	Site E natural source zone depletion rate estimates	222
Appendix F.1	Site F well logs	224
Appendix F.2	Site F GC-FID analytical and density results	228

## Tables

Table 1	Summary of information for each site including NSZD rates for each measurement method.	V
Table 2	Comparison of NSZD estimation methods applied to the six sites.	8
Table 3	Density and carbon ranges for the gas condensate source from site A.	12
Table 4	Summary of NSZD methods applied at monitoring wells and other data collected.	16
Table 5	Results of laboratory measured primary porosity from SiteA_Ref3 (2016).	18
Table 6	Table 6. Summary of reported apparent LNAPL thickness variations (mm).	20
Table 7	Summary of transmissivity results in $\text{m}^2 \text{day}^{-1}$ .	22
Table 8	Temperature logger (iButton) string location and depth configuration details.	26
Table 9	Construction details for monitoring wells for which manual temperature profiles were measured and in-well gas samples were collected.	26
Table 10	Summary of LI-COR measurements from SiteA_Ref4 (2016).	28
Table 11	Summary of LI-COR $\text{CO}_2$ flux sampling locations and conditions from SiteA_Ref4 (2016).	29
Table 12	Summary of LNAPL recovery by method from SiteA_Ref9 (2017) and SiteA_Ref16 (2018) between 21 April 2015 and 30 September 2018.	31
Table 13	Summary of results for iButton string, temperature-based NSZD.	32
Table 14	Summary of results for NSZD based on manual thermistors.	32



Table 15	Summary of results for NSZD based on gas vapour port data (location SV1).	34
Table 16	Summary of results for NSZD based on in-well gas data.	34
Table 17	Summary of E-Flux CO <sub>2</sub> trap analytical results from reports.	36
Table 18	Results from E-Flux CO <sub>2</sub> trap measurements from sampling in December 2016 and April 2017.	36
Table 19	Summary of LI-COR CO <sub>2</sub> flux measurements for the gas condensate plume and process formation water (PFW) plume.	37
Table 20	Tabulation of NSZD rates across methods used, and spatially-weighted mass losses per time.	42
Table 21	Type of recovery equipment from SiteB_Ref2 (2005).	50
Table 22	Summary of 2015 product recovery near locations D6 and D10.	55
Table 23	Summary of results from buried thermistors, temperature-based NSZD.	56
Table 24	Summary of results for NSZD based on gas vapour port data.	58
Table 25	Summary of results for NSZD based on in-well gas data.	58
Table 26	LI-COR results for site B.	59
Table 27	BTEX (and selected aromatic compound) concentrations and assessments for LNAPL samples from location D6 and D10.	65
Table 28	Tabulation of NSZD rates across methods used at D6 (diesel), and total site-wide mass losses per time.	70
Table 29	Tabulation of NSZD rates across methods used at D10 (crude oil), and total site-wide mass losses per time.	70
Table 30	Summary of short-term (2 to 3 h) aquifer pump tests for the six research wells CS01 to CS06 from SiteC_Ref3 (2014).	77
Table 31	Summary of hydraulic conductivity estimates derived from analysis of baildown test results from SiteC_Ref3 (2014).	77
Table 32	Apparent LNAPL thickness monitoring data as reported in SiteC_Ref10 (2018) and SiteC_Ref11 (2018).	81
Table 33	LNAPL transmissivity testing results from SiteC_Ref1 (2013).	82
Table 34	Summary of LNAPL recovery tests reported in SiteC_Ref3 (2014).	83
Table 35	Monitoring wells for which manual temperature profiles were recorded and in which iButtons temperature loggers installed.	85
Table 36	Monitoring wells for which major gas samples were measured in situ using a gas analyser or collected for laboratory analysis.	85

Table 37	Locations where surface carbon dioxide flux was measured using LI-COR chamber method and E-Flux sorbent trap method.	86
Table 38	LNAPL recovery operations at site C over a three-year period.	88
Table 39	Summary of results for NSZD based on manual thermistors from May and September 2019 and average NSZD values based iButton data.	89
Table 40	Summary of uncorrected NSZD rates based on in-well gas data (O <sub>2</sub> ) and fluid level at the time of measurement.	91
Table 41	Summary of E-Flux CO <sub>2</sub> trap analytical results from client. Traps deployed for seven days.	92
Table 42	Tabulation of NSZD rates across methods used and total site-wide mass losses per time.	94
Table 43	Monitoring wells for which manual temperature profiles were recorded and iButtons temperature loggers installed.	104
Table 44	Summary of results for NSZD based on manual thermistors and iButton measurements from September 2019.	106
Table 45	Summary of results for NSZD based on in-well gas data (O <sub>2</sub> ).	106
Table 46	Summary of results for NSZD based on three rounds of E-Flux.	107
Table 47	Tabulation of NSZD rates across methods used and total site-wide mass losses per time.	109
Table 48	Density and carbon ranges for a typical Jet A1.	110
Table 49	Details of skimming operations for site E from SiteE_Ref1.	114
Table 50	Summary of NSZD data used for comparison of hydrocarbon mass removal from SiteE_Ref1 (2017).	119
Table 51	LNAPL thickness from SiteF_Ref1 (2019).	126
Table 52	Monitoring wells for which manual temperature profiles were recorded and iButtons temperature loggers installed.	128
Table 53	Monitoring wells for which major gas samples were measured in situ using a gas analyser or collected for laboratory analysis.	128
Table 54	Mass of LNAPL removed (kg hexane equivalent) by MPE.	130
Table 55	Summary of results for NSZD based on thermistors from May and September 2019.	131
Table 56	Summary of results for NSZD based on in-well gas data (O <sub>2</sub> ).	133
Table 57	Tabulation of NSZD rates across methods used and total site-wide mass losses per time.	136

## Figures

Figure 1	Comparison of NSZD rates in L LNAPL $\text{ha}^{-1} \text{yr}^{-1}$ across the six sites and by method.	vi
Figure 2	Schematic diagram of LNAPL conceptual model.	3
Figure 3	Procedure developed for estimating the area associated with each NSZD measurement location.	10
Figure 4	Procedure for constructing Voronoi polygons for a site with unknown LNAPL plume dimensions.	11
Figure 5	GC-FID analysis of the source condensate from Site A.	13
Figure 6	Generalised map of sampling and monitoring locations and transect for Site A.	15
Figure 7	Transect SW-NE for Site A..	17
Figure 8	Cumulative LNAPL recovery: historical overview of active remediation from SiteA_Ref9 (2017) and SiteA_Ref16 (2018).	23
Figure 9	Voronoi polygon areas constructed using QGIS for iButton and thermistor measurement locations for site A.	33
Figure 10	Voronoi polygon areas constructed using QGIS for gas in-well measurement locations for site A, and the single location (SV1) for soil vapour port measurements at different depths.	35
Figure 11	Voronoi polygon areas constructed using QGIS for the E-Flux and LI-COR measurement locations for site A.	38
Figure 12	LNAPL remaining at selected locations (where LNAPL was present in 2018) from 2015 to 2019.	40
Figure 13	GC-FID chromatograms showing the composition of the unweathered condensate LNAPL from 2015 and changes due to weathering in 2015, 2018 and 2019.	41
Figure 14	Map view of Site B and areas of detailed investigation at locations D6 and D10 and background site, B6.	44
Figure 15	Close-up view of location B6.	46
Figure 16	Close-up view of location D6.	46
Figure 17	Close-up view of location D10.	47
Figure 18	Hydrograph of gauged fluid elevations near site D6 from 1998 to 2014.	48
Figure 19	Hydrograph of gauged fluid elevations near site D10.	49
Figure 20	Historical LNAPL recovery data for site B.	54
Figure 21	Weekly product recovery for 2015 from tanks in the vicinity of D6.	54
Figure 22	Weekly product recovery for 2015 from tanks in the vicinity of D10.	55

Figure 23	GC-FID analysis of LNAPL sample E3-RW-01 from location D6 in 2016.	61
Figure 24	GC-FID analysis of LNAPL sample DBMW3 from location D6 in 2006.	62
Figure 25	GC-FID analysis of LNAPL sample 55 from location D10.	63
Figure 26	GC-FID analysis of LNAPL sample 60 from location D10.	64
Figure 27	GC-FID analysis of TPH from selected samples from core 67 D6 location.	66
Figure 28	GC-MS analysis showing selected ion chromatograms (m/z 156) highlighting the dimethylnaphthalenes (DMN) in selected TPH samples from core 67 (location D6).	67
Figure 29	GC-FID analysis of TPH extracts from selected core samples from location D10.	68
Figure 30	Distribution of monitoring wells at site C.	73
Figure 31	Geological cross-section roughly perpendicular parallel to the coastline.	75
Figure 32	Geological cross-section roughly perpendicular to the coastline.	76
Figure 33	LNAPL corrected groundwater levels for a selection of wells near the inferred LNAPL extent as of October 2017 from SiteC_Ref11 (2018).	79
Figure 34	LNAPL thickness for a selection of wells near the inferred LNAPL extent as of October 2017 from SiteC_Ref11 (2018).	80
Figure 35	Voronoi polygon areas constructed using QGIS for thermistor measurement locations for site C in May 2019 and September 2019.	90
Figure 36	Examples of LI-COR installations and changes in vegetation between the two sampling campaigns.	92
Figure 37	Voronoi polygon areas constructed using QGIS for the E-Flux measurement locations for site C.	93
Figure 38	Distribution of monitoring sites at site D and land use.	96
Figure 39	Geological cross-section (east-west) based on logs provided in SiteD_Ref6 (2014) and SiteD_Ref9 (2017).	97
Figure 40	Geological cross-section (north-south) based on logs provided in SiteD_Ref6 (2014) and SiteD_Ref9 (2017).	98
Figure 41	LNAPL-corrected groundwater levels for a selection of wells along north-south and east-west transects of site D.	100
Figure 42	LNAPL thicknesses for a selection of wells along north-south and east-west transects of site D.	101
Figure 43	Daily and cumulative VOC vapour recovery for MPE conducted on 12 extraction wells.	102

Figure 44	Groups of four extraction wells per field for MPE conducted between June 2013 and July 2015.	103
Figure 45	Voronoi polygon areas constructed using QGIS for thermistor measurement locations for site D in September 2019.	106
Figure 46	Voronoi polygon areas constructed using QGIS for the E-Flux measurement locations for site D.	107
Figure 47	GC-FID analysis of typical Jet A1.	111
Figure 48	Location of site E investigation area relative to land use.	112
Figure 49	Sample locations and groundwater wells for site E from SiteE_Ref1 (2017).	112
Figure 50	Summary of LNAPL recovery produced from reported field notes.	116
Figure 51	Flux chamber (LI-COR) results contour with maximum background correction from SiteE_Ref1 (2017).	117
Figure 52	Flux chamber (LI-COR) results contour with average background correction from SiteE_Ref1 (2017).	118
Figure 53	CO <sub>2</sub> trap (E-Flux) results from SiteE_Ref1 (2017).	118
Figure 54	Area and data used to compare NSZD LNAPL degradation rates to LNAPL recovery rates from active skimming from SiteE_Ref1 (2017).	120
Figure 55	Voronoi polygon areas constructed using QGIS for LI-COR measurement locations for site E.	120
Figure 56	Voronoi polygon areas constructed using QGIS for E-Flux measurement locations for site E.	121
Figure 57	Layout of some of the monitoring and recovery wells on site F, along with groundwater contours and key site features (SiteF_Ref1, 2019).	122
Figure 58	Distribution of the monitoring and recovery sites at site F.	123
Figure 59	Conceptual site model from SiteF_Ref1 (2019).	124
Figure 60	Geological cross section (SiteF_Ref2, 2007).	125
Figure 61	Voronoi polygon areas constructed using QGIS for thermistor measurement locations for site F in May 2019 and September 2019.	132
Figure 62	Voronoi polygon areas constructed using QGIS for gas in-well measurement locations for site F in May 2019, and September 2019.	134

# Acknowledgements

---

## Authors of Technical Report

- John Rayner, CSIRO Land and Water
- Elise Bekele, CSIRO Land and Water
- Michael Donn, CSIRO Land and Water
- Trevor Bastow, CSIRO Land and Water
- Greg Davis, CSIRO Land and Water
- Robert Woodbury, CSIRO Land and Water
- Andrew Furness, CSIRO Land and Water
- Yasuko Geste, CSIRO Land and Water

## Technical Working Group

- Niall Johnston, Independent Chair
- Olivia Patterson, NSW EPA
- Joanne Stuart, NSW EPA
- Kristin Wasley, EPA Victoria
- Anne Northway, EPA Victoria
- Andrew Miller, WA DWER
- Rebecca Hughes, SA EPA
- Andrew Pruszinski, SA EPA
- Graham Cordingley, QLD DES
- Keith Osborne, NSW Department of Planning, Industry & Environment
- Greg Davis, CSIRO Land and Water
- David Reynolds, Geosyntec
- Jason Clay, Senversa
- Kristi Hanson, Senversa
- Warren Pump, Salient Plus
- Dave Thomas, Chevron
- Robin Wright, National Energy Resources Australia
- Andrew King, BP
- Mark Murrie, BP
- Rod Lukatelich, Petroleum LNAPL Forum
- Prashant Srivastava, CRC CARE

## CRC CARE Project Advisory Group

- Dennis Monahan, Independent Chair
- Joanne Stuart, NSW EPA
- Kristin Wasley, EPA Victoria
- Andrew Miller, WA DWER
- Andrew Pruszinski, SA EPA
- Tony Bradshaw, QLD DES
- Daniel Walters, ACT EPA
- Christopher Coombes, NT EPA
- Mirella Goetzmann, WA Health
- Craig Barnes, Air Services Australia

- Brian Priestly, Monash University
- Jack Ng, University of Queensland
- Andrew King, BP
- Damien Davidson, Caltex
- Dave Thomas, Chevron
- John Mikac, ExxonMobil
- Tanya Astbury, Viva Energy
- Tim Carr, Rio Tinto
- Paul Barrett, Australian Institute of Petroleum
- Peter Gniel, Australian Institute of Petroleum
- Rod Lukateliich, Petroleum LNAPL Forum
- Ravi Naidu, CRC CARE
- Prashant Srivastava, CRC CARE

### **Project Steering Committee**

- Robin Wright, National Energy Resources Australia
- Miranda Taylor, National Energy Resources Australia
- Tim Duff, National Energy Resources Australia
- Rod Lukateliich, Petroleum LNAPL Forum
- Prashant Srivastava, CRC CARE

### **Project Management**

- Robin Wright, National Energy Resources Australia
- Prashant Srivastava, CRC CARE

### **Funding acknowledgement**

The work has been supported by the Cooperative Research Centre for Contamination Assessment and Remediation of the Environment (CRC CARE), whose activity in this case was funded by National Energy Resources Australia (NERA), which is one of the Australian Government's Industry Growth Centres.

This work was also funded by following industry participants of Petroleum LNAPL Forum.

- BP
- BHP
- Caltex
- Viva Energy
- ExxonMobil
- Chevron
- Santos
- Quadrant Energy
- Rio Tinto

# 1. Introduction

---

Over the past decade there has been increasing awareness that remediation of sites contaminated with light non-aqueous phase liquids (LNAPLs) reach practical limits of LNAPL recoverability. During the past five years there has also been an improved understanding that rates of LNAPL mass removal by natural source zone depletion (NSZD) (or source zone natural depletion (SZND)) can be substantial and often higher than those achieved by active removal technologies.

To better understand the magnitude of these different mass removal approaches and technologies, and the role of NSZD in management of LNAPL contaminated sites a three-year research program 'Towards national guidance of natural source zone depletion (NSZD)' was initiated by CRC CARE and supported by National Energy Resources Australia (NERA). A key element of the program was to compare LNAPL recovery approaches at sites across Australia with NSZD rates estimated by a variety of methods. Sites were to represent typical representative geologies and to encompass a range of LNAPL types.

The objectives for the research program were:

- estimate and verify NSZD removal rates of subsurface liquid hydrocarbons under Australian conditions
- develop a technical guidance document on methodologies for monitoring subsurface liquid hydrocarbon removal rates by NSZD
- develop a guidance document for the management of sites contaminated with subsurface liquid hydrocarbon-impacted sites, including the use of NSZD as an accepted remedial technology, and
- involve stakeholders through the life of the project to ensure that methods and approaches are aligned with expectations for the management of sites contaminated by subsurface liquid hydrocarbons.

The role of the Commonwealth Scientific and Industrial Research Organisation (CSIRO) in the project was to:

- maintain impartial and anonymous interpretation of information from selected sites
- identify the data collection requirements for both NSZD and conventional hydrocarbon recovery systems
- collate the data and reports from the representative selected sites
- investigate and augment NSZD rates and data at additional sites where needed and feasible
- interpret the data and report the findings in the context of the project objectives, and
- assist with delivery of the complementary application and technical guidance documents (CRC CARE 2018, 2020).

This report complements the LNAPL NSZD application guidance document *The role of natural source zone depletion in the management of light non-aqueous phase liquid (LNAPL) contaminated sites* (Technical report 46, CRC CARE 2020) and the LNAPL NSZD measurement guidance document *Technical measurement guidance for LNAPL natural source zone depletion* (Technical report 44, CRC CARE 2018).



Here we provide detailed, Australian-specific measurements and case studies for six Australian sites and multiple LNAPL product types. For these sites we estimate NSZD rates for a range of LNAPLs such as crude oil, diesel, jet fuel and gas condensate (predominantly gasoline range). The NSZD rates are compared to the most representative active product recovery rates from each of these sites to provide context to the scale of the NSZD rates.

Separate sections outline the information and approaches taken for each of the six sites. Guidance on the desired level of data and measurements required at selected sites was previously reported (Donn *et al* 2017).

## 2. Key features, processes, and measurement of LNAPL behaviour and NSZD

The fate and behaviour of LNAPLs in the subsurface is reported in a number of technical documents (CL:AIRE 2014; ITRC 2009a; ITRC 2009b). As depicted in Figure 2, the elements of an LNAPL conceptual site model include an understanding of contaminant fate and transport in the vadose zone including partitioning and vapour behaviour, the interaction of LNAPL with groundwater at the water table and the subsequent migration and fate of LNAPL and any dissolved phase in groundwater within the hydrogeological setting.

Much research and investigation has been undertaken on particular elements of LNAPL transport, distribution and depletion, but few have integrated all processes at field scale to consider LNAPL mass loss holistically. Overall, there is a lack of publicly documented case-studies of NSZD of LNAPLs in Australia.

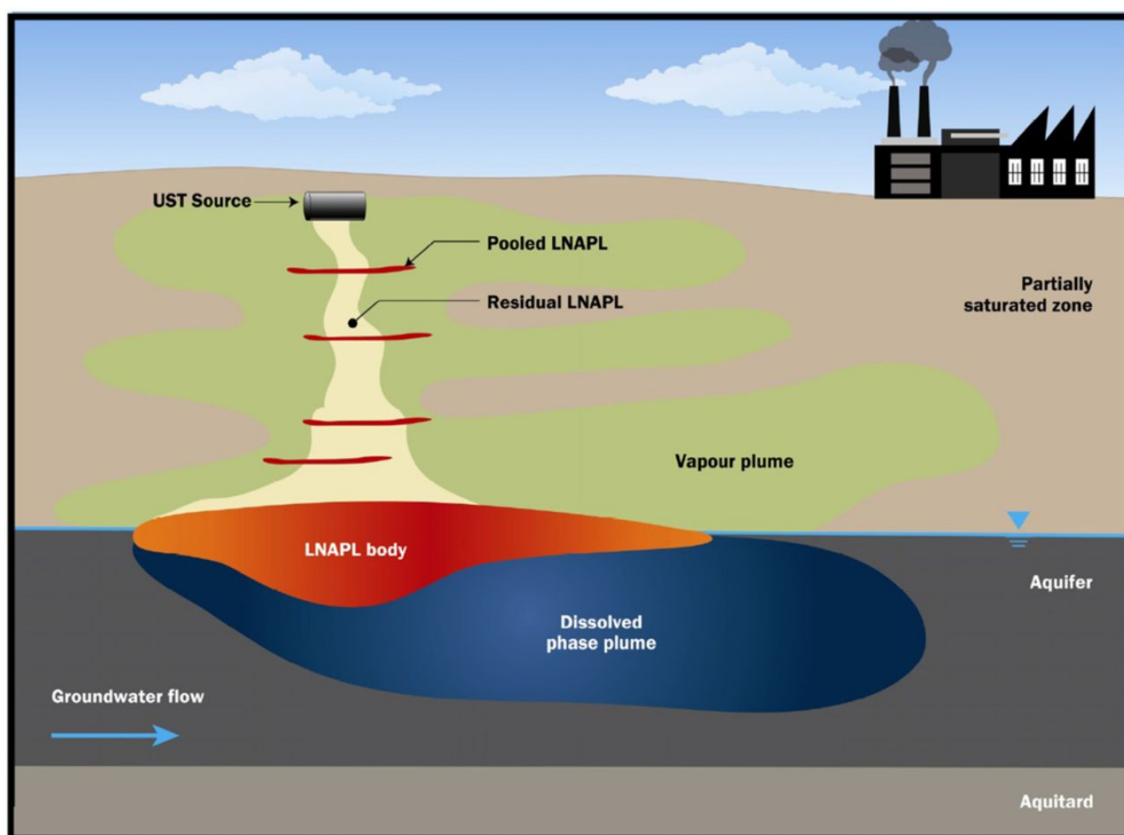


Figure 2. Schematic diagram of LNAPL conceptual model (CL:AIRE 2014)

### 2.1 LNAPL contamination

LNAPL can be distributed in the saturated and/or unsaturated zone. Under natural conditions in a homogeneous, unconfined aquifer, if there is sufficient release of a volume of LNAPL it will migrate toward the groundwater table due to gravity, mound at the water table and then can continue to migrate primarily laterally via advective flow (Suthersan *et al* 2017). If heterogeneities are present in the soil zone, LNAPL can

become trapped in soil pores as ganglia and lenses during passage through the vadose zone. If the volume of LNAPL contamination is insufficient, it may not reach the water table and will remain at residual levels in the vadose zone. As rainfall and other water sources infiltrate through the vadose zone, the water can dissolve soluble compounds from the residual LNAPL. This can act as a long-term source of dissolved contaminants to groundwater (Suthersan *et al* 2017; Wiedemeier *et al* 1999). Vertical redistribution of LNAPL can occur in an aquifer experiencing water level changes due to seasonal fluctuations or local pumping. In coastal sites, there are also potential tidal influences affecting water table dynamics and LNAPL behaviour. As the water table moves down, it can leave behind residual LNAPL in the pore spaces. As the water table rises, LNAPL and air can become entrapped below the water table (Dobson *et al* 2007; Kechavarzi *et al* 2005), forming discrete blobs, which become trapped in groundwater and only partially remobilised during water table fluctuations (Teramoto & Chang 2017; Yang *et al* 1995). A recent publication by Lenhard *et al* (2017) has contributed a quantitative model to predict different LNAPL saturations (i.e. free, residual, and entrapped), which accounts for fluctuating water levels.

## 2.2 Source zone depletion

Source zone depletion of LNAPL broadly refers to active and passive remedial technologies, such as hydraulic recovery of LNAPL from the source zone, and processes of natural mass removal and degradation. LNAPL mass recovery methods can involve the application of different technologies for varying durations with varying recovery rates and/or cumulative mass recovered (ITRC 2009b). Examples include the use of interceptor trenches, skimmer wells, single/dual well total fluids pumping, and vacuum enhanced recovery. For a description of these methods, see the *Illustrated handbook of LNAPL transport and fate in the subsurface* (CL:AIRE 2014).

Despite concerted remedial efforts, some LNAPL remains immobile (residual and entrapped) in the porous media, while some will exist at saturations above residual, i.e. mobile LNAPL (ITRC 2009a). The limits to hydraulic recovery of the mobile LNAPL depends on the type of product, age of the LNAPL plume, and the geological and hydrogeological conditions (CL:AIRE 2014). A recent publication has sought to characterise LNAPL recovery endpoints for different scenarios (e.g. skimming, skimming with drawdown, and vacuum-enhanced skimming with and without water table drawdown) and for a variety of different aquifer properties and LNAPL plume architectures (Sookhak Lari *et al* 2018).

## 2.3 LNAPL zone depletion processes

The design of effective source zone remediation may require the coupling of LNAPL recovery and NSZD processes, i.e. the result of volatilization, dissolution, sorption, and biodegradation processes that leads to mass losses of LNAPL (Eichert *et al* 2017; ITRC 2009b; Palaia 2016).

*In-situ* bioremediation of LNAPL involves the degradation of hydrocarbons by the activity of soil and water borne microorganisms that use organic compounds as an energy source and ultimately aid in decontamination of the polluted environment (Fiorenza and Ward 1997; Franzmann *et al* 1999; Pandey *et al* 2009). In order for

remediation to proceed, microbes require nutrients, electron acceptors, and other growth-favouring conditions (Yadav and Hassanizadeh 2011). Some of the crucial factors that affect microbial activity and the rate of contaminant transport/supply to the microorganisms include soil-water temperatures, salinity, water table dynamics and soil moisture changes (Kulkarni *et al* 2017; Yadav and Hassanizadeh 2011). Historically, electron acceptor-mediated biodegradation was the conceptual model adopted for hydrocarbon attenuation (Davis *et al* 1999; Garg *et al* 2017).

More recently, anaerobic methanogenic degradation of LNAPL sources, whereby hydrocarbons are converted to methane, carbon dioxide, and traces of hydrogen, has been highlighted as significant biodegradation process (Garg *et al* 2017; Kulkarni *et al* 2017). As with hydrocarbon vapours (Davis *et al* 2005; Davis *et al* 2009), methane will aerobically biodegrade in the vadose zone where oxygen is available, producing carbon dioxide.

## 2.4 Estimating rates of NSZD

An expanding area of NSZD research is measuring proxies for microbial respiration (i.e. biodegradation) and converting this information into rates of LNAPL mass depletion via biodegradation. Methods for measuring LNAPL degradation include measuring degradation products, such as carbon dioxide and heat (as temperature) and their changes through the vadose zone and at the ground surface. Additionally, changes in LNAPL composition can provide estimates of LNAPL mass loss. CRC CARE Technical Report 44 (2018) provides details of different methods used to estimate NSZD. Briefly, several of these methods, which pertain to the sites investigated in this report, are presented here. The methods used to estimate NSZD at the six sites investigated in this report are in Table 2.

Three methods can be used to measure the soil gas flux: gradient, passive flux trap and dynamic closed trap (CRC CARE 2018). Common to all three of the soil gas flux methods is that stoichiometry is used to determine a mass based NSZD rate based on assuming a representative hydrocarbon and using soil gas flux data. At an individual location, a gas flux measurement can be used to estimate the NSZD rate using Equation 1:

$$R_{NSZD} = \left[ \frac{J_{NSZD} m_r MW}{10^6} \right] \times \frac{86400s}{d} \quad \text{Equation 1}$$

Where:

$R_{NSZD}$  = the total hydrocarbon degraded or NSZD rate ( $\text{g m}^{-2} \text{d}^{-1}$ ),

$J_{NSZD}$  = the background corrected soil gas flux in micromoles per square metre per second ( $\mu\text{mol m}^{-2} \text{s}^{-1}$ ),

$m_r$  = the stoichiometric molar ratio of hydrocarbon degraded (unitless)

MW = the molecular weight of the representative hydrocarbon ( $\text{g mol}^{-1}$ )

CRC CARE Technical Report 44 (2018) provides a table of representative hydrocarbons and  $\text{CO}_2$  stoichiometric conversion factors that one can use in Equation 1. As described in CRC CARE report, soil gas flux methods require some element of data correction and other data processing procedures. In particular, a correction for

natural soil respiration reactions, which are considered background must be quantified and subtracted from the gas flux associated with NSZD. The exact methods for implementing background corrections are specific to each of the three soil gas flux measurement methods as described in more detail in CRC CARE Technical Report 44 (2018).

#### **2.4.1 Gradient method for soil gas flux**

This method relies on measuring change in gas concentration with depth at a monitoring location to estimate the diffusive flux through the vadose zone. Either the diffusive flux of O<sub>2</sub> or CO<sub>2</sub> can be stoichiometrically related to an NSZD rate. The gradient method is based on Fick's first law of diffusion (Equation 2):

$$J = D_v^{eff} \left( \frac{dC}{dZ} \right) \quad \text{Equation 2}$$

Where:

$J$  = the steady-state diffusive flux (g m<sup>-2</sup>(soil) s<sup>-1</sup>)

$dC/dZ$  = the soil gas concentration gradient (g m<sup>-4</sup>)

$D_v^{eff}$  = the effective vapour diffusion coefficient (m<sup>2</sup> s<sup>-1</sup>) and is specific to the soil and gas being measured.

To determine the soil gas concentration gradient ( $dC/dZ$ ), one can use nested soil vapour monitoring probes or existing monitoring wells.

Refer to CRC CARE Technical Report 44 (2018) for further details about how to implement the gradient method and the underlying assumptions.

#### **2.4.2 Passive flux trap**

This method involves the collection of CO<sub>2</sub> released from the subsurface to the atmosphere using a caustic sorbent material. Generally, the method involves the collection of the gas over two weeks. The company E-Flux, LLC (Fort Collins, Colorado, USA) commercialised the method and passive flux trap results presented in this report utilised this method. Appendix A.1 provides details of the equipment used for E-Flux measurements. Refer to CRC CARE Technical Report 44 (2018) for further details about how to implement the passive flux method and the underlying assumptions.

#### **2.4.3 Dynamic closed chamber (DCC) method**

The DCC method directly measures soil gas emitted at the ground surface. The company LI-COR Biosciences, Inc. (Lincoln, Nebraska, USA) commercialised the method and DCC results presented in this report utilised this method. The LI-COR system uses a ground-mounted chamber, which collects soil gas. The chamber is connected to a vapour pump and soil gas analyser. The device measures changes in the concentration of CO<sub>2</sub> over time to derive a measure of soil gas efflux. Appendix A.2 provides details of the equipment used for LI-COR measurements. Refer to CRC CARE Technical Report 44 (2018) for further details about how to implement the LI-COR method and the underlying assumptions.

#### 2.4.4 Biogenic heat method

NSZD rate estimate using temperature data relies on the biogenic heat method (CRC CARE 2018). The heat emitted by biologically mediated, exothermic reactions can be thermodynamically equated to a NSZD rate. Johnston *et al* (2008) and Warren and Bekins (2015) were among the first to measure heat production from microbial degradation in the field and infer rates of degradation based on temperature data. The use of soil calorimeters to measure and relate heat production to microbial activity is well documented (e.g. Braissant *et al* 2010).

Assuming that heat conduction is the only method of heat transfer and that processes are largely operating in one-dimension vertically, then the biogenic heat produced through biodegradation is determined through application of Fourier's Law (Equation 3):

$$q_H = -K_T(\Delta T/\Delta z) \quad \text{Equation 3}$$

where

$q_H$  is the heat flux ( $\text{J m}^{-2} \text{s}^{-1}$ )

$K_T$  is the thermal conductivity of the soil ( $\text{J m}^{-1} \text{K}^{-1} \text{s}^{-1}$ )

$\Delta T$  is the change in background-corrected temperature (K)

$\Delta z$  (m) is the depth interval across which the heat flux is calculated

#### 2.4.5 LNAPL compositional change method

Weathering of LNAPL can result in significant changes to the composition of petroleum due to physical (volatilisation and dissolution) and biodegradation processes (Brauner *et al* 2004). The weathering process may alter the LNAPL properties, such as increasing the viscosity, and alter the potential transport of LNAPL through the porous media (Newell *et al* 1995). Physical losses of the volatile and soluble compounds generally affect the lighter components <C10, with the aromatic and aliphatic components both affected by volatilisation and mainly the aromatics affected by dissolution into water. For example, LNAPL components, such as benzene, toluene, ethylbenzene, and xylenes, have both lower molecular weights and higher solubilities compared to other constituents (Vasudevan *et al* 2016). These are readily volatilised and partition into groundwater, thus leaving behind heavier molecular weight constituents in the source zone (Suthersan *et al* 2017).

Biodegradation of LNAPL results in an apparent stepwise depletion of compounds in a specific order, based on their susceptibilities to biodegradation (Kaplan *et al* 1996; Peters & Moldowan 1993; Volkman *et al* 1984). For instance, *n*-alkanes have a high susceptibility to biodegradation relative to isoprenoids and this has led to the development of ratios to assess the extent of biodegradation as well as estimate the spill age of petroleum (Christensen & Larsen 1993; Wade 2001) based on the *n*-alkanes being completely removed after approximately 20 years (Christensen & Larsen 1993).

Relative mass losses can be calculated from compositional changes in LNAPLs due to weathering and biodegradation of some compounds compared with a conservative tracer, over a specified time. Samples needed to calculate mass losses include either LNAPL samples from the same location sampled at different times or the actual source

product released at the site for comparison with recovered LNAPL samples. Where the source or older recovered LNAPL samples are unavailable for the site, an estimate of mass losses can be obtained by comparison with a generic unweathered product of the same type. Samples can be taken from monitoring wells or from the extraction of soil cores.

The selection of a conservative tracer is generally based on it being one of the most non-volatile, water insoluble and biodegradation resistant components present in the LNAPL samples in sufficient relative abundances to measure (i.e. the concentration of the conservative tracer will increase as more soluble, more volatile and less biodegradation resistant compounds in the LNAPL are depleted). LNAPL constituents that can be used as a conservative tracer will depend on a number of factors including, the product type (e.g. gasoline, jet fuel, diesel), extent of weathering and the source organic matter that formed the crude oil (e.g. algal, land-plants, bacteria) used to refine into the product type. Concentration increases of the selected conservative tracers in the LNAPL samples allow losses to be calculated, for example a two-fold increase in the conservative tracer concentration over time would give an estimated loss of 50%. LNAPL depletion or losses over time are based on changes in a conservative tracer ( $H$ ) concentration, using Equation 4 (Douglas *et al* 1996).

$$\% \text{ oil depletion} = (1 - (H_0/H_1)) \times 100 \quad \text{Equation 4}$$

Where  $H_0$  is the concentration of the conservative tracer in the initial LNAPL released (or the starting period for the mass loss calculation) and  $H_1$  is the concentration of the conservative marker in the depleted LNAPL at a later time on a weight basis (w/w). This approach has been used to calculate the % losses of LNAPL by number of researchers (Baedecker *et al* 2018; Douglas *et al* 1996; Douglas *et al* 2012; Johnston *et al* 2007).

**Table 2. Comparison of NSZD estimation methods applied to the six sites. Methods that were not implemented (grey-shaded cells) and those that were implemented but did not yield meaningful results to compare with active recovery (orange-shaded cells) are indicated.**

Description of NSZD estimation method		Site A	Site B	Site C	Site D	Site E	Site F
Soil temperature gradient	iButton	√		√	√		√
	Thermistor	√	√	√	√		√
Soil gas concentration gradient	Soil vapour port	√	√				
	In-well	√	√	√	√		√
Soil surface CO <sub>2</sub> flux	E-Flux	√		√	√	√	
	LI-COR flux chamber	√	√	√		√	

## 2.5 Total site-wide rate estimation for NSZD and active recovery

A methodology for combining NSZD rate data from various locations around a site to obtain a site-wide total NSZD rate is briefly described in CRC CARE Technical Report 44 (2018). A description of the computational tools and a methodology developed specifically for this study are provided below. For active recovery, a site-

wide total mass of product recovered in tonnes per year was calculated based on volumetric recovery data converted to a mass basis using an estimate of the density of LNAPL. For purposes of comparison, an LNAPL density of 703 kg m<sup>-3</sup> was used.

### **2.5.1 Area determination**

A geographic information system (GIS)-based approach was used to estimate the area associated with each NSZD measurement location. The method involves dividing a site into polygons whereby the sides of each polygon is equidistant from each adjacent measuring location. A recognised method for this uses Voronoi/Thiessen polygons (Howarth 2017). The Voronoi polygon tool within the open source GIS desktop application, QGIS (QGIS Development Team 2019), was used for this purpose. Figure 3 is a schematic diagram depicting the procedure developed for estimating the area associated with each NSZD measurement location. To compute Voronoi polygons, the dataset of monitoring locations must have more than two locations.

For each case study, the areal extent of the site for constructing polygons was constrained by the total, assumed area of the plume (if known) or guided by background measurement locations indicating no evidence of LNAPL contamination. If there are insufficient data to delineate an assumed area of the plume, an arbitrary buffer around the outermost measurement locations can be used (CRC CARE 2018). The buffer extends the calculated polygon area and assumes that the outer measurement locations for NSZD are within the LNAPL contaminated area (CRC CARE 2018).

If approximate dimensions of the LNAPL plume are unknown, a procedure was developed for constructing a buffer around the outer measurement locations as shown in Figure 3 (right panel in the diagram). Although the procedure outlined in CRC CARE Technical Report 44 (2018) considers the measurement locations from each NSZD estimate method separately, in the case studies where approximate dimensions of the LNAPL plume were unknown, it was decided to compile all locations across multiple methods of estimating NSZD (see justification outline below). If there were measurement locations beyond the boundary of the assumed dimensions of the LNAPL plume (source zone) that showed substantial NSZD, the outermost measurement locations were used to delineate the buffer instead of using the plume dimensions.



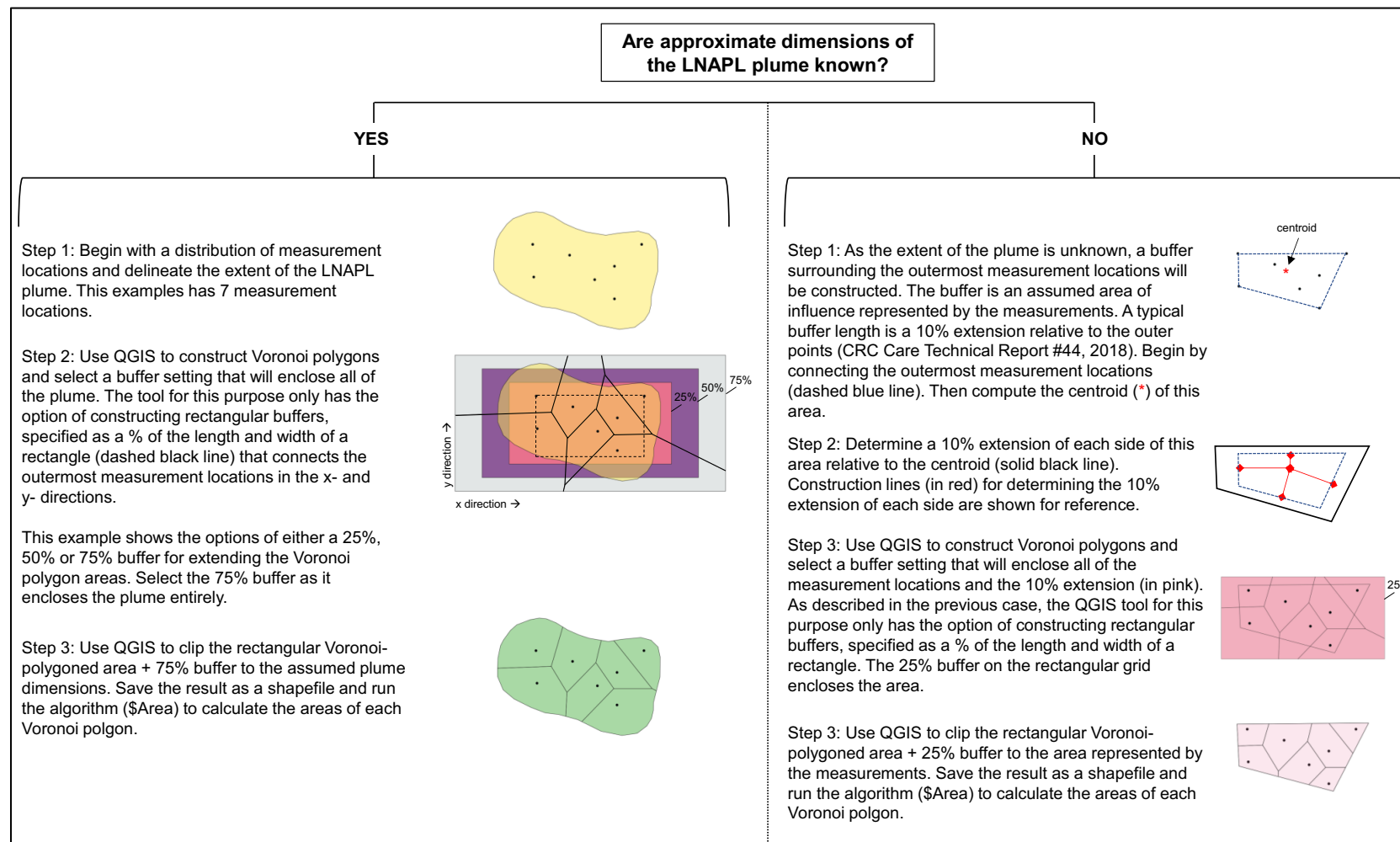


**Figure 3. Procedure developed for estimating the area associated with each NSZD measurement location**

Figure 4 depicts an example involving two different datasets of measurement locations for two methods of estimating NSZD. A couple of the measurement locations are identical for the two methods, but most of the locations are different and create different areas delimiting the measurement datasets. Presumably, NSZD extends throughout both areas; therefore, the union of the two datasets of measurement locations should be used. The solution involved combining the two datasets of locations and then constructing Voronoi polygons as described in Figure 3.

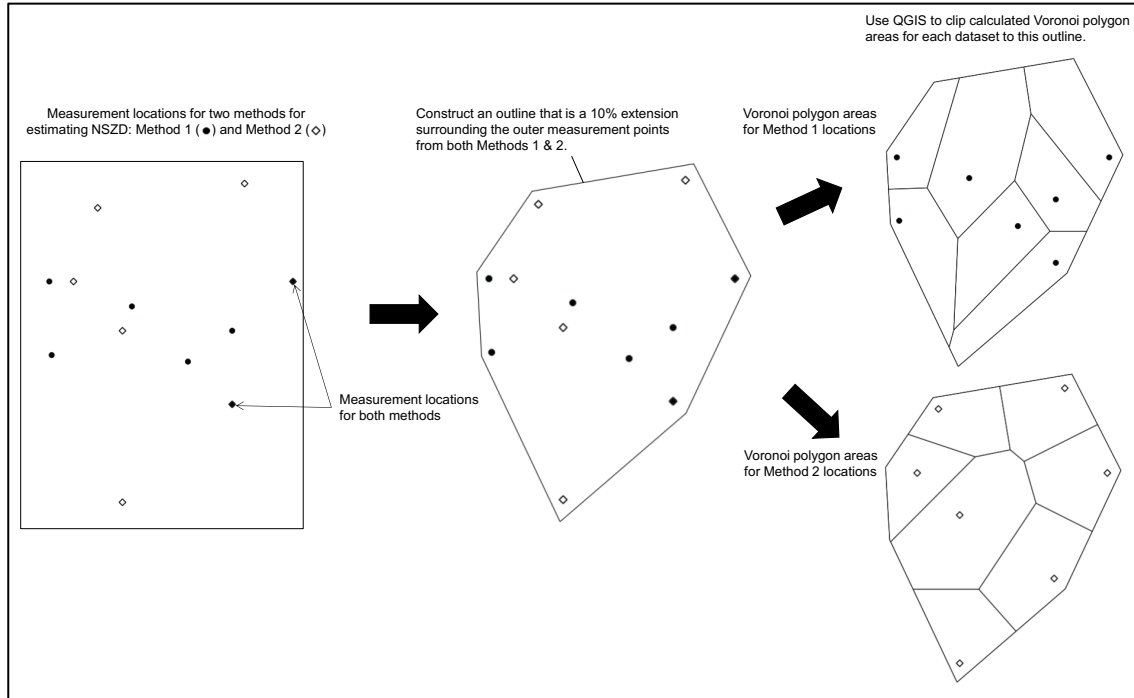


**Figure 4. Procedure for constructing Voronoi polygons for a site with unknown LNAPL plume dimensions, showing the measurement locations for method 1 (black dots) and method 2 (open diamonds) for estimating NSZD. The outer measurement locations for both methods were used to determine the 10% extension buffer.**

### 2.5.2 Geospatial integration

To obtain an estimate of the site-wide rate of hydrocarbon mass removal by NSZD, a simple summation of the product of the rate and the respective Voronoi polygon area was used, using the following equation from CRC CARE Technical Report 44 (2018):

$$R_{NSZD-site} = \left( \sum_{i=1}^n R_{NSZD-i} * A_i \right) * \left( \frac{1 \text{ kg}}{1000 \text{ g}} \right) * \left( \frac{365 \text{ d}}{1 \text{ yr}} \right) \quad \text{Equation 5}$$

where  $R_{NSZD-site}$  is the site-wide total NSZD rate (kg/yr),  $R_{NSZD-i}$  is the NSZD rate for Area  $i$  ( $\frac{g}{m^2 d}$ ),  $A_i$  is the area of the Voronoi polygon Area  $i$  ( $m^2$ ) associated with

$R_{NSZD-i}$ , and  $n$  is the number of Voronoi polygon areas. As discussed in CRC CARE Technical Report 44 (2018), if there are multiple events of site-wide measurements made throughout the year, one can integrate over the year to obtain an annual average site-wide rate of hydrocarbon mass removal.

## 3. Site A

### 3.1 Introduction

The petroleum in the subsurface at site A was a result of a gas condensate release estimated to have occurred in 2012. The gas condensate contained C4–C26 carbon range hydrocarbons dominated by the C6–C10 carbon range components. The gas condensate contained high relative abundances of aromatic compounds (including, alkylbenzenes and alkylnaphthalenes) with toluene, methylcyclohexane and *m/p*-xylene the highest concentration components in the source condensate (Figure 5). Density and carbon ranges for the source condensate from site A are shown in Table 3.

**Table 3. Density and carbon ranges for the gas condensate source from site A**

Petroleum type	Carbon range <sup>1</sup>	Density kg m <sup>-3</sup> (15 °C) <sup>2</sup>	Density kg m <sup>-3</sup> (20 °C) <sup>1</sup>
Gas condensate	C4–C26	788	784

<sup>1</sup>CSIRO data, <sup>2</sup>Density calculated using AS 2520-1981 (1981) Petroleum measurement tables.

### 3.2 Site description

Site A covers an area of 28 ha, is a sparsely vegetated coastal environment, with a low-elevation (maximum elevation of 18 mAHD) and its surface soils and aquifers are comprised of limestone or lime-cemented dune sand (SiteA\_Ref11 2017). Aeolian sand dunes are present overlying the limestone in the southern and western parts of the site (SiteA\_Ref6 2016).

The climate is arid subtropical (high humidity summer, warm winter) with an annual average rainfall of about 280 mm. Groundwater recharge is largely rainfall infiltration, however, a significant portion of the site area is sealed, resulting in reduced or negligible infiltration in those areas (SiteA\_Ref12 2017). Saturated horizons are mainly in the limestone and potentially in the overlying sand closer to the coastline (SiteA\_Ref12 2017). There are strong tidal influences on groundwater levels at the site, though the magnitude varies spatially and is unrelated to the distance from the coast.

LNAPL in the subsurface at site A arises mainly from an uncontrolled historic release of product from a pipeline, which leaked between 2012 and 2014 with a maximum estimated extent of 4.5 ha (SiteA\_Ref2 2016). The resulting plume is referred to here as the gas condensate plume. In addition, there is a dissolved phase hydrocarbon (DPH) plume on the periphery of the gas condensate plume. Estimates of condensate mass in the subsurface from in well product thickness, approximately one year after the leak was discovered, are between 1000 and 4000 tonnes (SiteA\_Ref3 2016).

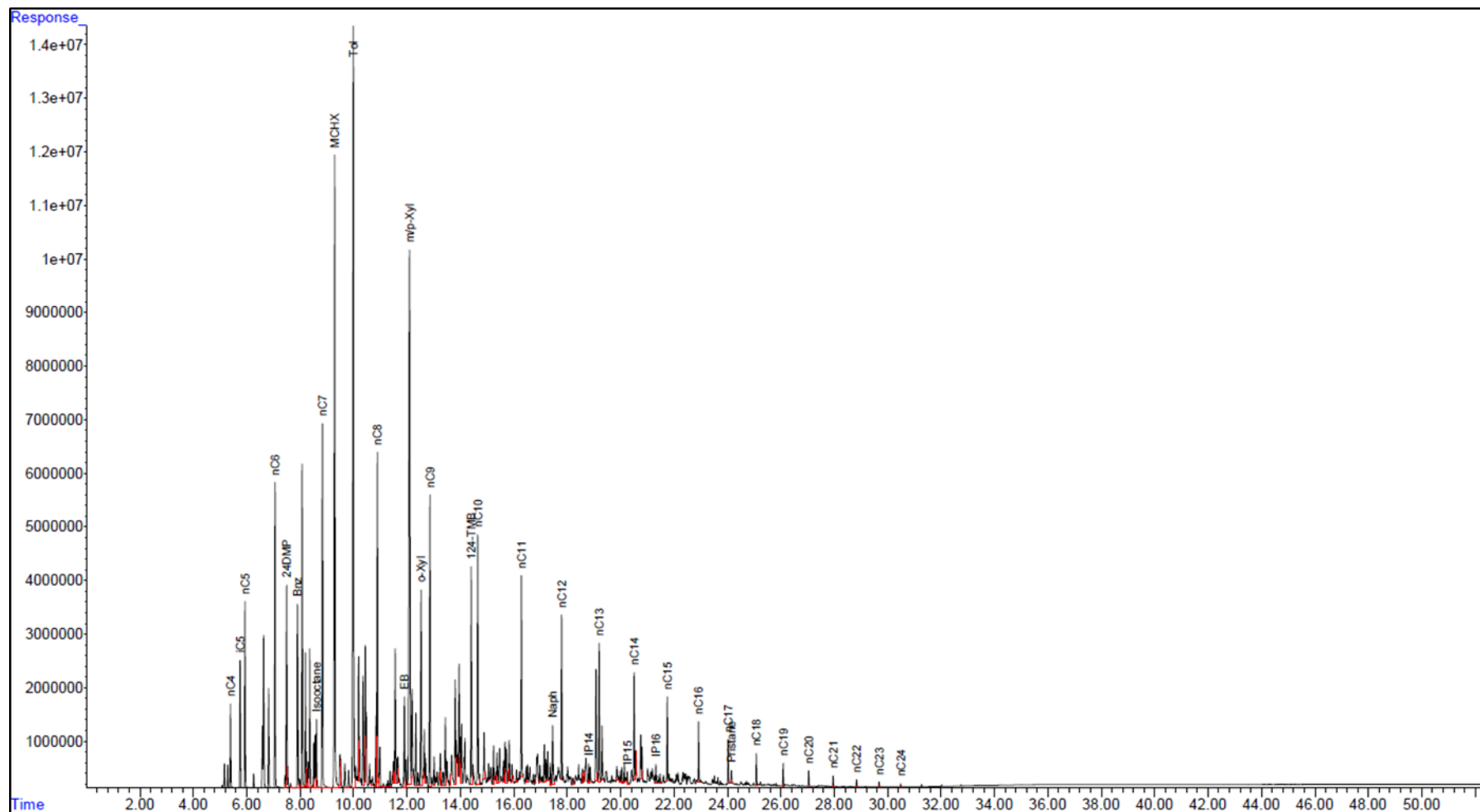


Figure 5. GC-FID analysis of the source condensate from site A. Benz: benzene, CHX: cyclohexane, Cx: straight or branched alkane containing x carbons, D: di, E: ethyl, i: iso, IP: isoprenoid, M: methyl, n: normal, Naph: naphthalene, P: pentane, TMB: trimethylbenzene, Tol: toluene, Xyl: xylene

The DPH plume forms a halo around the source area resulting from the dissolution of the gas condensate, increasing the affected area of groundwater by 4 ha. There is some evidence to suggest there are concentrations of hydrocarbons within the DPH plume above the solubility limit, suggesting the presence of non-dissolved hydrocarbons (or LNAPL bias). This is currently being investigated by filtering to remove possible non-dissolved hydrocarbons from groundwater sampled (based on guidance in CRC CARE Technical Report 44 (2018)) within the DPH plume and comparing this with non-filtered samples. For practical purposes the plumes in this report are as outlined in Figure 6. The DPH plume is not considered further in the assessment of NSZD. The DPH plume mass is considered small compared to the mass of the LNAPL condensate plume, although dissolution from the LNAPL into groundwater is a strong pathway for mass loss given the high solubility and high relative abundance of aromatic components in the condensate, and hence a pathway for biodegradation within groundwater.

### **3.2.1 Distribution of wells and measurement methods**

Figure 6 shows the inferred extent of the gas condensate LNAPL plume and associated DPH plume as of April 2018 (SiteA\_Ref13 2018) and the distribution of monitoring wells and locations of surface measurements for the following:

- LI-COR (sites labelled FS1 to FS6 and PFW01) from SiteA\_Ref4 (2016)
- soil vapour ports (Summa canisters, sites labelled SV1 and SV1QA) from SiteA\_Ref11 (2017), and
- and E-Flux (site labelled E-Flux near FS5, and sites T1 to T4) from SiteA\_Ref13 (2018) and SiteA\_Ref14 (2017).

Table 4 summarises the methods applied to the monitoring wells and other supporting data referred to in this report. Transect A-A' (Figure 7) shows the stratigraphy and the typical range of groundwater levels influenced by tides.

### **3.2.1 Profile stratigraphy**

For the logged wells, maximum drilled depths range from 12 to 30 mbg based on well log data and a geological cross-section of the site (Figure 7, SiteA\_Ref6 2016). The wells intersect mainly limestone from the surface to their maximum drilled depths. There is a greater thickness of sand overlying limestone to the northeast (e.g. 4.5 m in MW40 and 7.5 m of sand in MW58). Solution cavities are present in the upper portion of the aquifer. Localised heterogeneous flows may exist due to solution cavities and fractures in the limestone. Solution channels of up to 50 mm diameter were observed during historical drilling works (SiteA\_Ref6 2016). There are larger cavities, 'as great as 1.5 m in extent [that] were reported at some locations' (SiteA\_Ref6 2016).

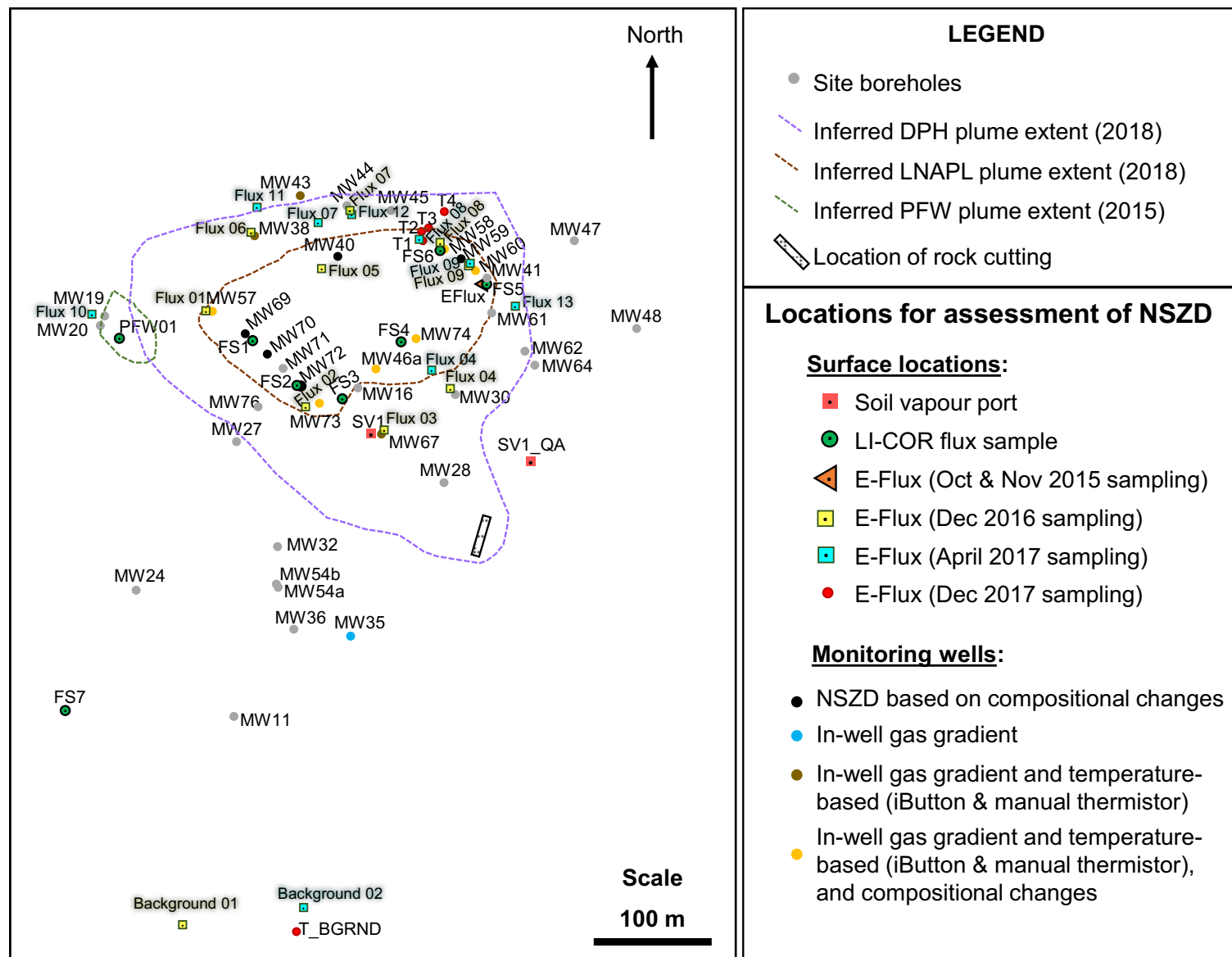


Figure 6. Generalised map of sampling and monitoring locations and transect for site A

**Table 4. Summary of NSZD methods applied at monitoring wells and other data collected. Note, LI-COR and E-Flux measurements were not conducted at well locations**

Monitoring wells	NSZD rate methods			Comments on other supporting data referred to in this report
	Temperature-based (iButton & manual thermistor)	In-well gas gradient	Inferred from NAPL compositional changes	
MW35	—	Yes	—	Well log
MW38	Yes	Yes	—	LNAPL thickness data
MW40	—	—	Yes	LNAPL thickness data, petroleum density, analysis of tidal variations in water level
MW41	—	—	—	Transmissivity estimate, recovery data, analysis of tidal variations in water level
MW43	Yes	Yes	—	Analysis of tidal variations in water level
MW46A	Yes	Yes	Yes	Well log, transmissivity estimate, recovery data, petroleum density, analysis of tidal variations in water level
MW57	Yes	Yes	Yes	Well log & recovery data, petroleum density
MW58	Yes	Yes	Yes	Well log, transmissivity estimate, recovery data, petroleum density, analysis of tidal variations in water level
MW59	—	—	Yes	LNAPL thickness data, petroleum density
MW60	Yes	Yes	Yes	Well log, LNAPL thickness data, petroleum density
MW67	Yes	Yes	—	Well log, transmissivity estimate, recovery data
MW69	—	—	Yes	Transmissivity estimate, recovery data, petroleum density, analysis of tidal variations in water level
MW70	—	—	Yes	Transmissivity estimate, recovery data, petroleum density
MW72	—	—	Yes	Well log, transmissivity estimate, recovery data, petroleum density
MW73	Yes	Yes	Yes	Well log & recovery data, petroleum density
MW74	Yes	Yes	Yes	Well log, transmissivity estimate, recovery data; petroleum density

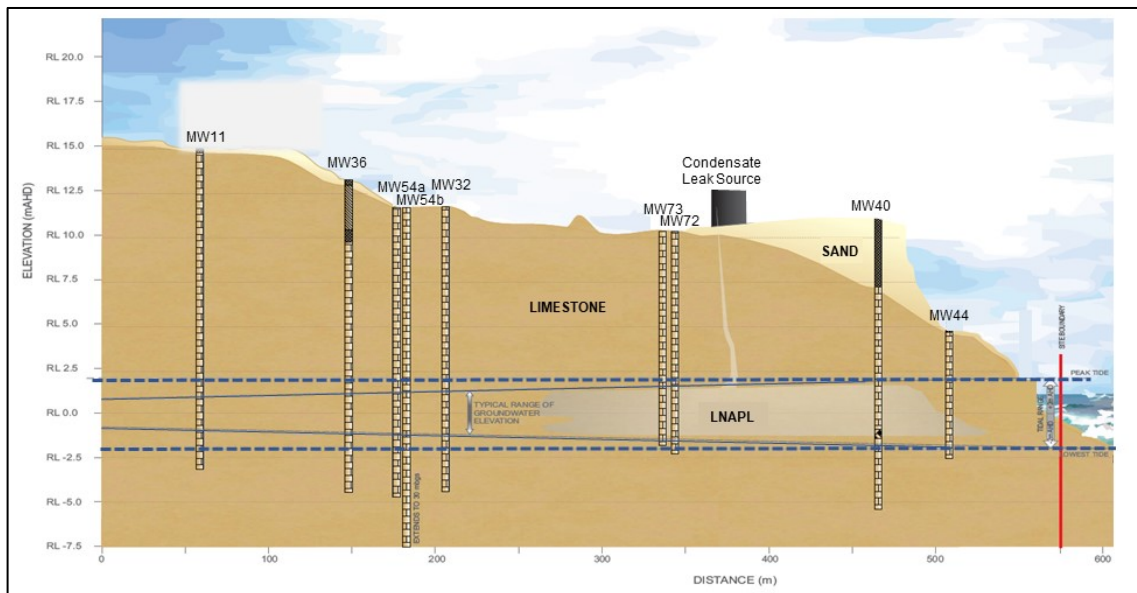


Figure 7. Transect SW-NE for site A (modified after SiteA\_Ref6 2016)

### 3.3 Data supplied by site owner

Consultancy reports dated from January 2015 to January 2018 (total number = 14), a file of recovery data (April 2015–September 2018) and selected figures from a report dated July 2015 were provided. To preserve the confidential nature of these reports, citations are coded and reference to the file name is provided in Section 12. In addition, the owner provided CSIRO with field data for interpretation and well logs. Briefly, the contents of the publications included the following:

- CO<sub>2</sub> sorbent trap (E-Flux) locations and LNAPL degradation rates dated from sampling in December 2016 and April 2017 (SiteA\_Ref15 2017)
- skimmer trials from 2015–2016, including enhanced skimmer and total fluids trials (SiteA\_Ref2, 2016; SiteA\_Ref7 2016)
- multiple and individual multiphase extraction (MPE) trials (SiteA\_Ref7 2016)
- remedial action plans in 2016 (SiteA\_Ref6 2016)
- NSZD rates from LI-COR measurements taken in 2015 (SiteA\_Ref4 2016) and from E-Flux measurements taken in 2015 and 2017 (SiteA\_Ref14 2017)
- estimation of removal of the dissolved hydrocarbon phase based on secondary indicators of natural attenuation (SiteA\_Ref5 2016)
- estimation of the mass of LNAPL over the extent of the site (SiteA\_Ref5 2016)
- estimation of LNAPL transmissivity and porosity (SiteA\_Ref2 2016)
- LNAPL saturation and hydrocarbon mass (SiteA\_Ref3 2016)
- differentiation of possible petroleum sources (SiteA\_Ref8 2016)
- data from soil vapour monitoring (SiteA\_Ref11 2017)
- groundwater remediation and a mandatory Auditor's report from 2017 (SiteA\_Ref12 2017)
- estimates of CO<sub>2</sub> flux and NSZD rates from E-Flux measurements (SiteA\_Ref14 2017)
- a schedule of field work to assess NSZD undertaken in 2018 (SiteA\_Ref13 2018), and



- historical recovery data from April 2015 to the end of September 2018 (SiteA\_Ref16 2018).

CSIRO analysed additional field data from the site. This included application of the gas gradient method to estimate NSZD using soil vapour monitoring data (O<sub>2</sub> and CO<sub>2</sub>) from 2016, and similar calculations based on in-well measurements of O<sub>2</sub> and CO<sub>2</sub> (data collected in 2018). Furthermore, gradient methods were used to estimate NSZD based on subsurface temperature data (iButton and manual thermistors) from 2018.

LNAPL compositional analysis was undertaken for samples collected from bores and an assessment of the extent of weathering (i.e. LNAPL loss (% w/w)) relative to source based on pristane concentration changes in the samples) are presented for samples up to 2019.

### **3.3.1 Hydrogeological parameters**

Estimates of hydraulic conductivity within the limestone range from 130 to 8000 m day<sup>-1</sup> based on recent measurements from pumping tests (SiteA\_Ref6 2016; SiteA\_Ref12 2017). The transmissivity of the aquifer has not been estimated.

Limestone can have both primary and secondary porosity. The former is the space within the cemented limestone matrix, and the latter is fracture or dissolution conduit pathways through the limestone. Primary porosity values are given for three locations (Table 5). Estimates of secondary porosity in the limestone were 37% and 25% based on photographic analysis of rock cuttings from a location in the southeast portion of the site (Figure 6, SiteA\_Ref1 2016). LNAPL was not detected in crushed core material recovered from depths and locations indicated in Table 5 (Figure 6). This might provide a line of evidence that LNAPL resides in the secondary porosity, but results are limited.

**Table 5. Results of laboratory measured primary porosity from SiteA\_Ref3 (2016)**

<b>Sample</b>	<b>Porosity (%)</b>	<b>Density (t m<sup>-3</sup>)</b>
MW44 (5.0–6.0 m)	5.7	2.422
MW46A (8.8–9.8 m)	17.8	1.935
MW57 (8.0–9.0 m)	10.4	2.133

### **3.3.2 Groundwater levels and flows**

Well construction logs for site A are in Appendix A.3.

The monitoring wells depicted in Figure 6 are located <220 m from the coast. The water table is tidally influenced and was found to vary by approximately 1.2 m between low and high tide (Figure 7). Based on the surveyed ground elevations and depths to water measured during well logging, the water table is at or near sea level. Due to the topographic variation across the site, the depth to water varies between 4 and 15 mbg.

The following statements describe the relationship between groundwater flow directions and tides:

‘when the tide is rising or high, the inferred groundwater flow direction is to the north; as the tide falls, the inferred groundwater flow direction turns to

the west rotating anticlockwise; when the tide and groundwater levels are at their lowest, the predominant groundwater flow direction is to the south; and groundwater levels then rise in response to a rising tide and the flow direction returns to the north' (SiteA\_Ref12 2017, p. 50).

### **3.3.3 Product thicknesses in local wells on the site over time**

LNAPL thickness measurements are referred to in the following reports:

- *Skimmer relocation plan, Jan. 2016* (SiteA\_Ref1 2016)
- *Remedial action plan, April 2016* (SiteA\_Ref6 2016)
- *Skimmer pump and total fluids pump optimisation trials, May 2016* (SiteA\_Ref2 2016)
- *LNAPL Saturation and Hydrocarbon Mass, May 2016* (SiteA\_Ref3 2016)
- *25-day trial MPE event, Sept. 2016* (SiteA\_Ref7 2016), and
- *Source zone natural depletion-field data, April 2018* (SiteA\_Ref13 2018).

A summary of these data is in Table 6. Plots showing LNAPL thickness relative to corrected water table elevation for 13 monitoring wells are in Appendix A.4

Statements given in these reports related to LNAPL thickness are:

'The greatest LNAPL thickness was observed at the second half of the falling tide; LNAPL thickness is likely affected by primary porosity and presence or absence of localised, secondary porosity features' (SiteA\_Ref1 2016, p. 4).

'...the average apparent thickness of LNAPL across the Condensate Plume is 0.12 m.', but this is, 'likely to underestimate the LNAPL thickness as most of the monitoring wells used to measure LNAPL are located towards the perimeter of the LNAPL plume where thickness is expected to be less than what may be present towards the middle of the plume' (SiteA\_Ref3 2016, p. 8).

**Table 6. Summary of reported apparent LNAPL thickness variations (mm)**

Monitoring well	SiteA_Ref1 (2016) <sup>1</sup>	SiteA_Ref2 (2016) <sup>3</sup>	SiteA_Ref6 (2016) <sup>2</sup>	SiteA_Ref3 (2016) <sup>3</sup>	SiteA_Ref7 (2016) <sup>4</sup>		SiteA_Ref13 (2018) Data collected: 16 Jan 2018
					Pre-MPE Trial (9–13 Aug 2016)	Post-MPE Trial (3 Sept & 4 Sept 2016)	
MW16	N.D.	N.D.	59–71 (2 March 2016)	N.D.	55–70	0–4	0
MW28	N.D.	N.D.	N.D.	5 (11 Oct 2015)	N.D.	N.D.	N.D.
MW38	N.D.	N.D.	N.D.	3 (28 Oct 2015)	N.D.	N.D.	N.D.
MW40	5–60 (14 Oct 2015)	N.D.	88–101 (18 Feb 2016)	35 (28 Oct 2015)	N.D.	N.D.	74
MW41	N.D.	155; 185 (20 Jan 2016)	124–159 (18 Feb 2016)	107 (28 Oct 2015)	N.D.	N.D.	3
MW44	N.D.	N.D.	22–30 (21 Jan 2016)	N.D.	N.D.	N.D.	0
MW46A	N.D.	246 (21 Jan 2016)	22–56 (2 Mar 2016)	302 (28 Oct 2015)	207–225	229–231	54
MW57	N.D.	N.D.	20–57 (18 Feb 2016)	11 (28 Oct 2015)	19–35	0–4	21
MW58	262 (14 Oct 2015)	68; 178 (31 Oct 2015)	196–262 (18 Feb 2016)	188 (28 Oct 2015)	N.D.	N.D.	38
MW59	N.D.	121; 147 (21 Jan 2016)	142–183 (18 Feb 2016)	90 (28 Oct 2015)	N.D.	N.D.	130
MW60	N.D.	N.D.	95–125 (18 Feb 2016)	86 (28 Oct 2015)	N.D.	N.D.	43

Monitoring well	SiteA_Ref1 (2016) <sup>1</sup>	SiteA_Ref2 (2016) <sup>3</sup>	SiteA_Ref6 (2016) <sup>2</sup>	SiteA_Ref3 (2016) <sup>3</sup>	SiteA_Ref7 (2016) <sup>4</sup>		SiteA_Ref13 (2018) Data collected: 16 Jan 2018
					Pre-MPE Trial (9–13 Aug 2016)	Post-MPE Trial (3 Sept & 4 Sept 2016)	
MW67	N.D.	204, 197 (1 Mar 2016)	103 (1 Mar 2016)	289 (28 Oct 2015)	93, 125	63–80	1
MW69	N.D.	374 (1 Mar 2016)	102–334 (2 Mar 2016)	78 (28 Oct 2015)	263	261–275	110
MW70	262 (14 Oct 2015)	262, 290 (11 Oct 2015)	63–162 (13 Mar 2016)	242 (28 Oct 2015)	160–204	207–259	225
MW71	380 (14 Oct 2015)	380, 481 (11 Oct 2015)	292–296 (2 Mar 2016)	220 (28 Oct 2015)	184–215	100–144	7
MW72	N.D.	71, 163 (21 Jan 2016)	115 (2 Mar 2016)	75 (28 Oct 2015)	122–153	99–101	70
MW73	N.D.	N.D.	78–98 (18 Feb 2016)	71 (28 Oct 2015)	151–163	48–69	20
MW74	N.D.	360 (21 Jan 2016)	339–414 (2 Feb 2016)	270 (28 Oct 2015)	229–239	0–42	58

<sup>1</sup> Depth to LNAPL and water measured every 30 minutes – a pressure transducer was installed in each well to monitor the change in head of water plus LNAPL above the logger at 5-minute intervals; <sup>2</sup> This report provides these results from an earlier report, which was not provided, and the methods are not described. As both reports were by the same company, it is assumed similar methods were used as in SiteA\_Ref1 (2016); <sup>3</sup> Wells were gauged prior to bail down testing using an LNAPL/water interface probe; <sup>4</sup> Wells were gauged with an interface probe for depth to water and LNAPL thickness. Post-MPE, all extraction wells were gauged after the applied vacuum was stopped and then gauged a short time later; N.D. = no data (not measured).

### 3.3.4 Measurements of LNAPL transmissivity

Transmissivity estimates were reported from baildown testing data interpreted using *API LNAPL transmissivity workbooks* provided in SiteA\_Ref1 (2016) and SiteA\_Ref2 (2016, Table 7).

According to SiteA\_Ref1 (2016), it remains uncertain whether the aquifer is confined or unconfined, but the analysis was conducted assuming unconfined conditions and ‘the API Workbook failed to provide an analytical solution of the data based on a confined system’. Furthermore, ‘due to tidal effects and aquifer heterogeneity, only the first 10 to 15 minutes of recovery data was found to be suitable for assessment’. Analysis of diagnostic gauge plots (LNAPL thickness vs potentiometric head) indicates wells exhibiting both confined and unconfined behaviour.

A follow-up study conducted in April 2016 involved baildown testing of 10 wells (SiteA\_Ref6 2016) and considered recovery data throughout the tidal cycle. According to this report,

‘...potential variations in LNAPL transmissivity that may be caused by the tidal cycle are likely insignificant to other potential sources of variability most likely associated with the heterogeneous secondary porosity of the site geology’ (SiteA\_Ref6 2016, p. 20).

It was also noted that the low transmissivity estimate for MW59 is likely an underestimate in view of data from remedial trial results.

**Table 7. Summary of transmissivity results in  $\text{m}^2 \text{day}^{-1}$ . Average based on Bower & Rice, Cooper & Jacob, and Cooper, Bredehoeft & Papadopoulos methods**

Monitoring well	SiteA_Ref1 (January 2016)	SiteA_Ref6 (April 2016)
MW41	—	0.08
MW46A	—	0.145
MW58	—	0.207
MW59	—	0.004
MW67	—	0.135
MW69	—	0.256
MW70	0.14	0.057
MW71	0.129	0.029
MW72	—	0.054
MW74	—	0.127

### 3.3.5 LNAPL sampling and analysis (compositional analyses)

Sampling of LNAPL was carried out by a contractor in 2015, 2018 and 2019. The analyses of LNAPL, water and LNAPL, water equilibration, and estimates of LNAPL loss were conducted by CSIRO (see Section 3.4.3).

### 3.3.6 LNAPL recovery operations

An historical overview of active remediation at site A is shown in Figure 8 (SiteA\_Ref9 2017 and SiteA\_Ref16 2018). This covers the period from April 2015 to the end of September 2018. The methods undertaken involved skimming pumps (enhanced skimmer and long skimmer), a total fluid pump (TFP) and multi-phase extraction (MPE) equipment. As depicted in Figure 8, there has been a decline in the rate of recovery of product from wells after late 2017, indicating that recovery has started to plateau.

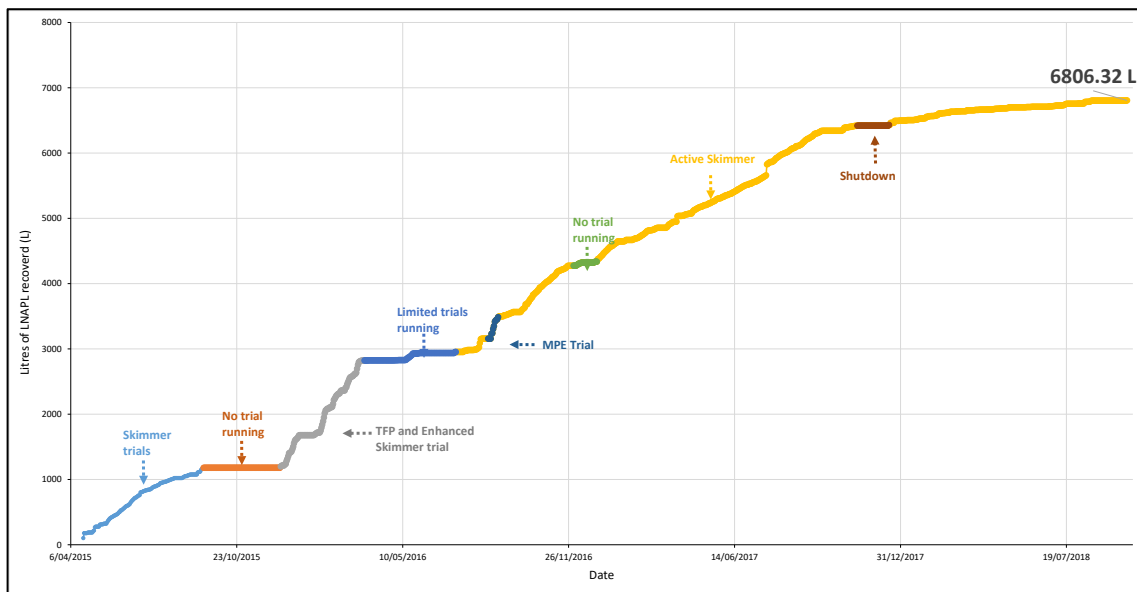


Figure 8. Cumulative LNAPL recovery: historical overview of active remediation from SiteA\_Ref9 (2017) and SiteA\_Ref16 (2018)

## 3.4 Methods

### 3.4.1 Active recovery

#### Type of method used to recover LNAPL

- LNAPL recovery started with skimmer trials (April 2015 to September 2015) in two wells (MW16 & MW41).
- Enhanced skimmer and total fluids pumping commenced in December 2015 and continued until March 2016. The trials were conducted in either one or two of the wells (MW41, MW46A, MW58, MW59, MW69, and MW70) at different times over this period. Total fluids pumping was conducted in MW41, MW46A, MW69, and MW70.
- Following a period of limited trials (April to end of June 2016), enhanced skimmer and long skimmer trials commenced in July 2016, with mainly long skimmer operations conducted in multiple wells (i.e. MW41, MW60, MW69, MW70, MW71, and MW72) and continuing until the end of September 2018.

- Individual MPE trials were conducted between 16 August and 2 September 2016 in the following wells: MW16, MW46A, MW57, MW67, MW69, MW70, MW71, MW72, MW73, and MW74.
- Multiple well MPE trials were conducted 24-31 August 2016 in MW16, MW46A, MW57, MW67, MW69, MW70, MW71, MW72, MW73, and MW74.

### **How recovery data was estimated**

The fluid stream was directed into an aboveground storage tank (AST) for each of the three LNAPL recovery methods used (i.e. skimmer pumps, TFP and MPE; SiteA\_Ref9 2017). In the situation where multiple wells directed fluids to a single AST, recovery performance of a particular well was monitored by taking the depth to fluid at the time of changeover from well to well (SiteA\_Ref9 2017). In the situation where a skimmer pump was used in particular wells, bucket tests were performed frequently whereby the delivered fluid stream was diverted into a graduated cylinder and the ratio of LNAPL to water was recorded (SiteA\_Ref9 2017). The latter was mainly used to optimise the skimmer pump performance and not for quantifying recovery volumes (SiteA\_Ref9 2017).

For the skimmer trials conducted between April and September 2015:

‘the active skimmer pumps used on site had a float element incorporating a hydrophobic membrane at the LNAPL-water interface to preferentially allow hydrocarbon to pass into the skimmer’s pump bladder whilst excluding water’ (SiteA\_Ref9 2017, p. 9).

Based on a series of optimisation assessments, a refinement was made to the standard skimmer pump arrangement. Beginning in December 2015:

‘one skimmer pump was fitted with a purpose-designed and built “lifter” that automatically positioned the down-well skimmer pump inlet throughout the changes in the SWL due to tidal influence’ (SiteA\_Ref9 2017, p. 10).

The MPE system trialled in late August 2016 used:

‘a combination of a mobile containerised MPE system and existing recovery wells on site. Well drop-tubes (spears) were inserted into nominated extraction wells at the required depth to extract from the LNAPL/groundwater interface. Fuel or static rated hose was used to connect the well head assembly to the pump on the containerised unit’ (SiteA\_Ref7 2016, p. 5).

‘Each targeted extraction well [was] pumped under vacuum at pressures of up to -80 kPa to remove LNAPL and dissolved phase impact in the groundwater as well as well VOCs in the form of vapour from the sites subsurface’ (SiteA\_Ref7 2016, p. 5).

The vacuum pump provided two duties in this system: (1) initially it provided recovery of LNAPL, potentially impacted groundwater and associated vapour; and (2) the vacuum needed for desorption of volatile organic compounds (VOC) from the carbon after capture in granular activated carbon (GAC) vessels (SiteA\_Ref7 2016).

The system cycled between MPE operations and desorption in automatic mode according to set times (SiteA\_Ref7 2016). Furthermore:

- ‘...liquids removed as part of the process were contained within a 10 kL storage tank before being transferred through a coalescing plate separator for treatment where LNAPL was separated from water’ (SiteA\_Ref7 2016, p. 6), and
- tank losses were observed due to LNAPL pooling on the surface of biological growth which inhibited skimming and prompted volatilisation in the vented tank (SiteA\_Ref7 2016, p. 6).

Between December 2015 and March 2016 TFP was conducted (SiteA\_Ref9 2017). The procedure used:

- ‘a modified skimmer pump not reliant on a float mechanism to selectively target an LNAPL thickness, to direct LNAPL and hydrocarbon impacted groundwater by positive displacement pumping to the surface’ (SiteA\_Ref9 2017, p. 11), and
- ‘a submersible, pneumatically powered pump, which fills and empties automatically when the pump bladder is full of fluid’ (SiteA\_Ref9 2017, p. 11).

### **3.4.2 NSZD rate estimation**

#### **Subsurface temperature measurement and analysis (iButton and thermistors)**

Subsurface temperatures were measured in existing wells using two techniques: emplacement of temperature loggers at set depths and manual temperature profiling down boreholes. The brief methodology for these techniques is outlined below. Further details can be found in the Appendix A.5.

##### *Temperature loggers*

Temporal changes in subsurface temperatures were monitored using strings of temperature loggers (iButtons) emplaced at set depths below ground surface in four wells, MW35 (background), MW57, MW60 and MW74. Six temperature loggers were installed in each well with the depth of the loggers determined accounting for the mean water table elevation (0 mAHD), the tidal fluctuation in the water table elevation and the depth of the vadose zone. The depths of the temperature loggers are provided in Table 8. The temperature loggers were deployed between 5 December 2017 and 11 January 2018. In addition, a pressure transducer was installed in MW35 to monitor groundwater levels during the deployment period with barometric correction provided by a second pressure transducer deployed at the top of the well casing.

##### *Manual temperature profiling*

In-well temperature profiles were obtained for ten monitoring wells on 13 and 14 January 2018 (Table 9). The temperature profiling was conducted following the in-well gas sampling (outlined in Section 0). A single NTC thermistor (10k Ohm Betacurve, 10K3A1B, matched to YSI 44036) was lowered to a depth less than 0.5 m above the standing water level and resistance measurements recorded at this point and every 0.5 m increments vertically upwards for at least 4.5 m in the lower profile and 1.0 m increments in the upper profile.



**Table 8. Temperature logger (iButton) string location and depth configuration details**

	Monitoring well ID							
Equipment ID	MW35		MW57		MW60		MW74	
Units	mBTOC	mAHD	mBTOC	mAHD	mBTOC	mAHD	mBTOC	mAHD
Button 1	2.02	11.45	2.08	7.13	2.03	8.28	4.55	8.57
Button 2	5.51	7.96	4.12	5.09	4.45	5.86	7.07	6.05
Button 3	9.00	4.47	6.16	3.05	6.88	3.43	9.59	3.53
Button 4	12.47	1.00	8.21	1.00	9.31	1.00	12.12	1.00
Button 5	13.47	0.00	9.21	0.00	10.31	0.00	13.12	0.00
Button 6	16.03	-2.56	11.58	-2.37	12.53	-2.22	15.25	-2.13
Pressure transducer	17.02	-3.55	—	—	—	—	—	—

**Table 9. Construction details for monitoring wells for which manual temperature profiles were measured and in-well gas samples were collected**

Well ID	Ground elevation	Top of casing elevation	Casing diameter	Total depth	Top of screen
Units	mAHD	mAHD	mm	mBGL	mBGL
MW35	12.45	13.38	100	16.5	10.5
MW38	11.05	11.00	100	15.0	9.0
MW43	5.25	5.87	50	7.5	2.5
MW46a	9.57	10.53	80	13.2	7.2
MW57	8.13	9.21	80	12.0	6.0
MW58	10.45	11.32	80	13.3	7.3
MW60	9.28	10.31	80	12.8	6.8
MW67	11.66	12.76	80	15.0	9.0
MW73	8.15	9.05	100	12.0	6.0
MW74	12.17	13.12	80	16.0	10.0

### *Temperature data analysis*

In-well resistance measurements were converted to temperatures using the thermistor manufacturer's polynomial calibration algorithm while daily average iButton temperatures were calculated to remove variation related to tidally induced water table fluctuations. Since the thickness of the vadose zone was generally greater at the background location (MW35) the temperature was interpolated between the measurement locations and subtracted from the other profiles at equivalent depths below ground surface. This background correction method assumes that heat transfer processes other than those associated with NSZD processes are equivalent between the background and NSZD test location.

As described in Section 2.4, this method uses Fourier's Law (Equation 3). For this site,  $\Delta T$  was assigned the maximum difference measured and  $\Delta z$  is relative to the ground

surface. It was assumed that the thermal conductivity was  $1.0 \text{ J m}^{-1} \text{ K}^{-1} \text{ s}^{-1}$  since the thermal conductivity of the profile at Site A was unknown and this lies in the range for soil (Sweeney and Ririe 2014). The heat flux was converted to a NSZD rate ( $\text{L ha}^{-1} \text{ yr}^{-1}$ ), assuming that octane was the LNAPL hydrocarbon undergoing biodegradation with a  $\Delta H$  of  $52 \text{ kJ g}^{-1}$  (Sweeney and Ririe 2014) and a density of  $703 \text{ kg m}^{-3}$  at  $20^\circ \text{C}$ .

## **Gas sampling and analyses (soil vapour port and in-well)**

### *Soil vapour gas sampling*

Multi-level soil vapour probes had been previously installed at SV21 with screen depths of 2.0 m, 4.0 m, 6.5 m and 8.5 m. Details of sampling from these is presented in Appendix A.6.

The gas gradient method for determining NSZD rates was applied to soil vapour data in the following manner:

- $\text{O}_2$  and  $\text{CO}_2$  concentrations with depth data were obtained from SiteA\_Ref11 (2017) at sample locations SV1 and SV1\_QA (background, Figure 6), which were measured in December 2016.
- Gas gradient calculations were undertaken by CSIRO (for this study) between 2.0 m and 4.0 m and between 2.0 m and 8.5 m below ground level, using the 2016 data.

### *In-well gas sampling*

Appendix A.7 provides details of in-well gas sampling. Samples were sent to CSIRO for analysis as outlined below.

### *Major gas analysis*

Analyses were carried out using an Agilent 7890 gas chromatograph (GC) fitted with a 10 port sampling valve, thermal conductivity detector (TCD), a flame ionising detector (FID), an air actuated heated valve box (containing gas sampling loops,  $2 \times 0.25 \text{ mL}$ ), a packed column (60/80 Carboxen-1000 Supleco,  $15' \times 1/8''$  SS) connected to the TCD and a capillary column (CA-1  $30 \text{ m} \times 0.32 \text{ mm ID} \times 3.0 \mu\text{m FT}$ ) connected to FID. Helium was used as carrier gas at a constant pressure and the GC oven was initially held isothermal at  $35^\circ \text{C}$  for 5 min, heated to  $225^\circ \text{C}$  at  $6^\circ \text{C min}^{-1}$  and then held at  $225^\circ \text{C}$  for 5 min. Samples were injected to the GC sample port via an Agilent 7697A headspace sampler.

NSZD rates were determined between the sampling location and the soil surface for in-well major gas measurements and depths as indicated above for the soil vapour samples, using the gradient method described in Section 2.4 and in CRC CARE Technical Report 44 (2018). To calculate NSZD rates, the gradient method for soil gas flux was applied using Equation 2 (see Section 2.4). The effective vapour diffusion coefficient for  $\text{O}_2$  and  $\text{CO}_2$  were assigned the values of  $2.59\text{E-}06$  and  $2.37\text{E-}06 \text{ m}^2 \text{ s}^{-1}$ , respectively.

## Soil surface carbon dioxide flux measurements (E-Flux and LI-COR flux chamber)

An E-Flux CO<sub>2</sub> trap was installed near the flux sampling location FS5 and deployed between 29 October 2015 and 3 November 2015 (SiteA\_Ref4 2016). Appendix A.1 provides additional details of the E-Flux method. A second set of E-Flux traps were deployed 8–21 December 2017 (locations T1 to T4 and a background site (T\_BGRND)). Duplicate samples were collected and sent to E-Flux LLC for analysis (SiteA\_Ref4 2016). The total fossil fuel CO<sub>2</sub> in the sample was corrected based on results for a travel blank sample. An additional correction was made for background CO<sub>2</sub> fluxes using carbon isotope <sup>14</sup>C analysis (SiteA\_Ref4 2016).

A LI-COR 10 cm survey chamber, analyser control unit and application software were deployed in selected locations. Appendix A.2 provides additional details of the LI-COR methodology.

Table 10 records the LI-COR flux chamber measurements that were collected for three sampling dates (SiteA\_Ref4 2016). Location (FS07) was used for taking background measurements to correct all the other measurements (Figure 6). The sample locations intercepted different portions of the tidal cycle as summarised in Table 11.

**Table 10. Summary of LI-COR measurements from SiteA\_Ref4 (2016)**

Sampling location	Number of measurements at each location		
	30 Oct 2015	3 Nov 2015	9 Dec 2015
FS1	10	--	--
FS2	10	--	--
FS3	10	--	--
FS4	10	30	--
FS5	10	30	--
FS6	10	--	--
FS7 (background)	10	30	30
PFW01	--	---	10

**Table 11. Summary of LI-COR CO<sub>2</sub> flux sampling locations and conditions from SiteA\_Ref4 (2016)**

Sampling location	Date Start and end time	Tidal cycle	Surface observations
FS1	30 Oct 2015 14:50–15:50	Full tide	Gravelly sand, very compacted at 0.05 m
FS2	29 Oct 2015 13:38–14:38	High tide	Trace ground cover, gravelly sand, very compacted at 0.05 m
FS3	30 Oct 2015 12:30–13:30	High tide	Some low-lying dead shrubs, gravelly sand, very compacted covered with gravel
FS4	30 Oct 2015 11:00–12:00	Incoming tide	Small creepers to east of sample location, gravelly sand with very compacted fill underlain, soil covered in gravel
FS4	03 Nov 2015 10:40–11:40	Incoming tide	Blue quarry gravel with gravelly sands, then very compacted fill, gravelly sands
	03 Nov 2015 13:00–14:00		
	03 Nov 2015 15:25–16:25		
FS5	30 Oct 2015 8:02–9:00	Low tide	Low shrubs with compacted gravelly sand underlain with fill
FS5	03 Nov 2015 9:20–10:20	Incoming tide	Gravelly sand, very compacted fill underlain
	03 Nov 2015 11:50–12:50		
	03 Nov 2015 14:10–15:10		
FS6	30 Oct 15 9:50–10:50	Incoming tide	Gravelly sand, very compacted at 0.05 m
FS7 (background)	30 Oct 2015	Outgoing tide	Small shrub (some dead, some living), gravelly sand, natural stone at 0.06 m
	30 Oct 2015	Low tide, incoming	Gravelly sand, very compacted, possible refusal on natural stone at 0.05 m
	9 Dec 2015 Start/end not provided	Not provided	Not provided
PFW01	9 Dec 2015 Start/end not provided	Not provided	Not provided

### **3.4.3 NSZD: LNAPL sampling and analysis (compositional analyses to assess the extent of weathering)**

Sampling of LNAPL was carried out by a contractor in 2015, 2018 and 2019. The analyses of LNAPL, water and LNAPL, water equilibration, and estimates of LNAPL loss were conducted by CSIRO.

#### *LNAPL condensate analysis (C4–C40) using GC-FID*

GC-FID analysis of LNAPL samples was performed at CSIRO, using an HP 6890 GC fitted with a vaporising injector (operating in split mode), helium carrier gas, an autosampler and a FID. The GC was equipped with a 60 m x 0.25 mm internal diameter column coated with a 0.25 µm thick film of dimethyl polysiloxane (DB-1 UI J&W).

### *LNAPL condensate and water analysis by GC-MS (C7–C24)*

Gas chromatography-mass spectroscopy (GC-MS) analysis was performed using an Agilent 7890 GC fitted with a vaporizing injector (operating in splitless mode), helium as carrier gas, an auto-sampler and an Agilent 7000 mass spectrometer. The GC-MS was fitted with a capillary GC column (AT-5MS Alltech, 30 m length, 0.25 mm internal diameter and 1.0  $\mu\text{m}$  thick film of dimethylpolysiloxane).

### *Estimating LNAPL mass losses*

Estimated percentage mass losses over a time period were based on concentration increases in the LNAPL of a conservative tracer (one of the most non-volatile, water insoluble and biodegradation resistant components present in the samples) as a result of other components decreasing in the LNAPL due to volatilisation, dissolution and biodegradation. Pristane was selected in this instance as it was unaffected by volatilisation, dissolution and biodegradation in the LNAPL samples studied (based on the ratio of pristane to n-heptadecane) as well as being one of few higher molecular weight components present due to the limited and low molecular weight range of the gas condensate.

Pristane concentration changes in the LNAPL samples relative to the unweathered condensate released at the site allowed estimation of LNAPL losses to be calculated, where a concentration of pristane (w/w) in an LNAPL sample twice that of source condensate would afford an estimated loss of 50% (w/w). Estimates of LNAPL depletion or losses over time were based on changes in the pristane concentration (conservative tracer, H) using Equation 4 (See Section 2.4).

## **3.5 Results**

### ***3.5.1 Estimation of total hydrocarbon mass removal by active recovery***

Based on SiteA\_Ref16 (2018):

As of 30 September 2018, a total of:

- 6806 L of LNAPL was recovered across the three LNAPL recovery methods used (i.e. skimmer pumps, TFP and MPE).
- Active recovery occurred over an effective period of 1185 days (i.e. combined duration across the three LNAPL recovery methods used).
- Average LNAPL recovery rates were  $\sim 5.1 \text{ L day}^{-1}$  for skimming,  $\sim 18 \text{ L day}^{-1}$  for TFP and  $\sim 16.5 \text{ L day}^{-1}$  for MPE' (Table 12).

**Table 12. Summary of LNAPL recovery by method from SiteA\_Ref9 (2017) and SiteA\_Ref16 (2018) between 21 April 2015 and 30 September 2018**

Method	LNAPL recovered (L)	Effective recovery period (days)	Average recovery (L day <sup>-1</sup> )
Skimmer pumping	5678.3	1121	5.1
Total fluids pumping	798.5	44	18.1
Multi-phase <sup>1</sup> extraction	329.6	20	16.5

<sup>1</sup>Indicative vapour concentrations are about 3000 L recovered from MPE during the same time period that the liquid NAPL was recovered (SiteA\_Ref7 2016).

Recovery techniques including skimming, total fluids pumping and multiphase extraction had an average rate of recovery of 5 L day<sup>-1</sup>, 18 L day<sup>-1</sup> and 17 L day<sup>-1</sup> respectively from April 2015 to September 2018 (SiteA\_Ref16 2018). During this period, a total of 6806 L was recovered over a total period of 1185 days. Some of the recovery was limited by operational infrastructure impeding access to the entire extent of the subsurface LNAPL plume as well as prohibitively high in well vapour concentrations. Active recovery employing three methods over the last three years has achieved on average circa 13.2 L day<sup>-1</sup> (~3.7 t yr<sup>-1</sup>) LNAPL removal, assuming an LNAPL density of 703 kg m<sup>-3</sup>.

### **3.5.2 NSZD results: measurements and total site-wide rate estimates**

#### **Temperature results**

NZSD rate calculations are based on the methods described in Section 2.4 and in CRC CARE Technical Report 44 (2018).

Interpretation of the recent data by CSIRO (this study), reveals the background corrected NSZD rates based on the iButton string data range from 0 to 3276 L LNAPL ha<sup>-1</sup> yr<sup>-1</sup> (Table 13) and the rates based on the manual thermistors range from 200 to 4471 L LNAPL ha<sup>-1</sup> yr<sup>-1</sup> (Table 14). The variability in iButton string NSZD rates for MW57 and MW74 reflects increases in the  $\Delta T$  observed over the 37-day monitoring period potentially related to seasonal changes, however longer temperature records are required to confirm this. The differences observed for the manual thermistor measurements reflect spatial variability in NSZD rates at this site. It should be noted that there is no clear spatial pattern and further measurements would be required to determine the spatial distribution.

**Table 13. Summary of results for iButton string, temperature-based NSZD**

Well location	Date	NSZD (L LNAPL ha <sup>-1</sup> yr <sup>-1</sup> )
MW57	7 Dec 2017	0
	23 Dec 2017	0
	10 Jan 2018	564
MW60	7 Dec 2017	3260
	23 Dec 2017	3264
	10 Jan 2018	3276
MW74	7 Dec 2017	609
	23 Dec 2017	726
	10 Jan 2018	908

**Table 14. Summary of results for NSZD based on manual thermistors**

Well location	Date	NSZD (L LNAPL ha <sup>-1</sup> yr <sup>-1</sup> )
MW38	13 Jan 2018	892
MW43	14 Jan 2018	1239
MW46a	13 Jan 2018	4471
MW57	13 Jan 2018	971
MW58	14 Jan 2018	1980
MW60	14 Jan 2018	3610
MW67	14 Jan 2018	200
MW73	13 Jan 2018	680
MW74	13 Jan 2018	200

The polygon areas used to compute site-wide total NSZD rates for the temperature results are shown in Figure 9. The site-wide total NSZD rates for the iButton and manual thermistor-based methods were 3.7 and 5.6 t yr<sup>-1</sup>, respectively. The outline surrounding the measurement locations for NSZD encompasses 54,762 m<sup>2</sup> (5.5 ha).

### Gas sampling results

Based on interpretation of the data by CSIRO (this study), the gas gradient method applied to soil vapour and in-well measurements of O<sub>2</sub> and CO<sub>2</sub> yielded the following results:

- vapour port data: 10,069 to 35,753 L LNAPL ha<sup>-1</sup> yr<sup>-1</sup> (Table 15), and
- in-well gas data: 34 to 8924 L LNAPL ha<sup>-1</sup> yr<sup>-1</sup> from O<sub>2</sub> data and 27 to 8984 L LNAPL ha<sup>-1</sup> yr<sup>-1</sup> from CO<sub>2</sub> data (Table 16).

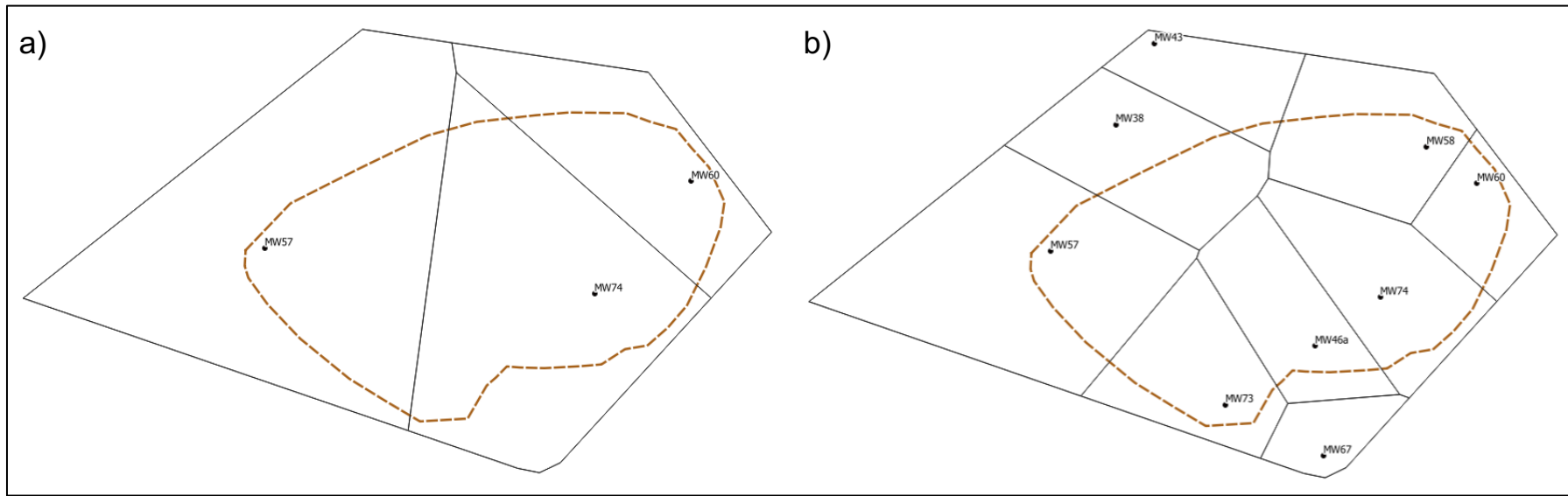


**Figure 9. Voronoi polygon areas constructed using QGIS for (a) iButton and (b) thermistor measurement locations for site A. The inferred LNAPL plume extent (2018) is shown for reference (dashed brown line).**



**Table 15. Summary of results for NSZD based on gas vapour port data (location SV1)**

Location	Date	Gas	NSZD (L LNAPL ha <sup>-1</sup> yr <sup>-1</sup> )
SV1 between 2 & 4m	15 Dec 2016	O <sub>2</sub>	34,776
SV1 between 2 & 8.5m	15 Dec 2016	O <sub>2</sub>	10,961
SV1 between 2 & 4m	15 Dec 2016	CO <sub>2</sub>	35,753
SV1 between 2 & 8.5m	15 Dec 2016	CO <sub>2</sub>	10,069

**Table 16. Summary of results for NSZD based on in-well gas data**

Location	Date/time	Gas	NSZD (L LNAPL ha <sup>-1</sup> yr <sup>-1</sup> )
MW35 background	14 Jan 2018 16:50	O <sub>2</sub>	34
	14 Jan 2018 16:50	CO <sub>2</sub>	27
MW38	13 Jan 2018 14:00	O <sub>2</sub>	90
	13 Jan 2018 14:00	CO <sub>2</sub>	74
MW43	14 Jan 2018 14:00	O <sub>2</sub>	4153
	14 Jan 2018 14:00	CO <sub>2</sub>	3350
MW46a	13 Jan 2018 16:30	O <sub>2</sub>	8438
	13 Jan 2018 16:30	CO <sub>2</sub>	8577
MW57	13 Jan 2018 14:50	O <sub>2</sub>	2425
	13 Jan 2018 14:50	CO <sub>2</sub>	2251
MW58	13 Jan 2018 14:55	O <sub>2</sub>	7380
	13 Jan 2018 14:55	CO <sub>2</sub>	8458
MW60	14 Jan 2018 14:45	O <sub>2</sub>	8924
	14 Jan 2018 14:45	CO <sub>2</sub>	8984
MW67	14 Jan 2018 16:00	O <sub>2</sub>	4661
	14 Jan 2018 16:00	CO <sub>2</sub>	3943
MW73	13 Jan 2018 15:45	O <sub>2</sub>	6287
	13 Jan 2018 15:45	CO <sub>2</sub>	5461
MW74	13 Jan 2018 17:00	O <sub>2</sub>	6695
	13 Jan 2018 17:00	CO <sub>2</sub>	6405

The polygon areas used to compute site-wide total NSZD rates for the gas in-well sampling results are shown in Figure 10. The site-wide total NSZD rates for the gas in-well (O<sub>2</sub> and CO<sub>2</sub>) were 19 and 18 t yr<sup>-1</sup>, respectively and the site-wide total NSZD rates for the gas vapour port (O<sub>2</sub> and CO<sub>2</sub>) were 42 to 130 t yr<sup>-1</sup> and 39 to 140 t yr<sup>-1</sup>, respectively. As measurements were taken from only one gas vapour port across different depth intervals, no polygons were constructed to compute a site-wide total NSZD rate. Instead, the NSZD rates based on gas gradients at this location were scaled using the area encompassing the measurement locations for NSZD rate estimation (54,762 m<sup>2</sup>) as a multiplier.

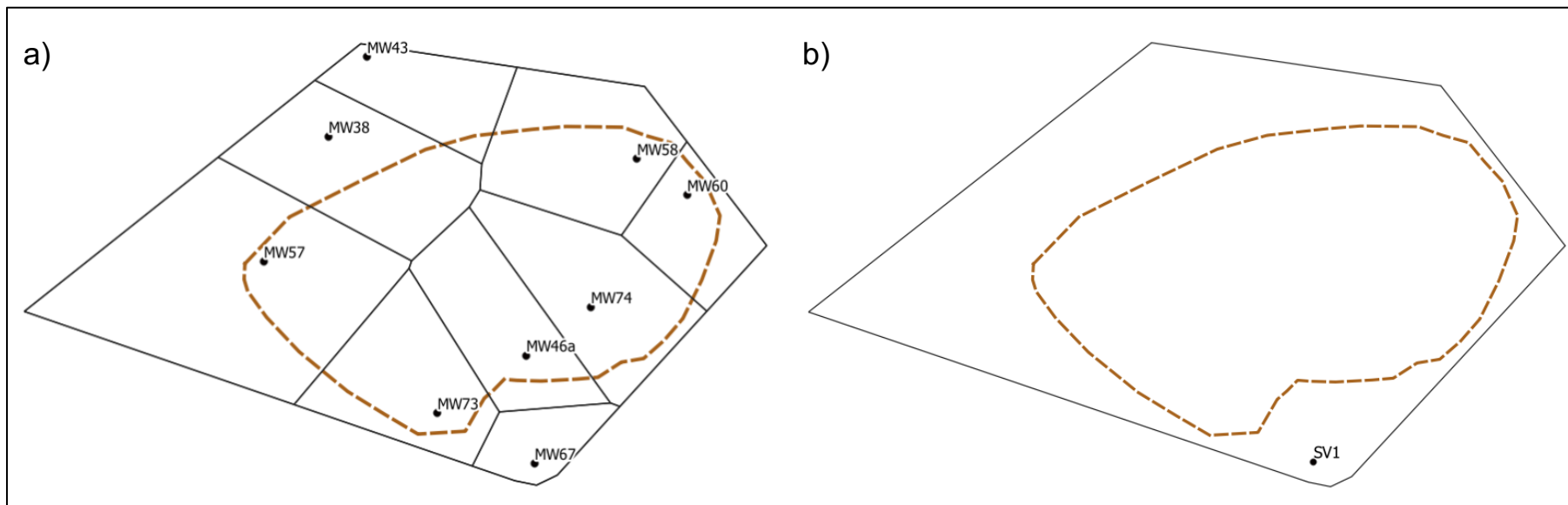


**Figure 10. Voronoi polygon areas constructed using QGIS for (a) gas in-well measurement locations for site A, and (b) the single location (SV1) for soil vapour port measurements at different depths. The inferred LNAPL plume extent (2018) is shown for reference (dashed brown line).**

## Soil surface carbon dioxide flux results

### E-Flux results

The analytical results for the E-Flux CO<sub>2</sub> trap sampling near FS5 are shown in Table 17 for traps deployed for the period between 29 October 2015 and 3 November 2015. Also shown are results from 2017 sampling (Table 17). LNAPL degradation rates derived from E-Flux CO<sub>2</sub> traps sampled in December 2016 and April 2017 are summarised in Table 18 (SiteA\_Ref15 2017).

**Table 17. Summary of E-Flux CO<sub>2</sub> trap analytical results from reports (locations are on Figure 3). Traps deployed in 2015 and 2017**

Date	Sample	Deployment days	CO <sub>2</sub> flux <sup>a</sup> ( $\mu\text{mol m}^{-2}\text{s}^{-1}$ )	Modern CO <sub>2</sub> flux <sup>b</sup> ( $\mu\text{mol m}^{-2}\text{s}^{-1}$ )	Fossil fuel CO <sub>2</sub> flux <sup>b</sup> ( $\mu\text{mol m}^{-2}\text{s}^{-1}$ )	Equivalent fossil fuel NAPL loss rate <sup>c</sup> (L ha <sup>-1</sup> yr <sup>-1</sup> )	Source of data
2015 samples	E-Flux location near FS5	5.163	1.32	1.13	0.20	1140	SiteA_Ref14 (2016)
2017 samples	T1	13.17	2.7	1.93	0.8	4653	SiteA_Ref14 (2017)
	T2	13.16	2.7	1.58	1.07	6261	
	T3	13.15	7.0	2.17	4.83	28,210	
	T4	13.14	1.3	1.21	0.09	533	
	T_Background	13.10	1.5	1.45	0.03	159	

<sup>a</sup> Blank corrected results; <sup>b</sup> Blank corrected, <sup>14</sup>C analysis results; <sup>c</sup> Blank corrected, <sup>14</sup>C analysis results that reported in gal. acre<sup>-1</sup> yr<sup>-1</sup> have been converted to L ha<sup>-1</sup> yr<sup>-1</sup>.

**Table 18. Results from E-Flux CO<sub>2</sub> trap measurements from sampling in December 2016 and April 2017 as shown on a map provided in SiteA\_Ref15 (2017)**

Date	Sample	LNAPL degradation (L ha <sup>-1</sup> yr <sup>-1</sup> )	Date	Sample	LNAPL degradation (L ha <sup>-1</sup> yr <sup>-1</sup> )
Dec. 2016 samples	Flux 01	2132	April 2017 samples	Flux 04	3329
	Flux 02	954		Flux 07	5760
	Flux 03	2768		Flux 08	6919
	Flux 04	3301		Flux 09	12,127
	Flux 05	1244		Flux 10	1935
	Flux 06	1889		Flux 11	34,118
	Flux 07	2693		Flux 12	3908
	Flux 08	12,651		Flux 13	13,342
	Flux 09	7265		Background 02	1141
	Background 01	2104			

## LI-COR results

The average CO<sub>2</sub> fluxes for each sampling location are provided in Table 19 from SiteA\_Ref4 (2016). Results for sampling location FS03 are not shown as review of the data indicated the chamber seal likely failed at this location. Average CO<sub>2</sub> fluxes have been corrected for background CO<sub>2</sub> flux measured at FS07 and the average flux converted to a volumetric flux (LNAPL loss rate) per mole of octane assuming a hydrocarbon density of 0.77 (SiteA\_Ref4 2016).

**Table 19. Summary of LI-COR CO<sub>2</sub> flux measurements for the gas condensate plume and process formation water (PFW) plume (locations are in Figure 3)**

	30 Oct 2015						3 Nov 2015			9 Dec 15	
Sample location	FS1	FS2	FS4	FS5	FS6	FS7	FS4	FS5	FS7	PFW01	FS7
Number of observations used to compute average	10	10	8	10	10	10	30	30	30	10	30
Average flux (μmol m <sup>-2</sup> s)	0.51	0.88	0.73	1.02	2.36	0.23	0.72	1.13	0.22	6.47	0.55
Average flux corrected for background (μmol m <sup>-2</sup> s)	0.28	0.65	0.50	0.78	2.13	0.00	0.50	0.90	0.00	5.92	0.00
Volumetric flux of LNAPL (L ha <sup>-1</sup> yr <sup>-1</sup> )	1654	3801	2910	4585	12,474	0.00	2910	5288	0.00	34,620	0.00

FS7 results are of background CO<sub>2</sub> flux

The polygon areas used to compute site-wide total NSZD rates for the soil surface carbon dioxide flux results are shown in Figure 11. The site-wide total NSZD rates for the E-Flux and LI-COR methods were 16 and 33 t yr<sup>-1</sup>, respectively.

### 3.5.1 NSZD results: LNAPL composition

Recovered LNAPL samples all seemed unaffected by intrinsic biodegradation based on indicators of biodegradation. The ratios of isoprenoids (pristane, Pr) to *n*-alkanes (*n*-heptadecane, *n*C17) were used as an indicator of biodegradation (Christensen & Larsen 1993; Wade 2001) and the recovered LNAPL samples and unweathered gas condensate had similar ratios of Pr/*n*C17 (Appendix Table A.8-1) suggesting the samples were unaffected by biodegradation as biodegradation would generally preferentially deplete the *n*-alkanes. Losses to volatilisation that the recovered LNAPL samples have experienced were minor up to the 2015 with losses largely due to dissolution. This is based on depletion of the more water-soluble components (benzene, toluene, xylenes, Appendix Table A.8-1) relative to lighter insoluble components (low molecular weight alkanes, *n*C6 Appendix Table A.8-1), compared to the source condensate. Increases in the lighter insoluble components in the LNAPLs is likely a result of losses of the water-soluble components increasing the relative proportion of the non-water-soluble components in the LNAPL.

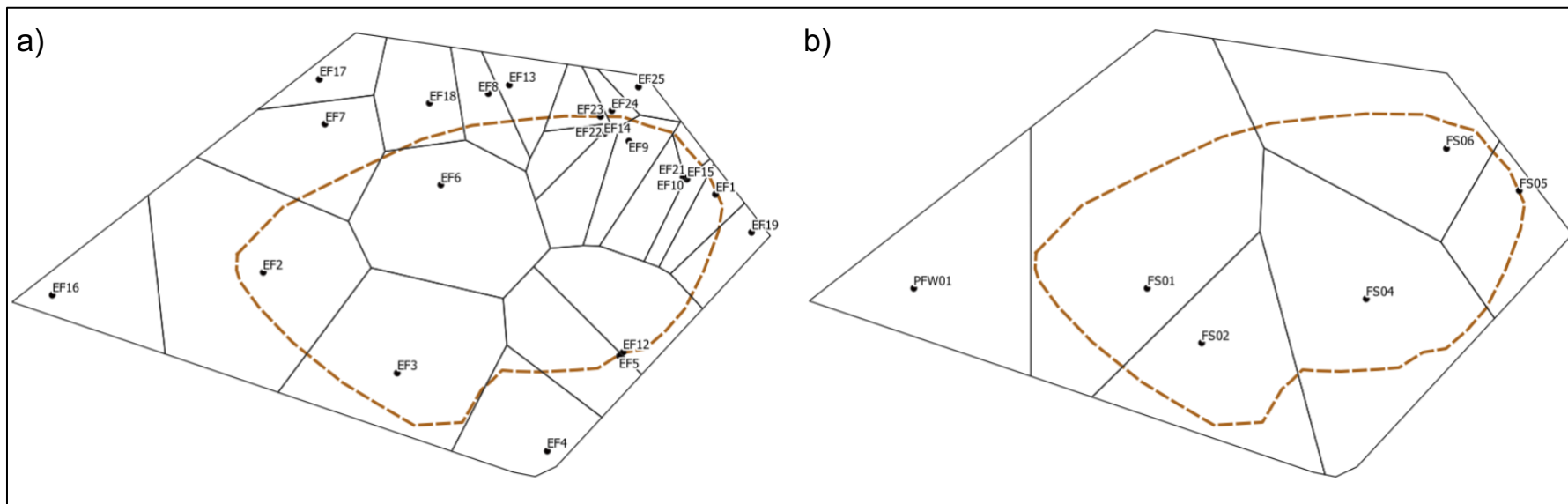


**Figure 11. Voronoi polygon areas constructed using QGIS for the (a) E-Flux and (b) LI-COR measurement locations for site A. The inferred LNAPL plume extent (2018) is shown for reference (dashed brown line).**

In 2015, estimated LNAPL losses were from 3% to 24% (based on comparison with the unweathered condensate, Appendix Table A.8-1 and Figure 12) after the end of the release in 2014 (so effectively over a one-year period). Whereas losses in 2019 were larger (52% to 79%) due to both dissolution of the more water-soluble components (BTEX in 2019 ranging from 0.2% to 4.7%, BTEX in source condensate 16%) and volatilisation of the lower molecular weight components (over a five-year period). Some of this increased loss may be due to MPE remediation activities that were carried out in 2016. GC-FID chromatograms (Figure 13) show compositional changes in the recovered LNAPL from 2015 to 2019 losses (from different locations showing typical changes observed) compared to the unweathered condensate. These results suggest that direct biodegradation of the condensate LNAPL has not been a dominant process as all the changes to the LNAPL up to 2018 have been related to physical changes (dissolution and volatilisation), although components that have partitioned into the gas and water phases are undergoing biodegradation in these phases. However, in 2019 some samples (MW58, MW59, MW60, MW67, MW69 and MW73) are showing indications of the lower molecular *n*-alkanes undergoing biodegradation (depletion of *n*C10 and *n*C11, Appendix Table A.8-1 and Figure 13).

good relationship was observed with percentage loss and density (Appendix Figure A.9-1) suggesting density and percent loss data is valid. The relationship with percent loss and density likely works well in this situation due to the high proportion of lighter components resulting in significant density changes to the LNAPL when they are lost. Based on this the relationship with percentage loss and density may be applicable to gasoline range products. Percentage loss and time also show a relationship (Appendix Figure A.9-2) suggesting extrapolation of the relationship (assuming a linear relationship with percent loss and time) may allow a time window to be predicted for the complete removal of the condensate from the monitoring locations.

While dissolution and volatilisation processes currently dominate the changes to LNAPL, subsequent biodegradation of these components in groundwater and the vadose zone, respectively, contributes to the NSZD. Thus, a site-wide estimate of NSZD based on LNAPL compositional changes was obtained for January 2018, of between 26 and 64% mass losses since the release occurred. This equates to 35,000 and 87,000 L LNAPL ha<sup>-1</sup> yr<sup>-1</sup>. No polygons were constructed to compute a site-wide total NSZD rate. Instead, the NSZD rates were scaled using the area encompassing the measurement locations for NSZD rate estimation (54,762 m<sup>2</sup>) as a multiplier to obtain an estimated range between 110 and 280 t yr<sup>-1</sup>.

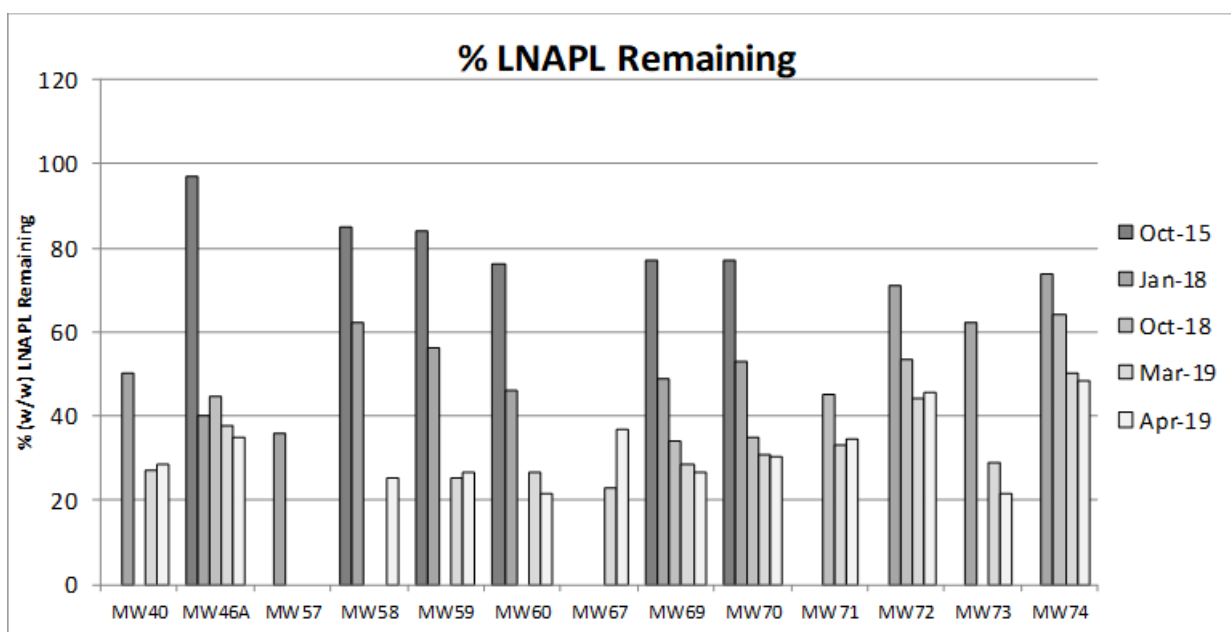


Figure 12. LNAPL remaining at selected locations from 2015 to 2019

### 3.6 Overview of hydrocarbon mass removal – recovery and NSZD

Table 20 provides a review of site-wide total NSZD rates reported in Section 3.5. The active recovery of LNAPL on site ( $3.7 \text{ t yr}^{-1}$ ) is much lower than the estimated NSZD rates by between ~5 and ~50 times for temperature methods and vapour port gas compositions respectively. It is noted that active recovery was restricted by operational infrastructure limiting access to the entire extent of the subsurface LNAPL plume.

At this site, it appears mass loss processes which do not fall under active recovery or vadose zone NSZD measurement techniques, have accounted for perhaps two orders of magnitude more LNAPL removal than what has been quantified in the methods being compared in this case study. These losses are associated with dissolution into groundwater, volatilisation into the vadose zone, and subsequent biodegradation processes. These are the subject of further investigation.

It is recognised that the depletion rate of all these processes will change over time as both the removal of more biodegradable and lower molecular weight components through partitioning processes occurs. Thus, while it is recognised that these processes have occurred based on the LNAPL compositional changes it is unlikely that the contribution of these processes to mass loss can be retrospectively quantified without additional fate and transport modelling.

NSZD rates ranged from zero or low values for some methods and locations up to  $34,000 \text{ L LNAPL ha}^{-1} \text{ yr}^{-1}$  based on E-Flux measurements and as high as  $36,000 \text{ L LNAPL ha}^{-1} \text{ yr}^{-1}$  based on the gradient method for  $\text{CO}_2$  flux using vapour port monitoring data. The upper estimates of the range of NSZD rates from temperature data were in general lower than those determined by other methods.

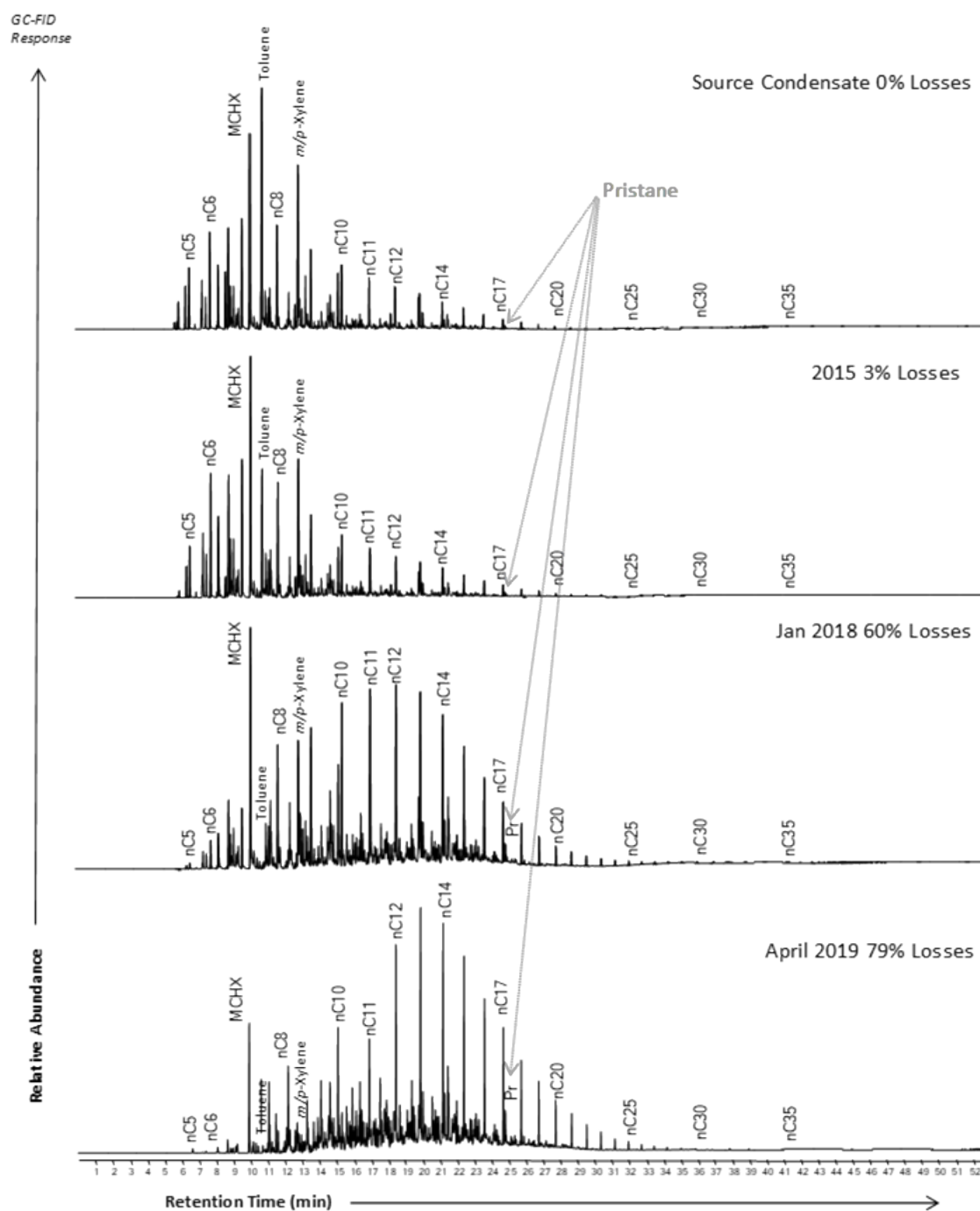


Figure 13. GC-FID chromatograms showing the composition of the unweathered condensate LNAPL from 2015 and changes due to weathering in 2015, 2018 and 2019. Benz: benzene, CHX: cyclohexane, Cx: straight or branched alkane containing x carbons, D: di, E: ethyl, i: iso, IP: isoprenoid, M: methyl, n: normal, Naph: naphthalene, P: pentane, TMB: trimethylbenzene, Tol: toluene, Xyl: xylene.



**Table 20. Tabulation of NSZD rates across methods used, and spatially-weighted mass losses per time**

NSZD methods	Intrinsic rate estimates (L LNAPL ha <sup>-1</sup> yr <sup>-1</sup> )*	Rate mass/time (t yr <sup>-1</sup> )**
Soil surface CO <sub>2</sub> flux	<ul style="list-style-type: none"> <li>E-Flux: 160 to 34,000</li> <li>LI-COR: 1700 to 12,000</li> </ul>	<ul style="list-style-type: none"> <li>E-Flux: 16</li> <li>LI-COR: 33</li> </ul>
Temperature:	<ul style="list-style-type: none"> <li>iButton strings: 0 to 3300</li> <li>Manual thermistors: 200 to 4500</li> </ul>	<ul style="list-style-type: none"> <li>iButton: 3.7</li> <li>Manual thermistor: 5.6</li> </ul>
Gas sampling (in-well)	<ul style="list-style-type: none"> <li>O<sub>2</sub>: 34 to 8900</li> <li>CO<sub>2</sub>: 27 to 9000</li> </ul>	<ul style="list-style-type: none"> <li>O<sub>2</sub>: 19</li> <li>CO<sub>2</sub>: 18</li> </ul>
Gas sampling (gas vapour port data)	<ul style="list-style-type: none"> <li>O<sub>2</sub>: 11,000 to 35,000</li> <li>CO<sub>2</sub>: 10,000 to 36,000</li> </ul>	<ul style="list-style-type: none"> <li>O<sub>2</sub>: 42 to 130<sup>†</sup></li> <li>CO<sub>2</sub>: 39 to 140<sup>†</sup></li> </ul>
LNAPL compositional changes	<ul style="list-style-type: none"> <li>35,000 to 87,000</li> <li>Based on between 26 and 64% mass loss since release to January 2018</li> </ul>	<ul style="list-style-type: none"> <li>140 to 340</li> </ul>

\* Rates have been determined across a number of locations (except for the vapour port), the range denotes variability across different locations at the site. Values are rounded to two significant figures. For the vapour port data the range is estimated by different assumed depth interval concentration gradients.

\*\* A polygon areal weighting approach has been adopted to determine these rates, with the polygon areas scaled to the LNAPL plume area at the site (5.5 ha), except where noted (†).

NSZD rates from temperature data ranged from zero to 4471 L LNAPL ha<sup>-1</sup> yr<sup>-1</sup>. There appears no systematic trend in rates with distance from the LNAPL, since sites like MW57 and MW74 within the LNAPL plume delineation (Figure 3) have low NSZD rates (0 to 908 L LNAPL ha<sup>-1</sup> yr<sup>-1</sup>) compared to others like location MW43 beyond the boundary of the DPH plume, which have comparable or higher rate estimates (1239 L LNAPL ha<sup>-1</sup> yr<sup>-1</sup>). Further data over longer time frames, and closer monitoring of ambient conditions, will yield greater certainty around rates determined via the thermal method.

In contrast at MW74, NSZD rates estimated from in-well gas data give rates nearer 6500 L LNAPL ha<sup>-1</sup> yr<sup>-1</sup>, whilst at MW43 the estimated rates are close to 4000 L LNAPL ha<sup>-1</sup> yr<sup>-1</sup>. The highest rates determined from in-well gas data are close to 9000 L LNAPL ha<sup>-1</sup> yr<sup>-1</sup> (at MW60 and MW46a).

E-Flux estimates in the T transect (Table 17) ranged from 28,210 L LNAPL ha<sup>-1</sup> yr<sup>-1</sup> at T3 to 533 L LNAPL ha<sup>-1</sup> yr<sup>-1</sup> at T4. T4 is located furthest away from the LNAPL source (see Figure 3) and the T4 rate accords somewhat with the estimate from the background location (at T\_background) which gave an estimate of 159 L LNAPL ha<sup>-1</sup> yr<sup>-1</sup>. Other E-Flux rates (Table 18) ranged from 1141 L LNAPL ha<sup>-1</sup> yr<sup>-1</sup> equivalent at a background location up to 34,118 L LNAPL ha<sup>-1</sup> yr<sup>-1</sup>.

Some measurements of NSZD using different methods were in close proximity to each other on the northern boundary of the site (Figure 6). MW58 and MW60 are in the near vicinity of the E-Flux locations T1, T2, T3, Flux 08 and Flux 09, and the LI-COR location FS6 (see Figure 6). At MW58 and MW60, NSZD rate estimates from temperature data were 1980–3610 L LNAPL ha<sup>-1</sup> yr<sup>-1</sup> and from gas data were 7380–8984 L LNAPL ha<sup>-1</sup> yr<sup>-1</sup> – the upper end of the range across all locations for each of these methods. These are somewhat comparable to the range of E-Flux rate estimates across T1-T3 of 4653–28,210 L LNAPL ha<sup>-1</sup> yr<sup>-1</sup> and 6919–12,651 L LNAPL ha<sup>-1</sup> yr<sup>-1</sup> for the Flux 08 and Flux 09 locations, albeit lower than the upper end of the range for the flux canister measurements. The LI-COR estimate from FS6 is also comparable at

12,474 L LNAPL ha<sup>-1</sup> yr<sup>-1</sup>. Across these measurement techniques the higher rates across the range found at the site seem to occur in this location on site (note MW46a also has high rates but not all methods were used near MW46a). It provides some confidence that the methods at the higher rates are somewhat in agreement.

Whilst NSZD rate comparisons between methods and locations are promising, some rates contrast with one another especially at lower or intermediate rate estimates. Lower NSZD rates yield lower temperature contrasts, lower consumption of oxygen and production of carbon dioxide – these may lead to subdued changes that are more difficult to measure and may require longer time series of data or a greater intensity of data to gain greater surety and consistency. This variability at lower rates creates challenges in then interpolating data spatially from point and local estimates across large areas. Application of the NSZD rates across large areas requires considered understanding of variability across a site and an understanding of the distribution and the status of LNAPL in the subsurface. Such interpolation of the data will be further investigated.

### **3.7 Sources of uncertainty in hydrocarbon mass loss estimation**

The largest uncertainty in estimates of mass recovery are quantifying mass vapour emissions during multiphase extraction activities. This is mainly due to quantifying extraction fluxes and VOC concentrations in a mixed phase system composed of light hydrocarbons and saline water.

The main source of uncertainty in the determination of NSZD rates is assigning realistic physical properties (thermal conductivity and gas diffusion coefficients) to the subsurface material. The principle fluid conducting pathways are in the secondary porosity consisting of fractures and voids with varying continuity, whereas the dominant heat conduction will be through more competent rock. While selected literature values have been used to derive rates at this site, verification through direct measurement coupled with inverse modelling would improve the confidence and certainty of estimates.

## 4. Site B

### 4.1 Introduction

Site B is a large site with multiple LNAPL sources and located in a coastal district. It has stored a range of petroleum products including crude oil, diesel, gasoline and aviation fuels. According to maps of contoured LNAPL thickness  $\geq 50$  mm for 2015, the distribution of LNAPL was approximately 51 ha in summer (December) and 21 ha in winter (July). (SiteB\_Ref11 2016). It has operated since 1953 and there is subsurface contamination arising from a variety of product types due to past releases (SiteB\_Ref1 2004, Figure 14).

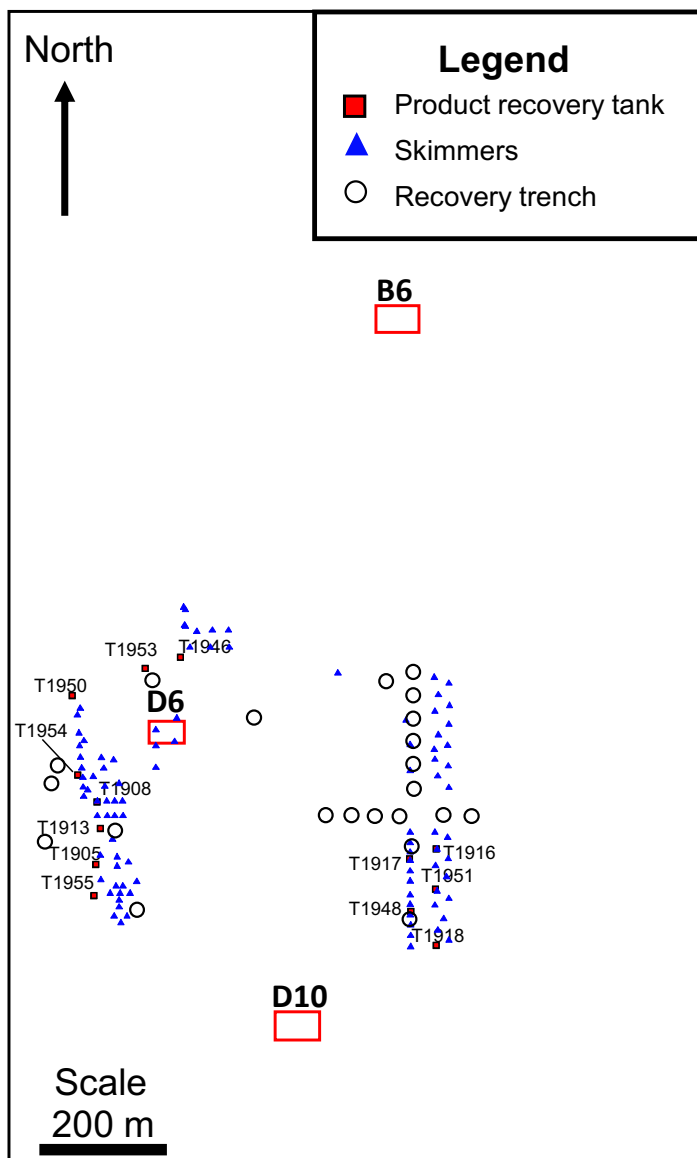


**Figure 14. Map view of site B and areas of detailed investigation at locations D6 and D10 and background site, B6. The rectangles marking these sites are shown enlarged in Figure 15–Figure 17. Only recovery operations relevant to sites D6 and D10 are shown.**

## 4.2 Site description

Three locations were examined on site B, referred to as locations D6, D10 and a background location B6. The recovery of LNAPL began in the 1980s and is still continuing (SiteB\_Ref1 2004). The three locations in this study are 370 m (D6), 420 m (D10), and 600 m (B6) from the coastline. The surface geology is mainly sand with surface elevations generally less than 15 mAHD. The site is comprised of aeolian sands overlying limestone.

The area has a mediterranean climate characterised by cool wet winters and hot dry summers. Annual average rainfall is approximately 630 mm (Queensland Government 2019). Groundwater recharge is predominantly from rainfall infiltration. The relatively permeable surface deposits allow for rapid downward migration of any hydrocarbon leakage (SiteB\_Ref4 2006).

LNAPL contamination at site B has arisen from leaks and spills of different products. According to a review of product contamination at the site conducted in 2005, location D6 is mapped as having diesel contamination, whereas near D10, there is crude oil contamination (SiteB\_Ref6 2013).

### **4.2.1 Distribution of wells and measurement methods**

All three study sites (B6, D6 and D10 – Figure 15 to Figure 17) have a similar distribution of measurement points that include:

- groundwater monitoring wells (for in-well temperature measurements and gas sampling)
- thermistor strings
- vadose zone gas sampling string, and
- LI-COR measurement locations.

The LI-COR measurements at B6, D6, and 10, referred to as LI0# a, b, c, were about 90 cm from the vadose zone gas sampling string.

### **4.2.1 Profile stratigraphy**

The soil profile and surficial aquifer consists of a sequence of aeolian and littoral calcareous sands. Sometimes thin carbonate-cemented layers are encountered in the vadose zone. Often creamy-tan-coloured sands extended to 2–3 mbg, where a change to grey-coloured sand might occur down to the depth of the bottom of the sand sequence. The sands typically have low organic matter content with the fraction of organic carbon less than 0.03%.

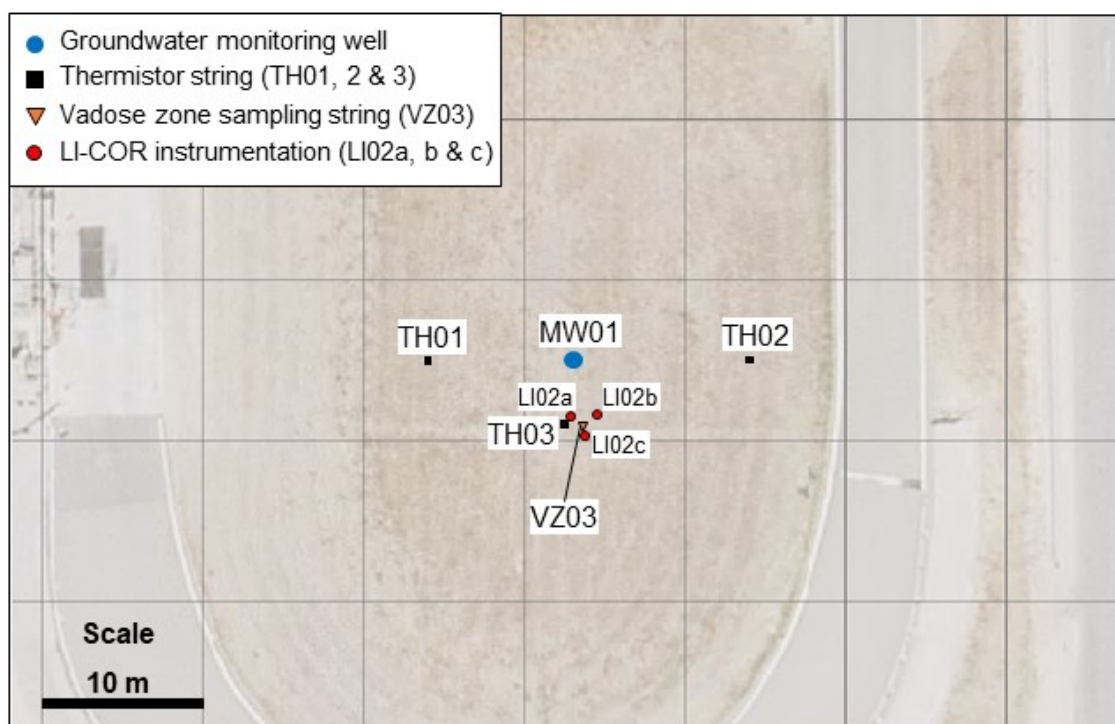


Figure 15. Close-up view of location B6

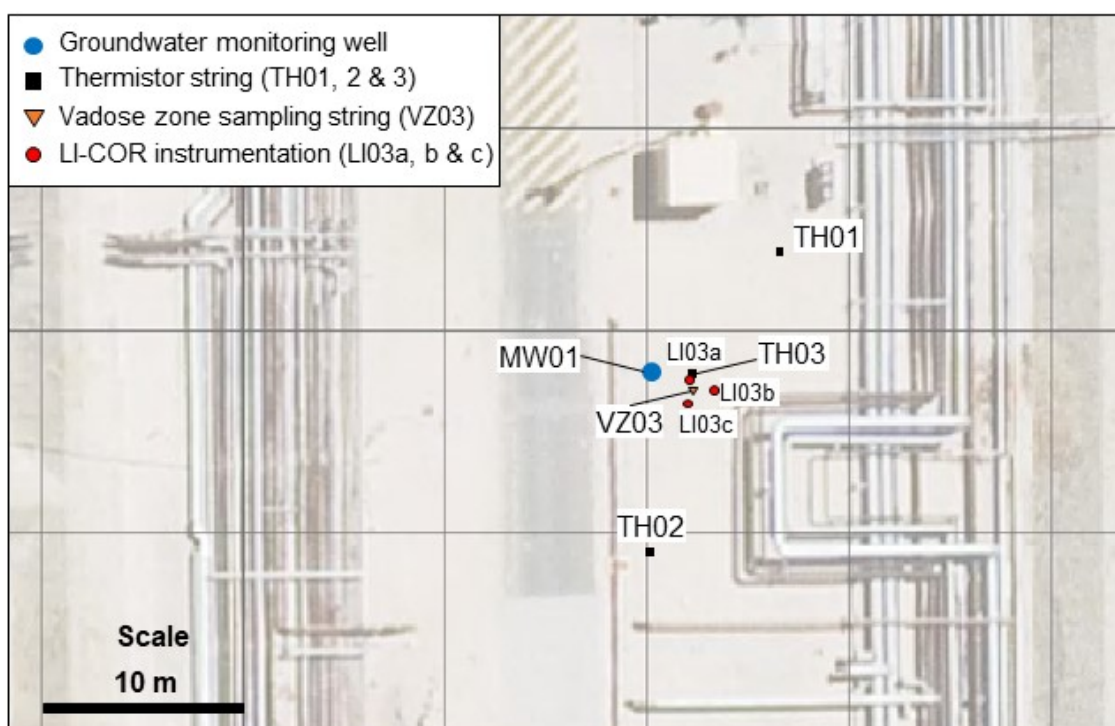


Figure 16. Close-up view of location D6

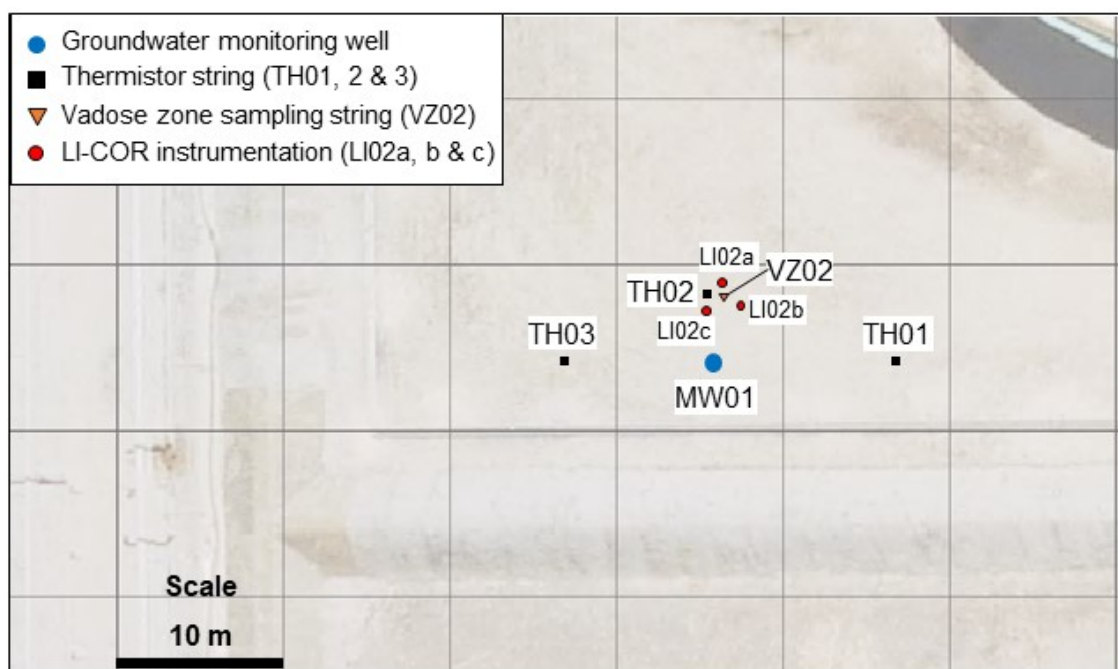


Figure 17. Close-up view of location D10

### 4.3 Data supplied by site owner

The material available for site B consisted of extensive records from more than three decades of CSIRO involvement in a research capacity. Previous CSIRO reports and files are cited. To preserve the confidential nature of these reports, citations are coded and reference to the file name is given in the Section 12.

In addition, additional data collected at site B in 2018 were interpreted by CSIRO and are presented for the first time in this report. These include estimation of NSZD rates based on subsurface temperature and soil surface CO<sub>2</sub> flux measurements (chamber, LI-COR), and gas sampling to determine major gas composition. In 2004–2005, a subsurface LNAPL characterisation study was conducted. The characterisation measured both physical properties (density and viscosity) and chemical composition to construct a map of the product types comprising the LNAPL source zone.

#### 4.3.1 Hydrogeological parameters

The uppermost sand and limestone layers comprise the superficial aquifers. The limestone is highly permeable. In eastern portions of the site, a clay aquitard layer hydraulically isolates the sand and limestone aquifers, such that the latter is confined. The average porosity of the calcareous sand is around 50%. The sands are predominantly fine to medium-grained. At a depth of around 3.84 m, the sand is laminated and has layers of larger grain size materials. The layering is often sub-horizontal. Thin layers of coarser grain size sands are generally absent below 3.84 m. The hydraulic conductivity of the sand in this area is 10 to 30 m day<sup>-1</sup>.

#### 4.3.2 Well construction and mean groundwater levels

In June–September 2016 the water table was ~ 4.6 mbg at location D6, but tidally influenced, and was ~ 3.6 mbg at D10 (SiteB\_Ref10 2016). Groundwater levels vary across the site to 2.5 to 4.0 mbg with an annual fluctuation of around 0.5 m from seasonal winter rainfall.

Monitoring wells at each site are 50 mm diameter, class 18 PVC with threaded couplings. Generally, the screens are between 3 and 4.5 m in length and set from at least 1 m above and 2 m below the average water table elevation. The screen slot size is 0.5 mm and gravel pack (1.8 to 3.2 mm in diameter) backfilled to 0.5 m above the top of the screen. A bentonite seal was placed above this.

Thermistors and vapour sampling ports were installed by coring with a percussion geoprobe drill rig using a dual tube 37 coring system. The installations were backfilled with white, washed silica sand of similar grain size to the formation sand (100 to 300  $\mu\text{m}$ ).

#### 4.3.3 Product thicknesses in local wells

Product thickness over time is shown for well 182, which is located near D6, and for well 418, which is near D10, Figure 18 and Figure 19, respectively.

Over a 16-year period LNAPL thicknesses varied from 0 m to close to 1 m, with decreasing trends over this time period.

#### 4.3.1 Measurements of LNAPL transmissivity

Near D6, measured LNAPL transmissivities ranged from 0.01 to 0.34  $\text{m}^2 \text{day}^{-1}$  in 2009 and other estimates from baildown testing in 2015 were 0.01 to 0.5  $\text{m}^2 \text{day}^{-1}$ , according to sources cited in SiteB\_Ref9 (2016) and SiteB\_Ref7 (2016).

No direct measurements were undertaken near D10 (SiteB\_Ref7 2016).

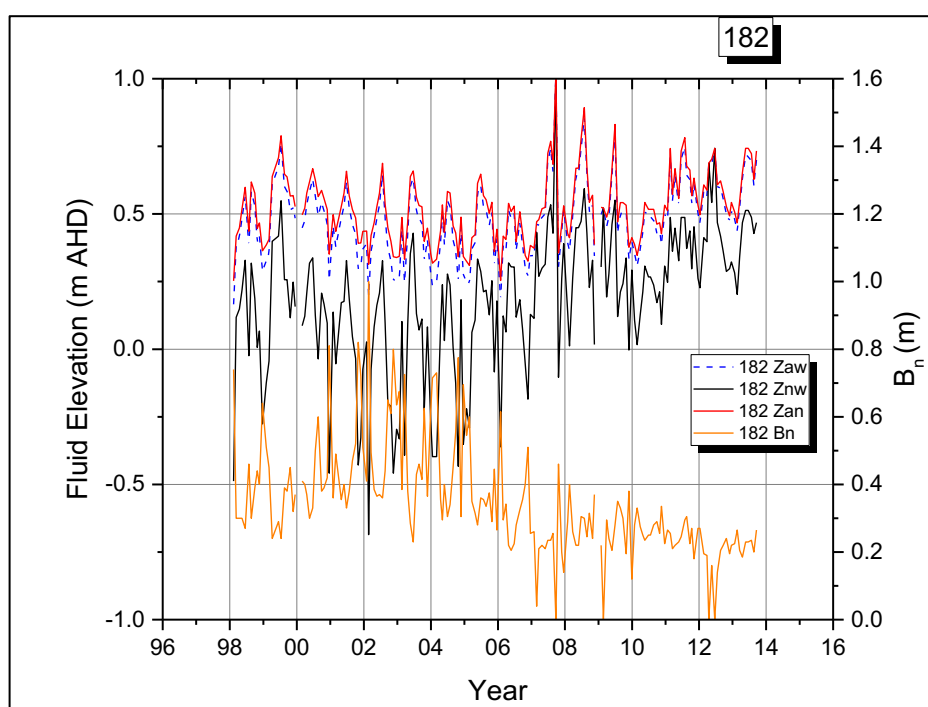


**Figure 18. Hydrograph of gauged fluid elevations near site D6 from 1998 to 2014. Zan is air-NAPL elevation, Znw is NAPL-water elevation and Zaw is the calculated potentiometric surface elevation and (Bn) is the product thickness for Well 182 (SiteB\_Ref9 2016)**

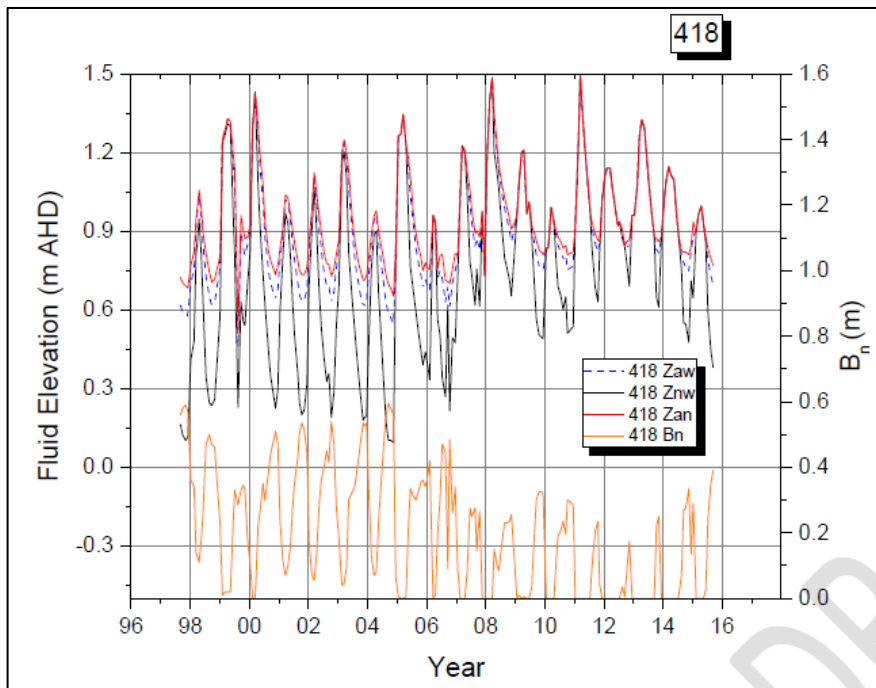


**Figure 19. Hydrograph of gauged fluid elevations near site D10. Zan is air-NAPL, Znw is NAPL-water and Zaw is the calculated potentiometric surface elevation and (Bn) is the product thickness for Well 418 (SiteB\_Ref9 2016)**

### 4.3.2 LNAPL recovery operations

The client provided cumulative and annual recovery data to illustrate trends. Whilst detailed recovery data per well was not provided, weekly product recovery history data for 2015 were provided on a cumulative basis for regions serviced by above ground storage tanks. Cumulative recovered tonnages for tank regions near D6, D10 and B8 were analysed for this report and are based on a previous CSIRO report, referred to here as SiteB\_Ref8 (2016).

## 4.4 Methods

### 4.4.1 Active recovery

#### Type of method used to recover LNAPL

According to *Site B LNAPL recovery report* (2016), product recovery has been used for decades and is recovered throughout the whole seasonal cycle (low water table conditions conducive to recovery), using clusters of LNAPL skimming wells. Within a 200 m radius of site D6, there are about 87 recovery wells and within a 200 m radius of site D10, there are eight recovery wells.

An inventory of recovery equipment used in 2005 indicates the predominant use of skimmers for recovering product (Table 21, SiteB\_Ref2 2005). A number of the skimmers remained in a fixed position, and others were moved around different areas to optimise product recovery (Figure 14, SiteB\_Ref3 2006). Figure 14 shows the locations of trenches as of 2005.



**Table 21. Type of recovery equipment from SiteB\_Ref2 (2005)**

Method	Description	% of recovery (October 2005)
Passive trenches	<ul style="list-style-type: none"> <li>• Network of about 40 trenches</li> <li>• Daily to weekly removal of free product by vacuum truck</li> </ul>	30%
Single phase skimmer	Inventory of over 50 single phase skimmers and associated pneumatic pumps, control systems and above ground storage tanks	58%
Solar systems	<ul style="list-style-type: none"> <li>• Solar units used to power air compressor for pneumatic pumps</li> <li>• Used to run single phase skimmers</li> </ul>	
Dual phase +VEP	8 dual phase units with VEP's connected to a few	12%

#### **4.4.2 NSZD rate estimation**

##### **Subsurface temperature measurement (thermistors)**

###### *In-ground temperature profiling*

Buried thermistor strings were also used to provide subsurface temperatures. These consist of a number of NTC thermistors (10k Ohm Betacurve, 10K3A1B, matched to YSI 44036) positioned at various points along a multi-core cable. The resistance of each thermistor was measured with a multimeter (Fluke 28 II EX). At each site temperature measurements were taken at three thermistor strings approximately 10 m apart (Figure 15 to Figure 17).

###### *Temperature data analysis*

The manual resistance measurements were converted to temperatures using the thermistor manufacturer's polynomial calibration. Since the water table was closer to the surface at the background site (B6) than at the contaminated sites B6 and D10 the depths were converted to relative depths with the land surface set to 0 m and the depth to groundwater set to 1 m as outlined by Warren and Bekins (2015). The depth to groundwater was determined from the closest monitoring bore (see Figure 15 to Figure 17). Background subtraction was performed using the average temperature values for the three background strings.

The biogenic heat method was used to calculate NSZD rates. As described in Section 2.4, this method uses Fourier's Law (Equation 3). For this site,  $\Delta T$  was assigned the maximum difference measured and  $\Delta z$  is relative to the ground surface. It was assumed that the thermal conductivity was  $1.0 \text{ J m}^{-1} \text{ K}^{-1} \text{ s}^{-1}$  since the thermal conductivity of the profile at Site B was unknown and this lies in the range for soil (Sweeney and Ririe, 2014). The heat flux was converted to a NSZD rate ( $\text{L ha}^{-1} \text{ yr}^{-1}$ ), assuming that octane was the LNAPL hydrocarbon undergoing biodegradation with a  $\Delta H$  of  $52 \text{ kJ g}^{-1}$  (Sweeney & Ririe 2014) and a density of  $703 \text{ kg m}^{-3}$  at  $20^\circ \text{C}$ .

### *Anthropogenic heat at the site*

There are sources of anthropogenic heat at the site. These needed to be avoided. A number of sources were identified:

- 'steam traps
- oily water sewer
- steam oils around tanks
- oil pipes, and
- heat from process units at ground level' (SiteB\_Ref5 2010, p. 7).

Possibly the most significant sources are from, 'heat arising from leaking steam traps and oily water sewer junction boxes...losses from a steam trap can be at rates up to 50 kg of steam per hour for a 25 mm steam trap' (SiteB\_Ref5 2010, p. 7).

### **Gas sampling and analyses (soil vapour port and in-well)**

Gas samples were collected from 6–8 vapour sampling points buried in the vadose zone depending on the site and depth to groundwater for major gas analysis. The first vapour sampling port was 0.25 m below groundwater level and then at every 0.5 mbg. Sample lines were purged prior to collection of a 50 mL sample in a 60 mL plastic syringe connected via three-way taps to the sampling line.

Gas samples were also collected from the closest bore to the vapour sampling location for major gas analysis. Following purging of the sample line a gas sample was also collected using a 60 mL syringe: a gas volume of 50 mL was pulled into the syringe. A 3-way stopcock was then closed to prevent sample loss.

The samples were then returned to the CSIRO laboratory for major gas analysis. Samples were analysed using the same procedure as outlined in Section 3.4.4. NSZD rates were determined using the gradient method (CRC CARE 2018) between the sampling location showing greatest degradation (lowest O<sub>2</sub> and highest CO<sub>2</sub> concentration) and the closest vapour sampling point to the surface (0.25 m).

To calculate NSZD rates, the gradient method for soil gas flux was applied using Equation 2 (Section 2.4). The effective vapour diffusion coefficient for O<sub>2</sub> and CO<sub>2</sub> were assigned the values of 2.59E-06 and 2.37E-06 m<sup>2</sup> s<sup>-1</sup>, respectively.

### **Soil surface carbon dioxide flux measurements (LI-COR flux chamber)**

Soil surface carbon dioxide flux was measured using a LI-COR LI8100A Automated soil carbon dioxide (CO<sub>2</sub>) flux system connected to a 20 cm survey chamber (8100-103) (LI-COR Lincon, NE). At each site three evenly spaced PVC soil collars (20 cm diameter x 12 cm) were installed ~90 cm from the vadose zone sampling locations used for gas sampling (Figure 15–Figure 17). The collars were installed to a depth of ~8.5 cm seven days prior to CO<sub>2</sub> flux measurements. Three repeat CO<sub>2</sub> flux measurements were collected for each collar at two times at each site on 11 April 2018. The raw data was processed using the manufacturer supplied software (LI-8100 file viewer 3.1.1) and either a linear or exponential function fitted to the data to determine the CO<sub>2</sub> flux rate. The CO<sub>2</sub> flux rates were then averaged for the three replicates. The average background CO<sub>2</sub> flux rate for the two sampling times were then used to determine the CO<sub>2</sub> flux rate due to NSZD for corresponding sampling times at

the LNAPL impacted sites. The CO<sub>2</sub> flux rates were then converted to a NSZD rate in L LNAPL ha<sup>-1</sup> yr<sup>-1</sup> using octane as the representative LNAPL (density of 703 kg m<sup>-3</sup>).

#### **4.4.3 NSZD: LNAPL sampling and analysis (compositional analyses to assess the extent of weathering)**

LNAPL sampling involved lowering a 40 mL VOA vial directly into the well on nylon fishing line to just below the fluid (LNAPL) interface and the vial was retrieved, capped and sent to the laboratory for analysis.

Core sampling involved driving in a core barrel (DT 37 coring system) via a percussion drilling rig into clear, polycarbonate tubes. The tubes were sectioned in the field, put into tins with an airtight seal, placed in an esky of ice and sent to the laboratory. In the lab, cores were sub-sampled and extracted into solvent. Soil weights, liquid contents and core dimensions were measured to enable the volumetric calculation of fluids and sediments.

##### *Laboratory analyses: LNAPL analysis methods (C4–C40)*

GC-FID analysis was performed using a HP 6890 GC fitted with an autosampler, a vaporising injector (operating in split mode), helium carrier gas (flow 1 mL min<sup>-1</sup>), an autosampler and a FID. The GC was equipped with a 60 m x 0.25 mm internal diameter column coated with a 0.25 µm thick film of dimethyl polysiloxane (DB-1 UI, J&W). Compound identifications were based on known retention time and mass spectra characteristics for components present in gasoline and diesel.

##### *Laboratory analyses: core soil sample extraction and analysis from 2006*

Soil samples (3–5 g) from cores were extracted using 5 mL of a mixture of diethylether and acetone (1:1 v/v) containing deuterated internal standards (*d6*-benzene, *d8*-toluene, *d10-p*-xylene and *d8*-naphthalene). The soil samples were extracted using a tumbling method followed by sonication to consolidate the soil at the base of the extraction tubes. The extract was sub-sampled twice into 2 mL vials providing samples ready for GC analyses.

GC-MS analysis was performed using a Varian model 3400 gas chromatograph fitted with an auto-sampler (Varian 8100), used helium as the carrier gas and was coupled to a Varian Saturn IV mass spectrometer. The GC-MS was fitted with a capillary GC column (Alltech, AT-5 ms, 30 m length, 0.25 mm internal diameter and 0.25 µm thick film of dimethyl polysiloxane 5% phenyl/95% dimethyl polysiloxane or equivalent column). Quantitation of the total petroleum hydrocarbon (TPH) and selected compounds was performed using external standards containing the same internal standards used for the samples.

##### *Laboratory analyses: core soil sample extraction and analysis from 2015 to 2017*

Soil samples (3–5 g) from cores were extracted using 4 mL of dichloromethane (DCM) containing deuterated internal standards (*d6*-benzene, *d8*-toluene, *d10-p*-xylene, *d8*-naphthalene and *d14-p*-terphenyl). The soil samples were extracted using a tumbling method followed by sonication which also allowed the extraction solvent to accumulate in the base of vials which was removed by pipette. The extracts were placed into tared 5 mL vial and the soil washed with small portions of DCM to provide a total extract volume of 4.8 mL. The extract was sub-sampled twice into 2 mL vials (each containing 1.9 mL of extract) for GC analyses and the remaining 1.0 mL in the 5 mL vials were

allowed to evaporate providing a gravimetric determination of TPH for the >C<sub>10</sub> carbon range hydrocarbons in the core samples.

GC-FID analysis of TPH was performed using an Agilent 6890 GC fitted with a vaporizing injector (operating in split mode), with helium as carrier gas, an auto-sampler using a FID. The GC-FID was fitted with a capillary GC column (Phenomenex ZB-1ms, 30 m length, 0.25 mm internal diameter and 0.25 µm thick film of dimethyl polysiloxane or equivalent column). Quantitation of TPH was performed using external standards containing the same internal standards used for the samples.

GC-MS analysis of selected components was performed using an Agilent 7890 GC fitted with a vaporizing injector (operating in split mode), with helium as carrier gas, an auto-sampler and an Agilent 7000 mass spectrometer. The GC-MS was fitted with a capillary GC column (Phenomenex, ZB-1ms, 30 m length, 0.25 mm internal diameter and 0.25 µm thick film of dimethyl polysiloxane or equivalent column). The mass spectrometer was operated with an ionisation energy of 70 eV at 230 °C in scan and SIM modes. Quantitation of selected compounds was performed using external standards containing the same internal standards used for the samples.

#### *Estimated LNAPL losses at the D6 site*

Estimated percentage mass losses over a time period were based on concentration increases in the LNAPL of a conservative tracer (one of the most non-volatile, water insoluble and biodegradation resistant components present in the samples) as a result of other components decreasing in the LNAPL due to volatilisation, dissolution and biodegradation. The rearranged drimanes were selected in this instance as they were unaffected by volatilisation, dissolution and biodegradation in the LNAPL samples from the D6 location as comparison of the samples after 10 years showed few differences with only minor depletion of the pristane relative to the other isoprenoids (pristane/norpristane  $1.64 \pm 0.014$  for E3-RW-01 and  $1.88 \pm 0.024$  for DBMW3). Therefore the drimanes (C<sub>15</sub> bicyclic alkanes) are ubiquitous to petroleum and are generally present at significant relative abundances (Alexander *et al* 1984) and should be unaffected by biodegradation at this extent of biodegradation as the isoprenoids are only at the biodegradation level where they are just being altered (based on scales for assessing biodegradation of petroleum (Peters & Moldowan 1993; Volkman *et al* 1983; Volkman *et al* 1984)). Therefore, a rearranged drimane (C<sub>15</sub> rearranged drimane IV, Alexander *et al* 1984) was selected to use as the conservative tracer for calculating mass losses and afforded a mass loss of 5% ( $\pm 2$ ) for the ~ 10-year period. Estimates of LNAPL depletion or losses over time were based on changes in the rearranged drimane relative concentration (conservative tracer, H) using Equation 4 (Section 2.4).

## **4.5 Results**

### **4.5.1 Estimation of total hydrocarbon mass removal by active recovery**

Figure 20 shows the total LNAPL mass removed by active recovery spanning the years 1985 to 2018 from all recovery operations on site. The annual mass recovery ranges from a maximum of 3600 t in 1988 to a minimum of 21 t in 2018. In general, there has been a substantial reduction in mass recovery over three decades, with occasional spikes due to new releases (for example 2004). In 2018 the 21 t recovered comprised of c. 17.5 t coming from diesel impacted areas, with no recovery from the crude oil

areas due to limited recoverable LNAPL, with no measurable in-well thickness  $\geq 50\text{mm}$ . This value given above for the maximum LNAPL liquid diesel recovery rates in 2018 (circa 17.5 t) is compared with total site-wide, diesel NSZD rates in Section 4.6.

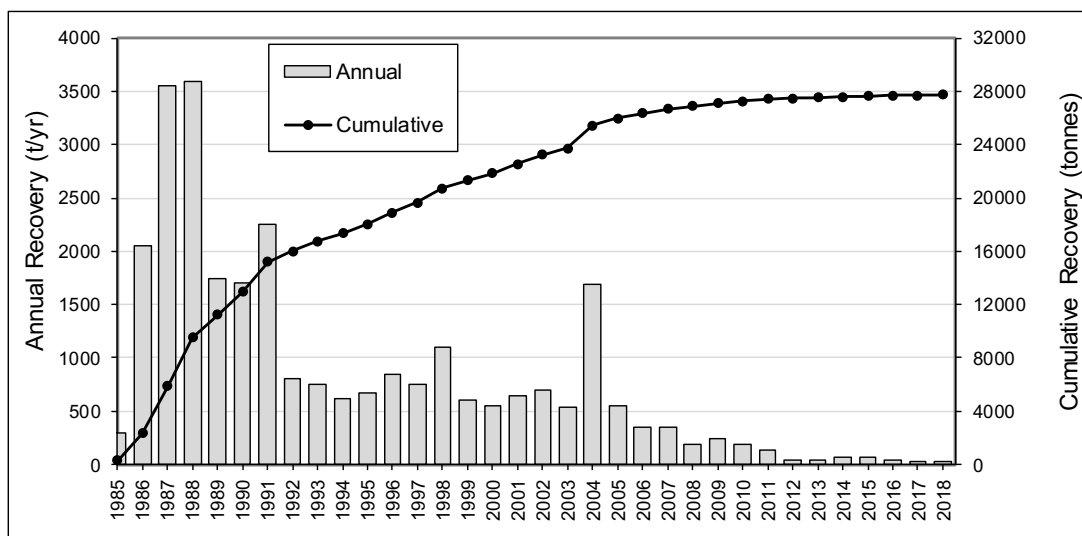


**Figure 20. Historical LNAPL recovery data for site B**

Figure 21 and Figure 22 show product recovery history in 2015 for each of the product recovery tanks near locations D6 and D10, respectively. Each product recovery tank may have a variable number of local recovery points providing product to the tank over different periods of any one year (SiteB\_Ref8 2016). Based on maps of site B of recovery well and tank locations, a rough estimate of the number of wells supplying each of the recovery tanks was obtained (Table 22). Tanks T1946, T1954 and T1905 in D6 stored the majority of product recovered in 2015 with approximately 7 to 8 tonnes of product stored in each of these tanks. The annual totals of product recovered for the tanks near D10 were lower, <2 tonnes of product for 2015 in each tank.

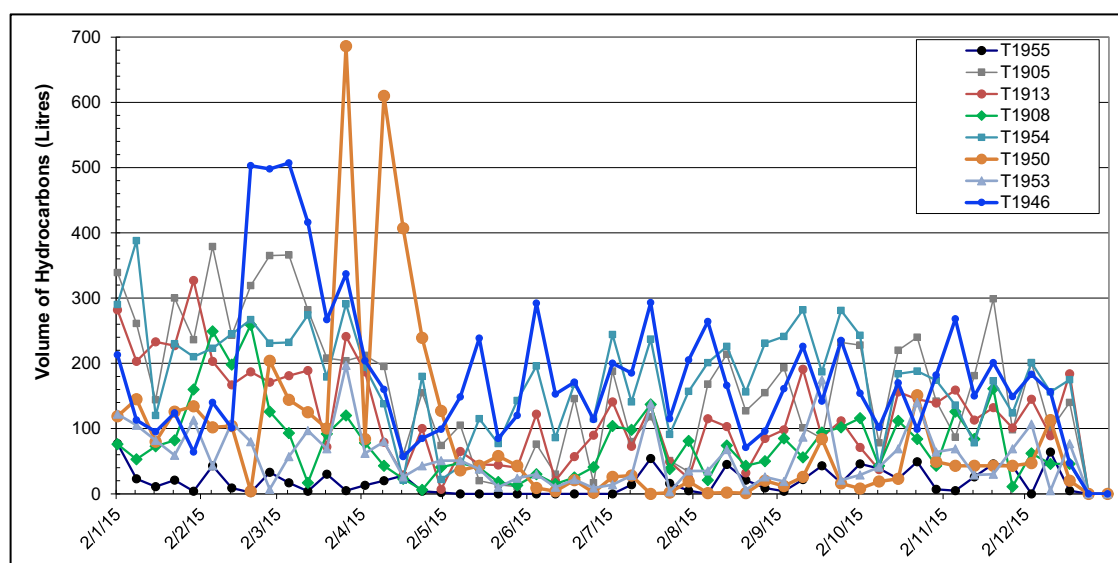


**Figure 21. Weekly product recovery for 2015 from tanks in the vicinity of D6**

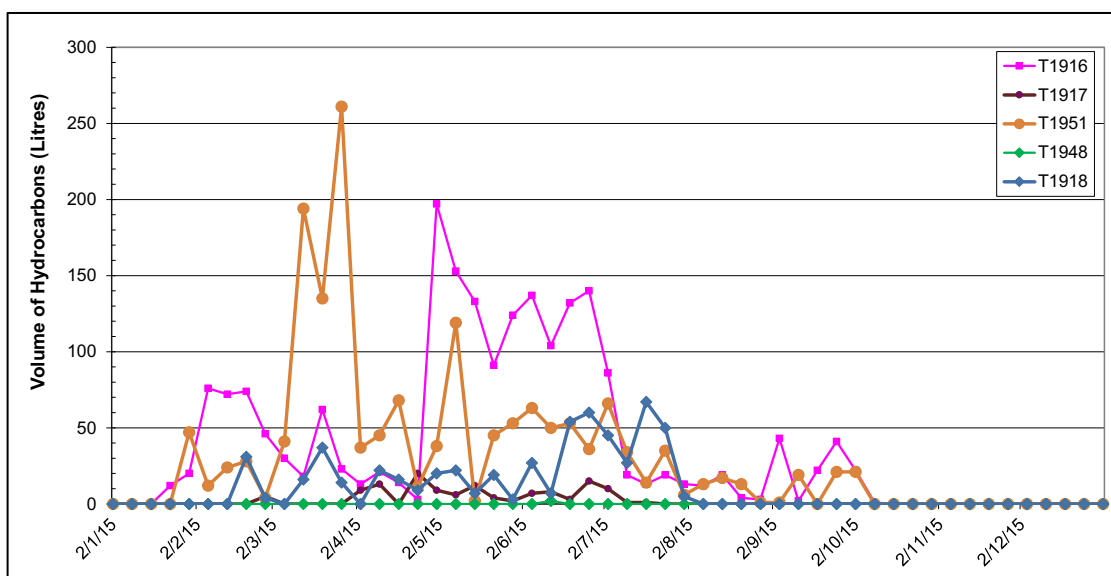


Figure 22. Weekly product recovery for 2015 from tanks in the vicinity of D10

Table 22. Summary of 2015 product recovery near locations D6 and D10

Site	Tank number	Approximate number of recovery wells per tank	Product (L)	Product (tonnes)
D6	T1946	18	9525	8.3
	T1954	23	9225	8.0
	T1905	19	8519	7.4
	T1913	12	6284	5.5
	T1950	2	4595	4.0
	T1908	13	3935	3.4
	T1953	16	2980	2.6
	T1955	11	949	0.8
D10	T1916	8	2014	1.8
	T1951	7	1627	1.4
	T1918	4	562	0.5
	T1917	11	125	0.1
	T1948	15	2	<0.002

#### 4.5.2 NSZD rate results: measurements and total site-wide rate estimates

In the following section, intrinsic rate estimates are provided based on the temperature, gas sampling, and LI-COR methods. No spatial weighting of NSZD rates at measurement locations was conducted to obtain total site-wide rate estimates. Instead, the intrinsic rate estimates expressed in terms of  $L \text{ LNAPL ha}^{-1} \text{ yr}^{-1}$  were multiplied by the product of LNAPL density (an assumed value of  $703 \text{ kg m}^{-3}$  as octane) and the areal extent of LNAPL. The areal extent of diesel LNAPL is 28 ha and the areal extent of crude oil LNAPL is 6 ha. This is based on the 2004 distribution determined by a combination of LNAPL density, viscosity and whole oil analysis (by GC-FID).

## Temperature results

Based on interpretation of the data by CSIRO (this study), the NSZD rates estimated from the buried thermistor data range from 1034 to 8799 L LNAPL ha<sup>-1</sup> yr<sup>-1</sup> (Table 23). The average NSZD for the two sites, D10 and D6 were quite distinct at 2254 and 7575 L LNAPL ha<sup>-1</sup> yr<sup>-1</sup>, respectively.

Despite this, the NSZD rates at D10 (crude oil location) and D6 (diesel location) separately yielded a reasonably tight range across the dates and multiple thermistor strings of 1034 to 3061 L LNAPL ha<sup>-1</sup> yr<sup>-1</sup> (4.4 to 13 t yr<sup>-1</sup>) for D10 and 6018 to 8799 L LNAPL ha<sup>-1</sup> yr<sup>-1</sup> (120 to 170 t yr<sup>-1</sup>) for D6. The reason for the difference in the magnitude of the average rates at the two locations is not clear – however the weathered crude oil at D10 contains components over a larger carbon range and these may be less biodegradable than the narrower carbon range of components present in the weathered diesel at D6.

**Table 23. Summary of results from buried thermistors, temperature-based NSZD**

Well location	String	Date	NSZD (corrected) (L LNAPL ha <sup>-1</sup> yr <sup>-1</sup> )
D10 (Crude oil contaminated site)	TH01	19 February 2018	3061
	TH01	5 April 2018	2653
	TH01	11 April 2018	2283
	TH02	19 February 2018	1471
	TH02	5 April 2018	1859
	TH02	11 April 2018	1960
	TH02	11 April 2018	1034
	TH03	19 February 2018	2452
	TH03	5 April 2018	2831
	TH03	11 April 2018	2935
D6 (Diesel contaminated site)	TH01	19 February 2018	6450
	TH01	5 April 2018	6018
	TH01	11 April 2018	6090
	TH02	19 February 2018	8799
	TH02	5 April 2018	8428
	TH02	11 April 2018	8614
	TH03	19 February 2018	8538
	TH03	5 April 2018	7374
	TH03	11 April 2018	8589
	TH03	11 April 2018	6845

## Gas sampling results

As described in the methods section, the gas gradient method applied to soil gas and in-well measurements of O<sub>2</sub> and CO<sub>2</sub> determined by CSIRO yielded the following results.

### *Vapour port multi-depth gas data*

Based on the data in Table 24, the average, corrected NSZD rates from gas sampling (gas vapour port):

- D6:
  - O<sub>2</sub> 10,460 L LNAPL ha<sup>-1</sup> yr<sup>-1</sup>
  - CO<sub>2</sub> 11,607 L LNAPL ha<sup>-1</sup> yr<sup>-1</sup>
- D10:
  - O<sub>2</sub> 15,325 L LNAPL ha<sup>-1</sup> yr<sup>-1</sup>
  - CO<sub>2</sub> 16,858 L LNAPL ha<sup>-1</sup> yr<sup>-1</sup>

### *In-well gas data:*

Based on the data in Table 25, the average, corrected NSZD rates from gas sampling (in-well):

- D6:
  - O<sub>2</sub> 13,034 L LNAPL ha<sup>-1</sup> yr<sup>-1</sup>
  - CO<sub>2</sub> 13,968 L LNAPL ha<sup>-1</sup> yr<sup>-1</sup>
- D10:
  - O<sub>2</sub> 6799 L LNAPL ha<sup>-1</sup> yr<sup>-1</sup>
  - CO<sub>2</sub> 7459 L LNAPL ha<sup>-1</sup> yr<sup>-1</sup>

For both sites and gas methods (in-well or depth profile), there is a high degree of consistency between the rates calculated based on oxygen data or based on carbon dioxide data. It is also consistent between the two sampling dates (Table 24 and Table 25). This is to be hoped for, if there is mole for mole production of carbon dioxide during the consumption of oxygen in the subsurface. Interestingly for the multi-depth data, location D10 had higher average, corrected rate estimates (15,325–16,858 L LNAPL ha<sup>-1</sup> yr<sup>-1</sup>) than location D6 (10,460–11,607 L LNAPL ha<sup>-1</sup> yr<sup>-1</sup>), whereas for the in-well gas data location D10 had lower average rate estimates (6799–7459 L LNAPL ha<sup>-1</sup> yr<sup>-1</sup>) than location D6 (13,034–13,968 L LNAPL ha<sup>-1</sup> yr<sup>-1</sup>). The explanation for this reversal of trends is not clear; however, the weathered crude oil at D10 has more lower carbon range components (or VOCs that are likely more recalcitrant due to weathering) than the weathered diesel at D6 and the differences in NSZD rates using the different techniques may be a result of the VOCs from the crude oil at D10 undergoing degradation in the soil profile further away from the LNAPL. And the narrower carbon range and therefore lower complexity of the weathered diesel at D6 may afford higher NSZD of the residual LNAPL at the source. Ongoing monitoring will provide an expanded data set which will assist. Additionally, oxygen, carbon dioxide and volatile organic compound probes (Patterson & Davis 2008; Patterson *et al* 2000; Patterson *et al* 2013) are to be placed at these locations to provide real time continuous monitoring of gases and changes over time for the depth profile. This will provide more definitive gas data for estimation of NSZD rates.

NSZD rates determined at the background site (B6) are relatively small compared to the rates determined for the LNAPL impacted sites. No LNAPL has been measured at site B6 during drilling and coring operations.



**Table 24. Summary of results for NSZD based on gas vapour port data. D6 is the diesel contaminated site; D10 is the crude oil contaminated site**

Location	Date	NSZD (uncorrected) (L LNAPL ha <sup>-1</sup> yr <sup>-1</sup> )		NSZD (corrected) (L LNAPL ha <sup>-1</sup> yr <sup>-1</sup> )	
		O <sub>2</sub>	CO <sub>2</sub>	O <sub>2</sub>	CO <sub>2</sub>
B6_VZ03	5 April 2018	268	803	-	-
D10_VZ02	5 April 2018	15,418	17,149	15,150	16,346
D6_VZ03	5 April 2018	11,262	12,283	10,994	11,480
B6_VZ03	11 April 2018	382	809	-	-
D10_VZ02	11 April 2018	15,881	18,178	15,499	17,369
D6_VZ03	11 April 2018	10,308	12,543	9,926	11,734

**Table 25. Summary of results for NSZD based on in-well gas data. D6 is the diesel contaminated site; D10 is the crude oil contaminated site**

Location	Date	NSZD (uncorrected) (L LNAPL ha <sup>-1</sup> yr <sup>-1</sup> )		NSZD (corrected) (L LNAPL ha <sup>-1</sup> yr <sup>-1</sup> )	
		O <sub>2</sub>	CO <sub>2</sub>	O <sub>2</sub>	CO <sub>2</sub>
B6_MW01	5 April 2018	1555	238	-	-
D10_MW01	5 April 2018	10,067	9209	8512	8971
D6_MW01	5 April 2018	16,222	15,527	14,667	15,289
B6_MW01	11 April 2018	1734	174	-	-
D10_MW01	11 April 2018	6819	6121	5085	5947
D6_MW01	11 April 2018	13,135	12,821	11,401	12,647

In summary, intrinsic NSZD rates based on the gas sampling (in-well) method, on average, are of the order of 6800 (O<sub>2</sub>) L LNAPL ha<sup>-1</sup> yr<sup>-1</sup> and 7500 (CO<sub>2</sub>) L LNAPL ha<sup>-1</sup> yr<sup>-1</sup> for the crude oil contaminated site and 13,000 (O<sub>2</sub>) L LNAPL ha<sup>-1</sup> yr<sup>-1</sup> and 14,000 (CO<sub>2</sub>) L LNAPL ha<sup>-1</sup> yr<sup>-1</sup> for the diesel contaminated site. This yields total, site-wide NSZD rates for the crude oil site of 29 and 31 t yr<sup>-1</sup> for O<sub>2</sub> and CO<sub>2</sub>, respectively, and 260 and 280 t yr<sup>-1</sup> for O<sub>2</sub> and CO<sub>2</sub>, respectively, for the diesel contaminated sites based on the gas in-well method.

Average, intrinsic NSZD rates based on the gas sampling (vapour port) method are of the order of 15,000 (O<sub>2</sub>) L LNAPL ha<sup>-1</sup> yr<sup>-1</sup> and 17,000 (CO<sub>2</sub>) L LNAPL ha<sup>-1</sup> yr<sup>-1</sup> for the crude oil contaminated site and 10,000 (O<sub>2</sub>) L LNAPL ha<sup>-1</sup> yr<sup>-1</sup> and 12,000 (CO<sub>2</sub>) L LNAPL ha<sup>-1</sup> yr<sup>-1</sup> for the diesel contaminated site. This yields total, site-wide NSZD rates for the crude oil site of 65 and 71 t yr<sup>-1</sup> for O<sub>2</sub> and CO<sub>2</sub>, respectively, and 210 and 230 t yr<sup>-1</sup> for O<sub>2</sub> and CO<sub>2</sub>, respectively, for the diesel contaminated sites based on the gas vapour port method.

### Soil surface carbon dioxide flux results

Measuring the carbon dioxide flux using LI-COR and converting it to average total LNAPL NSZD rates (or soil respiration results for the background location) for each location gave:

- B6: 7724 L LNAPL ha<sup>-1</sup> yr<sup>-1</sup> (background)
- D10: 13,774 L LNAPL ha<sup>-1</sup> yr<sup>-1</sup> (or corrected 5761 L LNAPL ha<sup>-1</sup> yr<sup>-1</sup>), and
- D6: 13,853 L LNAPL ha<sup>-1</sup> yr<sup>-1</sup> (or corrected 5931 L LNAPL ha<sup>-1</sup> yr<sup>-1</sup>).

Average NSZD rates at the two LNAPL locations were effectively the same (Table 26). However, despite similar average NSZD rates at the two locations, rates for D10 had a reasonably narrow range (4490–6390 L LNAPL ha<sup>-1</sup> yr<sup>-1</sup> corrected) compared to D6 (3088–8575 L LNAPL ha<sup>-1</sup> yr<sup>-1</sup> corrected). The broader range at D6 may be due to ground surface variability, product type difference or other effects.

**Table 26. LI-COR results for site B**

Location		Date/time	Total soil respiration (L LNAPL ha <sup>-1</sup> yr <sup>-1</sup> )	NSZD (corrected) (L LNAPL ha <sup>-1</sup> yr <sup>-1</sup> )
B6	LI02a	11 April 2018 10:00	7430	-
	LI02b	11 April 2018 10:00	7315	-
	LI02c	11 April 2018 10:00	5636	-
	LI02a	11 April 2018 13:00	9116	-
	LI02b	11 April 2018 13:00	8220	-
	LI02c	11 April 2018 13:00	8625	-
D10	LI02a	11 April 2018 11:00	11,862	4490
	LI02b	11 April 2018 11:00	13,655	6283
	LI02c	11 April 2018 11:00	13,143	5771
	LI02a	11 April 2018 13:00	14,710	6056
	LI02b	11 April 2018 13:00	15,052	6398
	LI02c	11 April 2018 13:00	14,219	5565
D6	LI03a	11 April 2018 9:00	14,821	7449
	LI03a	11 April 2018 9:00	15,077	7705
	LI03b	11 April 2018 9:00	10,530	3158
	LI03c	11 April 2018 9:00	13,181	5809
	LI03a	11 April 2018 13:00	17,229	8575
	LI03b	11 April 2018 13:00	11,742	3088
	LI03c	11 April 2018 13:00	14,390	5736

*Note: Results have been converted to L ha<sup>-1</sup> yr<sup>-1</sup>, assuming octane.*

The background LI-COR values representing natural soil respiration on average are approximately 50% of the rates measured at the LNAPL impacted sites. Corrected NSZD data are shown in Table 26. It should also be noted that NSZD rates can vary both over small areas and over the several hours between measurements.

Intrinsic NSZD rates based on the LI-COR method are of the order of 5800 and 6000 L LNAPL ha<sup>-1</sup> yr<sup>-1</sup> for the crude oil and diesel contaminated sites, respectively. This yields total, site-wide NSZD rates of 24 t yr<sup>-1</sup> and 120 t yr<sup>-1</sup> for the crude oil and diesel contaminated sites, respectively, based on the LI-COR method.

#### **4.5.3 NSZD results: LNAPL composition**

##### *Location D6: LNAPL diesel sample (E3-RW-01)*

The LNAPL sample (E3-RW-01) from location D6 (Figure 23 and Table 27) was likely weathered diesel as the relative abundance of hydrocarbon carbon range present is Gaussian with a limited carbon range (C9 to C28) typically observed in diesel fuels (C8 to C28). Severe weathering has resulted in the removal of *n*-alkanes and likely altered

the distribution of methylalkanes and isoprenoids. Biomarker analysis showed the presence of higher plant markers (cadalene, retene and bicadinanes) suggesting the diesel was produced from crude oils sourced from South East Asia due to the presence of bicadinanes (related to extant dammar resin common to South East Asia (van Aarssen *et al* 1990)). An LNAPL sample from a nearby well (Figure 24, DBMW3 within 3 m of E3-RW-01) was obtained in 2006 and was consistent with the product obtained in 2016 (containing the same higher plant markers). Comparison of the samples after 10 years showed few differences with only minor depletion of pristane relative to the other isoprenoids with a calculated mass loss of 5% ( $\pm 2$ ) for the  $\sim 10$ -year period (based on the rearranged drimanes).

#### *Location D10: LNAPL crude oil samples (55 and 60)*

The LNAPL samples (55 and 60, Figure 25, Figure 26 and Table 27) from location D10 were both likely weathered crude oil as the hydrocarbon carbon ranges present seem uniform and covers an extended range (C7 to C40) larger than typically observed for single fuel types. Biodegradation has resulted in the removal of *n*-alkanes and an altered distribution of methylalkanes and isoprenoids. Both samples are practically identical with no significant differences (and may be part of the same continuous release in the subsurface). Biomarker analysis showed the presence of higher plant markers (cadalene, retene and bicadinanes) suggesting the crude oil was sourced from South East Asia due to presence of bicadinanes (related to extant dammar resin common to South East Asia (van Aarssen *et al* 1990)).

#### *Location D6: Core 67 (weathered diesel)*

TPH analyses of the core samples from location D6 (core 67 samples 171–203, Figure 27 and Appendix Table B.1-1) showed the fuel type and extent of biodegradation (weathered diesel, *n*-alkanes removed and isoprenoids altered) in the core samples match well with LNAPL recovered in the same area (E3-RW-01, Figure 23). The composition of the TPH with depth showed the shallower samples (3.2–3.45 m) were affected slightly more by biodegradation (fewer peaks and some specific isoprenoids like pristane more depleted relative to other isoprenoids such as phytane, Pr/Ph Figure 27 and Table B.1-1) compared to the higher concentration samples more central in the subsurface contamination (core sample 182 3.9–3.95 m, Figure 27 and Table B.1-1), pristane has been reported to be less resistant to biodegradation than phytane (Hansen *et al* 2002; Johnston *et al* 2007). The deeper samples from 4.05 m (core sample 185 4.05–4.1 m) had altered distributions of dimethylnaphthalenes (1,6-dimethylnaphthalene depleted in core sample 185 (4.05–4.1 m) and completely removed in core samples deeper than sample 186 (4.1–4.15 m, Figure 28) suggesting these deeper samples have been affected by biodegradation differently compared to the shallower samples. 1,6-Dimethylnaphthalene has been shown to biodegrade preferentially to other dimethylnaphthalenes (Fisher *et al* 1996). Also, the deeper samples (>4.1 m) unlike the shallower samples did not show changes resulting in fewer peaks or depletion of pristane relative to the other isoprenoids. The GC analyses of this core showed that biodegradation is occurring in the shallower and deeper samples and that the different subsurface conditions are resulting in different components being preferentially biodegraded.

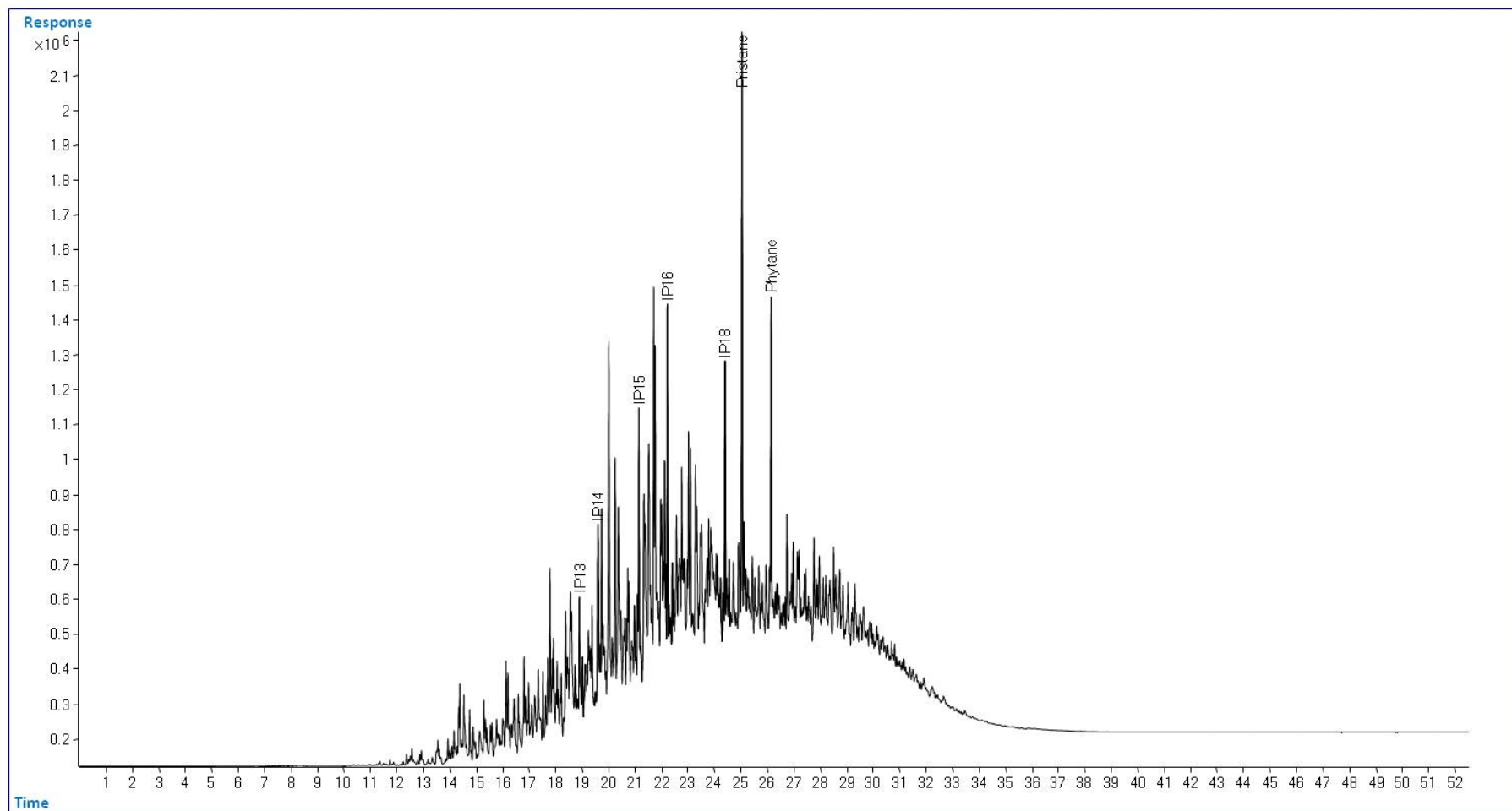


**Figure 23. GC-FID analysis of LNAPL sample E3-RW-01 from location D6 in 2016. IP: isoprenoid**

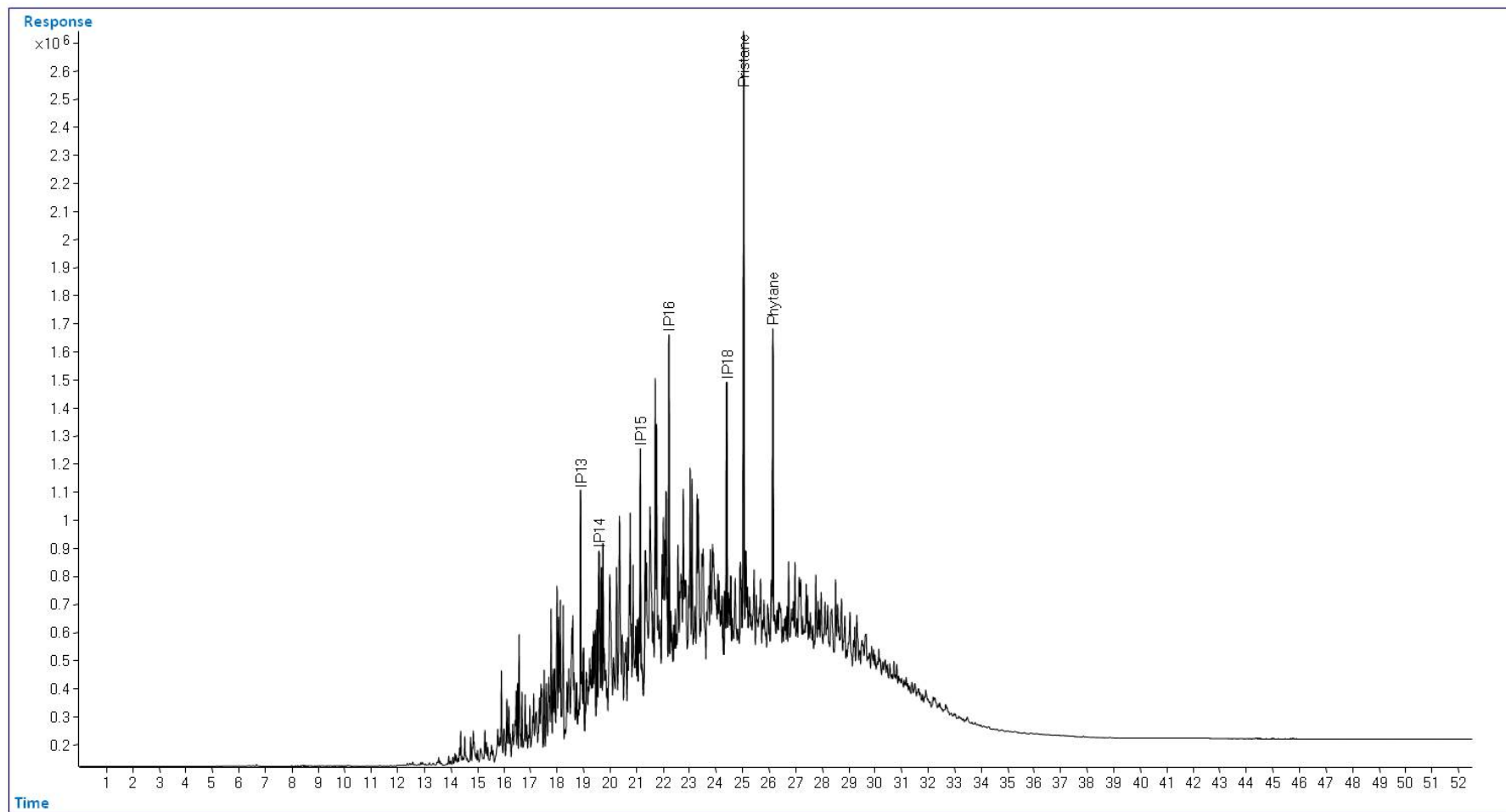


Figure 24. GC-FID analysis of LNAPL sample DBMW3 from location D6 in 2006. IP: isoprenoid

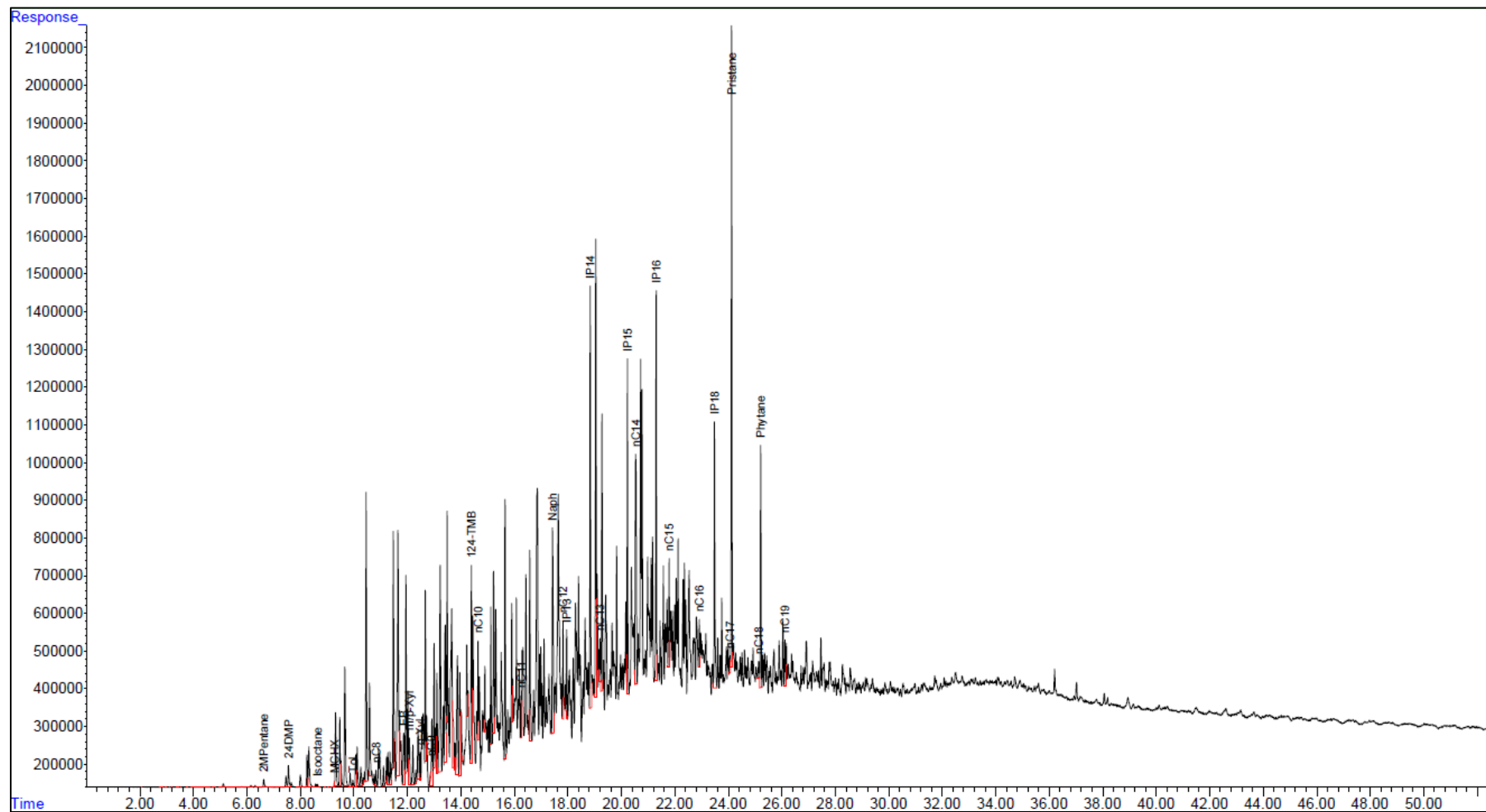


Figure 25. GC-FID analysis of LNAPL sample 55 from location D10. CHX: cyclohexane, Cx: straight or branched alkane containing x carbons, EB: ethylbenzene, IP: isoprenoid, Tol: toluene, Xyl: xylene

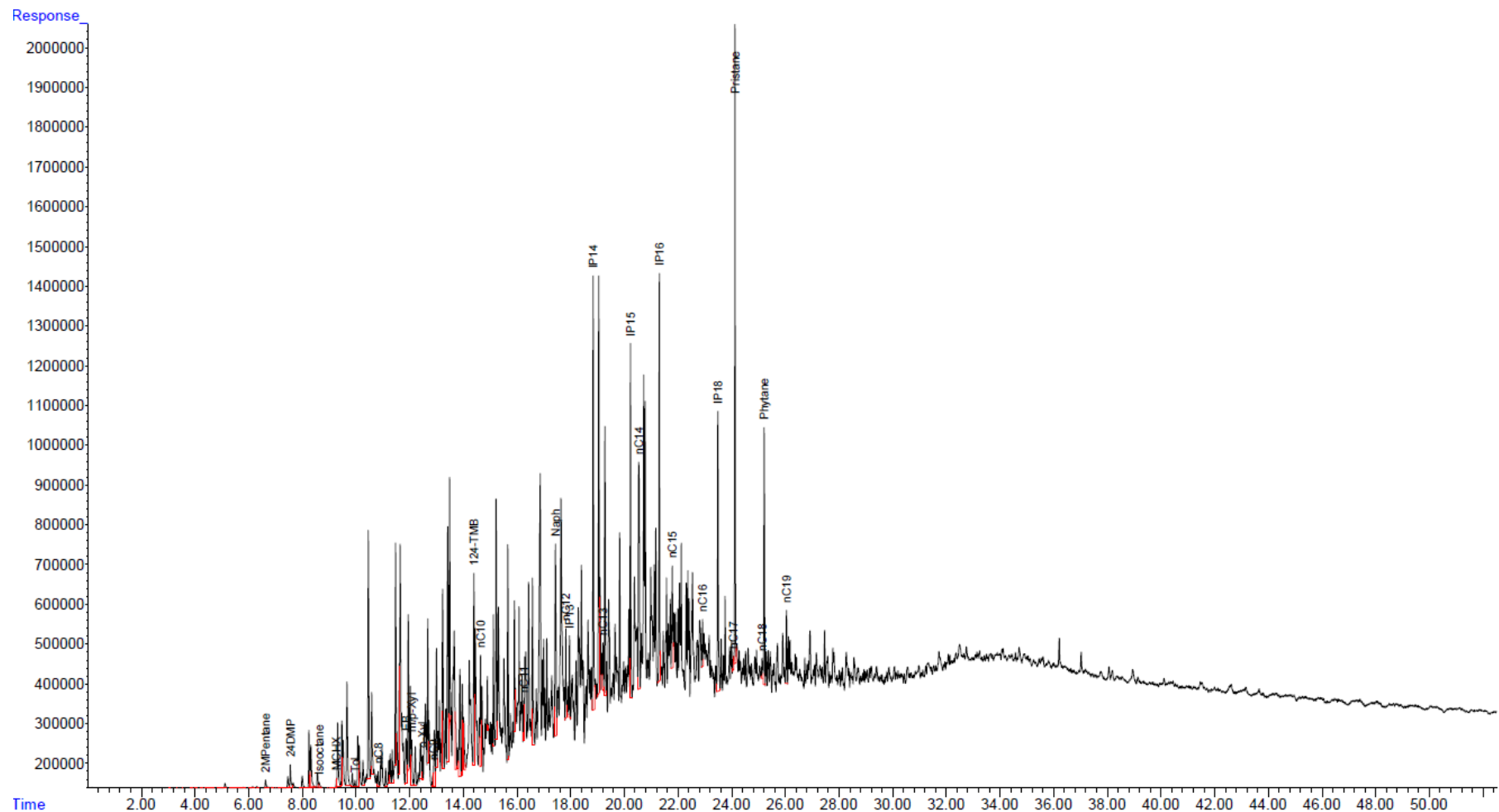


Figure 26. GC-FID analysis of LNAPL sample 60 from location D10. CHX: cyclohexane, Cx: straight or branched alkane containing x carbons, EB: ethylbenzene, IP: isoprenoid, Tol: toluene, Xyl: xylene

**Table 27. BTEX (and selected aromatic compound) concentrations and assessments for LNAPL samples from location D6 and D10. Units are % (w/w)**

Sample IDs	B	T	EB	m/p-X	o-X	135-TMB	124-TMB	123-TMB	Naph	2-MN	1-MN	Likely LNAPL type	Carbon range present	Extent of biodegradation
D6 E3-RW-01 16018	<0.01	<0.01	0.01	0.02	0.01	0.06	0.11	0.03	0.20	0.68	0.33	Diesel	C9-C28	<i>n</i> -Alkanes removed, methylalkanes isoprenoids altered
D6 DBMW3 06105	<0.01	<0.01	<0.01	<0.01	<0.01	0.01	0.04	0.02	0.17	0.39	0.19	Diesel	C9-C28	<i>n</i> -Alkanes removed, methylalkanes isoprenoids altered
D10 55 16018	<0.01	0.01	0.09	0.06	0.03	0.13	0.24	0.06	0.30	0.51	0.28	Crude Oil	C7-C40	<i>n</i> -Alkanes removed, methylalkanes isoprenoids altered
D10 60 16018	<0.01	0.01	0.08	0.06	0.02	0.10	0.21	0.04	0.26	0.45	0.26	Crude Oil	C7-C40	<i>n</i> -Alkanes removed, methylalkanes isoprenoids altered

*B* : Benzene, *T* : Toluene, *EB* : Ethylbenzene, *mpX* : *m/p*- Xylene, *oX* : *o*-Xylene, *Naph* : Naphthalene, *2-MN* : 2-Methylnaphthalene, *1-MN* : 1-Methylnaphthalene, *TMB* : Trimethylbenzene



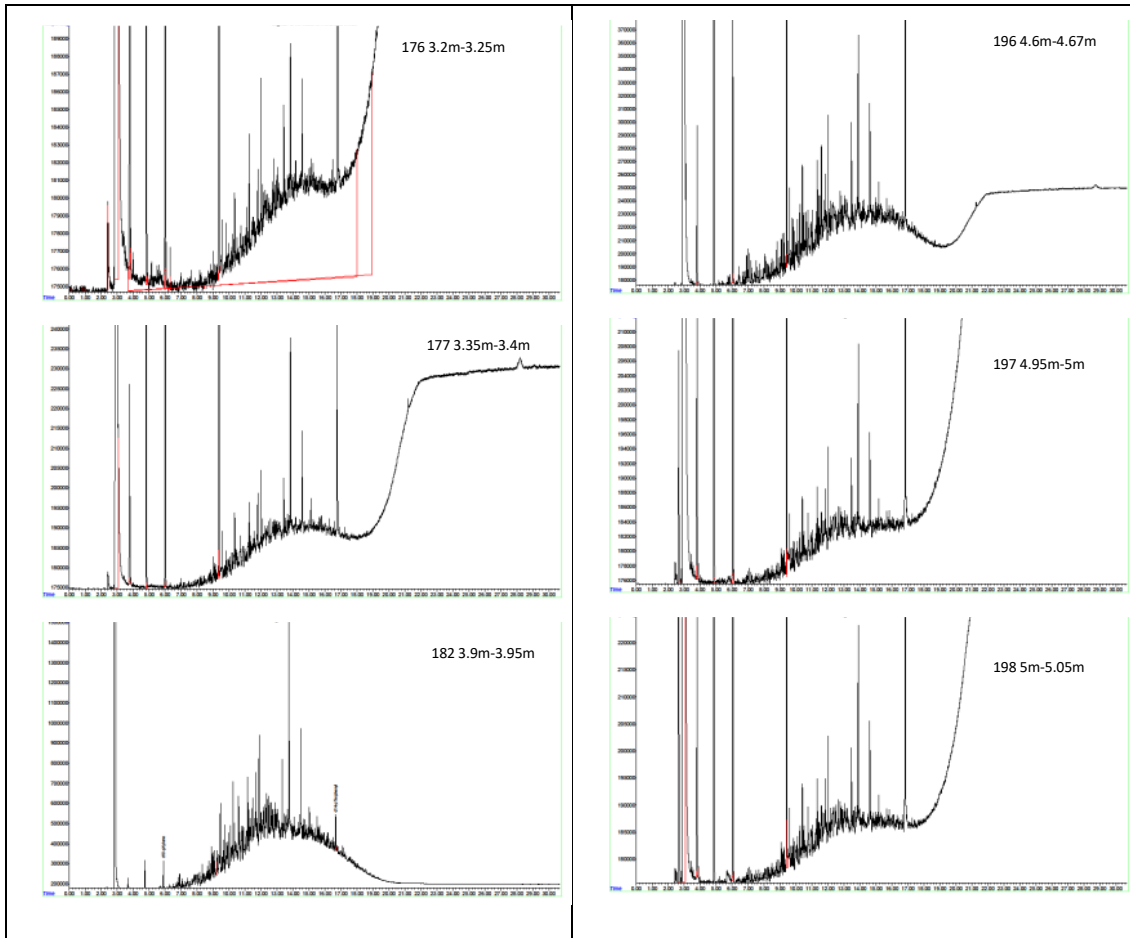
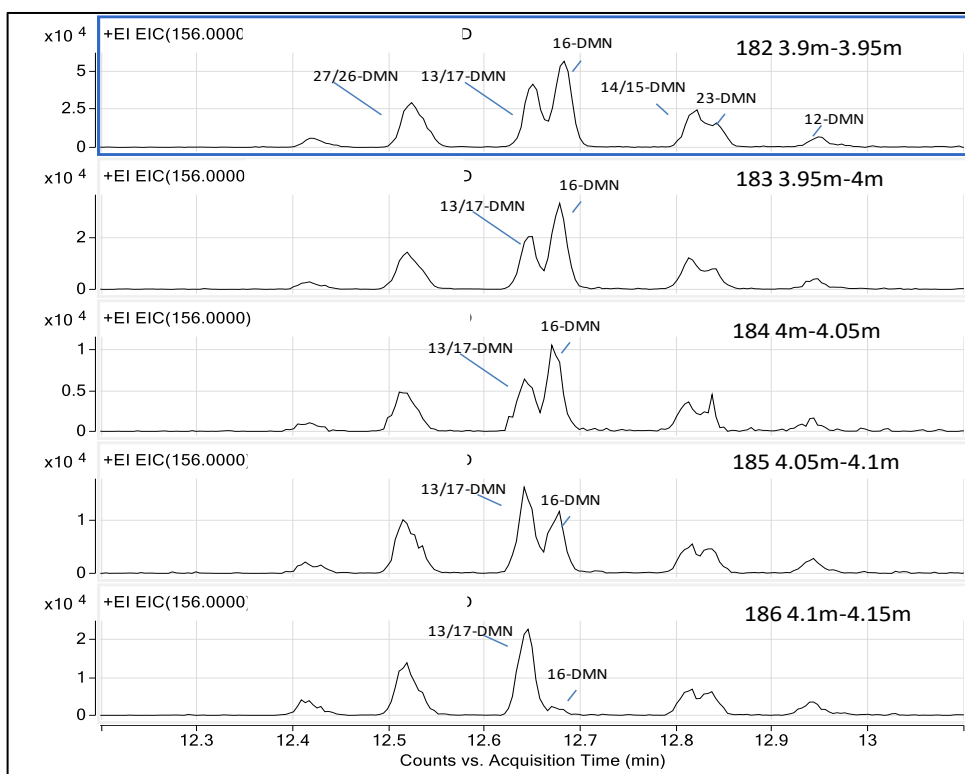


Figure 27. GC-FID analysis of TPH from selected samples from core 67 D6 location



**Figure 28. GC-MS analysis showing selected ion chromatograms (m/z 156) highlighting the dimethylnaphthalenes (DMN) in selected TPH samples from core 67 (location D6)**

#### *Location D10: cores C70 and C71*

TPH analyses of samples from the D10 location (two sets of core samples, core C70 261-293 (1.2–5.65 m) and core C71 294-318 (1.3–4.55 m, Figure 29, Appendix Tables B.1-2 and B.1-3) showed the fuel type and extent of biodegradation in the core samples (weathered crude oil, with *n*-alkanes removed and isoprenoids altered) match well with LNAPL recovered from the same area (55 and 60, Figure 25 and Figure 26). TPH was detected shallower and deeper (below the water table) in the C70 core (3.1– 4.1 m) compared to the C71 core (3.2–3.9 m). The higher concentration TPH samples in core C71 were typically more weathered (fewer peaks) than the higher concentration TPH samples in core C70. The composition of the TPH with depth showed significant changes in the shallower samples. The TPH in the shallower core samples (core C70 3.1–3.3 m and core C71 3.2–3.3 m) were extremely weathered, consisting mainly of an unresolved complex mixture (UCM or hump) with few if any peaks on the UCM (*n*-alkanes, methylalkanes and isoprenoids removed). The shallow core samples immediately after the extremely weathered samples (3.3–3.35 m in both cores) unlike the shallower core samples now contained isoprenoids and they had more altered distributions (pristane depleted relative to phytane, Pr/Ph) than subsequent core samples, suggesting they are more biodegraded than deeper core samples (pristane has been reported to biodegrade preferentially to phytane (Hansen *et al* 2002; Johnston *et al* 2007)). The GC analyses of these core samples shows that biodegradation is occurring in the shallower samples.

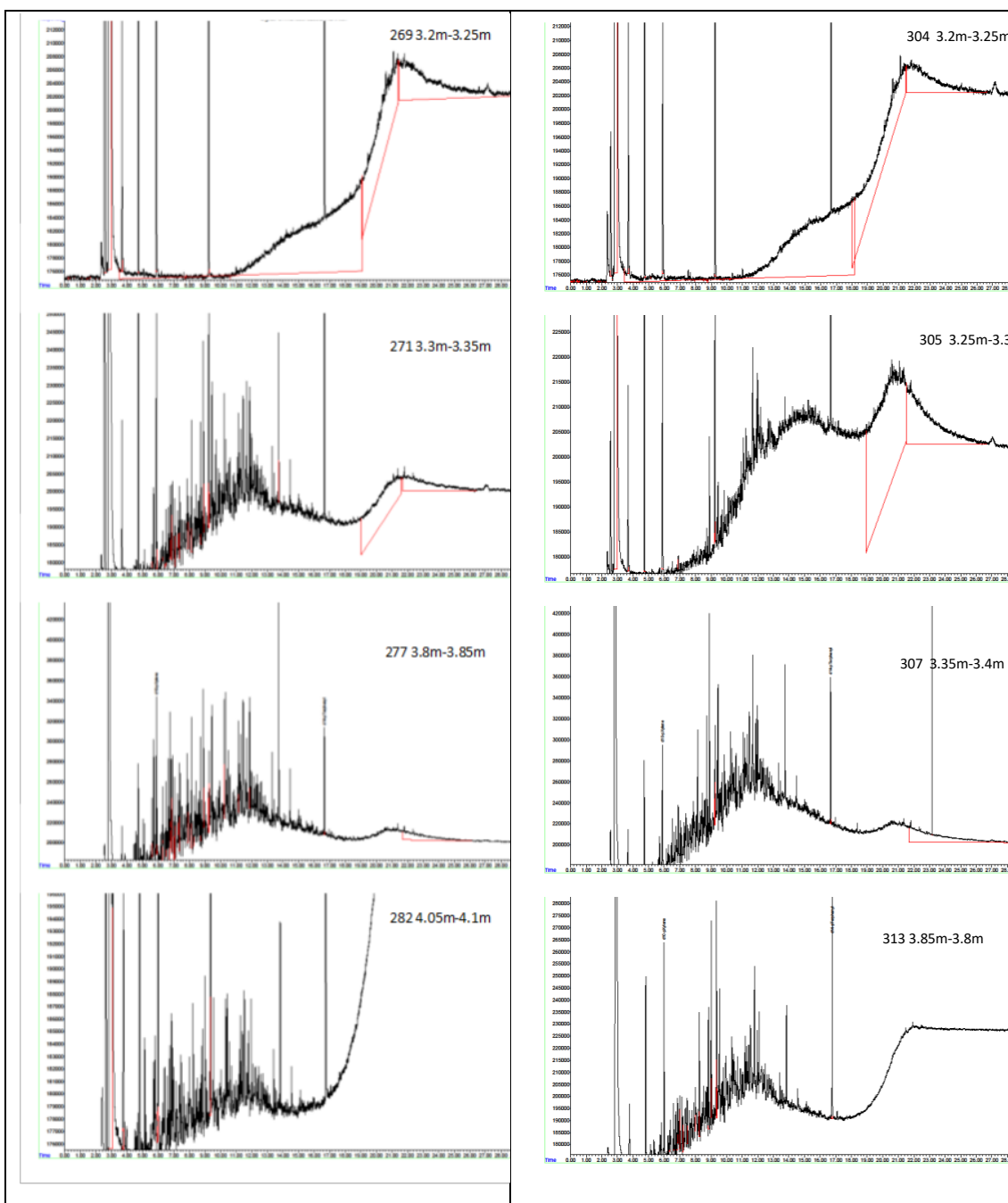


**Figure 29. GC-FID analysis of TPH extracts from selected core samples from location D10**

*LNAPL composition changes and mass loss estimates at a nearby diesel release site*

Samples of the weathered LNAPL diesel from 28 monitoring wells, along with LNAPL from cores, in a 2-ha plume were characterised by GC-MS techniques. The relative extent of biodegradation was assessed using ratios of partially degraded and resistant compounds including *n*-alkanes (*n*C17), pristane and phytane. Age relationships were also investigated from the LNAPL composition. In a spill thought to be perhaps older than 50 years (about 300 m from D6), these analyses also identified a range of mass loss between 65 and 80% of the initial spilled diesel mass (largely losses of *n*-alkanes) through biodegradation and other natural attenuation processes.

## 4.6 Overview of hydrocarbon mass removal – recovery and NSZD

Remedial mass recovery efforts at site B have plateaued across a large area at less than 50 t yr<sup>-1</sup> (as at 2015). LNAPL composition changes determined from cores indicated preferential biodegradation of LNAPL in the vertical profile. Overall mass loss was not possible to estimate from LNAPL compositional changes, especially because of the range of product types present at site B. In one area, mass losses up to 65–80% of the initial spill release was estimated for a spill that was perhaps greater than 50 years. The initial volume of this release is unknown.

Using temperature data, NSZD rate estimates were consistent across three thermistor strings and three dates for each location D10 (crude oil) and D6 (diesel), but the locations had distinctly different rates, 2254 L LNAPL ha<sup>-1</sup> yr<sup>-1</sup> versus 7575 L LNAPL ha<sup>-1</sup> yr<sup>-1</sup> respectively, when averaged across the three thermistor strings and dates.

For the gas methods (in-well or depth profile), there was a high degree of consistency between the rates calculated based on oxygen data or based on carbon dioxide data, and across different dates. The multi-depth data gave higher average, corrected rate estimates for location D10 (15,325–16,858 L LNAPL ha<sup>-1</sup> yr<sup>-1</sup>) than location D6 (10,460–11,607 L LNAPL ha<sup>-1</sup> yr<sup>-1</sup>), whereas the in-well gas data gave lower average rate estimates (6799–7459 L LNAPL ha<sup>-1</sup> yr<sup>-1</sup>) for D10 than location D6 (13,034–13,968 L LNAPL ha<sup>-1</sup> yr<sup>-1</sup>). The explanation for this reversal of trends is not clear – ongoing manual and on-line monitoring using buried probes is planned to provide an expanded data set.

Based on LI-COR measurements of carbon dioxide fluxes, the estimated average NSZD rates at D10 and D6 were effectively the same. The range of rates at location D10 (4490–6390 L LNAPL ha<sup>-1</sup> yr<sup>-1</sup> – corrected for background) was narrower and provides greater confidence in the average than at D6. The broader range at D6 (3088–8575 L LNAPL ha<sup>-1</sup> yr<sup>-1</sup> – corrected for background) may be due to ground surface variability, product type differences or other effects.

Estimates based on temperature were largely lower than those determined by the other methods, especially at D10. The average estimate at D6 (7575 L LNAPL ha<sup>-1</sup> yr<sup>-1</sup>) based on temperature is comparable to the corrected LI-COR estimate at D6.

Overall, average NSZD rate estimates at D10 (crude location) varied from 2254 L LNAPL ha<sup>-1</sup> yr<sup>-1</sup> based on temperature to 16,858 L LNAPL ha<sup>-1</sup> yr<sup>-1</sup> based on multi-depth gas data, with LI-COR carbon dioxide flux providing an estimate between the two (5761 L LNAPL ha<sup>-1</sup> yr<sup>-1</sup>).

Similarly, for D6 (diesel location), average NSZD rate estimates varied from 7575 L LNAPL ha<sup>-1</sup> yr<sup>-1</sup> based on temperature to 13,968 L LNAPL ha<sup>-1</sup> yr<sup>-1</sup> based on in-well gas data, but in this case the LI-COR carbon dioxide flux provided an estimate comparable to the temperature estimate (5931 L LNAPL ha<sup>-1</sup> yr<sup>-1</sup>).

Overall, NSZD rates ranged from a few hundred to ~ 9000 L LNAPL ha<sup>-1</sup> yr<sup>-1</sup> at the background site where we know there is no LNAPL present (based on oxygen and carbon dioxide profiles). Where LNAPL is present, NSZD rates were consistently above 2000 L LNAPL ha<sup>-1</sup> yr<sup>-1</sup> and more typically 7500–17,000 L LNAPL ha<sup>-1</sup> yr<sup>-1</sup>.

Table 28 and Table 29 provide a review of site-wide total NSZD rates reported in Section 4.5.

**Table 28. Tabulation of NSZD rates across methods used at D6 (diesel), and total site-wide mass losses per time**

NSZD methods	Intrinsic rate estimates (L LNAPL ha <sup>-1</sup> yr <sup>-1</sup> )*	Rate mass/time (t yr <sup>-1</sup> )**
Soil surface CO <sub>2</sub> flux	<ul style="list-style-type: none"> <li>LI-COR: 6000</li> </ul>	<ul style="list-style-type: none"> <li>120</li> </ul>
Temperature:	<ul style="list-style-type: none"> <li>Buried thermistors: 6,000 to 8,800</li> </ul>	<ul style="list-style-type: none"> <li>120 to 170</li> </ul>
Gas sampling (in-well)	<ul style="list-style-type: none"> <li>O<sub>2</sub>: 13,000</li> <li>CO<sub>2</sub>: 14,000</li> </ul>	<ul style="list-style-type: none"> <li>260</li> <li>280</li> </ul>
Gas sampling (gas vapour port data)	<ul style="list-style-type: none"> <li>O<sub>2</sub>: 10,000</li> <li>CO<sub>2</sub>: 12,000</li> </ul>	<ul style="list-style-type: none"> <li>210</li> <li>230</li> </ul>

\* All rates are background corrected. The LI-COR are averages across three replicates at three locations within 2–5 m of the central gas sampling locations. NSZD temperature ranges are from three thermistor strings. Values are rounded to two significant figures. \*\*Assumed an LNAPL density of 703 kg m<sup>-3</sup> (as octane), and areal extent of diesel LNAPL (28 ha) from the 2004 distribution determined by a combination of LNAPL density, viscosity and whole oil analysis (by gas chromatography).

**Table 29. Tabulation of NSZD rates across methods used at D10 (crude oil), and total site-wide mass losses per time**

NSZD methods	Intrinsic rate estimates (L LNAPL ha <sup>-1</sup> yr <sup>-1</sup> )*	Rate mass/time (t yr <sup>-1</sup> )**
Soil surface CO <sub>2</sub> flux	<ul style="list-style-type: none"> <li>LI-COR: 5800</li> </ul>	<ul style="list-style-type: none"> <li>24</li> </ul>
Temperature:	<ul style="list-style-type: none"> <li>Buried thermistors: 1000 to 3100</li> </ul>	<ul style="list-style-type: none"> <li>4.4 to 13</li> </ul>
Gas sampling (in-well)	<ul style="list-style-type: none"> <li>O<sub>2</sub>: 6800</li> <li>CO<sub>2</sub>: 7500</li> </ul>	<ul style="list-style-type: none"> <li>29</li> <li>31</li> </ul>
Gas sampling (gas vapour port data)	<ul style="list-style-type: none"> <li>O<sub>2</sub>: 15,000</li> <li>CO<sub>2</sub>: 17,000</li> </ul>	<ul style="list-style-type: none"> <li>65</li> <li>71</li> </ul>

\* All rates are background corrected. The LI-COR are averages across three replicates at three locations within 2–5 m of the central gas sampling locations. NSZD temperature ranges are from three thermistor strings. Values are rounded to two significant figures. \*\*Assumed an LNAPL density of 703 kg m<sup>-3</sup> (as octane), and areal extent of crude oil LNAPL (6.0 ha) from the 2004 distribution determined by a combination of LNAPL density, viscosity and whole oil analysis (by gas chromatography).

We note that total mass removal rates by NSZD may be reduced if soil gas movement is inhibited – as it might occur below concreted or asphalt areas within the 28 and 6 ha areas used for converting intrinsic to total, site wide NSZD rates; or if soils have high moisture contents. Inhibiting oxygen ingress reduces NSZD biodegradation rates.

For the diesel location, the highest NSZD rates were estimated by major gas analysis. The oxygen and carbon dioxide in-well and depth profile multilevel data provide similar rates of 10,000–14,000 L LNAPL ha<sup>-1</sup> yr<sup>-1</sup> (or 210 to 280 t yr<sup>-1</sup>). Surface flux and temperature estimates were comparable to each other in the range 6000–8800 L LNAPL ha<sup>-1</sup> yr<sup>-1</sup> and (or 120 to 170 t yr<sup>-1</sup>).

For the crude oil location, intrinsic NSZD rates were highest when estimated by major gas analysis. However, in contrast to the diesel location, the oxygen and carbon dioxide depth profile multilevel data at the crude oil location provided two to three times higher NSZD rate estimates of 15,000–17,000 L LNAPL ha<sup>-1</sup> yr<sup>-1</sup> (or 65 to 71 t yr<sup>-1</sup>) compared to the in-well major gas method. The temperature method yielded the lowest NSZD rates of 1000–3000 L LNAPL ha<sup>-1</sup> yr<sup>-1</sup> (or 4.4 to 13 t yr<sup>-1</sup>). Surface flux and in-well gas sampling methods yielded comparable estimates.

NSZD rate estimates from temperature data were consistent across multiple thermistor strings and measurement times. Rate estimates for the diesel location were 3 to 4 times higher compared to the crude oil location. Active LNAPL recovery from the D6 (diesel) location was approximately 17.5 t in 2018. NSZD mass loss is of the order of 120 to 280 t y<sup>-1</sup> across the estimated extent of the diesel LNAPL plume.

At the D10 (crude oil) location, there was no active LNAPL recovery due to limited recoverable LNAPL, with no measurable in-well thickness ≥ 50 mm. There is a large range of calculated LNAPL mass removal across all NSZD methods of 4.4 to 71 t y<sup>-1</sup> representing the crude oil plume, largely due to low rates derived from temperature gradient methods. If temperature estimates are excluded, crude oil NSZD mass estimates were in the narrower range of 24 to 71 t y<sup>-1</sup>.

Overall diesel NSZD rates are seven to 15 times higher than the maximum LNAPL liquid diesel recovery rates in 2018. For crude oil a direct comparison could not be made in 2018 due to there being no crude oil available for removal via active recovery. Therefore, mass losses associated with crude oil were solely as a result of NSZD. Across all methods, NSZD rates for diesel were comparable to those for crude oil, with differences between methods of up to a factor of two (excluding temperature). Research into the variability between NSZD methods caused by compositional, spatial and temporal conditions is the subject of ongoing investigations at this field site.

## 4.7 Sources of uncertainty in hydrocarbon mass loss estimation

Uncertainty in mass estimates from active recovery operations at this site are mainly from interference in recovered fluid volumes from water entrained in the LNAPL. This can be corrected by dipping recovery tanks with an oil/water interface probe, however when estimated from vacuum tankers recovering from large diameter wells the product ratio needs to be estimated. Experience and periodic testing over time has improved the estimation overall.

While the soil profiles are relatively uniform across site B, and hence application of uniform soil properties when calculating NSZD rates is more applicable, there are still a few considerations that may influence uncertainty. Firstly, generic soil properties for sands was used to generate NSZD rates, and secondly, seasonal changes in soil moisture content and groundwater level are not assessed. The measurement of the thermal conductivity and gas diffusion coefficient would assist in reducing the uncertainty with the estimation of NSZD rates using the thermal and major gas gradient methods.

A second area of uncertainty relates to the assessment of site-wide NSZD rates. The monitoring program designed for site B was not intended for this purpose. The monitoring locations have been set up to provide detailed side-by-side comparisons of different techniques for determining NSZD rates and areas for direct comparison of mass reduction NSZD and recovery for specific product types. As such the monitoring design does not provide extensive spatial coverage of site B. The uncertainty is introduced when these point measurements are extrapolated to determine site-wide NSZD rates for crude oil and diesel, also noting that for surface cover overlying the diesel plume is not fully represented by the study locations and this may impact NSZD rates.

## 5. Site C

---

### 5.1 Introduction

Site C is a historic refuelling facility, located adjacent to a large site-based workshop and ancillary services facility. The location is coastal, underlain by alluvial deposits and a thin veneer of clay overlying ridges of heavily weathered basalt. It is estimated approximately 1,000 m<sup>3</sup> of diesel was spilled or leaked into the subsurface at the facility over a lengthy period, notionally between 1997 and 2000 and potentially later (SiteC\_Ref1 2013). According to this report:

‘A recovery system was installed in 1998 and approximately 50 m<sup>3</sup> of diesel was extracted until the system was decommissioned. More recently an upgraded new recovery system was installed to further abstract PSH. Anecdotal information from [...] indicates that an insignificant volume has been removed since June 2012, with commissioning and debottlenecking process improvements currently underway in order to improve runtime and extraction performance. Hence, based on estimated spill and leakage volumes and on remediation system recovery records approximately 950 m<sup>3</sup> of product potentially remains in the subsurface. This estimate does not consider any potential biodegradation or volatilisation that may be occurring’ (SiteC\_Ref1 2013, p. 76).

The extent of the LNAPL plume was estimated at 7 ha (SiteC\_Ref3 2014). Based on the contoured plume shown for October 2017 (SiteC\_Ref11 2018), the extent of the LNAPL plume estimated from the appearance of product in wells is about 3.5 ha. The extent of residual and entrapped LNAPL in the subsurface is likely to be much larger than this and may be in the order of 18 ha.

Petroleum contamination has likely resulted from multiple historic LNAPL releases as determined by differences in the product types and extents of weathering observed in the LNAPL samples from the site including diesel and lube oil range product types.

### 5.2 Site description

The presence of fractures in the basalt makes for a complex system for the movement and interaction of multi-phase LNAPL, groundwater and VOCs (SiteC\_Ref3 2014). The vadose zone contains preferential flow paths such that the water table is highly responsive to infrequent, high intensity storms, typical of the climate at site C. The overall annual variation in the water table is large, typically around 4 m (Site C\_Ref3 2014). Due to the low transmissivity of much of the aquifer, an increase in the water table elevation following a rainstorm event, tends to persist over an extended recession period (SiteC\_Ref3 2014). Mobility of the LNAPL in the aquifer is dependent on variation in the water table, which controls whether the LNAPL is isolated from or connected with conducting fracture systems.

#### **5.2.1 Distribution of wells and measurement methods**

Figure 30 indicates the locations of monitoring wells and methods referred to in this report.

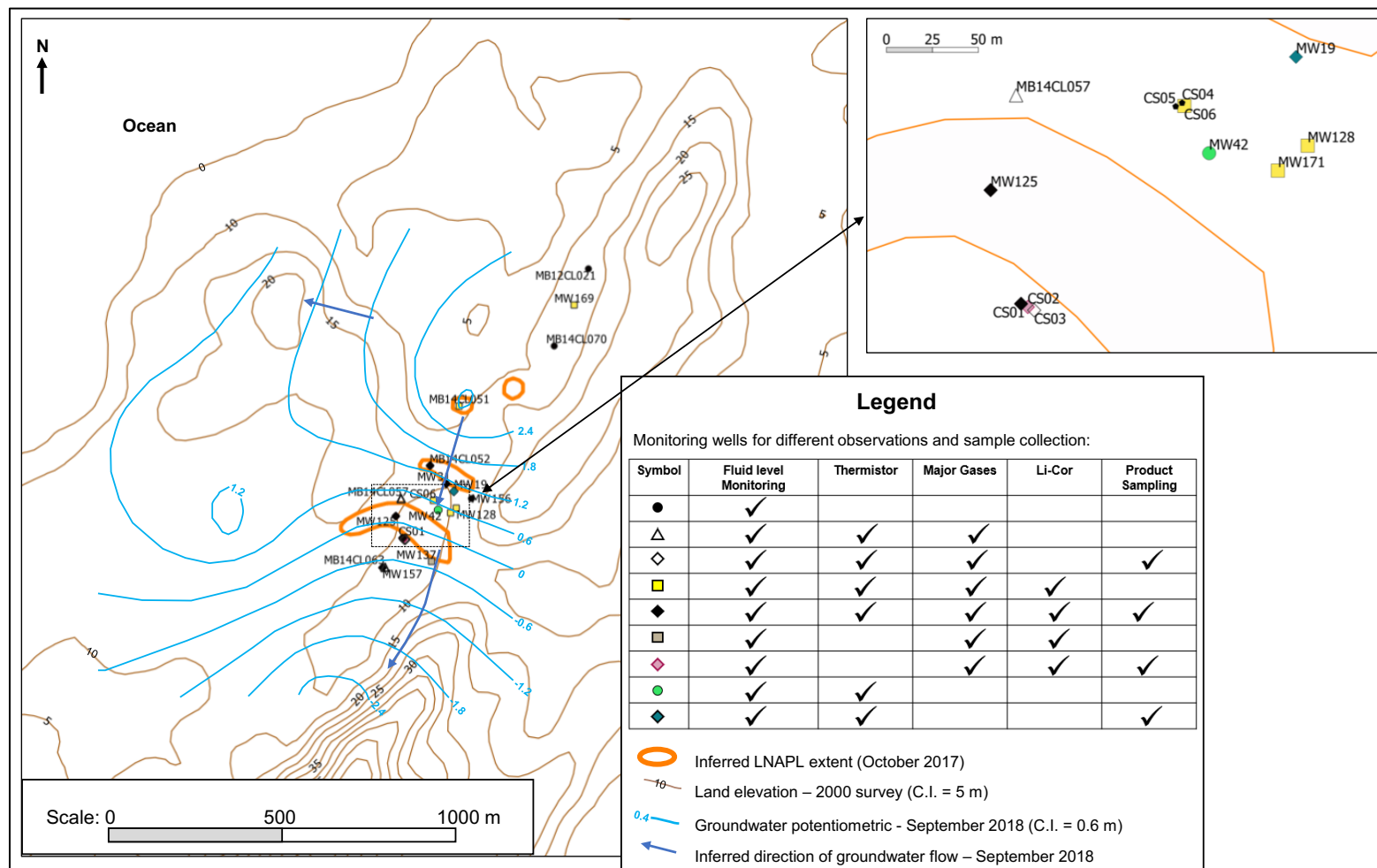


**Figure 30. Distribution of monitoring wells at site C. Note, LI-COR collar locations are approximate and are shown as the nearest monitoring well. Groundwater potentiometric contours and inferred LNAPL extent from SiteC\_Ref11 (2018). Land elevation from survey conducted in 2000 (Geoscience Australia 2019). The inset shows an enlarged view of CSIRO research well locations (CS01 to CS06) relative to the other wells.**



### 5.2.2 Profile stratigraphy

Land surface elevations are largely controlled by two northeast-southwest trending ridges of basalt and an intervening valley (SiteC\_Ref9 2016). As depicted in Figure 30, the topography varies between about 5 and 13 m AHD near the inferred LNAPL extent (SiteC\_Ref9 2016).

Site C is underlain by alluvial and colluvial sediments, and a thin veneer of clay overlying ridges of heavily weathered basalt (SiteC\_Ref1 2013; SiteC\_Ref3 2014). Two stratigraphic cross-sections constructed using well logs from SiteC\_Ref1 (2013) and SiteC\_Ref10 (2018) depict the variable thickness of poorly graded sand and weathered basalt overlying more cohesive, fresh basalt (Figure 31 and Figure 32). The upper portion of fractured basalt forms an unconfined aquifer system (SiteC\_Ref3 2014).

## 5.3 Data supplied by site owner and other data

### 5.3.1 Hydrogeological parameters

The porosity of the basalt depends on the extent of weathering. According to SiteC\_Ref1 (2013), the range of porosity is between 3 and 35% and unfractured basalt is likely to have porosity values less than 3%. The best estimates of porosity at the location of LNAPL is 10% (range between 1 and 30%, SiteC\_Ref1 2013).

SiteC\_Ref1 (2013) describes the hydrostratigraphy assigned in a three-layer groundwater model constructed for site C:

‘Layer 1 is 2.7 m thick and was assigned properties representative of alluvial and fill deposits with a hydraulic conductivity of 4.0 m/day. Because depth to water is greater than 2.7 m in some areas of the site a portion of this layer is simulated to not contain water;

Layer 2 is 3.7 m thick and was assigned properties representative of weathered basalt with the hydraulic conductivity ranging from 0.001 to 4.0 m/day. The lowest hydraulic conductivities were assigned to the eastern, up-gradient part of the site and the more permeable units were assigned to the western part of the site; and

Layer 3 is mostly 10 m to 25 m thick and was assigned properties representative of fresh basalt. The hydraulic conductivity ranged between 0.001 and 0.1 m/day with the lowest hydraulic conductivity along the eastern part of the site where the bedrock was assumed less weathered’ (SiteC\_Ref1 2013, p. 72).

Aquifer tests results reported in SiteC\_Ref3 (2014) provide a range of hydraulic conductivity ( $K_w$ ) values, which were estimated from the transmissivity by dividing by the aquifer thickness (Table 30). Estimates of  $K_w$  based on baildown test results were also provided in SiteC\_Ref3 (2014, Table 31). As described in SiteC\_Ref3 (2014), p. 60:

‘[t]he range of  $K_w$  for the wells measured extends over three orders of magnitude from 0.001 to 1 m day<sup>-1</sup>. The median value is around 0.037 m day<sup>-1</sup> which represents an upper value for basalt and lower value for permeable basalt (Domenico and Schwartz 1998)’.

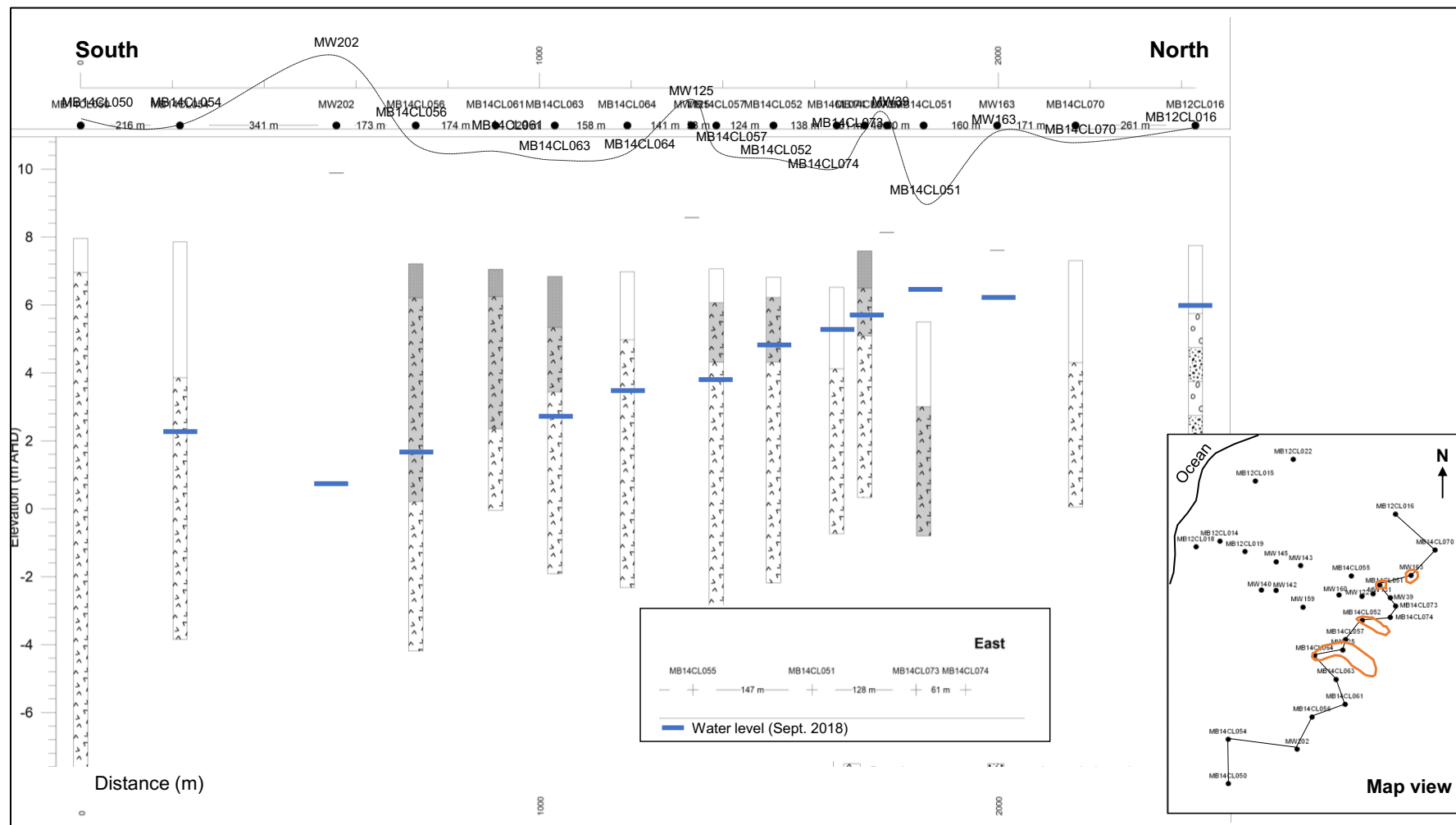


Figure 31. Geological cross-section roughly perpendicular parallel to the coastline. The inset shows a map view and the location of the coastline and inferred LNAPL extent as of October 2017 (in orange) for reference from SiteC\_Ref11 (2018). Stratigraphic cross-section constructed using well logs from SiteC\_Ref1 (2013), SiteC\_Ref6 (2015), and SiteC\_Ref10 (2018). Groundwater level for September 2018 (SiteC\_Ref11 2018).

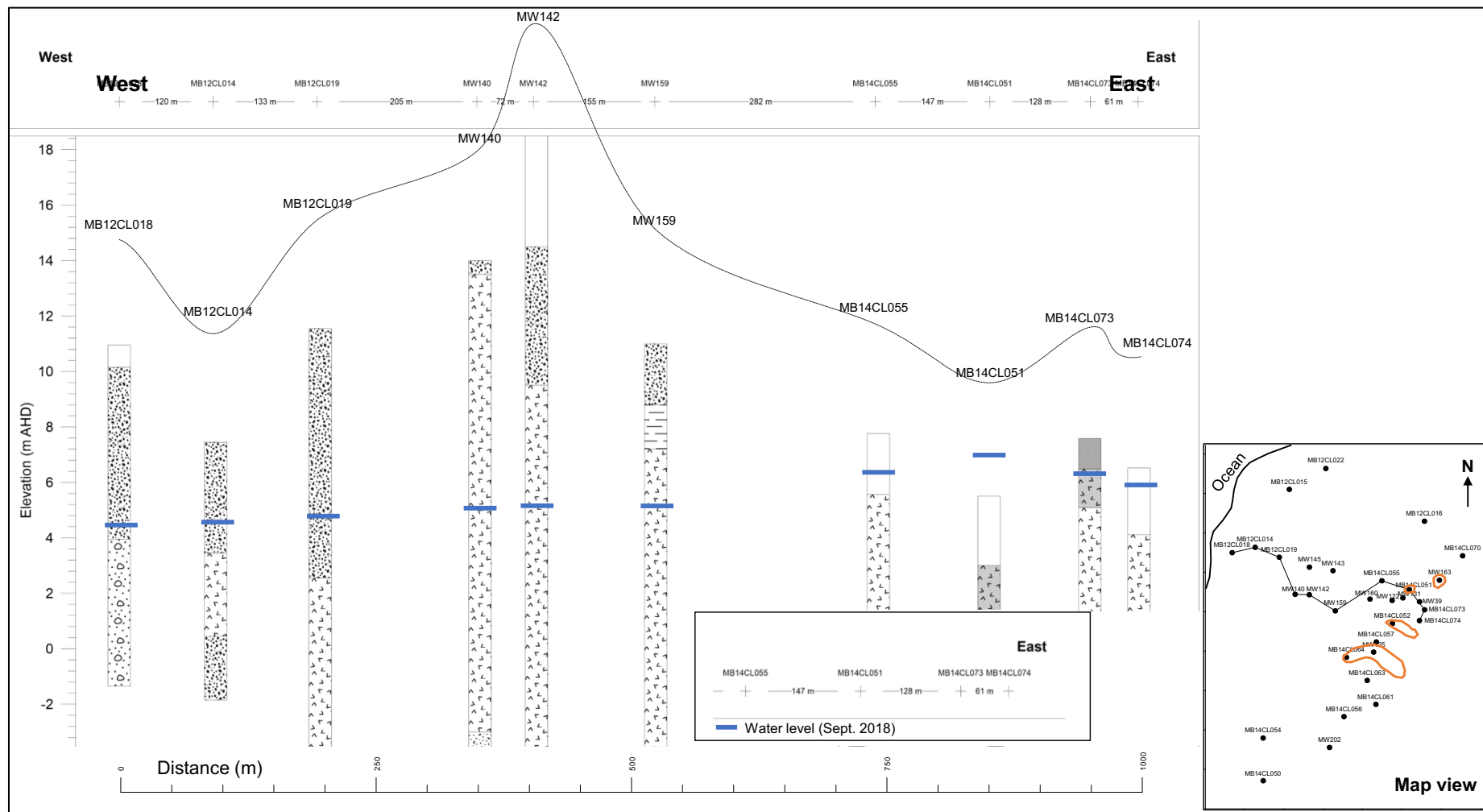


Figure 32. Geological cross-section roughly perpendicular to the coastline. The inset shows a map view and the location of the coastline and inferred LNAPL extent as of October 2017 (in orange) for reference from SiteC\_Ref11 (2018). Stratigraphic cross-section constructed using well logs from SiteC\_Ref1 (2013), SiteC\_Ref6 (2015), and SiteC\_Ref10 (2018). Groundwater level for September 2018 (SiteC\_Ref11 2018).

**Table 30. Summary of short-term (2 to 3 h) aquifer pump tests for the six research wells CS01 to CS06 from SiteC\_Ref3 (2014)**

Well	Date	Aquifer thickness (m)	Transmissivity (m <sup>2</sup> day <sup>-1</sup> )	Hydraulic conductivity (m day <sup>-1</sup> )
CS01	9 May 2012	7.85	8.12	1.03
CS02	5 May 2012	8.05	1.97	0.245
CS03	9 May 2012	7.95	0.543	0.068
CS04	6 May 2012	9.1	0.789	0.087
CS05	7 May 2012	9.15	0.056	0.0061
CS06	8 May 2012	9.35	0.171	0.018

**Table 31. Summary of hydraulic conductivity estimates derived from analysis of baildown test results from SiteC\_Ref3 (2014)**

Well	Date	Hydraulic conductivity (m day <sup>-1</sup> )
MW19	19 August 2011	0.001
MW31	20 August 2011	0.079
MW23A	20 August 2011	0.01
MW157	20 August 2011	0.204
MW139	21 August 2011	0.028
MW171	21 August 2011	0.015
MW128	21 August 2011	0.005
MW42	21 August 2011	0.046
MW37	23 August 2011	0.012
CS02	8 May 2012	0.166
CS05	9 May 2012	0.022
MW157	9 May 2012	0.038
CS06	9 May 2012	0.047
MW171	9 May 2012	0.037
MW128	10 May 2011	0.009
CS01	19 May 2011	0.996
CS02	20 May 2011	0.233
CS03	21 May 2011	0.452

### **5.3.2 Well construction and mean groundwater levels**

Well construction logs from six wells (CS01 to CS06) drilled for a research program conducted by CSIRO are shown in Appendix C.2 (SiteC\_Ref3 2014). Their locations are shown in Figure 30. Well construction and stratigraphic log files were also provided for sixty additional wells and a selection of these were used to construct the cross-sections shown in Figure 31 and Figure 32.

Also shown in Figure 31 and Figure 32 is the interpolated position of the groundwater level for September 2018, which varied across the site between 3 and 16 mbg and extended mainly within the basalt. Contours of the potentiometric surface depicted in Figure 30 are shown for September 2018 (SiteC\_Ref11 2018). Interpreted groundwater flow directions are to the west and to the south-west (Figure 30). Depictions of the potentiometric surface from earlier reports from November 2013 (SiteC\_Ref2 2014), October 2015 (SiteC\_Ref8 2016), September/October 2017 (SiteC\_Ref10 2018) and September 2018 (SiteC\_Ref11,2018) were compared. These show groundwater flow primarily toward the coast in November 2013 and development of a stronger component of flow to the south in October 2015, and then to the south-west in later reports (September/October 2017 and September 2018).

The elevation of the water table is strongly controlled by large intense rainfall events, characteristic of the climate, as well as by pumping and dewatering activities (SiteC\_Ref3 2014). LNAPL corrected groundwater levels are compared with monthly rainfall data between August 2002 and November 2014 (Figure 33) for a selection of wells near the LNAPL plume with long term fluid level monitoring data. These indicate the highly responsive groundwater level to intense rainfall events, depending on the magnitude of the rainfall event. MW156 showed a 4.9 m increase in groundwater level in response to the 238 mm storm in June 2013 (SiteC\_Ref3 2014).

#### ***5.3.1 Product thicknesses in local wells on the site over time***

Time series of LNAPL thickness between August 2002 and November 2014 are shown for a selection of monitoring wells near the inferred extent of the plume (Figure 34). As of October 2016, apparent LNAPL thicknesses were within historic ranges (SiteC\_Ref9 2016). However, in the reports for 2018, observed increase and decrease in LNAPL thicknesses relative to historic levels were reported (Table 32).

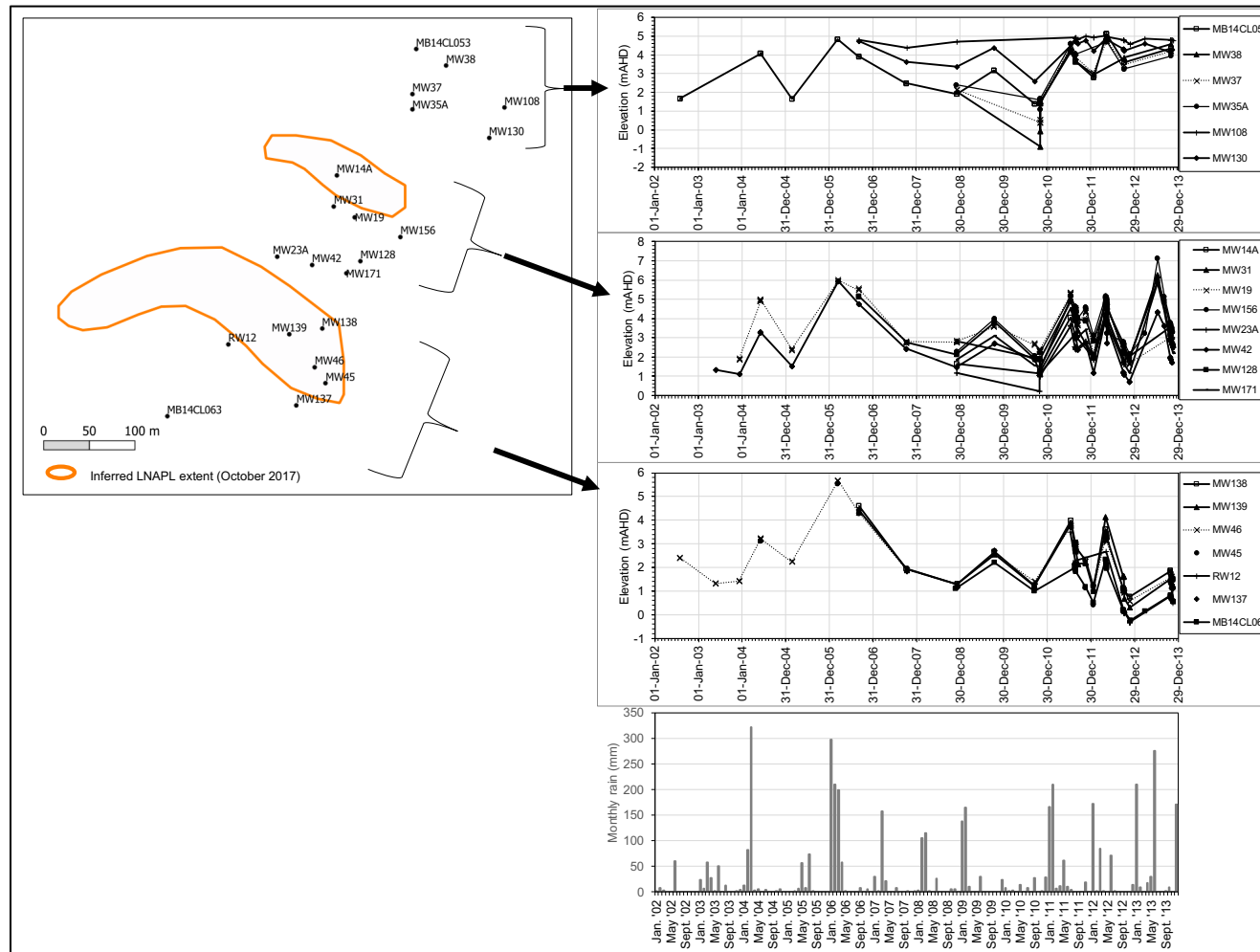
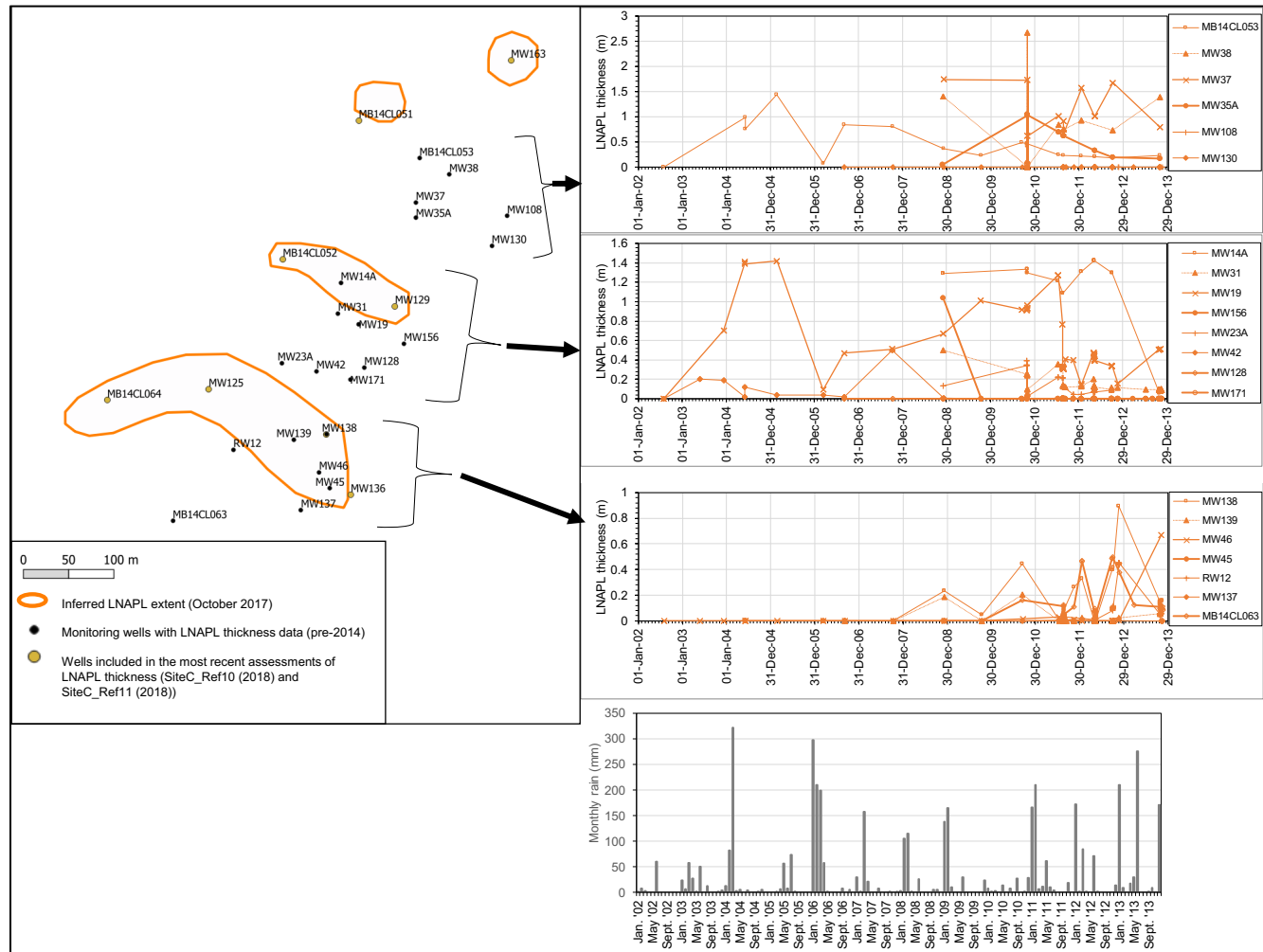


Figure 33. LNAPL corrected groundwater levels for a selection of wells near the inferred LNAPL extent as of October 2017 from SiteC\_Ref11 (2018). Groundwater data up to July 2011 were provided by the client and data post-August 2011 were measured by CSIRO (SiteC\_Ref3 2014). Monthly rainfall is shown for comparison (Queensland Government 2019).



**Figure 34. LNAPL thickness for a selection of wells near the inferred LNAPL extent as of October 2017 from SiteC\_Ref11 (2018). LNAPL thickness data were compiled from the client and CSIRO as reported in SiteC\_Ref3 (2014). Monthly rainfall is shown for comparison (Queensland Government 2019).**

**Table 32. Apparent LNAPL thickness monitoring data as reported in SiteC\_Ref10 (2018) and SiteC\_Ref11 (2018)**

Well	Apparent LNAPL thickness (m)						Observations
	Jun-15	Oct/Nov 2015	May-16	Oct-16	Oct-17	Sep-18	
MW125	0.074	0.985	0.923	0.905	0.56	Well not gauged	Approx. 34.5 cm decline compared to Oct 2016, noting that groundwater elevation increased by approx. 23 cm
MW129	1.314	0.48	0.75	0.539	Well not gauged	Well not gauged	--
MW136	0.039	0.515	0.168	0.065	0.02	Well not gauged	Approx. 4.5 cm decline compared to Oct 2016, noting that groundwater elevation decreased by approx. 1.27 m
MW138	0.621	0.523	0.765	0.417	0.095	Well not gauged	Approx. 32 cm decline compared to Oct 2016, noting that groundwater elevation increased by approx. 2.36 m
MB14CL052	0.012	0.967	1.152	1.051	0.504	Well not gauged	Approx. 55 cm decline compared to Oct 2016, noting that groundwater elevation increased by approx. 40 cm
MB14CL064	0.098	0.25	0.413	0.802	0.853	Well not gauged	Approx. 5 cm increase compared to Oct 2016, noting that groundwater elevation increased by approx. 42 cm
MW163	not detected	0.124	0.138	0.063	Well not gauged	0.31	Approx. 25 cm increase compared to October 2016, noting that groundwater increased by approximately 48 cm.
MB14CL051	not detected	not detected	0.013	0.022	Well not gauged	0.04	Approx. 2 cm increase compared to October 2016, noting that groundwater increased by approximately 63 cm.



### 5.3.2 Measurements of LNAPL transmissivity

LNAPL transmissivity was estimated based on LNAPL bail down testing at two monitoring wells (MW138 and MW19, well locations shown in Figure 34).

**Table 33. LNAPL transmissivity testing results from SiteC\_Ref1 (2013)**

Date	Location	Transmissivity ( $T_n$ ) ( $\text{m}^2 \text{ day}^{-1}$ )
13 Oct 2012	MW138	0.016
13 Oct 2012	MW19	0.015

### 5.3.3 LNAPL sampling and analysis (compositional analysis and extent of weathering)

According to SiteC\_Ref3 (2014), GC-MS analysis of LNAPL samples from the site showed that they all contained weathered diesel-range product as well as mixtures containing weathered diesel-range product and lube-range product. Many of these samples were re-analysed by CSIRO in 2019 along with additional samples obtained for this study.

### 5.3.4 LNAPL recovery operations

The client provided a report containing an approximate volume of total diesel recovered between 1998 and 2013 (SiteC\_Ref1 2013). In addition, recovery operations and test results from 2013–2013 reported in SiteC\_Ref3 (2013) and SiteC\_Ref13 (2014).

## 5.4 Methods

### 5.4.1 Active recovery

#### Type of method used to recover LNAPL

As indicated in a report dated October 2013:

‘Remediation to recover the free phase product commenced in May 1998 and since then approximately 50,000 L of diesel has been recovered; this original system which consisted of recovery wells, bladder pumps connected to skimmers and operated by a pneumatic control stations, has been decommissioned’ (SiteC\_Ref1 2013, p. 23).

Regarding LNAPL recovery operations conducted as part of the CSIRO research program in 2012–2013:

‘Testing was conducted on consecutive days to evaluate continued stress on the aquifer. Continuous over-night operation was not possible... The length of tests varied due to various factors. It should be noted that the duration reported in [Table 34] is the total and does not necessarily represent the total time of actual recovery’ (SiteC\_Ref3 2014, p. 69).

**Table 34. Summary of LNAPL recovery tests reported in SiteC\_Ref3 (2014)**

Test #	Well	Technology	Start date	Duration (min)	Total LNAPL (L)
1	CS02	Drawdown	30 September 2013	350	0
2	CS02	total fluids	1 October 2012	411	9.1
3	CS02	total fluids	2 October 2012	288	3.8
4	CS02	skimmer-drawdown	3 October 2012	485	7.6
5	CS02	skimmer-drawdown	4 October 2012	511	2.5
6	CS01	skimmer-drawdown	20 November 2012	323	5.7
7	CS01	skimmer-drawdown	21 November 2012	433	7.8
8	CS03	skimmer-drawdown	22 November 2012	565	7.2
9	CS03	Skimmer	27 November 2012	90	2.3
10	CS03	VER-skimmer-drawdown	1 November 2013	0	0
11	CS03	VER-skimmer	2 November 2013	199	0
12	CS03	VER-skimmer-drawdown	2 November 2013	150	-
13	CS03	VER-skimmer-drawdown	3 November 2013	465	0.3
14	CS02	VER-skimmer-drawdown	4 November 2013	269	2.9
15	CS02	VER-skimmer-drawdown	5 November 2013	457	3.6
16	CS02	VER-skimmer-drawdown	6 November 2013	366	1.7
17	CS01	VER-skimmer-drawdown	9 November 2013	554	1.8 <sup>+</sup>
18	CS01	VER-skimmer-drawdown	10 November 2013	323	0.3 <sup>+</sup>
19	CS03	MPE	11 November 2013	570	
20	CS03	MPE	12 November 2013	192	0.1
21	CS02	MPE	12 November 2013	157	1
22	CS02	MPE	13 November 2013	530	2.7
23	CS01	MPE	14 November 2013	433	1.4
24	CS01	MPE	15 November 2013	517	0.5 <sup>+</sup>
25	CS04	MPE	17 November 2013	519	0.8
26	CS04	MPE	18 November 2013	268	0.5

The well test results in Table 34 were used to estimate longer-term LNAPL recovery rates for each method (total fluids, skimming and drawdown, vacuum enhanced recovery (VER) and MPE) as described in Section 5.5.1.

#### **How recovery data was estimated**

For the 2012–2013 recovery tests, the following details were provided for each test.

Total fluids:

'Liquid discharge rates were measured using either a digital impeller-type flow meter, or volumetrically with different size buckets and measuring cylinders. The relative volumes of groundwater and LNAPL were determined by timed collection into measuring cylinders where the water

and LNAPL were allowed to separate and the volumes of each determined' (SiteC\_Ref3 2014, p. 31).

Drawdown and skimming:

'LNAPL discharge rates were measured by collecting volumes of LNAPL in a measuring cylinder over timed intervals' (SiteC\_Ref3 2014, p. 32).

VER:

'Liquids were quantified in the same manner as the drawdown plus skimming recovery described above' (SiteC\_Ref3 2014, p. 34).

MPE:

'...all fluids are removed through a common 'straw'. Groundwater and LNAPL accumulated in the knockout drum of the SVE unit and were then transferred to a 200-L drum for quantification and sampling. The liquid discharge was typically water with a fine dispersed phase of LNAPL. ...The liquid discharge was then left to settle prior to the next batch of liquid from the SVE unit. After settling, any LNAPL that had separated under gravity was retained and bulked up for volumetric measurement over various periods of the recovery. The total volume of liquid extracted was determined from flow metering the liquid collected in the drum' (SiteC\_Ref3 2014, p. 34).

#### **5.4.2 NSZD rate estimation**

##### **Subsurface temperature measurement and analysis (iButton and thermistor)**

Subsurface temperatures were measured using two techniques, instantaneous measurements using thermistors and longer-term temporal measurements using iButtons. Both of these methods involved the hanging of the temperature sensors in existing monitoring wells. Instantaneous temperature measurements were obtained during two separate sampling campaigns (6–10 May 2019 and 24–25 September 2019) while 4 iButton strings were installed between 10 May 2019 and 22 June 2019 and then again for a short period 24 September 2019 to 25 September 2019. The monitoring wells in which temperature was measured are shown in Table 35.

For the thermistor method a string of thermistors was hung within the monitoring bore for at least 1 hour to equilibrate with the subsurface temperature. The thermistor string was made up of 10 NTC thermistors (10k Ohm Betacurve, 10K3A1B, matched to YSI 44036) spaced at 1 m intervals along a multi-core cable. Electrical resistance was measured using a multimeter (Fluke 28 II Ex) and converted to temperature using the thermistor manufacturer's polynomial calibration algorithm. Background correction and NSZD calculation was done according to the method outlined for site A.

The iButtons logged temperature at 15 min intervals. This data was assessed and then averaged over either daily or monthly periods which were then corrected against the background well (MW169). The temperature differences were then reviewed and the largest background temperature difference above the water table was used to generate the thermal gradient. The gradient was then multiplied by the thermal conductivity to calculate the heat flux, which was then related stoichiometrically to the LNAPL degradation rate.

**Table 35 Monitoring wells for which manual temperature profiles were recorded and iButtons temperature loggers installed**

Method	Well ID
Thermistor	
May 2019	CS01, CS03, CS06, MW19, MW31, MW125, MW128, MW157, MW169, MW171, MB14CL051, MB14CL052, MB14CL057, MB14CL063
September 2019	CS01, CS02, CS06, MW19, MW31, MW42, MW125, MW157, MW169, MB14CL052, MB14CL063
iButton	MW169, MB14CL052, MW157, CS03

### Gas sampling and analyses (in-well)

Major gas samples were obtained during two separate sampling campaigns (6–10 May 2019 and 24–25 September 2019) from the locations in Table 36. Gas concentrations were determined in situ using a portable gas analyser and for the May campaign on gas samples collected and analysed in the laboratory.

Gas sampling was undertaken by lowering a weighted, nylon tube into the well casing such that the intake was 0.3 m above the fluid-air interface determined previously using an interface meter (H.OIL, Heron Instruments Inc.). An Eagle II gas analyser (RKI Instruments) equipped with oxygen, carbon dioxide and methane sensors, was used to measure the gas concentrations. Following zeroing with ambient air the Eagle II was connected to the nylon tubing and readings taken every 30 s for 3 min. Final oxygen and carbon dioxide concentrations were used to calculate NSZD rates.

Samples for laboratory analysis were collected following the in-situ readings using a 60 mL plastic syringe and a foil sampling bag. The sampling procedure is outlined in detail in Appendix A.7. Major gas analysis was performed as outlined in Section 3.4.2 for site A.

NSZD rates were determined between the sampling location and the soil surface for in-well major gas using the gradient method described in Section 2.4 and in CRC CARE Technical Report 44 (2018). To calculate NSZD rates, the gradient method for soil gas flux was applied using Equation 2 (see Section 2.4). The effective vapour diffusion coefficient for O<sub>2</sub> and CO<sub>2</sub> were assigned the values of 0.41E-06 and 0.37E-06 m<sup>2</sup> s<sup>-1</sup>, respectively.

**Table 36 Monitoring wells for which major gas samples were measured in situ using a gas analyser or collected for laboratory analysis**

Sampling campaign	Gas analysis method	Well ID
May 2019	Gas analyser	CS01, CS02, CS03, CS06, MW31, MW125, MW128, MW137, MW157, MW169, MW171, MB14CL051, MB14CL052, MB14CL057, MB14CL063
May 2019	Laboratory	CS01, CS03, CS06, MW31, MW125, MW128, MW137, MW157, MW169, MW171, MB14CL051, MB14CL052, MB14CL057, MB14CL063
September 2019	Gas analyser	CS01, CS02, CS06, MW19, MW31, MW42, MW125, MW157, MW169, MB14CL051, MB14CL052, MB14CL057, MB14CL063

## Soil surface carbon dioxide flux measurements (E-Flux and LI-COR flux chamber)

Soil surface carbon dioxide flux was measured using a LI-COR LI8100A Automated Soil Carbon Dioxide (CO<sub>2</sub>) Flux System connected to a 20 cm survey chamber (8100-103, LI-COR Lincon, NE) during two sampling campaigns (8–10 May 2019 and 24–25 September 2019). At each monitoring location (Table 37) a PVC soil collar (20 cm diameter x 12 cm) was installed generally within 1 m of a monitoring bore. Several locations (MW169, MW157 and MW171) had two collars installed to test the within site variability during the May 2019 sampling campaign. Three repeat CO<sub>2</sub> flux measurements were collected for each collar for between 1 and 3 times in May (9 times on MW169) and two times in September. The raw data was processed using the manufacturer supplied software (Soil Flux Pro v4.0.1) and either a linear or exponential function fitted to the data to determine the CO<sub>2</sub> flux rate. The CO<sub>2</sub> flux rates were then averaged for the three replicates. The average background CO<sub>2</sub> flux rate was then used to determine the CO<sub>2</sub> flux rate due to NSZD for corresponding sampling campaign at the LNAPL impacted sites. The CO<sub>2</sub> flux rates were then converted to a NSZD rate in L LNAPL ha<sup>-1</sup> yr<sup>-1</sup> using octane as the representative LNAPL (density of 703 kg m<sup>-3</sup>).

E-Flux CO<sub>2</sub> traps were installed at five locations (Table 37) and deployed between 17 and 24 September 2019. Appendix A.1 provides additional details of the E-Flux method. The total fossil fuel CO<sub>2</sub> in the sample was corrected based on results for a travel blank sample. An additional correction was made for background CO<sub>2</sub> fluxes using carbon isotope <sup>14</sup>C analysis.

**Table 37 Locations where surface carbon dioxide flux was measured using LI-COR chamber method and E-Flux sorbent trap method**

Method	Sampling campaign	Location
LI-COR	May 2019	MW169 (background; two locations), CS01, CS02, CS06, MW31, MW125, MW157 (2 locations), MW128, MW137, MW171 (two locations), MB14CL051, MB14CL052
LI-COR + E-Flux	September 2019	MW169 (background), CS01, CS06, MW31, MW125

### 5.4.3 NSZD: LNAPL compositional analyses to assess the extent of weathering

LNAPL sampling involved lowering a 40 mL VOA vial directly into the well on nylon fishing line to just below the fluid (LNAPL) interface and the vial was retrieved, capped and sent to the laboratory for analysis.

#### *LNAPL analysis using GC-FID and GC-MS*

GC-FID analysis of LNAPL samples (C<sub>4</sub>–C<sub>40</sub> carbon range) was performed at CSIRO, using an HP 6890 GC fitted with a vaporising injector (operating in split mode), helium carrier gas, an autosampler and a FID. The GC was equipped with a 60 m x 0.25 mm internal diameter column coated with a 0.25 µm m thick film of dimethyl polysiloxane (DB-1 UI, J&W).

GC-MS analysis (C7–C40 carbon range) of selected components was performed using an Agilent 7890 GC fitted with a vaporizing injector (operating in split mode), with helium as carrier gas, an auto-sampler and an Agilent 7000 mass spectrometer. The LNAPL samples (5 µL) were diluted in dichloromethane containing internal standards (*d*6-benzene, *d*8-toluene, *d*10-p-xylene, *d*8-naphthalene and *d*34-hexadecane) to allow quantitation of selected analytes. The GC-MS was fitted with a capillary GC column (Phenomenex, ZB-1ms, 30 m length, 0.25 mm internal diameter and 0.25 µm thick film of dimethyl polysiloxane or equivalent column). The mass spectrometer was operated with an ionisation energy of 70 eV at 230 °C in scan mode. Quantitation of selected compounds was performed using external standards containing the same internal standards used for the samples.

#### *Estimating LNAPL mass losses*

Estimated percentage mass losses over a time period were based on concentration increases in the LNAPL of a conservative tracer (one of the most non-volatile, water insoluble and biodegradation resistant components present in the samples) as a result of other components decreasing in the LNAPL due to volatilisation, dissolution and biodegradation. Pristane was selected in this instance as it was unaffected by volatilisation, dissolution and biodegradation in the LNAPL samples studied (the ratio of pristane to phytane is constant at locations over time, suggesting pristane and phytane are unaffected by biodegradation). Pristane concentration changes in the LNAPL samples from individual locations over time at the site allowed estimation of LNAPL losses to be calculated at individual locations, such that where a concentration of pristane (w/w) in an LNAPL sample twice that of less weathered LNAPL would afford an estimated loss of 50% (w/w). Estimates of LNAPL depletion or losses over time were based on changes in the pristane concentration (conservative tracer, H) using Equation 4 (See Section 2.4).

## **5.5 Results**

### ***5.5.1 Estimation of total hydrocarbon mass removal by active recovery***

Table 38 summarises mass recovery data. Recovery ranged from 6 to 13 L day<sup>-1</sup> (approximately 1.8–3.8 t yr<sup>-1</sup>) with short term LNAPL recovery peaking at 33 L day<sup>-1</sup>. Recovery rates in these active recovery trials were dominated by the water table elevation. Between the single and dual phase recovery operations in 2012 and the more aggressive technologies in 2013, there was a single torrential rainfall event of 226 mm, resulting in a 3 to 4 m water table rise. This caused much of the mobile LNAPL becoming water occluded, immobile and largely unrecoverable during these operations.

**Table 38. LNAPL recovery operations at site C over a three-year period (SiteC\_Ref13 2014)**

Method	Relative water table condition	Average in-well LNAPL thickness (m)	Short term LNAPL recovery rate (L/day)	Long term LNAPL recovery rate (L/day)	Water made during recovery (L/d)	Comments
Total fluids/skimming and drawdown	Low	0.5	33	6	2000 to 5000	--
VER	0.5 m higher than in 1. above	0.01 to 0.07	9	3.5	2250 to 7300	Comparable LNAPL mass recovery with vapour phase
MPE	As for VER above	0.006		13	430 to 16,600	Less LNAPL recovered in vapour phase

### **5.5.2 NSZD rate results: measurements and total site-wide rate estimates**

#### **Temperature results**

Interpretation of the recent data by CSIRO (this study), reveals the background corrected NSZD rates based on the manual thermistors range from 0 to 12,531 L LNAPL ha<sup>-1</sup> yr<sup>-1</sup> and 0 to 3638 L LNAPL ha<sup>-1</sup> yr<sup>-1</sup> for May and September, respectively. Several NSZD rates derived from iButton data are shown for comparison (Table 39).

The polygon areas used to compute site-wide total NSZD rates for the thermistor results are shown in Figure 35. The site-wide total NSZD rates for the manual thermistor-based method are 35 and 11 t yr<sup>-1</sup> for May and September, respectively. The outline surrounding the measurement locations for NSZD encompasses 175,553 m<sup>2</sup> (18 ha).

**Table 39. Summary of results for NSZD based on manual thermistors from May and September 2019 and average NSZD values\* based iButton data**

Well location	Date	Manual thermistors NSZD (L LNAPL ha <sup>-1</sup> yr <sup>-1</sup> )	iButtons NSZD (L LNAPL ha <sup>-1</sup> yr <sup>-1</sup> )
CS01	7 May 2019	3483	
CS01	24 Sept 2019	262	
CS02	25 Sept 2019	3638	
CS03	7 May 2019	11,248	6940*
CS03	24-26 Sept 2019	-	2440*
CS06	7 May 2019	12,531	
CS06	25 Sept 2019	2182	
MB14CL051	7 May 2019	0	
MB14CL052	7 May 2019	0	3460*
MB14CL052	24 Sept 2019	0	1300*
MB14CL057	7 May 2019	2122	
MB14CL063	7 May 2019	7773	
MB14CL063	25 Sept 2019	1962	
MW125	7 May 2019	0	
MW125	24 Sept 2019	0	
MW128	7 May 2019	4333	
MW157	7 May 2019	8325	0*
MW157	24 Sept 2019	1998	0*
MW171	7 May 2019	0	
MW19	7 May 2019	0	
MW19	24 Sept 2019	0	
MW31	8 May 2019	0	
MW31	25 Sept 2019	3547	
MW42	10 May 2019	11,441	
MW42	25 Sept 2019	2528	
MW169 (background)	May and Sept 2019	0	

\* Note: iButton data is composed of averages of 15 minute readings for 10–31 May and 24–26 September 2019.



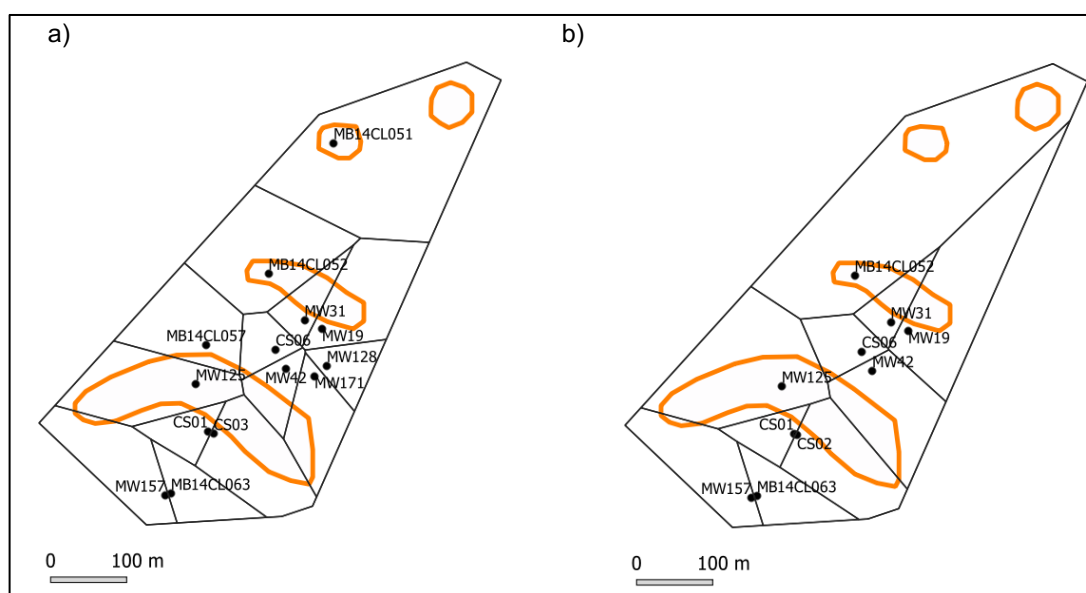


**Figure 35. Voronoi polygon areas constructed using QGIS for thermistor measurement locations for site C in (a) May 2019 and (b) September 2019. The inferred extent of LNAPL as of October 2017 is shown for reference (in orange).**

## Gas sampling results

A major rainfall event of ~460 mm occurred at site C 40 days prior to the initial sampling campaign in May 2019. As discussed in Section 5.2, these intense rainfall events have a profound effect on the water table elevation. As such groundwater levels during the May 2019 sampling campaign were at near peak levels and groundwater levels were above the screened interval of many of the monitoring wells. For the monitoring wells sampled across both sampling campaigns the depth to the air-LNAPL/water interface fell by between 0.64 and 3.38 m.

NSZD rates determined from in-well gas measurements were too uncertain to compute site-wide total rates for comparison with other methods and active recovery. The method relies on connection between the headspace within the monitoring bore and the formation via the well screen to measure gases influenced by hydrocarbon biodegradation. Of the monitoring wells considered for in-well gas measurements, screened interval details were only available for four of them. In May 2019, only two wells had exposed screened intervals, while in September 2019 there were four wells as the water table had dropped over between 2 and 3 m over this time.

Critically for the analysis of the results the groundwater level in the background (MW169) was above the screened interval in both May and September.

Despite the inability to correct for background oxygen consumption, the in-well gas data indicates that degradation is occurring (Table 40). The rate determined for MW157 is consistent between the sampling campaigns and upon the fall in groundwater levels the September NSZD rates for CS02 and MB14CL063 show a similar magnitude to MW157. Despite not knowing the screen interval it appears that MW125, MW19 and MW42 may also be indicative of NSZD. While a substantial decrease in groundwater level was observed at MW31 (~3 m) it appears from the O<sub>2</sub> concentrations and calculated NSZD rates that degradation is low at this location or the screen interval is deeper than 4.5 m.

**Table 40 Summary of uncorrected NSZD rates based on in-well gas data (O<sub>2</sub>) and fluid level at the time of measurement. NSZD rates in bold are reliable readings and those in italics are uncertain either from lack of screen interval data or fluid levels above the screen interval**

Well ID	Screen interval (mbg)	Top fluid elevation (mbg)	NSZD (L ha <sup>-1</sup> yr <sup>-1</sup> )	Top fluid elevation (mbg)	NSZD (L ha <sup>-1</sup> yr <sup>-1</sup> )
		May 2019		September 2019	
<b>MW157</b>	2.0 – 8.0	3.96	<b>3150</b>	6.52	<b>2300</b>
<b>CS03*</b>	3.0 – 12.5	3.68	<b>225</b>	6.32	nd
<b>CS02*</b>	4.5 – 12.5	3.75	<i>140**</i>	6.35	<b>1630</b>
<b>MB14CL063</b>	4.75 – 8.75	4.50	<i>180**</i>	7.07	<b>2330</b>
<b>MW125</b>	Unknown	4.29	<i>3120</i>	6.81	<i>2140</i>
<b>MW137</b>	Unknown	4.64	<i>470</i>	Nd	nd
<b>MW19</b>	Unknown	1.82	nd	4.73	<i>3030</i>
<b>MW31</b>	Unknown	1.58	<i>190</i>	4.51	<i>49</i>
<b>MW42</b>	Unknown	2.59	nd	5.90	<i>1130</i>

\* Monitoring well open (uncased) over screen interval; \*\* NSZD rate compromised due to fluid levels above the screened interval; nd = not determined.

## Soil surface carbon dioxide flux results

### LI-COR results

The total soil respiration rates (TSR, natural plus contaminant CO<sub>2</sub> flux) based on uncorrected LI-COR data for May 2019 range between 750 and 13,400 L ha<sup>-1</sup> yr<sup>-1</sup> and for September between 1,660 and 17,600 L ha<sup>-1</sup> yr<sup>-1</sup>. However, the TSR rate measured at the background site (MW169, attributable to only natural soil processes) is high relative to other sites, with an average of 10,200 L ha<sup>-1</sup> yr<sup>-1</sup> (standard deviation = 1,570 L ha<sup>-1</sup> yr<sup>-1</sup>, n = 9) in May and 4750 L ha<sup>-1</sup> yr<sup>-1</sup> (standard deviation = 1250 L ha<sup>-1</sup> yr<sup>-1</sup>, n = 2) in September. The high background is likely due to biological activity which decreases from May to September due to the drying of the landscape (see Figure 36). Vegetation cover varies spatially and temporally at the other LI-COR sampling locations (Figure 36), thus would likely have different natural contributions to the TSR.

The only location to record a consistent non-negative background corrected NSZD rate was MW31 with an average of 866 L ha<sup>-1</sup> yr<sup>-1</sup> in May and 12,700 L ha<sup>-1</sup> yr<sup>-1</sup> in September.

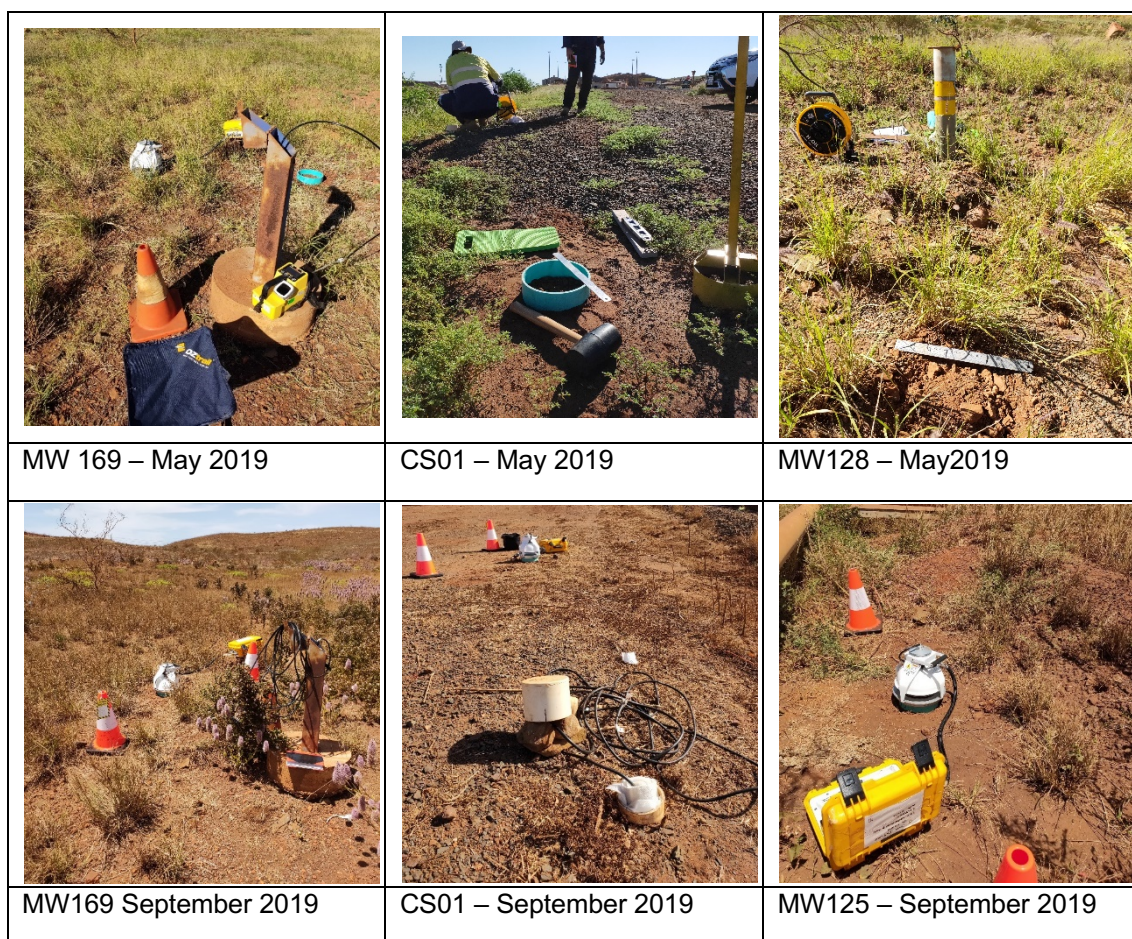


**Figure 36** Examples of LI-COR installations and changes in vegetation between the two sampling campaigns

### *E-Flux results*

The analytical results for the E-Flux CO<sub>2</sub> trap sampling are shown in Table 41. The NSZD rates range from 1141 to 10,185 L LNAPL ha<sup>-1</sup> yr<sup>-1</sup>. The E-Flux NSZD rate for MW31 compares well with the LI-COR NSZD rate.

**Table 41. Summary of E-Flux CO<sub>2</sub> trap analytical results from client. Traps deployed for seven days**

Well location	Deployment days	NSZD (L LNAPL ha <sup>-1</sup> yr <sup>-1</sup> )
CS06	7.1	1749
MW31	7.1	10,185
MW125	7.0	1141
CS01	7.1	1319
MW169 (background)	7.1	0

The polygon areas used to compute site-wide total NSZD rates for the soil surface carbon dioxide flux results are shown in Figure 37. The site-wide total NSZD rates for the E-Flux method is 69 t yr<sup>-1</sup>. This site-wide NSZD rate is likely to overestimate considering the site with the highest rate (MW31) represents more than half the area while the other three locations showed approximately one tenth of the rate (Table 41).

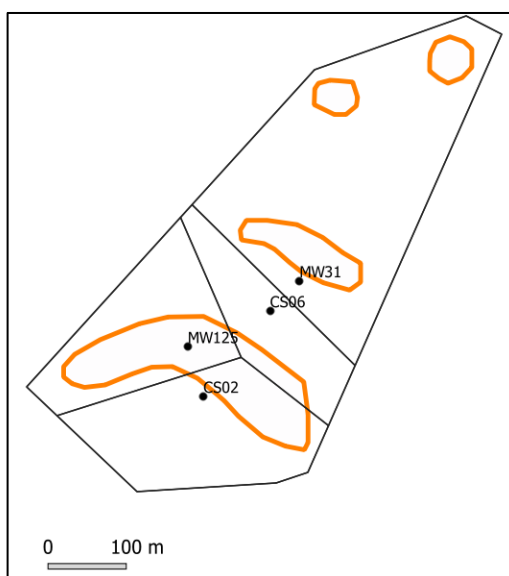


**Figure 37. Voronoi polygon areas constructed using QGIS for the E-Flux measurement locations for site C.**

### **5.5.3 NSZD results: LNAPL composition**

The LNAPL samples from site C spanned up to a ~seven year time period (2011 to 2018) and consisted of weathered diesel (except location MW31 which also contained lube oil range product) as the relative abundance of hydrocarbon carbon range present is Gaussian with a limited carbon range (C9 to C28, Appendix Figures C.1-1 to C.1-8) typically observed in diesel fuels (C8 to C28). Density and analytical results for LNAPL samples from site C are shown in Appendix Table C.1-1.

The weathering of the samples obtained in 2011 to 2013 has resulted in the depletion of *n*-alkanes (except samples MW19, MW31 where *n*-alkanes were removed). Whereas weathering has resulted in the complete removal of *n*-alkanes in the LNAPL samples obtained in 2018 (except sample MB14CL052 where *n*-alkanes were still present and depleted due to biodegradation). Losses to weathering from 2011 (2011 to 2013) to 2018 ranged from 3% to 21% (some samples had plasticizer contamination, CS02 2013 and MW157 2019).

## **5.6 Overview of hydrocarbon mass removal – recovery and NSZD**

As noted in SiteC\_Ref3 (2014), the remediation efforts at site C only achieved modest LNAPL recovery at best – typically up to  $3.8 \text{ t yr}^{-1}$ . This, perhaps, is not surprising given that observations from the site were that the LNAPL that was encountered in wells lacked any appreciable transmissivity or significant connection to fracture sets.

In comparison, the range of NSZD rates are provided in Table 42. NSZD rates for the iButton results (not spatially weighted) are  $5200 \text{ L LNAPL ha}^{-1} \text{ yr}^{-1}$  (average for May 2019) and  $1300 \text{ L LNAPL ha}^{-1} \text{ yr}^{-1}$  (September 2019). These correspond to  $66 \text{ t yr}^{-1}$  for May and September 2019, respectively (based on  $18 \text{ ha}$  area and  $703 \text{ kg m}^{-3}$ ).

Assuming an historical active recovery estimate of  $3.8 \text{ t yr}^{-1}$ , the NSZD rates are three to 20 times larger (E-Flux method) for Site C.

**Table 42. Tabulation of NSZD rates across methods used and total site-wide mass losses per time**

NSZD methods	Intrinsic rate estimates (L LNAPL ha <sup>-1</sup> yr <sup>-1</sup> )*	Rate mass/time** (t yr <sup>-1</sup> )
Temperature (thermistors)	May 2019: 0 to 13,000 Sept. 2019: 0 to 3,600	May 2019: 35 Sept. 2019: 11
E-Flux	1100 to 10,000	69
iButton	May 2019: 5200 Sept. 2019: 1300	66 <sup>†</sup> 16 <sup>†</sup>

\* Rates have been determined across a number of locations, the range denotes variability across different locations at the site. Values are rounded to two significant figures. \*\* A polygon areal weighting approach has been adopted to determine these rates, with the polygon areas scaled to the LNAPL plume area at the site (18 ha), except where noted (†).

## 5.7 Sources of uncertainty in hydrocarbon mass loss estimation

Uncertainty in determining representative active recovery estimates stem from the high dependency of recovery rates on water table elevation coupled with phase separation issues resulting from emulsified LNAPL associated with MPE. During MPE, high velocities of air, water and LNAPL through the suction straw and extraction manifold create emulsions which makes accurate quantification of LNAPL mass recoveries difficult. Regarding NSZD estimates at site C, one of the main uncertainties relate to the influence of rainfall on soil and groundwater conditions:

- The use of existing infrastructure to measure vadose zone gas concentrations is reliant on the screen intervals intercepting the vadose zone. However, as a result of the high groundwater levels across the site and potentially the purpose of the monitoring wells (e.g. LNAPL or groundwater) this methodology was of limited use at site C, especially in determining site-wide NSZD rates.
- Enhanced vegetation and associated biological activity were potentially increased across the site. It is likely that the increase in biological activity was not uniform being higher at the background, thus the background correction of the LI-COR data may overestimate the contribution of natural soil respiration to the total soil respiration reducing the NSZD rate.
- The antecedent moisture conditions are likely to influence the soil properties used to calculate NSZD rate (i.e. thermal conductivity and gas diffusion coefficient). Literature values for similar soil types were used with no vertical variability which may over- or under-estimate the NSZD. This may potentially be the reason for the variability observed between the two sampling campaigns. The only way to decrease uncertainty is to measure these properties and moisture conditions on-site.

The stratigraphy at site C is also complex with clays overlying highly weathered basalt and fresher basalt with different degrees of fracturing. Representing this profile with a single value for either thermal conductivity or gas diffusion coefficient was a necessary simplification due to the lack of data on these parameters. This introduces uncertainty along with the use of literature values.

The site wide NSZD rates have been calculated by different measurement techniques over two sampling campaigns at accessible locations. Spatial representation of measurements over the 18 ha area may require some additional analysis due to the difficulty in accessing some areas due to heavy infrastructure and operations.



## 6. Site D

---

### 6.1 Introduction

Site D consists of a former petroleum depot (SiteD\_Ref1 2011). LNAPL contamination is due to leaks from storage tanks and pipes and/or surface spills over several decades (SiteD\_Ref1 2000; SiteD\_Ref2 2011). The petroleum in the subsurface at site D contains a mixture of different product types including gasoline, kerosene, diesel and lube oil range products (C5–C40 carbon range) in various proportions (Appendix Figure D.1-1 to D.1-6). Density and analytical results for samples from site D are shown in Appendix Table D.1-1.

### 6.2 Site description

LNAPL contamination extends from the former petroleum depot into adjacent residential areas and parkland. The topography slopes gradually to the southeast and a river is located approximately 500 m from the boxed area shown in Figure 38. The direction of groundwater flow is to the southeast.

#### ***6.2.1 Distribution of wells and measurement methods***

Figure 38 indicates the locations of monitoring wells and methods referred to in this report. Background monitoring wells were OS68 for in-well gases, and OS36 for in-well gas, thermistor, and iButton measurements.

#### ***6.2.2 Profile stratigraphy***

According to drilling logs, the area is underlain by between 2 and 4 m of clay and sandy or silty clay overlying fractured, variably-weathered basalt (SiteD\_Ref6 2014; SiteD\_Ref9 2017). Figure 39 and Figure 40 show geologic cross-sections along east–west and north–south transects, respectively, that were constructed using the drilling log descriptions.

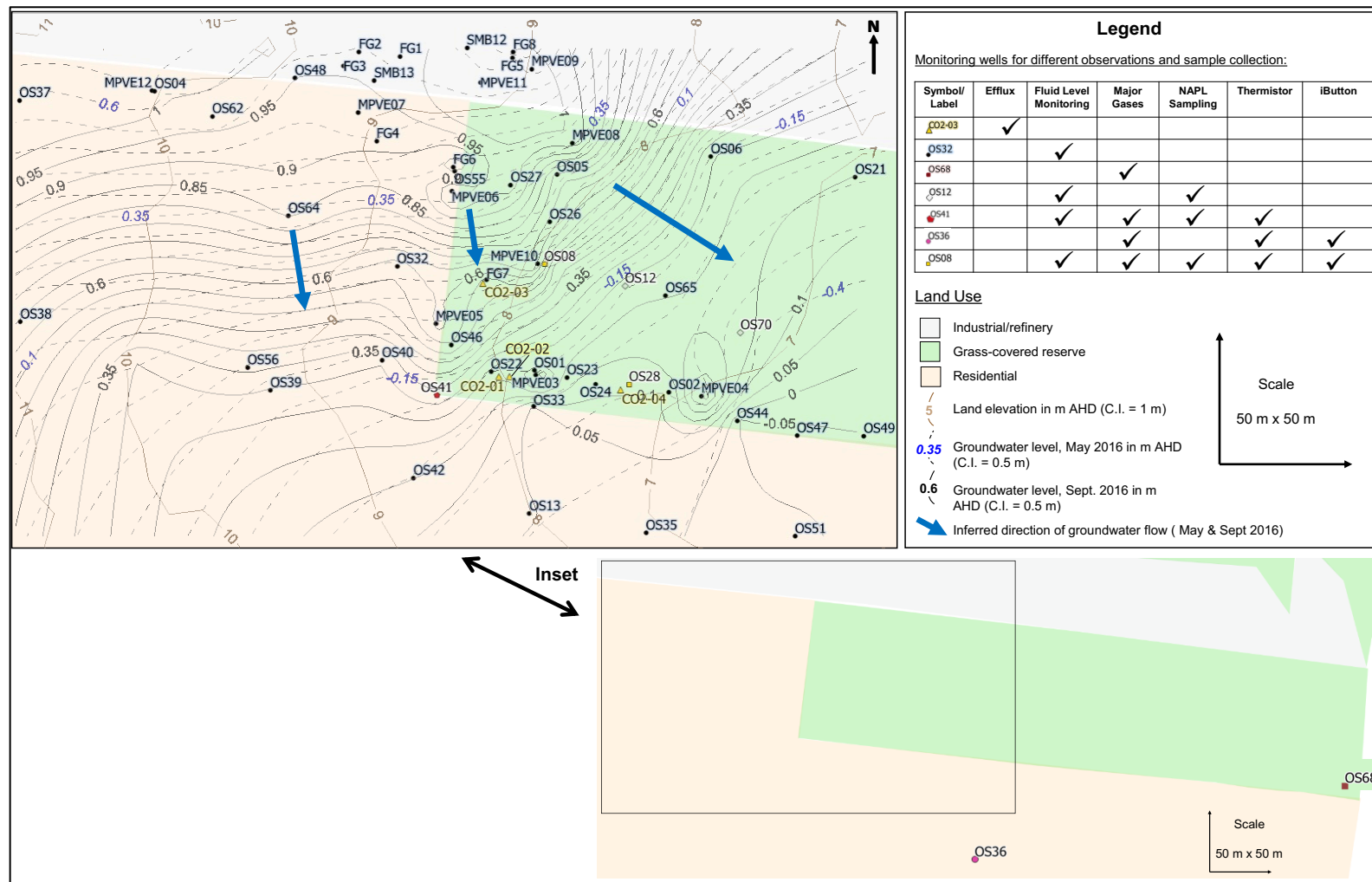


**Figure 38. Distribution of monitoring sites at site D and land use. Groundwater contours are depicted for the months of minimum and maximum groundwater levels in 2016, May and September respectively (CSIRO 2019). Land elevation from multiple surveys, latest 2015 (Geoscience Australia 2015). A river is located approximately 500 m east of the area.**

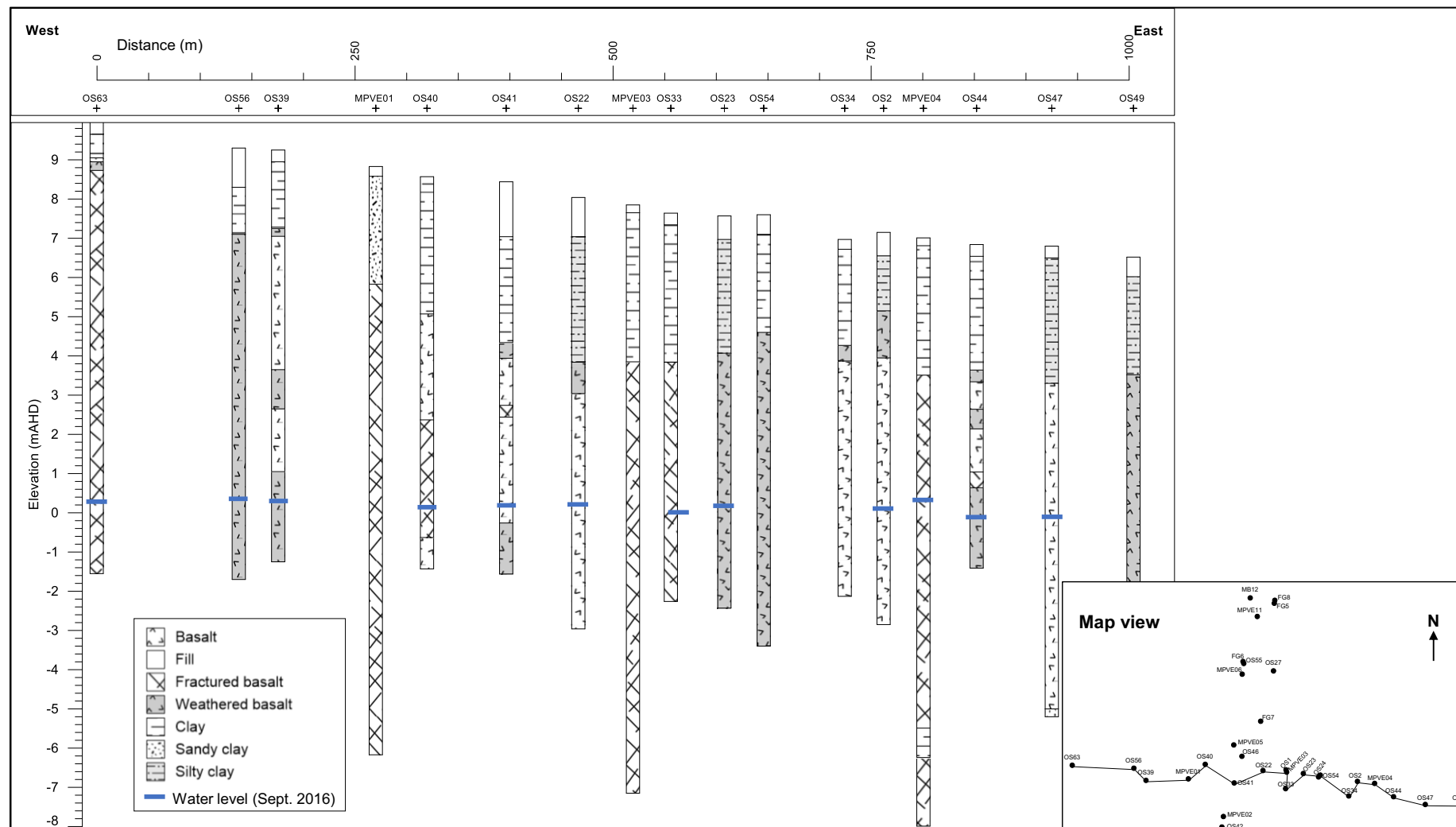


**Figure 39. Geological cross-section (east-west) based on logs provided in SiteD\_Ref6 (2014) and SiteD\_Ref9 (2017). LNAPL-corrected groundwater levels for September 2016 (CSIRO 2019 b). The inset shows the well locations in map view.**



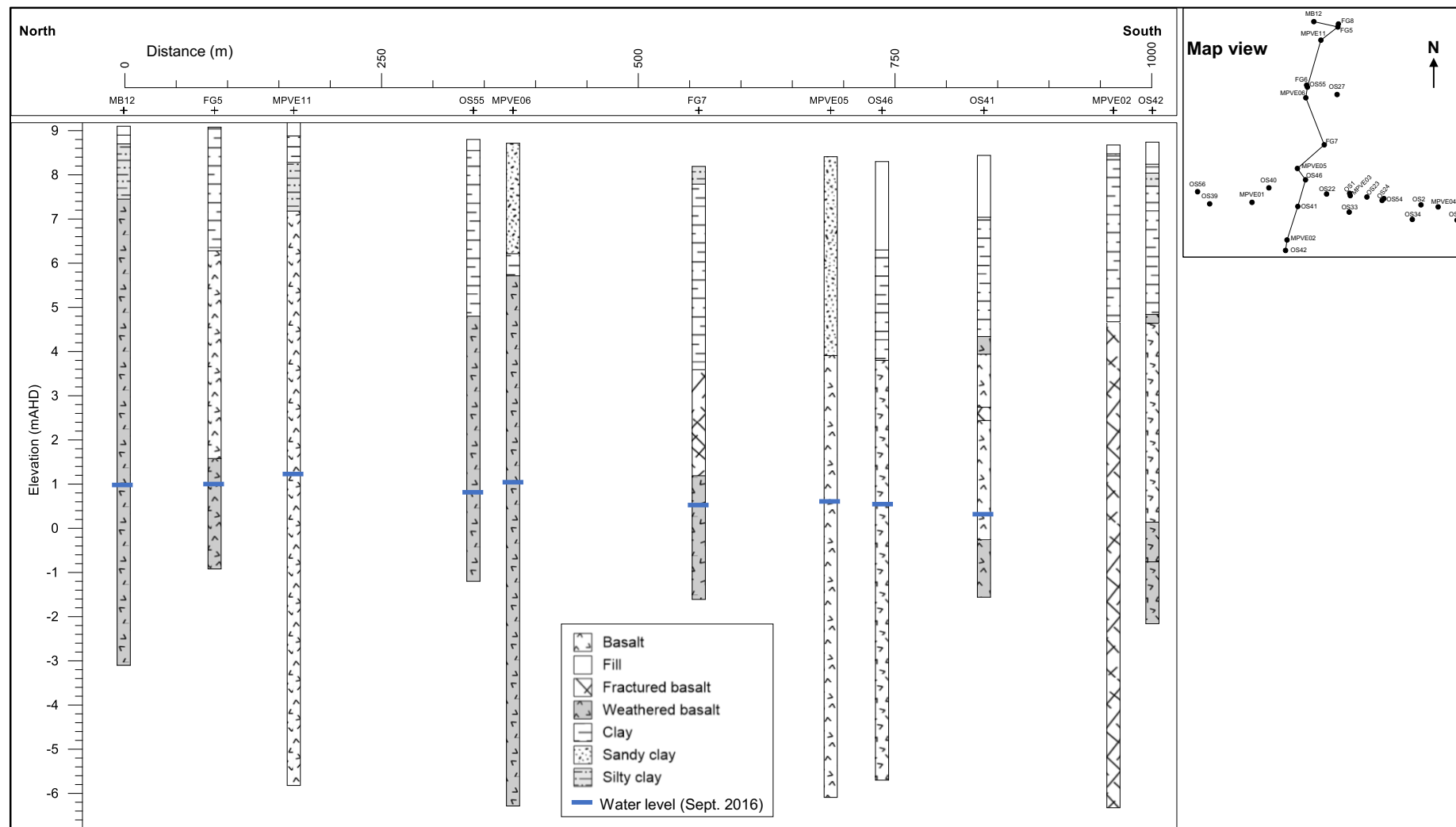


**Figure 40. Geological cross-section (north–south) based on logs provided in SiteD\_Ref6 (2014) and SiteD\_Ref9 (2017). LNAPL-corrected groundwater levels for September 2016 (CSIRO 2019 b). The inset shows the well locations in map view.**

## 6.3 Data supplied by site owner and other data

### 6.3.1 Hydrogeological parameters

None of the reports available contain hydrogeological parameters specifically for site D. However, pump tests were conducted in the same geological setting approximately 400 m north-east of the site (relative to the centre of the boxed area in Figure 38, SiteD\_Ref8 2014). Estimates of transmissivity ( $T_w$ ) for six individual wells, located approximately 400 m north-east of the site, range from 0.21 to 0.49  $\text{m}^2 \text{day}^{-1}$  (geometric mean of 0.31  $\text{m}^2 \text{day}^{-1}$ ) and the specific yield varied from 0.0011 to 0.0021 (SiteD\_Ref8 2014).

In view of regional studies of the volcanic strata (SiteD\_Ref1 2000) and the geologic logs for site D (SiteD\_Ref6 2014; SiteD\_Ref9 2017), it would seem the hydraulic properties of the basaltic aquifer are highly variable due to the heterogeneous and anisotropic nature. There may be high permeability joint opening and vesicles in the basalt, juxtaposed with clayey horizons, weathered zones and dense basalt that may act as aquitards. The hydraulic parameters are likely highly variable, depending on the development of secondary porosity. A report referring to the area approximately 400 m north-east of site D describes groundwater occurring in a discontinuous, perched aquifer consisting of fill material and silty clay, weathered basalt overlying the fractured basalt (SiteD\_Ref11 2018). A summary of regional hydraulic properties of the basalt aquifer indicates a range of hydraulic conductivity (0.18–35  $\text{m day}^{-1}$ ), transmissivity (40–170  $\text{m}^2 \text{day}^{-1}$ ) and porosity 1–5% (SiteD\_Ref1 2000).

### 6.3.2 Well construction and mean groundwater levels

There are 14 well construction and accompanying lithology logs provided in SiteD\_Ref6 (2014) and 123 additional logs provided in SiteD\_Ref9 (2017). A representative selection of eight well construction logs are shown in Appendix D.2.

A large dataset of LNAPL-corrected groundwater level data was available from the CSIRO fluid levels database for site D from monitoring conducted between 2003 and 2016, with much more frequent monitoring between 2011 and 2016 (mode of 47 measurements conducted per month). Analysis of water levels for 2016 showed significant differences between water levels in May (lowest) and September (highest) with seasonal differences of between 24 and 87 cm in groundwater level based on 53 wells used for contouring (Figure 38). Comparison of groundwater contours for May and September 2016 indicate the seasonal difference in water levels, but generally the same groundwater flow directions (south to south-east) during 2016. Mean groundwater levels vary across the site as shown in cross-section, e.g. in September 2016 groundwater depths were generally 6.8 to 9.6 mbg (Figure 39 and Figure 40). Comparison of groundwater levels for different monitoring wells between 2012 and 2017 (Figure 41) shows similar trends that are likely in response to varying rainfall

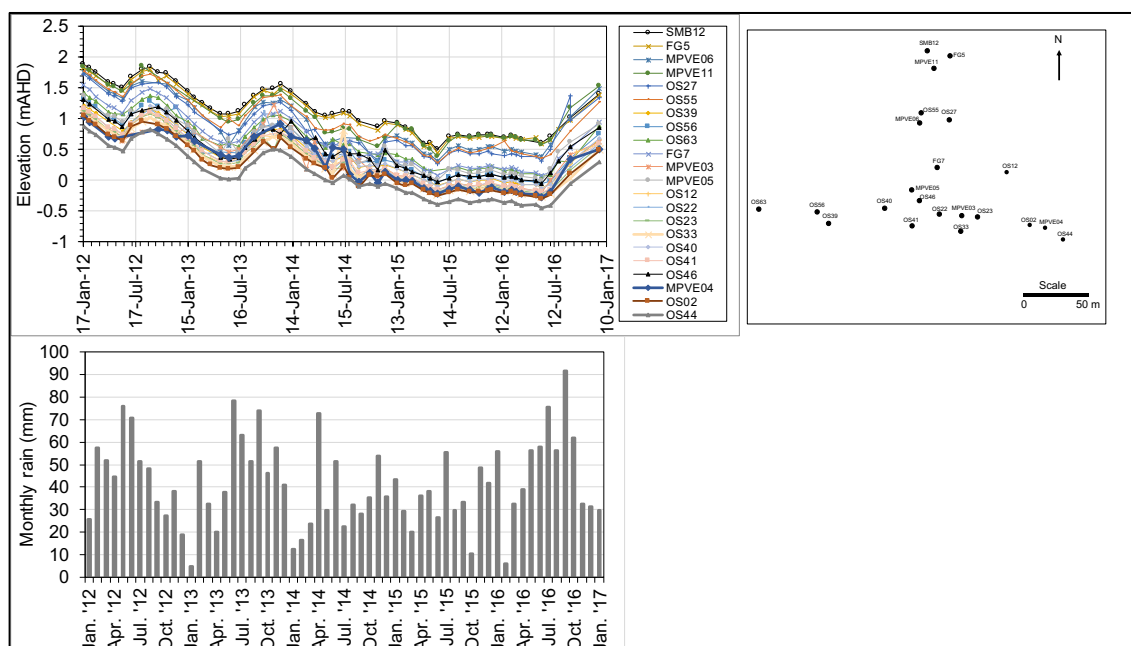


**Figure 41. LNAPL-corrected groundwater levels for a selection of wells along north–south and east–west transects of site D (CSIRO 2019 b). Monthly rainfall is shown for comparison (Queensland Government 2019).**

### 6.3.3 Product thicknesses in local wells on the site over time

LNAPL thickness data for years 2002 to 2017 are shown in Figure 42 for a selection of monitoring wells. According to a review conducted in 2014, the LNAPL thickness greater than 1 m observed in FG5 (September 2006) is likely a mis-observation as it is inconsistent with other observations from this well (SiteD\_Ref7 2014). The LNAPL thickness measured in OS63 in September 2016 (0.97 m) is also a likely mis-observation for the same reason. The review considered spatial variations in LNAPL thickness and noted the following:

‘Spatially, it is difficult to delineate a particular focus for the appearance of LNAPL in wells. However, the area roughly bounded by wells OS32, OS12, OS28, OS33 and OS41 seems to encompass those wells with most notable in-well LNAPL thickness’ (SiteD\_Ref7 2014, p. 15; Figure 42).

As indicated in Figure 42, the most notable in-well LNAPL thicknesses are in OS63, OS12, OS41 and OS22 as of the latest period of available monitoring (2016–2017).

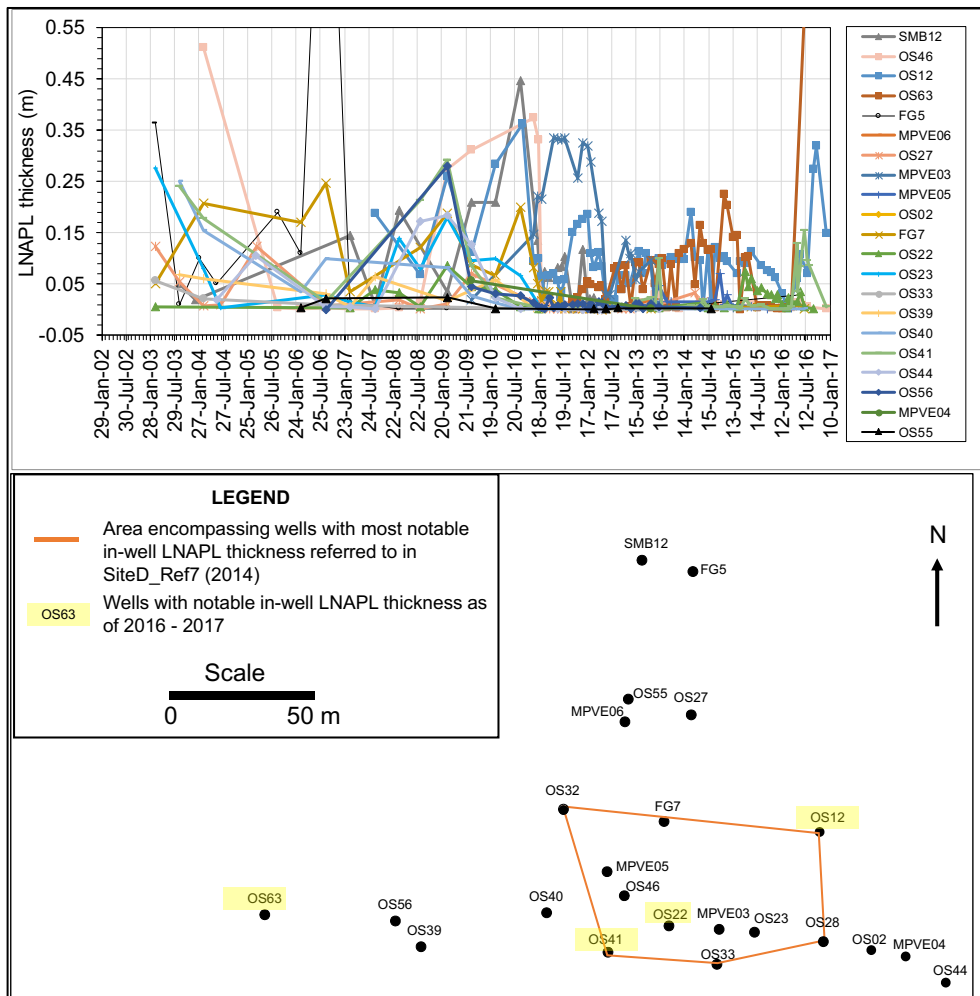


**Figure 42. LNAPL thicknesses for a selection of wells along north–south and east–west transects of site D (CSIRO 2019 b).**

### 6.3.4 Measurements of LNAPL transmissivity

There were no LNAPL transmissivity data provided in the reports for site D.

### 6.3.5 LNAPL compositional analysis and extent of weathering

There are limited historic composition data.

### 6.3.6 LNAPL recovery operations

An historical overview of active recovery at site D is shown in Figure 43 (SiteD\_Ref10 2017). This covers the period from June 2013 to July 2015. The method undertaken was MPE. Daily VOC vapour recovery (in kg) is shown relative to a daily target of 23 kg. As of July 2015, the total VOC mass recovered over the two-year period was 18,880 kg (~19 t, SiteD\_Ref10 2017).

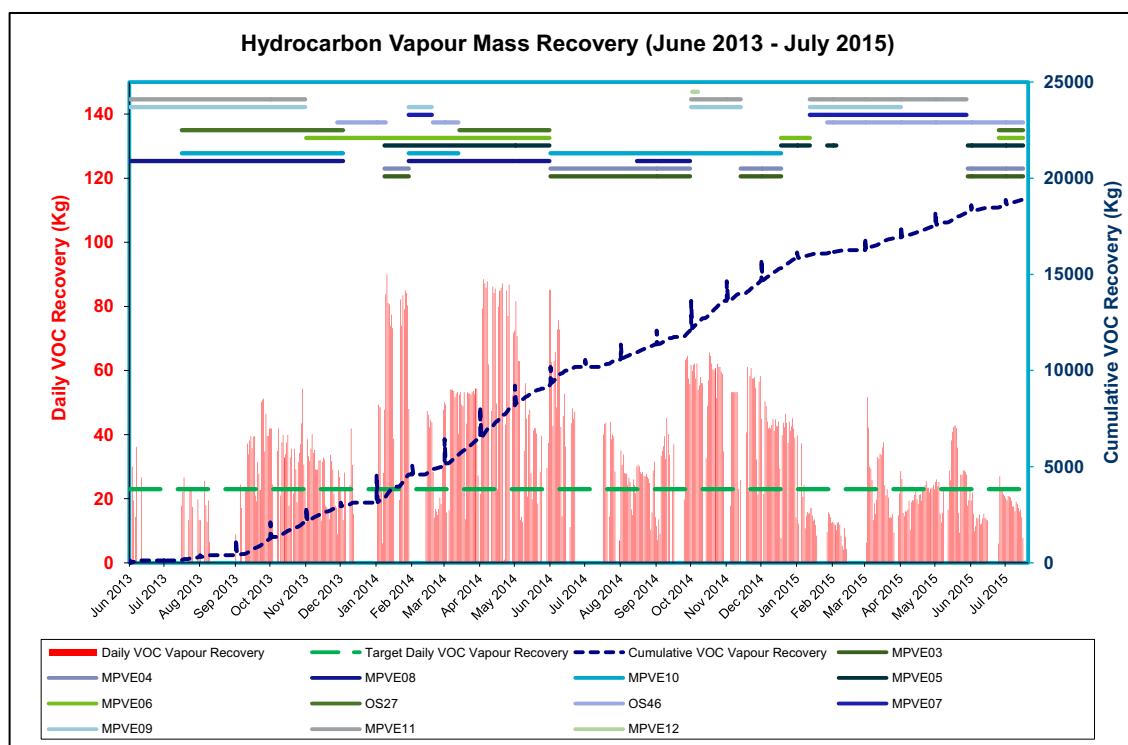


**Figure 43. Daily and cumulative VOC vapour recovery for MPE conducted on 12 extraction wells (SiteD\_Ref10 2017)**

## 6.4 Methods

### 6.4.1 Active recovery

#### Type of method used to recover LNAPL

A catalytic oxidation (CatOx) system was used for vapour extraction. As stated in a review report referring to recovery operations started in June 2013:

‘The MPE system consisted of 12 extraction wells manifolded to a single collection and treatment system. The extraction wells were arranged in three ‘fields’ of four connected wells. The lines from the fields are connected at the treatment system. So far, the system has only operated with extraction from one field at any time’ (SiteD\_Ref7 2014, p. 11).

The fields of extraction wells (four per field) are depicted in Figure 44.

#### How recovery data was estimated

Daily total VOC vapour recovery (in kg) across the 3 manifolds of connected extraction wells that were operating at a given time was used to estimate recovery and was provided as an Excel file (SiteD\_Ref10 2017). Estimates of daily VOC recovered were calculated based on the extraction pump duty and the temperature difference between the inlet and outlet on the CatOx system applying a conversion factor that accounts for the calorific value of fuel to produce the temperature change.

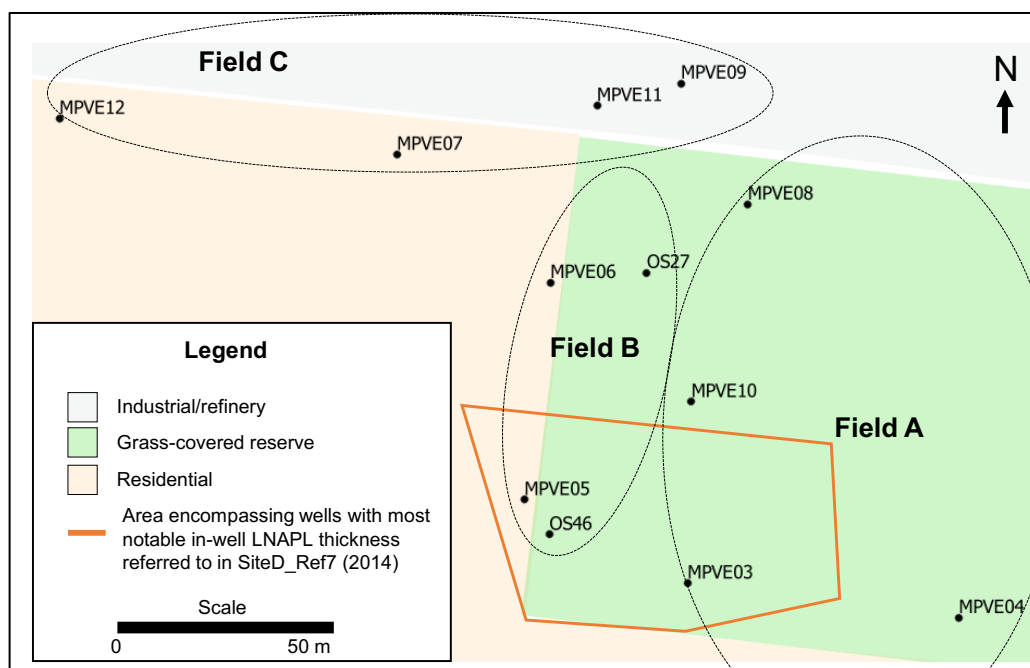


**Figure 44. Groups of four extraction wells per field for MPE conducted between June 2013 and July 2015**

#### 6.4.2 NSZD rate estimation

##### Subsurface temperature measurement and analysis (iButton and thermistors)

Subsurface temperatures were measured using two techniques, instantaneous measurements using thermistors and longer-term temporal measurements using iButtons. Both of these methods involved the hanging of the temperature sensors in existing monitoring wells. Instantaneous temperature measurements were obtained during a sampling campaign on 11 September 2019 while iButtons were installed 5 December 2018–28 February 2019 and for a second period from 11 September 2019 to 1 October 2019. The monitoring wells in which temperature was measured are shown in Table 43.

For the thermistor method a string of thermistors was hung within the monitoring bore for at least 1 hour to equilibrate with the subsurface temperature. The thermistor string was made up of 10 NTC thermistors (10k Ohm Betacurve, 10K3A1B, matched to YSI 44036) spaced at 1 m intervals along a multi-core cable. Electrical resistance was measured using a multimeter (Fluke 28 II Ex) and converted to temperature using the thermistor manufacturer's polynomial calibration algorithm. Background correction and NSZD calculation was done according to the method outlined for site A.

The iButtons were logged temperature at 15 min intervals. This data was assessed and then averaged over either daily or monthly periods which were then corrected against the background well (OS36). The temperature differences were then reviewed and the largest background temperature difference above the water table was used to generate the thermal gradient. The gradient was then multiplied by the thermal conductivity to calculate the heat flux, which was then related stoichiometrically to the LNAPL degradation rate.

**Table 43 Monitoring wells for which manual temperature profiles were recorded and iButtons temperature loggers installed**

Method	Well ID
Thermistor September 2019	OS08, OS28, OS36, OS41, OS63
iButtons	OS08, OS28, OS36

### Gas sampling and analyses (in-well)

Major gas samples were obtained during a sampling campaign conducted on 11 September 2019. Gas concentrations were determined in situ using a portable gas analyser.

Gas sampling was undertaken by lowering a weighted, nylon tube into the well casing such that the intake was 0.3 m above the fluid-air interface determined previously using an interface meter (H.OIL, Heron Instruments Inc.). An Eagle II gas analyser (RKI Instruments) equipped with oxygen, carbon dioxide and methane sensors, was used to measure the gas concentrations. Following zeroing with ambient air the Eagle II was connected to the nylon tubing and readings taken every 30 s for 3 min. Final oxygen and carbon dioxide concentrations were used to calculate NSZD rates.

NSZD rates were determined between the sampling location and the soil surface for in-well major gas using the gradient method described in Section 2.4 and in CRC CARE Technical Report 44 (2018). To calculate NSZD rates, the gradient method for soil gas flux was applied using Equation 2 (see Section 2.4). The effective vapour diffusion coefficient for O<sub>2</sub> and CO<sub>2</sub> were assigned the values of 0.41E-06 and 0.37E-06 m<sup>2</sup> s<sup>-1</sup>, respectively.

### Soil surface carbon dioxide flux measurements (E-Flux)

E-Flux data was supplied for three deployments April 2018 (20 days), October–November 2018 (23 days) and April–May 2019 (16 days). The total fossil fuel CO<sub>2</sub> in the sample was corrected based on results for a travel blank sample. An additional correction was made for background CO<sub>2</sub> fluxes using carbon isotope <sup>14</sup>C analysis.

#### **6.4.3 NSZD: LNAPL compositional analyses to assess the extent of weathering**

LNAPL sampling involved lowering a 40 mL VOA vial directly into the well on nylon fishing line to just below the fluid (LNAPL) interface and the vial was retrieved, capped and sent to the laboratory for analysis.

#### *LNAPL analysis using GC-FID and GC-MS*

GC-FID analysis of LNAPL samples (C4–C40 carbon range) was performed at CSIRO, using an HP 6890 GC fitted with a vaporising injector (operating in split mode), helium carrier gas, an autosampler and a FID. The GC was equipped with a 60 m x 0.25 mm internal diameter column coated with a 0.25 µm thick film of dimethyl polysiloxane (DB-1 UI, J&W).

GC-MS analysis (C7–C40 carbon range) of selected components was performed using an Agilent 7890 GC fitted with a vaporizing injector (operating in split mode), with helium as carrier gas, an auto-sampler and an Agilent 7000 mass spectrometer. The

LNAPL samples (5  $\mu\text{L}$ ) were diluted in dichloromethane containing internal standards (*d6*-benzene, *d8*-toluene, *d10-p*-xylene, *d8*-naphthalene and *d34*-hexadecane) to allow quantitation of selected analytes. The GC-MS was fitted with a capillary GC column (Phenomenex, ZB-1ms, 30 m length, 0.25 mm internal diameter and 0.25  $\mu\text{m}$  thick film of dimethyl polysiloxane or equivalent column). The mass spectrometer was operated with an ionisation energy of 70 eV at 230  $^{\circ}\text{C}$  in scan mode. Quantitation of selected compounds was performed using external standards containing the same internal standards used for the samples.

#### *Estimating LNAPL mass losses*

Estimated percentage mass losses over a time period were based on concentration increases in the LNAPL of a conservative tracer (one of the most non-volatile, water insoluble and biodegradation resistant components present in the samples) as a result of other components decreasing in the LNAPL due to volatilisation, dissolution and biodegradation. Pristane was selected in this instance as it was unaffected by volatilisation, dissolution and biodegradation in the LNAPL samples studied (based on the ratio of pristane to phytane remaining constant at locations over time). Pristane concentration changes in the LNAPL samples from individual locations over time at the site allowed estimation of LNAPL losses to be calculated, where a concentration of pristane (w/w) in an LNAPL sample twice that of less weathered LNAPL would afford an estimated loss of 50% (w/w). Estimates of LNAPL depletion or losses over time were based on changes in the pristane concentration (conservative tracer, H) using Equation 4 (Section 2.4).

## **6.5 Results**

### ***6.5.1 Estimation of total hydrocarbon mass removal by active recovery***

As described in Section 6.3.6, historical data provides an estimate of total VOC mass recovered of the order of 21 tons over a two-year period or about 10  $\text{t yr}^{-1}$ .

### ***6.5.2 NSZD rate results: measurements and total site-wide rate estimates***

#### **Temperature results**

Interpretation of the recent data by CSIRO (this study), reveals the background corrected NSZD rates based on the manual thermistors range from 2837 to 5140 L LNAPL  $\text{ha}^{-1} \text{yr}^{-1}$  for September (Table 44). The background corrected, monthly average iButton data was remarkably similar across the months of December 2018, January 2019, February 2019 and September 2019 and is also presented in Table 44. The iButton NSZD rates are too preliminary for determining site-wide rates using the polygon method.

The polygon areas used to compute site-wide total NSZD rates for the thermistor results are shown in Figure 45. The site-wide total NSZD rates for the manual thermistor-based method is 6.9  $\text{t yr}^{-1}$  for September. The outline surrounding the measurement locations for NSZD encompasses 26,783  $\text{m}^2$  (2.7 ha).



**Table 44. Summary of results for NSZD based on manual thermistors and iButton measurements from September 2019**

Well location	Date	Manual thermistor NSZD (L LNAPL ha <sup>-1</sup> yr <sup>-1</sup> )	iButtons NSZD (L LNAPL ha <sup>-1</sup> yr <sup>-1</sup> )
OS08	11 Sept 2019	3414	1720
OS28	11 Sept 2019	4413	2410
OS41	11 Sept 2019	5140	
OS63	11 Sept 2019	2837	

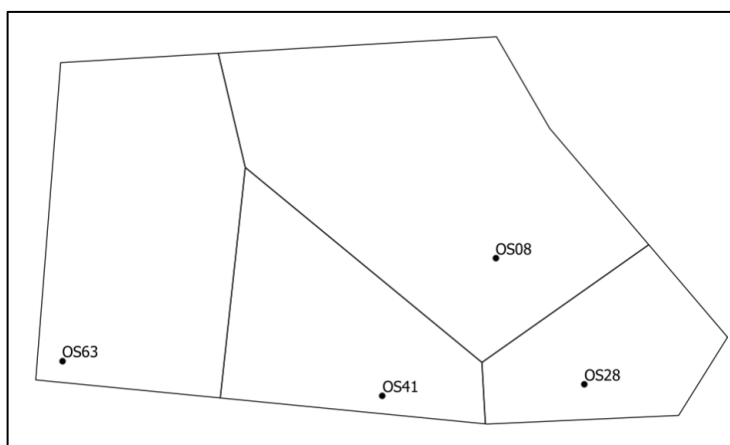


**Figure 45. Voronoi polygon areas constructed using QGIS for thermistor measurement locations for site D in September 2019**

## Gas sampling results

Independent of analysis method and sampling time CO<sub>2</sub> concentrations measured were stoichiometrically less than the depletion in O<sub>2</sub> concentrations associated with hydrocarbon degradation. This discrepancy between the O<sub>2</sub> and CO<sub>2</sub> concentrations could not be satisfactorily explained by the investigators. Thus, NSZD rates were only calculated using the measured O<sub>2</sub> concentrations as subsurface concentrations are related to diffusion of atmospheric oxygen into the subsurface and subsequent hydrocarbon degradation processes.

Based on interpretation of the data by CSIRO (this study), the in-well measurements of O<sub>2</sub> yielded NSZD rates that range from 278 to 1110 L LNAPL ha<sup>-1</sup> yr<sup>-1</sup> for September (Table 45).

**Table 45. Summary of results for NSZD based on in-well gas data (O<sub>2</sub>)**

Well location	Date	NSZD (L LNAPL ha <sup>-1</sup> yr <sup>-1</sup> )
OS08	11 Sept 2019	278
OS28	11 Sept 2019	751
OS41	11 Sept 2019	1110
OS63	11 Sept 2019	1079

To compute site-wide total NSZD rates for the gas in-well sampling results, the polygon areas used for the thermistor sites were used as the same wells were sampled. The site-wide total NSZD rates for the gas in well (O<sub>2</sub>) method is 1.4 t yr<sup>-1</sup>.

### Soil surface carbon dioxide flux results

The results provided by the client from three rounds of E-Flux range from 0 to 4436 L LNAPL ha<sup>-1</sup> yr<sup>-1</sup> (Table 46). Interestingly, rates varied considerably over time. In April 2018 three of the four well locations had some of the highest NSZD rates compared to other dates, whereas the fourth location CO2-03 gave a zero NSZD rate estimate. This location also yielded the lowest rate almost a year later in May 2019, and a low rate in October 2018 but not the minimum across all well locations at this time. The low rates in October 2018 may be related to the relatively high rainfall (55.2 mm) over the deployment period relative to the other two periods (7.0 mm in April 2018 and 1.4 mm in April 2019). Filling of soil pores during wetter periods, especially in finer textured soil potentially resulted in the lower CO<sub>2</sub> surface flux.

**Table 46. Summary of results for NSZD based on three rounds of E-Flux**

Well location	NSZD (L LNAPL ha <sup>-1</sup> yr <sup>-1</sup> )			
	4 April 2018	23 Oct 2018	31 May 2019	Average
CO2-01	4436	1020	3116	2857
CO2-02	3837	1525	1142	2168
CO2-03	0	833	1095	643
CO2-04	2639	374	1114	1376

The polygon areas used to compute site wide total NSZD rates for the soil surface carbon dioxide flux results are shown in Figure 46. The average NSZD rate from Table 46 was used to compute a site-wide total rate. The site-wide total NSZD rate for the E-Flux method based on the average of NSZD rates obtained from three sampling events is 1.9 t yr<sup>-1</sup>.

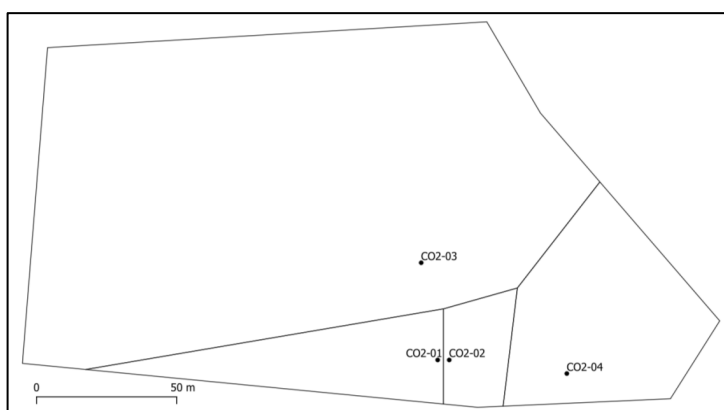


**Figure 46. Voronoi polygon areas constructed using QGIS for the E-Flux measurement locations for site D**

### 6.5.3 NSZD results: LNAPL composition

OS08, OS12, OS28, OS41, OS70

LNAPL from locations OS08, OS12, OS28, OS41 and OS70 consisted of weathered gasoline, kerosene, diesel and lube oil range products (Appendix Figures D.1-1 to D.1-5). From 2013 to 2018 mass losses for these samples maximised at 14% (Appendix Table D.1-1), losses were mainly due to losses of the lighter components in the gasoline range.

The weathered gasoline range product in these samples was depleted in *n*-alkanes, likely containing leaded gasoline (due to the presence of tetraethyllead based on GC-MS analyses as well as the complexity of the gasoline range product suggesting it was not highly refined) and unleaded gasoline (due to the presence of isooctane). From 2013 to 2018 the already depleted aromatics in the 2013 samples have been almost completely removed by 2018. The extent of weathering the diesel and lube oil range products have experienced in the 2013 samples has resulted in the almost complete removal of the *n*-alkanes and a steady decline in *n*-alkanes over time based on the pristane/*n*C17 ratio.

OS63

LNAPL from location OS63 consisted of weathered gasoline, kerosene and diesel range products, and contained a higher proportion of gasoline range product than the other samples from the site (Appendix Figures D.1-6). From 2013 to 2018 losses were estimated to be 24% (Appendix Table D.1-1) with the losses mainly due to losses of the lighter components as well aromatic components in the gasoline range (with the more water-soluble components suggesting significant losses to dissolution).

The weathered gasoline range product was depleted in *n*-alkanes and contained leaded gasoline (due to the presence of tetraethyllead based on GC-MS analyses as well as the complexity of the gasoline range product suggesting it was not highly refined) and a higher proportion of unleaded gasoline than other samples from site D (due to the higher relative abundance of isooctane). From 2013 to 2018 the already depleted aromatics in the 2013 LNAPL sample have been almost completely removed by 2018. The extent of weathering the diesel range product has experienced in 2013 resulted in the depletion of the *n*-alkanes and shows further depletion of the *n*-alkanes in the 2018 LNAPL sample (Pr/*n*C17 in 2013 1.9 and 6.7 in 2018, Appendix Table D.1-1).

## 6.6 Overview of hydrocarbon mass removal – recovery and NSZD

An estimate of the last six months of LNAPL recovery in 2015 is about 5.8 t yr<sup>-1</sup>. In comparison, the range of NSZD rates are provided in Table 47. The NSZD rate for the iButton results (not spatially weighted due to insufficient data points) is 2065 L LNAPL ha<sup>-1</sup> yr<sup>-1</sup> (average for September 2019), which corresponds to 3.9 t yr<sup>-1</sup> based on 2.7 ha area and 703 kg m<sup>-3</sup>. Polygon areal weighting yields NSZD rates of 1.4 to 6.9 t yr<sup>-1</sup> (Table 47). Overall current NSZD rates range from a factor of 4 lower to around 20 % higher than LNAPL recovery rates from 2015.

**Table 47. Tabulation of NSZD rates across methods used and total site-wide mass losses per time**

NSZD methods	Intrinsic rate estimates (L LNAPL ha <sup>-1</sup> yr <sup>-1</sup> )*	Rate mass/time (t yr <sup>-1</sup> )**
Temperature (thermistors)	Sept. 2019: 2800 – 5100	Sept. 2019: 6.9
Gas sampling (in-well, O <sub>2</sub> )	Sept. 2019: 280 – 1100	Sept. 2019: 1.4
E-Flux	0 to 4400	1.9
iButton	Sept. 2019: 2065	3.9 <sup>†</sup>

\* Rates have been determined across a number of locations, the range denotes variability across different locations at the site. Values are rounded to two significant figures. \*\* A polygon areal weighting approach has been adopted to determine these rates, with the polygon areas scaled to the LNAPL plume area at the site (2.7 ha), except where noted (†).

## 6.7 Sources of uncertainty in hydrocarbon mass loss estimation

One of the main uncertainties associated with estimation of NSZD rates for site D is related to the limited spatial coverage of sampling locations with only 4 within the 2.7 ha zone of highest LNAPL thickness. While limited the existing bore network (Figure 38) does offer the potential to conduct further NSZD measurements to provide greater confidence in site-wide NSZD rates.

The stratigraphy at site D is complex with varying thickness of clay and sandy or silty clay overlying fractured, variably-weathered basalt (Section 6.2.2). Representing this profile with a single value for either thermal conductivity or gas diffusion coefficient was a necessary simplification due to the lack of data on these parameters. This introduces uncertainty along with the use of literature values rather than values either measured in situ or onsite specific materials. Also depending on the antecedent soil moisture conditions flux of CO<sub>2</sub> out of the soil may be limited due to soil water filling the porosity of the soil.

Site D also consists of two main land uses, parkland and residential. The differences in covered surfaces (e.g. houses and roads) between the two different areas may result in different O<sub>2</sub> diffusion into the soil which may influence the degradation rate, however with only limited data it is not clear what role this may play. Thermal methods may also be influenced by the parkland and residential land uses with different heat transfer resulting from shading and different thermal conductivity of the surface materials (soil, grass, concrete, etc.). Shading is known to reduce heat transfer to the ground surface and reduce soil temperatures (Napoli *et al* 2016). The in-well temperature profiles from the manual thermistor measurements indicate that shading from buildings and trees may have resulted in lower temperatures in the upper part of the profile at the selected background location. This corollary of this, is that when these background temperatures are applied as corrections to locations within the source area, larger calculated temperature differences in the vicinity of the ground surface occurs which are unlikely to be caused by biodegradation processes. Therefore, some of this data has not been used to determine NSZD rates. Aspects of this warrant further investigation but reinforce the importance of identifying representative background locations for all the comparative NSZD methods.

## 7. Site E

### 7.1 Introduction

The petroleum contamination at site E was a result of a jet fuel (Jet A1) release in 2014. Jet A1 is a colourless liquid similar to kerosene range products containing C7 to C16 carbon range hydrocarbons with *n*-alkanes the dominant components (Figure 47). Density and carbon ranges for a typical Jet A1 that is likely similar to that released at site E are shown in Table 48.

**Table 48. Density and carbon ranges for a typical Jet A1**

Petroleum type	Carbon range <sup>1</sup>	Density kg m <sup>-3</sup> (15 °C) <sup>2</sup>	Density kg m <sup>-3</sup> (20 °C) <sup>3</sup>
Jet A1	C7–C16	775–840	771–836

<sup>1</sup>CSIRO information; <sup>2</sup>ASTM D1655-18a (2018); <sup>3</sup>Density calculated using AS 2520-1981 (1981) Petroleum measurement tables.

### 7.2 Site description

Site E is in an urban, intensively used, coastal site. The contaminated area is from a leak from a fuel storage facility (SiteE\_Ref1 2017). The fuel storage facility covers an area of about 42 ha and the leak extends beyond the boundary of the facility (SiteE\_Ref2 2017; SiteE\_Ref3 2015). Site E refers to the 0.96 ha investigation area shown as an inset in Figure 48 (SiteE\_Ref1 2017).

Site E has a warm temperate climate with an annual average rainfall of about 1033 mm with occasional intense rainfall due to low pressure events, typically in April and/or June (Queensland Government 2019).

The historical primary sources, including fuel delivery infrastructure remain on site, however, impacted soils from the jet fuel leak were considered to have been largely removed (SiteE\_Ref1 2017). The site is about 320 m west of a tidally-influenced creek and the regional groundwater flow regime is believed to be to the east north east of the site, towards the creek (SiteE\_Ref2 2017).

#### **7.2.1 Distribution of wells and measurement methods**

The land use near site E consists of commercial/industrial properties surrounded by residential or open space (Figure 48). The distribution of wells used for active skimming and the sample locations for the flux chamber and CO<sub>2</sub> traps methods are indicated in Figure 49.

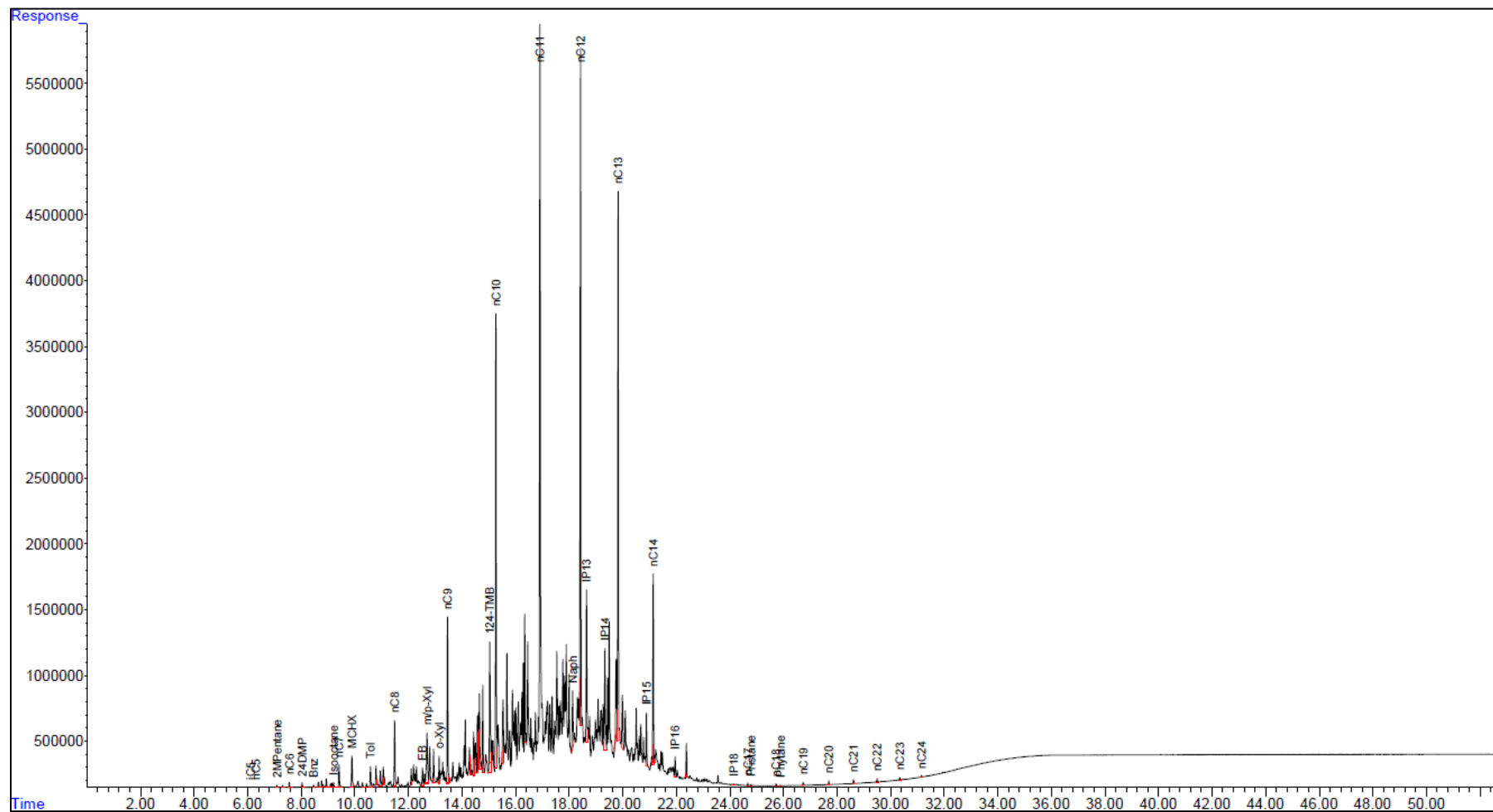
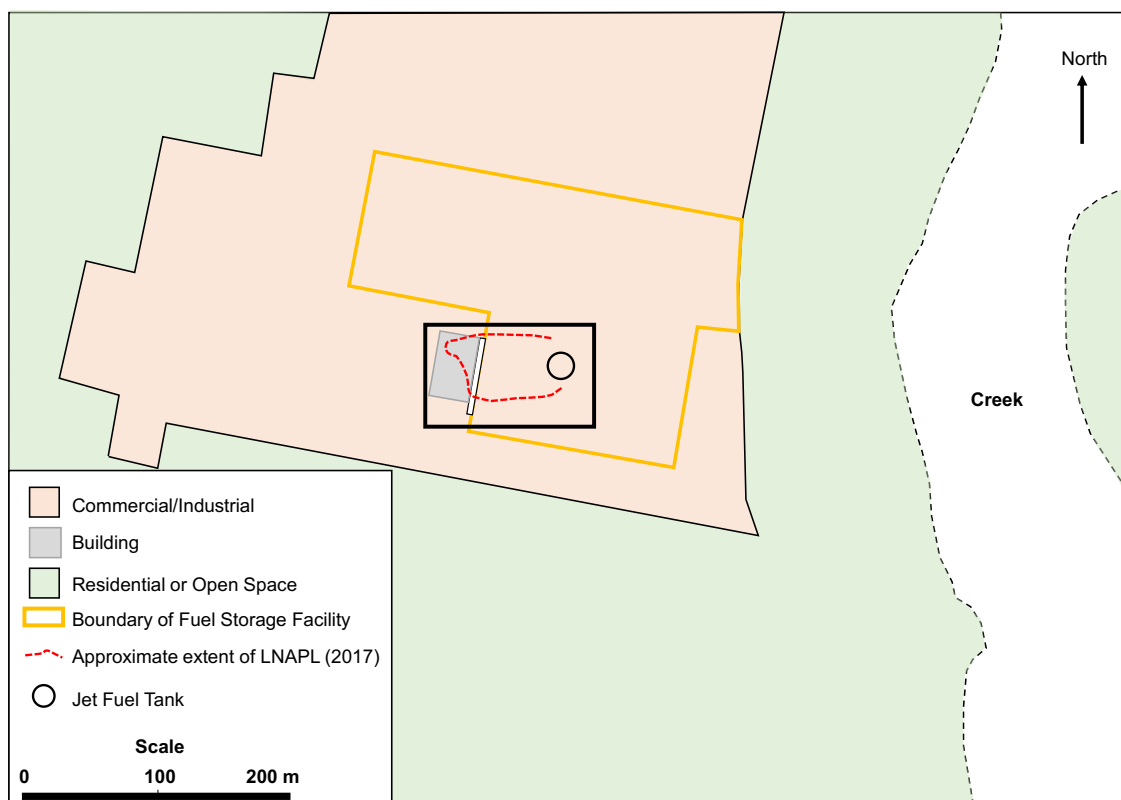
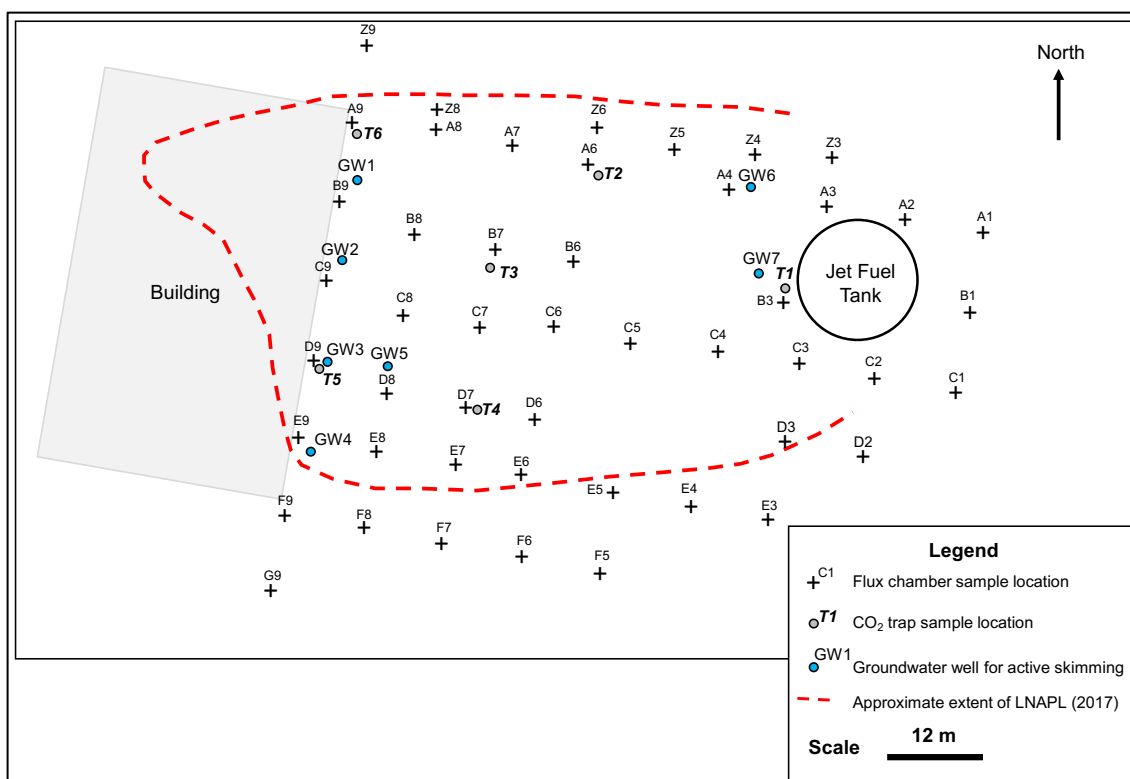


Figure 47. GC-FID analysis of typical Jet A1. B: Benzene, Benz: benzene, CHX: cyclohexane, Cx: straight or branched alkane containing x carbons, D: di, E: ethyl, EtOH: ethanol, i: iso, IP: isoprenoid, M: methyl, MeOH: methanol, n: normal, Naph: naphthalene Pr: pristane, Ph: phytane, Tol: toluene, Xyl: xylene



**Figure 48. Location of site E investigation area relative to land use. Sample and well locations for the boxed area are shown in Figure 49.**



**Figure 49. Sample locations and groundwater wells for site E from SiteE\_Ref1 (2017)**

### 7.2.2 Profile stratigraphy

The site is located on a low-lying alluvial plain consisting of fluvial, coastal and estuarine soil types with sand overlying bedrock composed of conglomerate and sandstone (SiteE\_Ref4 2014). The fluvial environment may mean the shallow horizon is a duplex soil, may have textural contrasts, and may be poorly drained. The soil may also have elevated concentrations of natural organic carbon which can play a role in sorption and also in generating carbon dioxide. Such information is currently unavailable.

The extent of subsurface heterogeneity is not known from the available reports, but descriptions of the catchment's depositional history from publicly available sources indicate fluvial and estuarine processes, which suggests the profile is at least moderately heterogeneous (SiteE\_Ref5 2003; SiteE\_Ref4 2014).

## 7.3 Data supplied by site owner and other data

To preserve the confidential nature of the reports, citations are coded and reference to the file name is given in the Section 12:

- The primary report is referred to as SiteE\_Ref1. It was focused on an assessment of NSZD dated May 2017. It consists of flux chamber and CO<sub>2</sub> trap results and a comparison with active skimming data.
- For this reporting, there were no data sets available of subsurface measurements to determine any NSZD rates from gradient methods (thermal or major gases).
- There was sparse information about the geology and hydrogeology of the location, therefore general references were consulted to provide the site description based on the location of the catchment. SiteE\_Ref1 covered LNAPL recovery operations and LNAPL degradation rates from CO<sub>2</sub> flux measurements (chamber and E-Flux).

General references consulted to provide the site description, included:

- a publicly available document entitled *Preliminary site investigation for contamination in relation to proposed apartment development by an external contractor* (SiteE\_Ref2 2017),
- a publicly available document entitled *pollution incident response management plan* (SiteE\_Ref3 2015),
- a publicly available document on the geology of the coastline (SiteE\_Ref4 2014), and
- a publicly available document on the coast and estuary management (SiteE\_Ref5 2003).

### 7.3.1 Hydrogeological parameters

There were no data provided for this item.

According to SiteE\_Ref2 (2017), the depth to the water table is believed to be <2.5 m below the surface and may be tidally influenced.



### 7.3.2 LNAPL recovery operations

Active skimming (see map of locations) to recover LNAPL was undertaken at the site. Planning for multi-phase vacuum extraction of LNAPL was reported in 2017.

## 7.4 Methods

### 7.4.1 Active recovery

#### Type of method used to recover LNAPL

Skimming for LNAPL recovery occurred between May 2015 and February 2017 (Table 49). SiteE\_Ref1 describes planned recovery via multi-phase vacuum extraction due to have commenced February 2017, but no data or report are available for that activity.

#### How recovery data was estimated

According to SiteE\_Ref1 (2017), active skimming was undertaken using tanks, hoses, downhole pumps, and telemetry and other test equipment. It was conducted in two stages with the target wells indicated in Table 49 (locations in Figure 49). Fluid levels (water and LNAPL) in the tank were measured using a dipstick and confirmed with a bailer. During skimming, levels were recorded using telemetry. Skimmers were regularly removed from the wells for maintenance (SiteE\_Ref1 2017).

The active skimming removal system consisted of four air supply pumps. During both stages of operations, there were periods where the system was stopped due to elevated groundwater levels which reduced the effectiveness of skimming, or the waste tanks reaching the safe fill level (water and LNAPL mixture, SiteE\_Ref1).

Table 49. Details of skimming operations for site E from SiteE\_Ref1

Stage	Period	Target wells
1	13 May 2015 to 30 September 2015	GW2, GW5, GW6, and GW7
2	8 January 2016 to 1 February 2017	GW2, GW5, GW4, GW3, GW1

### 7.4.2 NSZD rate estimation

#### Soil surface carbon dioxide flux measurements (E-Flux and LI-COR flux chamber)

Estimates of NSZD rates were obtained from CO<sub>2</sub> dynamic flux chamber measurements at 48 locations within the bund area, using LI-COR equipment (Figure 49). Readings were taken over the course of several minutes at a given location to estimate the short-term NSZD rates that were then used to determine the most suitable placement of passive CO<sub>2</sub> flux traps (SiteE\_Ref1 2017).

Six locations were instrumented with passive CO<sub>2</sub> flux traps, which remained in place for a total of six days and were subsequently retrieved and submitted to E-Flux, LLC (E-Flux) for laboratory analysis of total CO<sub>2</sub> concentration and the <sup>14</sup>C unstable isotope (SiteE\_Ref1 2017).

Each individual flux chamber result was corrected for background to isolate the portion of the measured CO<sub>2</sub> flux that is derived from fossil fuel/LNAPL (SiteE\_Ref1 2017).

Two different background correction estimates were calculated, one based on the maximum, modern (background) carbon flux from the CO<sub>2</sub> trap results, and another based on the average of the modern carbon fluxes reported in the CO<sub>2</sub> trap results (SiteE\_Ref1 2017). The background correction value was subtracted from each flux chamber result. The corrected flux chamber results were depicted in map view on contour plots (SiteE\_Ref1 2017).

The six laboratory CO<sub>2</sub> trap results were also shown in map view (not contoured) and compared with the flux chamber results. SiteE\_Ref1 comments that some discrepancy is expected between methods due to temporal variability in soil gas flow and because the sample duration is several days for the flux traps versus a few minutes with the flux chamber.

The following assumptions and calculations were used to estimate NSZD rates from CO<sub>2</sub> flux data:

- For flux chamber:
  - A molecular weight of octane (C<sub>8</sub>H<sub>18</sub>) of 114.23 g·mol<sup>-1</sup> and an LNAPL specific gravity of 0.77 (upper range for gasolines, SiteE\_Ref1 2017).
  - Based on the stoichiometry of octane and converting measurement units, this equates to  $625 \frac{\text{US gallon C}_8\text{H}_{18}}{\text{acre}\cdot\text{yr}}$ . This factor was rounded down to 600 U.S. gallons of LNAPL degraded per acre per year in the NSZD rate estimates.
  - It was also assumed that the estimated NSZD rates were representative of a 5-metre radius of influence from a given monitoring point to convert rates in units of volume of LNAPL degraded per unit area per unit time to units of volume of LNAPL degraded per unit time (SiteE\_Ref1 2017).
- For CO<sub>2</sub> trap:
  - The same values as indicated above for the flux chamber method were used, i.e. the molecular weight of octane (C<sub>8</sub>H<sub>18</sub>) of 114.23 g·mol<sup>-1</sup> and an LNAPL specific gravity of 0.77.
  - Converting the CO<sub>2</sub> flux from grams of CO<sub>2</sub> involved the cross-sectional area of the trap and the number of days that the trap was deployed in the field (SiteE\_Ref1 2017).

## 7.5 Results

### 7.5.1 Estimation of total hydrocarbon mass removal by active recovery

The data supplied for this study only referred to stage 2 of skimming, which involved the five wells closest to the building indicated in Figure 49. Active recovery took place over a period of 274 days (SiteE\_Ref1 2017). Several lengthy breaks occurred due to various issues and not all of the five wells were actively skimming simultaneously (SiteE\_Ref1 2017). A total of 208.25 L of LNAPL was recovered. Based on an assumed density of 0.84 kg L<sup>-1</sup> for jet fuel, this is equivalent to about 175 kg. This equates to an average recovery rate of approximately 0.6 kg day<sup>-1</sup> or 0.22 t yr<sup>-1</sup> (SiteE\_Ref1 2017).

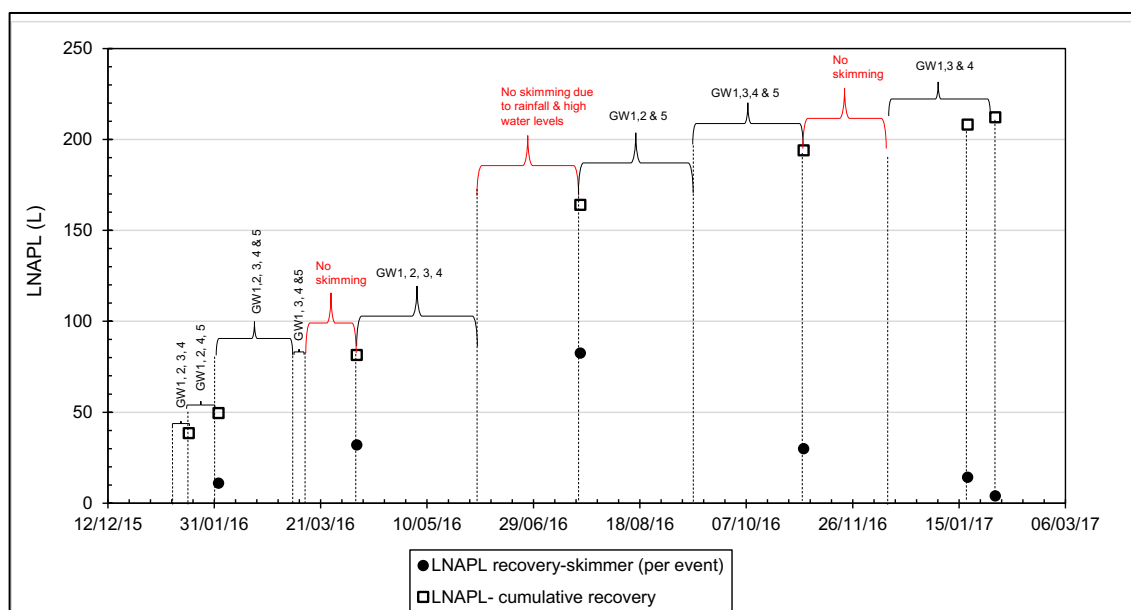


**Figure 50. Summary of LNAPL recovery produced from reported field notes. Dashed lines indicate site visits that refer to the skimmer pumps being removed and reinstalled in the selected wells from SiteE\_Ref1 (2017).**

### 7.5.1 NSZD rate results: measurements and total site-wide rate estimates

#### Soil surface carbon dioxide flux results

##### LI-COR results

Results for site E depicting estimates of NSZD rate contours using the maximum background correction and the average background correction based on 48 flux chamber locations are shown in Figure 51 and Figure 52. Regardless of which method is used to correct for background carbon fluxes, there are large portions of the study area with high NSZD rates (SiteE\_Ref1 2017).

Table 50 has spot measurements and conversions to L LNAPL ha<sup>-1</sup> yr<sup>-1</sup> for NSZD rates for the western boundary of the site. NSZD rates determined using the LI-COR flux chamber method ranged from 47,339 to 164,634 L LNAPL ha<sup>-1</sup> yr<sup>-1</sup> across six spot locations. The two rates listed in Table 50 refer to the maximum and average background corrected rates at each of the five sites were within 10–20% of each other.

##### E-Flux results

Figure 53 shows a data-posting plot of the six equivalent NSZD rates obtained using the CO<sub>2</sub> traps. The average and maximum, modern (background) carbon fluxes from the CO<sub>2</sub> trap results used for correcting the flux chamber results are 1.94 and 3.57 μmol m<sup>-2</sup> s<sup>-1</sup>, respectively (SiteE\_Ref1 2017).

E-Flux carbon dioxide traps provided NSZD rate estimates at two locations of 73,416 and 125,514 L LNAPL ha<sup>-1</sup> yr<sup>-1</sup>. Hence the two carbon dioxide surface flux methods at this site gave comparable and quite high estimates.

There is general agreement with the rates obtained from the LI-COR and E-Flux results (SiteE\_Ref1 2017). According to SiteE\_Ref1 (2017), discrepancy is expected between methods due to temporal variability in soil gas flow and because the sample duration is several days for the flux traps versus a few minutes with the flux chamber. Appendix

Table E.1-1 contains a table of the soil surface carbon dioxide flux results that are depicted in these figures (SiteE\_Ref1 2017).

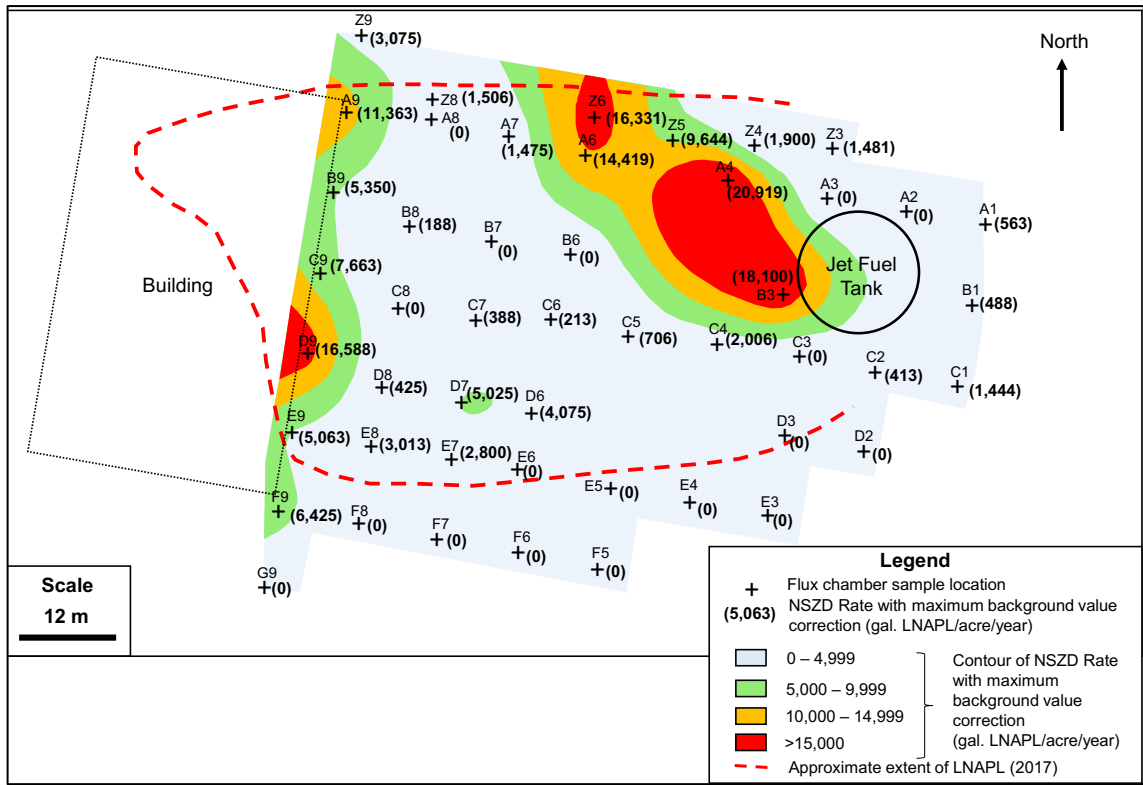
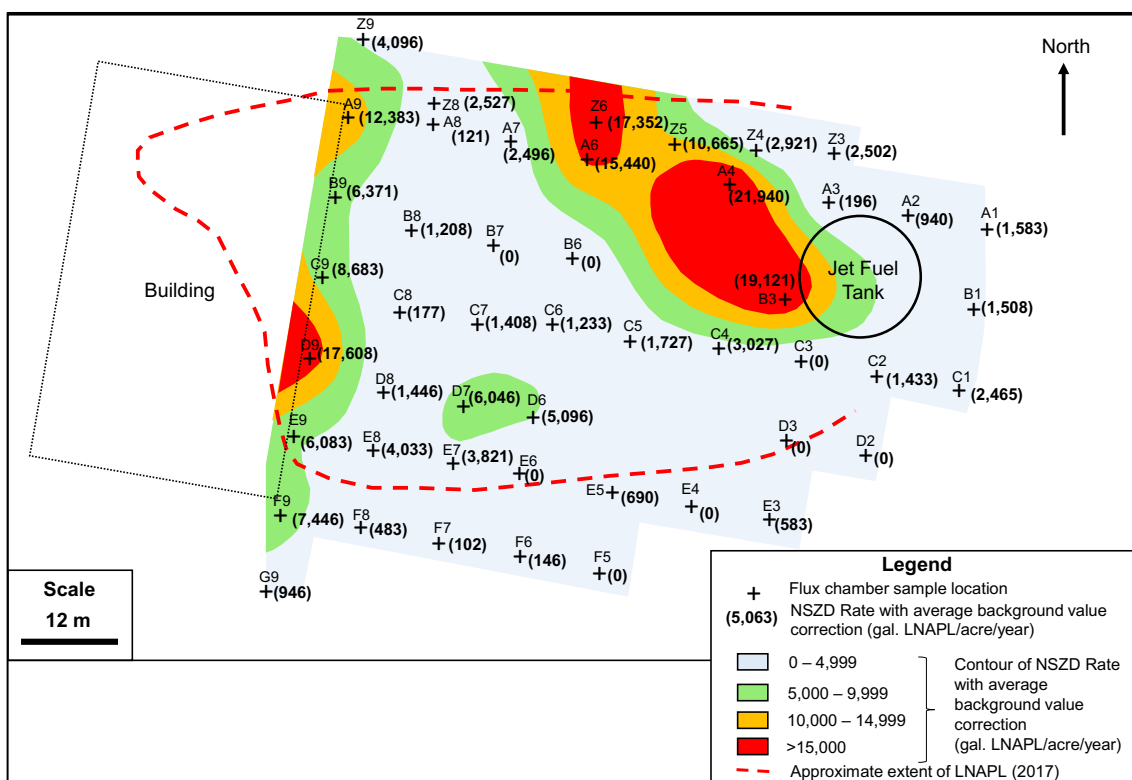
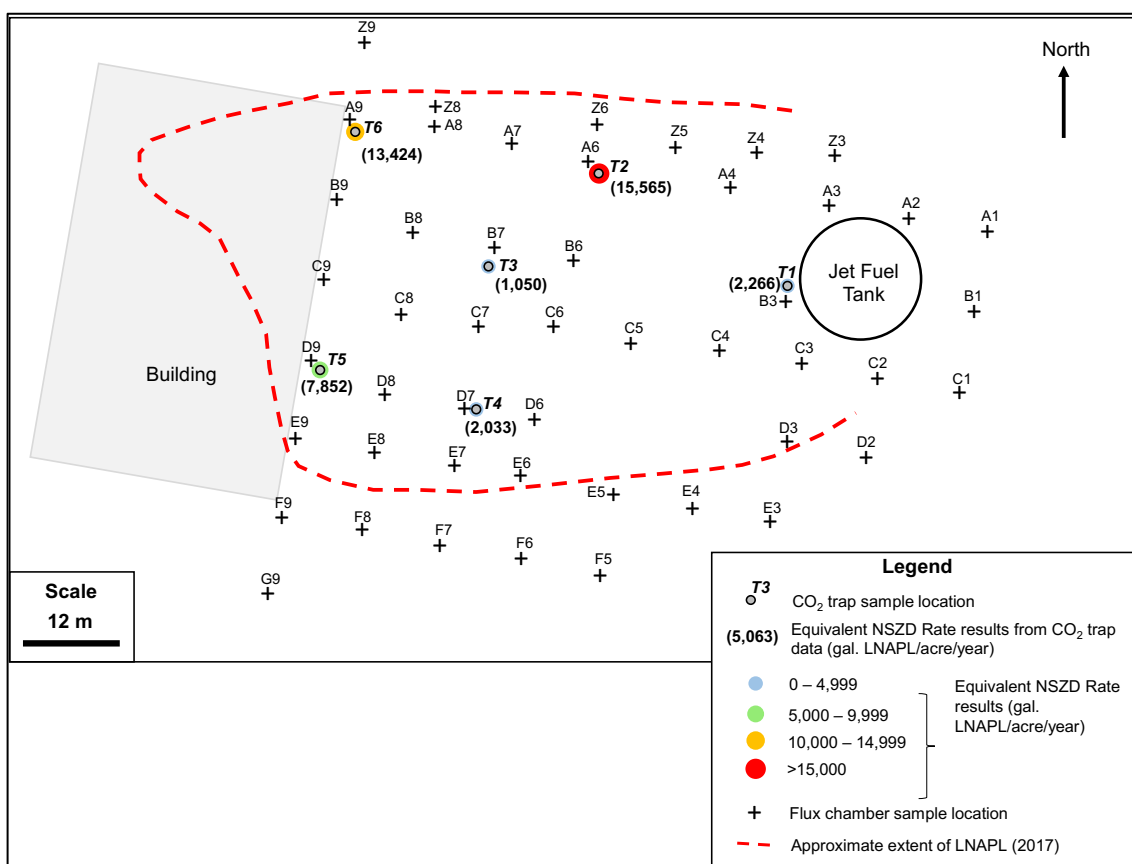


Figure 51. Flux chamber (LI-COR) results contour with maximum background correction from SiteE\_Ref1 (2017) (Note: 1 gal LNAPL acre<sup>-1</sup> year<sup>-1</sup> = 9.35 L LNAPL ha<sup>-1</sup> year<sup>-1</sup>)



**Figure 52. Flux chamber (LI-COR) results contour with average background correction from SiteE\_Ref1 (2017) (Note: 1 gal LNAPL acre<sup>-1</sup> year<sup>-1</sup> = 9.35 L LNAPL ha<sup>-1</sup> year<sup>-1</sup>)**



**Figure 53. CO<sub>2</sub> trap (E-Flux) results from SiteE\_Ref1 (2017) (Note: 1 gal LNAPL acre<sup>-1</sup> year<sup>-1</sup> = 9.35 L LNAPL ha<sup>-1</sup> year<sup>-1</sup>)**

**Table 50. Summary of NSZD data used for comparison of hydrocarbon mass removal from SiteE\_Ref1 (2017). The two NSZD rates listed at each LI-COR site refer to results using maximum and average background corrections, respectively.**

Method	Location	NSZD rate (gal LNAPL acre <sup>-1</sup> year <sup>-1</sup> )*	L LNAPL ha <sup>-1</sup> year <sup>-1</sup>	
LI-COR	A9	11,363; 12,383	106,244; 115,781	Average of LI-COR  86,508
	B9	5350; 6371	47,339; 59,569	
	C9	7663; 8683	71,649; 81,186	
	D9	16,588; 17,608	155,098; 164,635	
	E9	5063; 6083	47,339; 56,876	
	F9	6425; 7446	60,074; 69,620	
E-Flux	T5	7852	73,416	Average of E-Flux 99,465
	T6	13,424	125,514	
<b>Average</b>		<b>9,450</b>	<b>88,359</b>	

\*maximum and average background corrected values are given for the flux chamber method

## 7.6 Overview of hydrocarbon mass removal – recovery and NSZD

Very high estimates of NSZD rates have been determined at this site using the LI-COR and E-Flux methods for site E, ranging from 47,339 to 164,635 L LNAPL ha<sup>-1</sup> yr<sup>-1</sup> in a selected area along the western edge of the study area. The estimated fluxes are generally consistent between the two methods at the same locations.

According to SiteE\_Ref1 (2017), a comparison of methods was undertaken in the area of the previous active skimming operation – the area of about 175 m<sup>2</sup> between the building and the boundary of the fuel storage facility (Figure 54). The average corrected NSZD rate from the LI-COR and E-Flux results was 9,450 gal LNAPL acre<sup>-1</sup> yr<sup>-1</sup> or 88,359 L LNAPL ha<sup>-1</sup> yr<sup>-1</sup> based on the data in Table 50 for the area along the western boundary of the study area (SiteE\_Ref1 2017). A NSZD rate was reported as approximately 4 kg day<sup>-1</sup> (1.5 t yr<sup>-1</sup>) based on the area between the building and the boundary of the fuel storage facility (175 m<sup>2</sup>). The average NSZD rates for LI-COR and E-Flux were 86,508 (1.1 t yr<sup>-1</sup>) and 99,465 LNAPL ha<sup>-1</sup> yr<sup>-1</sup> (1.2 t yr<sup>-1</sup>), respectively. This is considerably higher than the LNAPL recovery rate from active skimming operations in the same area (0.8 L day<sup>-1</sup>, 0.2 t yr<sup>-1</sup>) (SiteE\_Ref1 2017).

According to SiteE\_Ref1 (2017):

- LNAPL degradation via NSZD was estimated to be occurring at rates of up to order of magnitude higher than LNAPL recovery rates from LNAPL skimming.
- Significant rates of LNAPL biodegradation, in some cases exceeding 15,000 US gallons of LNAPL depleted per acre per year (10.5 kg LNAPL per m<sup>2</sup> per year).
- Estimates of rates of LNAPL degradation obtained using CO<sub>2</sub> flux chamber are in general agreement with estimates obtained using the E-Flux method.

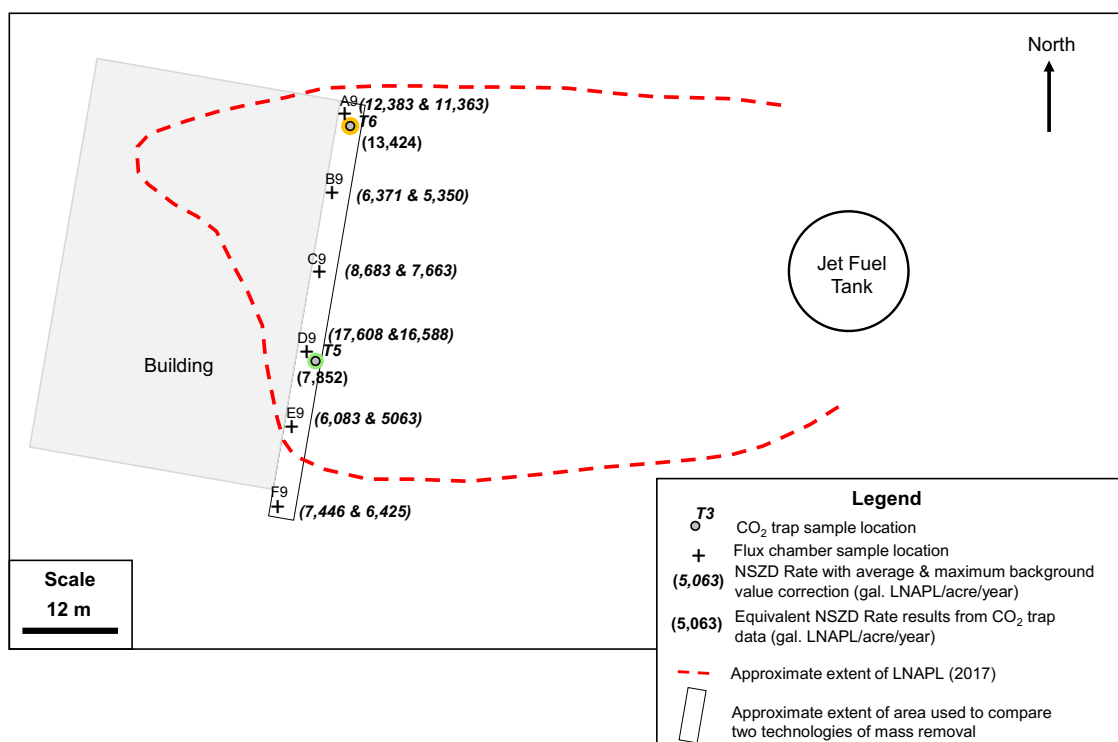


**Figure 54. Area and data used to compare NSZD LNAPL degradation rates to LNAPL recovery rates from active skimming from SiteE\_Ref1 (2017). (Note: 1 gal LNAPL acre<sup>-1</sup> year<sup>-1</sup> = 9.35 L LNAPL ha<sup>-1</sup> year<sup>-1</sup>).**

Surface flux estimates for both LI-COR and E-Flux were made using the entire data set across the site which lies within the plume boundary (0.48 ha). The polygon weighting method was used to weight each measurement location (Figure 55 and Figure 56) and these are summed to estimate annualised mass removal rates over the whole plume.

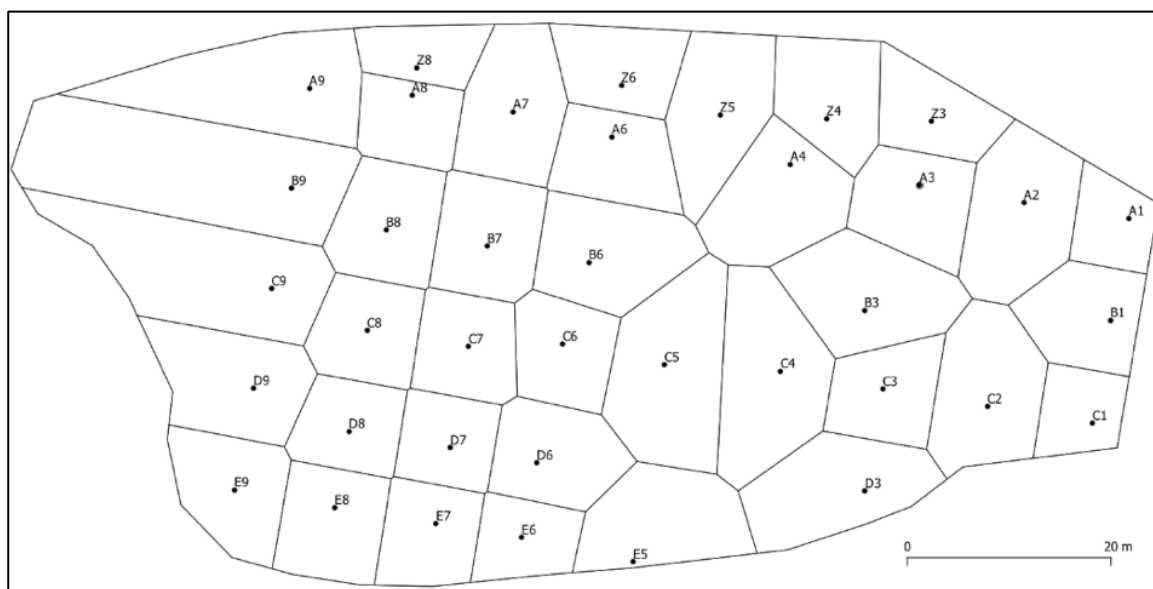


**Figure 55. Voronoi polygon areas constructed using QGIS for LI-COR measurement locations for site E. The inferred extent of LNAPL is shown by the polygon boundary**

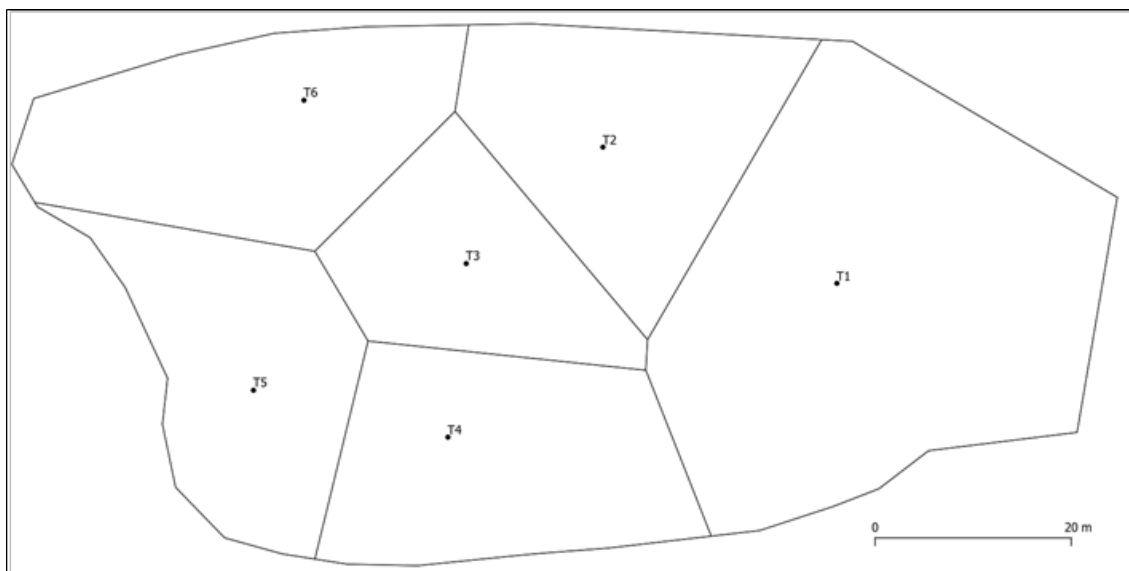


**Figure 56. Voronoi polygon areas constructed using QGIS for E-Flux measurement locations for site E. The inferred extent of LNAPL is shown by the polygon boundary**

The mass loss estimates derived from these methods is  $14 \text{ t yr}^{-1}$  for LI-COR and  $20 \text{ t yr}^{-1}$  for E-Flux. These losses are around two orders of magnitude greater than the active recovery operation which was based on skimming, bearing in mind this was concentrated on a small area ( $175 \text{ m}^2$ ) as described above.

## 7.7 Sources of uncertainty in hydrocarbon mass loss estimation

Uncertainties in estimating LNAPL NSZD rates may arise from a number of sources. The  $\text{CO}_2$  flux results may be influenced by soil stratigraphy, surface covers or compacted layers, edge effects due to the presence of buildings or paving, and barometric conditions and soil moisture content. At site E the building along the western boundary of the Fuel Storage Facility may provide such an effect on some of the  $\text{CO}_2$  flux results, by generating an altered or focussed diffusive flux. More data may be required to evaluate this possible effect and to determine temporal variability. Additional sample events were recommended to determine seasonal variations in rates and annual averages (SiteE\_Ref1 2017).

In addition to the  $\text{CO}_2$  flux, verification of the NSZD rates through alternative methods such as temperature/gas gradients assessment or temporal LNAPL composition changes would reduce uncertainty especially as the  $\text{CO}_2$  flux measurements appear to be localised (Figure 52).



## 8. Site F

### 8.1 Introduction

Site F is a fuel depot that is predominantly level and covers an area of 3.2 ha, of which 30% is covered with concrete or bitumen. Extensive investigations have been carried out at the site (Figure 57) and both MPE and NSZD rates have been determined. LNAPL on site is designated as motor spirit (gasoline) and diesel – recent analysis suggests the primary LNAPL in wells resembles weathered winter diesel that may have resulted from extensive weathering of the gasoline based on comparison with historic gasoline range product present at the site. The subsurface LNAPL area is estimated to be approximately 1 ha.

The petroleum in the subsurface at site F was a result of gasoline range product releases. The gasoline range product present at the site likely contained a mixture of leaded and unleaded gasolines. The product analysed at the site by CSIRO in 2008 showed the presence of mainly unleaded gasoline (due to the presence of high relative abundances of isooctane) as well a minor proportion of light diesel. The light diesel (possibly a similar carbon range as winter diesel) may have been associated with an underlying leaded gasoline (a less refined product). MPE carried out at the site has likely removed the gasoline range product leaving behind the light diesel range product.

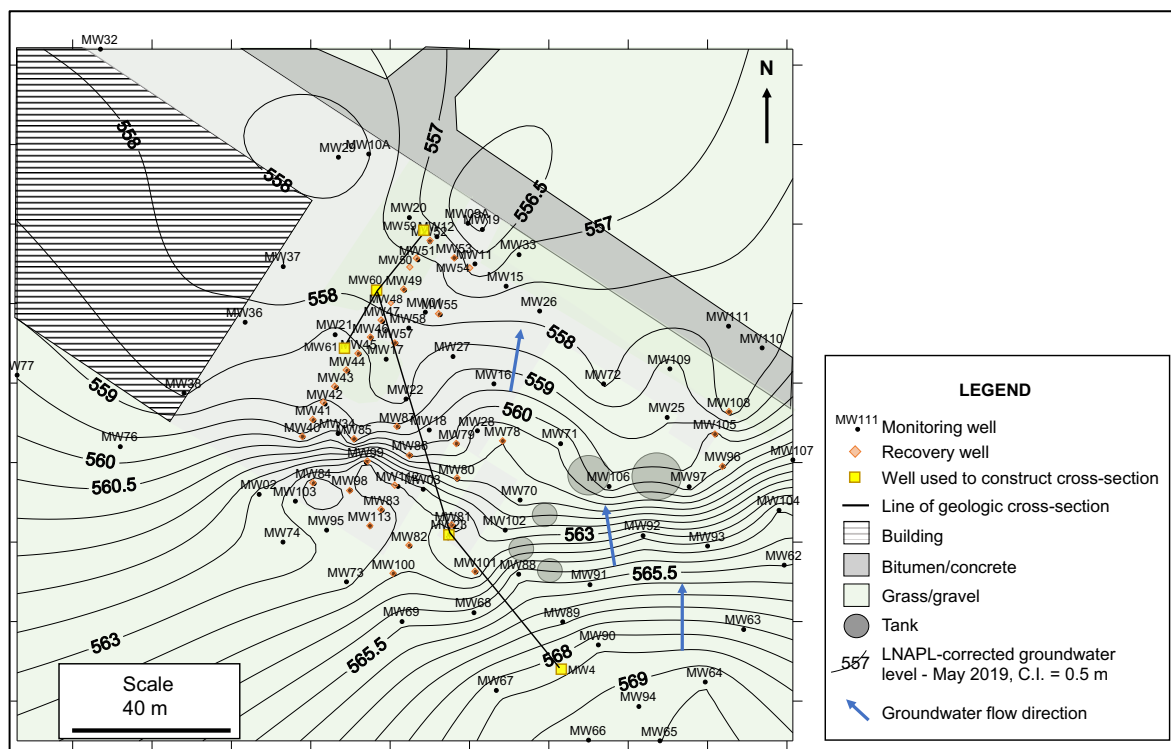


**Figure 57. Layout of some of the monitoring and recovery wells on site F, along with groundwater contours and key site features (SiteF\_Ref1 2019). Section lines for two geologic cross-sections refer to Figure 59 and Figure 60.**

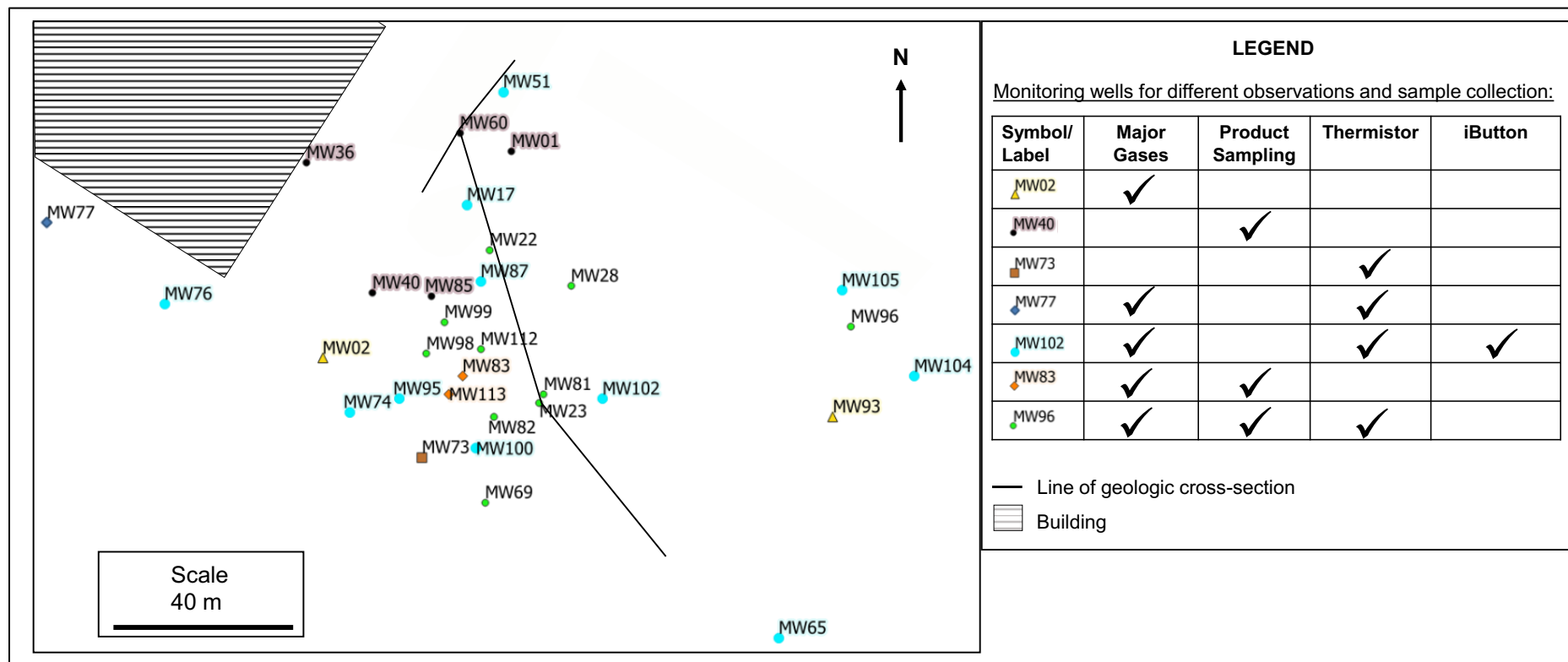


Figure 58. Distribution of the monitoring and recovery sites at site F.

## 8.2 Site description

### 8.2.1 Distribution of wells and measurement methods

Figure 58 indicates the location of monitoring wells and NSZD methods undertaken at site F referred to in this report.

### 8.2.2 Profile stratigraphy

The subsurface strata typically consist of 1 m of clay, overlying weathered phyllite (metamorphosed siltstone) over the next 3 m depth. Beneath this is a fractured phyllite. Two cross-sections are provided for site F. Figure 59 indicates the plume extent, whereas Figure 60 indicates hydraulic conductivity measurements, fracture frequency and the fracture planes in the upper 15 m of the section, which are also shown in the well logs for wells MW59, MW60 and MW61 (Appendix F.1, SiteF Ref2 2007).

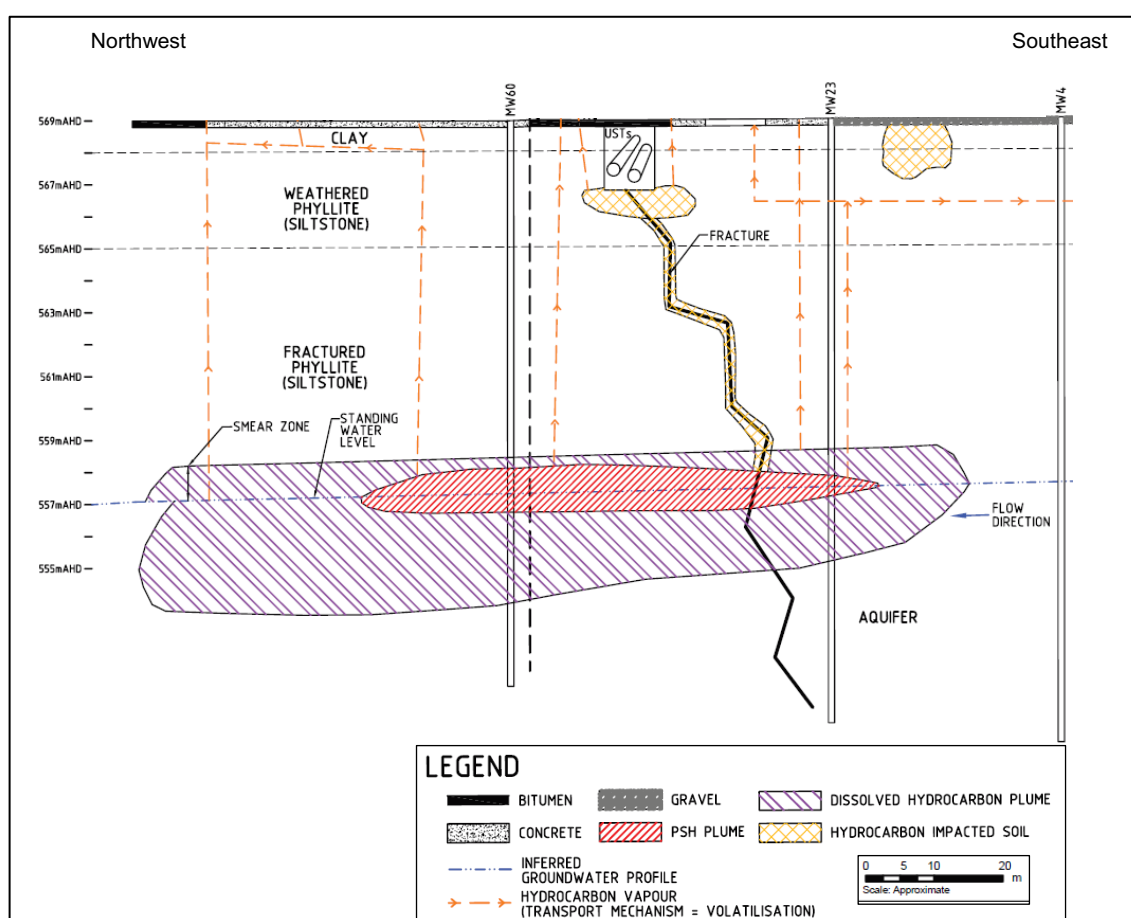


**Figure 59. Conceptual site model from SiteF\_Ref1 (2019). Refer to Figure 57 and Figure 58 for location**

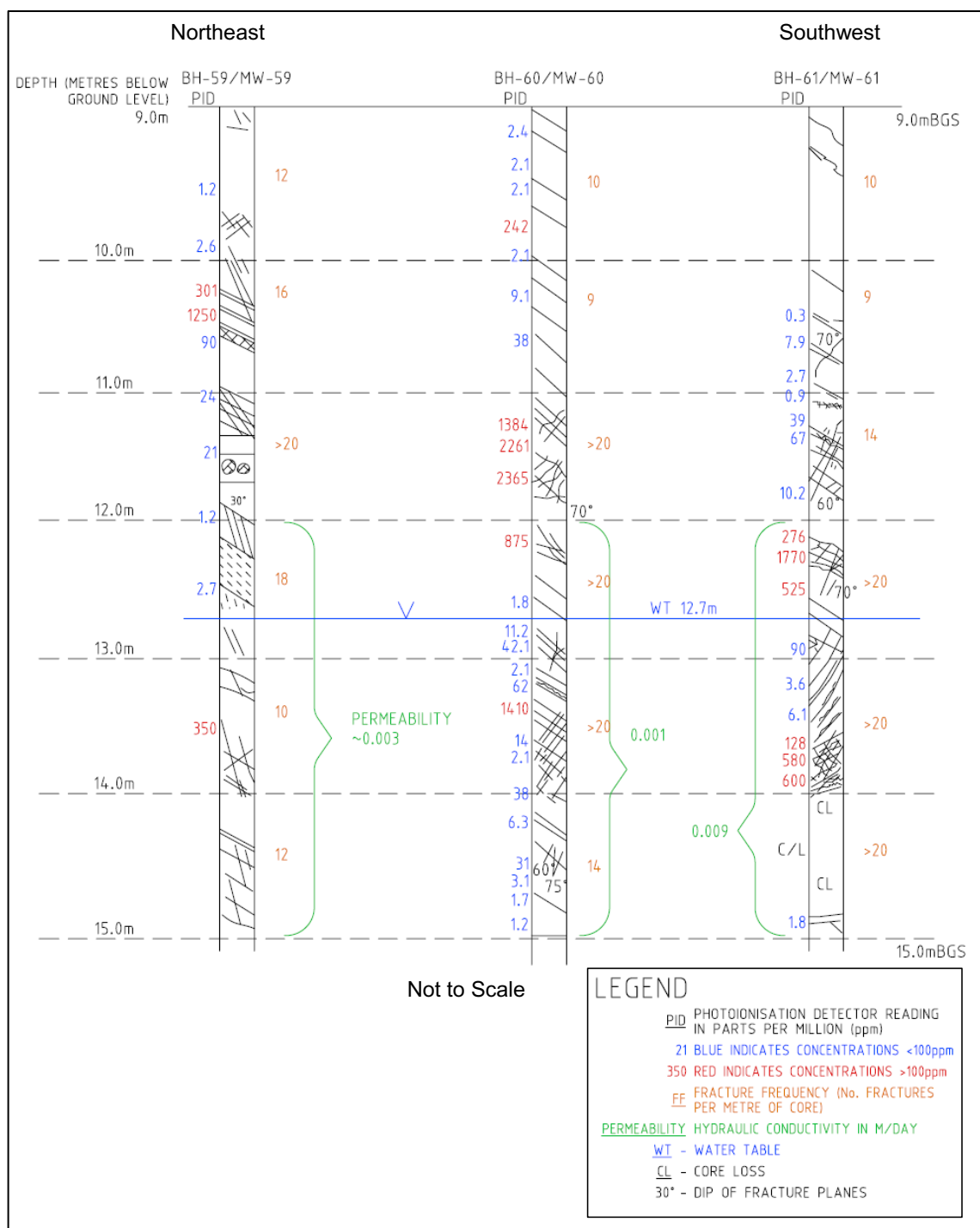


Figure 60. Geological cross section (SiteF\_Ref2 2007). Refer to Figure 57 for location.

## 8.3 Data supplied by site owner and other data

### 8.3.1 Hydrogeological parameters

The primary permeability is thought to be low. Hydraulic conductivity values depicted in Figure 60 are of the order of 0.001 to 0.009 m/day (SiteF\_Ref2 2007).

### 8.3.2 Well construction and mean groundwater levels

The water table has been measured as between 3 m and 14 m below ground surface, with significant inferred groundwater gradient across the site as indicated in Figure 57.

LNAPL-corrected groundwater levels were obtained from CSIRO fluid levels database for Site F from monitoring conducted in May 2019 and well construction details from SiteF\_Ref3 (2019).

Groundwater velocities of about 20 m/y have been estimated. Joint and fault system fractures appear to influence groundwater flows. Dissolved plumes have remained stable.

### **8.3.3 Product thicknesses in local wells on the site over time**

According to SiteF\_Ref1 (2019), MW112 and MW113 were installed during April 2018 with MW113 reporting the greatest apparent thickness (1.560 m) out of all wells (Table 51).

**Table 51. LNAPL thickness from SiteF\_Ref1 (2019)**

<b>Well</b>	<b>March 2017</b>	<b>August 2017</b>	<b>November 2017</b>	<b>February 2018</b>	<b>September 2018</b>
MW18	-	0.01	0.02	0.005	0.015
MW22	-	-	0.006	-	0.04
MW23	0.015	0.009	0.075	0.01	0.15
MW28	0.005	0.003	0.025	0.041	0.008
MW40	0.009	0.008	0.004	0.007	0.004
MW41	0.04	-	0.003	0.005	0.005
MW42	-	0.006	-	-	-
MW68	-	-	0.003	-	-
MW78	-	0.011	-	0.02	0.145
MW79	-	-	-	0.008	-
MW81	-	0.023	0.185	0.216	0.218
MW82	-	0.089	-	0.585	0.097
MW83	-	0.672	0.58	0.757	0.155
MW84	-	0.055	-	0.118	0.077
MW85	-	0.091	0.086	0.031	0.02
MW87	-	0.205	0.006	-	0.015
MW88	-	-	-	-	0.004
MW95	-	-	-	0.02	0.025
MW96	-	0.007	0.022	0.008	0.206
MW98	-	-	5.077	6.621	0.015
MW99	-	-	0.353	0.332	0.096
MW100	-	-	-	0.016	0.005
MW101	-	-	0.074	0.212	0.053
MW103	-	-	-	0.006	-
MW105	-	-	0.013	0.015	0.007
MW112	-	-	-	-	0.181
MW113	-	-	-	-	1.56

### **8.3.4 Measurements of LNAPL transmissivity**

Only one estimate of LNAPL transmissivity was provided 0.1 ft<sup>2</sup>/day (0.009 m<sup>2</sup>/day, SiteF\_Ref1 2019).

### **8.3.5 LNAPL sampling and analysis (compositional analyses)**

According to SiteF\_Ref1 (2019), no analytical data has been collected for the LNAPL present underlying the site. See Section 8.4.3 for details of sampling conducted by the CSIRO.

### **8.3.6 LNAPL recovery operations**

MPE was the main active recovery method used at the site over the period 2012–2018 from up to 37 well locations. A significant volume of LNAPL has been recovered over this period (up to 77,500 kg) with the majority in 2013, and a total of ~25,500 kg since 2015 (Table 54). LNAPL mass recovery has largely halved each year up to 2018 (Table 54), disproportionately to reduced run times. Proportional to run times, recovery rates have dropped from 3.8 kg/hr in 2015 to less than 1.0 kg/hr in 2018.

## **8.4 Methods**

### **8.4.1 Active recovery**

MPE data indicates that more than 99% of hydrocarbons removed has been through the vapour phase and measurement of vapour emissions are typically the most problematic to estimate accurately as a metric of MPE mass removal performance. Despite extensive MPE application, LNAPL still resides in wells local to LNAPL recovery areas, presumably due to the lack of interconnection between some areas across the site.

### **8.4.2 NSZD rate estimation**

#### **Subsurface temperature measurement and analysis (thermistor)**

Subsurface temperatures were measured using two techniques, instantaneous measurements using thermistors and longer-term temporal measurements using iButtons. Both of these methods involved the hanging of the temperature sensors in existing monitoring wells. Instantaneous temperature measurements were obtained during two separate sampling campaigns (27–29 May 2019 and 12 September 2019) where iButtons were installed between 29 May 2019 and 11 July 2019. The monitoring wells in which temperature was measured are shown in Table 52.

For the thermistor method a string of thermistors was hung within the monitoring bore for at least 1 hour to equilibrate with the subsurface temperature. The thermistor string was made up of 10 NTC thermistors (10k Ohm Betacurve, 10K3A1B, matched to YSI 44036) spaced at 1 m intervals along a multi-core cable. Electrical resistance was measured using a multimeter (Fluke 28 II Ex) and converted to temperature using the thermistor manufacturer's polynomial calibration algorithm. Background correction and NSZD calculation was done according to the method outlined for site A.

The iButtons were logged temperature at 15 min intervals. This data was assessed and then averaged over either daily or monthly periods which were then corrected against the background well (MW169). The temperature differences were then reviewed and the largest background temperature difference above the water table was used to generate the thermal gradient. The gradient was then multiplied by the thermal conductivity to calculate the heat flux, which was then related stoichiometrically to the LNAPL degradation rate.

**Table 52 Monitoring wells for which manual temperature profiles were recorded and iButtons temperature loggers installed**

Method		Well ID
Thermistor	May 2019	MW17, MW22, MW23, MW28, MW32, MW51, MW65, MW69, MW73, MW74, MW76, MW77, MW81, MW82, MW87, MW95, MW96, MW98, MW99, MW100, MW102, MW104, MW105, MW112
	September 2019	MW23, MW28, MW74, MW100, MW105, MW112
iButton		MW77, MW100, MW105, MW112

### Gas sampling and analyses (in-well)

Major gas samples were obtained during two separate sampling campaigns (27–29 May 2019 and 12 September 2019) from exiting monitoring wells (Table 53). Gas concentrations were determined in situ using a portable gas analyser and for the May campaign on gas samples collected and analysed in the laboratory.

Gas sampling was undertaken by lowering a weighted, nylon tube into the well casing such that the intake was 0.3 m above the fluid-air interface determined previously using an interface meter (H.OIL, Heron Instruments Inc.). An Eagle II gas analyser (RKI Instruments) equipped with oxygen, carbon dioxide and methane sensors, was used to measure the gas concentrations. Following zeroing with ambient air the Eagle II was connected to the nylon tubing and readings taken every 30 s for 3 min. Final oxygen and carbon dioxide concentrations were used to calculate NSZD rates.

Samples for laboratory analysis were collected following the in-situ readings using a 60 mL plastic syringe and a foil sampling bag. The sampling procedure is outlined in detail in Appendix A.7. Major gas analysis was performed as outlined in Section 3.4.2 for site A.

NSZD rates were determined between the sampling location and the soil surface for in-well major gas using the gradient method described in Section 2.4 and in CRC CARE Technical Report 44 (2018). To calculate NSZD rates, the gradient method for soil gas flux was applied using Equation 2 (see Section 2.4). The effective vapour diffusion coefficient for O<sub>2</sub> and CO<sub>2</sub> were assigned the values of 0.41E-06 and 0.37E-06 m<sup>2</sup> s<sup>-1</sup>, respectively.

**Table 53 Monitoring wells for which major gas samples were measured in situ using a gas analyser or collected for laboratory analysis**

Sampling campaign	Gas analysis method	Well ID
May 2019	Gas analyser	MW2, MW17, MW22, MW23, MW32, MW51, MW65, MW69, MW74, MW76, MW77, MW81, MW82, MW83, MW87, MW93, MW95, MW96, MW98, MW99, MW100, MW102, MW104, MW105, MW112, MW113
May 2019	Laboratory	MW17, MW22, MW23, MW69, MW74, MW76, MW77, MW81, MW87, MW95, MW96, MW99, MW100, MW102, MW105, MW112
September 2019	Gas analyser	MW23, MW28, MW74, MW76, MW83, MW98, MW99, MW100, MW105, MW112

#### **8.4.3 NSZD: LNAPL compositional analyses to assess the extent of weathering**

LNAPL sampling of 2019 samples involved lowering a 40 mL VOA vial directly into the well on nylon fishing line to just below the fluid (LNAPL) interface and the vial was retrieved, capped and sent to the laboratory for analysis. LNAPL sampling of pre-2019 samples was carried out by a contractor.

##### *LNAPL analysis using GC-FID and GC-MS*

2008 GC-FID analysis of LNAPL samples (C4–C40 carbon range) was performed at CSIRO, using an HP 5890 GC fitted with a vaporising injector (operating in split mode), hydrogen carrier gas, an autosampler and a FID. The GC was equipped with a 30 m x 0.25 mm internal diameter column coated with a 0.25 µm thick film of dimethyl polysiloxane (AT-1ms, Alltech).

2019 GC-FID analysis of LNAPL samples (C4–C40 carbon range) was performed at CSIRO, using an HP 6890 GC fitted with a vaporising injector (operating in split mode), helium carrier gas, an autosampler and a FID. The GC was equipped with a 60 m x 0.25 mm internal diameter column coated with a 0.25 µm thick film of dimethyl polysiloxane (DB-1 UI, J&W).

GC-MS analysis (C7–C40 carbon range) of selected components was performed using an Agilent 7890 GC fitted with a vaporizing injector (operating in split mode), with helium as carrier gas, an auto-sampler and an Agilent 7000 mass spectrometer. The LNAPL samples (5 µL) were diluted in dichloromethane containing internal standards (*d*6-benzene, *d*8-toluene, *d*10-p-xylene, *d*8-naphthalene and *d*34-hexadecane) to allow quantitation of selected analytes. The GC-MS was fitted with a capillary GC column (Phenomenex, ZB-1ms, 30 m length, 0.25 mm internal diameter and 0.25 µm thick film of dimethyl polysiloxane or equivalent column). The mass spectrometer was operated with an ionisation energy of 70 eV at 230 °C in scan mode. Quantitation of selected compounds was performed using external standards containing the same internal standards used for the samples.

##### *Estimating LNAPL mass losses*

Estimated percentage mass losses over a time period were based on concentration increases in the LNAPL of a conservative tracer (one of the most non-volatile, water insoluble and biodegradation resistant components present in the samples) as a result of other components decreasing in the LNAPL due to volatilisation, dissolution and biodegradation. 1,2,4-trimethylbenzene was selected to assess the relative losses of the 2008 samples (as well as the MW96 from 2019 containing mainly gasoline range product) as it was one of the major components present in significant relative abundances in the GC-FID chromatograms (LNAPL samples were no longer available however GC-FID chromatograms were available) and one of the components likely unaffected by volatilisation, dissolution and biodegradation at the extent of weathering the gasoline range LNAPL samples have experienced. Pristane was selected for 2019 samples (using the least weathered 2008 LNAPL pristane concentration as the reference for the initial LNAPL released at the site) as the gasoline range product present 2008 was no longer present in the 2019 samples and pristane was unaffected by volatilisation, dissolution and biodegradation in the LNAPL samples studied (based on the ratio of pristane to phytane). Pristane or 1,2,4-trimethylbenzene concentration changes in the LNAPL samples relative to the least weathered 2008 sample at the site



allowed estimation of LNAPL losses to be calculated, where a concentration of pristane or 1,2,4-trimethylbenzene (w/w) in an LNAPL sample twice that of least weathered 2008 sample would afford an estimated loss of 50% (w/w). Estimates of LNAPL depletion or losses over time were based on changes in the pristane or naphthalene concentration (conservative tracer, H) using Equation 4 (Section 2.4).

## 8.5 Results

### 8.5.1 Estimation of total hydrocarbon mass removal by active recovery

MPE was applied at the site over the period 2012-2018 from up to 37 well locations. A significant volume of LNAPL has been recovered over this period (up to 77,500 kg) with the majority in 2013, and a total of ~25,500 kg since 2015 (Table 54). LNAPL mass recovery has largely halved each year up to 2018 (Table 54), disproportionately to reduced run times. Proportional to run times, recovery rates have dropped from 3.8 kg/hr in 2015 to less than 1.0 kg/hr in 2018. Whilst seemingly successful, MPE data indicates that more than 99% of hydrocarbon removed has been through the vapour phase; and measurement of vapour emissions are typically the most problematic to do accurately as a metric of MPE mass removal performance. Despite extensive MPE application, LNAPL still resides in wells local to LNAPL recovery areas, presumably due to the lack of interconnection between some areas across the site.

**Table 54. Mass of LNAPL removed (kg hexane equivalent) by MPE**

LNAPL recovery	2015	2016	2017	2018	Total for 2015–2018
LNAPL mass removed (kg hexane)	13,817	6748	3209	1682	25,456
Run hours	3614	4058	2759	1774	12,205
LNAPL mass kg/hr	3.8	1.7	1.2	0.94	2.1

### 8.5.2 NSZD results: measurements and total site-wide rate estimates

#### Temperature results

Interpretation of the recent data by CSIRO (this study), reveals the background corrected NSZD rates based on the manual thermistors range from 0 to 15,151 L LNAPL ha<sup>-1</sup> yr<sup>-1</sup> and 0 to 8649 L LNAPL ha<sup>-1</sup> yr<sup>-1</sup> for May and September, respectively (Table 55). Several NSZD rates derived from iButton data are shown for comparison but are too preliminary for determining site-wide rates using the polygon method due to the limited spatial distribution.

The polygon areas used to compute site-wide total NSZD rates for the thermistor results are shown in Figure 61. The site-wide total NSZD rates for the manual thermistor-based method are 3.4 and 4.3 t yr<sup>-1</sup> for May and September, respectively. The outline surrounding the measurement locations for NSZD encompasses 11,204 m<sup>2</sup> (1.1 ha).

**Table 55. Summary of results for NSZD based on thermistors from May and September 2019**

Well location	Date	Manual thermistors NSZD (L LNAPL ha <sup>-1</sup> yr <sup>-1</sup> )	iButtons NSZD (L LNAPL ha <sup>-1</sup> yr <sup>-1</sup> )
MW100	28 May 2019	12,280	5360
MW100	12 Sept 2019	5680	
MW102	28 May 2019	2707	
MW104	27 May 2019	6608	
MW105	29 May 2019	2241	3270
MW105	12 Sept 2019	4474	
MW112	28 May 2019	12,821	
MW112	12 Sept 2019	4320	7580
MW17	29 May 2019	1127	
MW22	28 May 2019	1810	
MW23	28 May 2019	8118	
MW23	12 Sept 2019	4529	
MW28	27 May 2019	8479	
MW28	12 Sept 2019	8649	
MW51	27 May 2019	3945	
MW65	27 May 2019	0	
MW69	27 May 2019	6912	
MW73	27 May 2019	5023	
MW74	28 May 2019	0	
MW74	12 Sept 2019	0	
MW81	28 May 2019	15,151	
MW82	28 May 2019	13,082	
MW87	28 May 2019	1773	
MW95	28 May 2019	4176	
MW96	29 May 2019	2141	
MW98	29 May 2019	7692	
MW99	29 May 2019	2283	

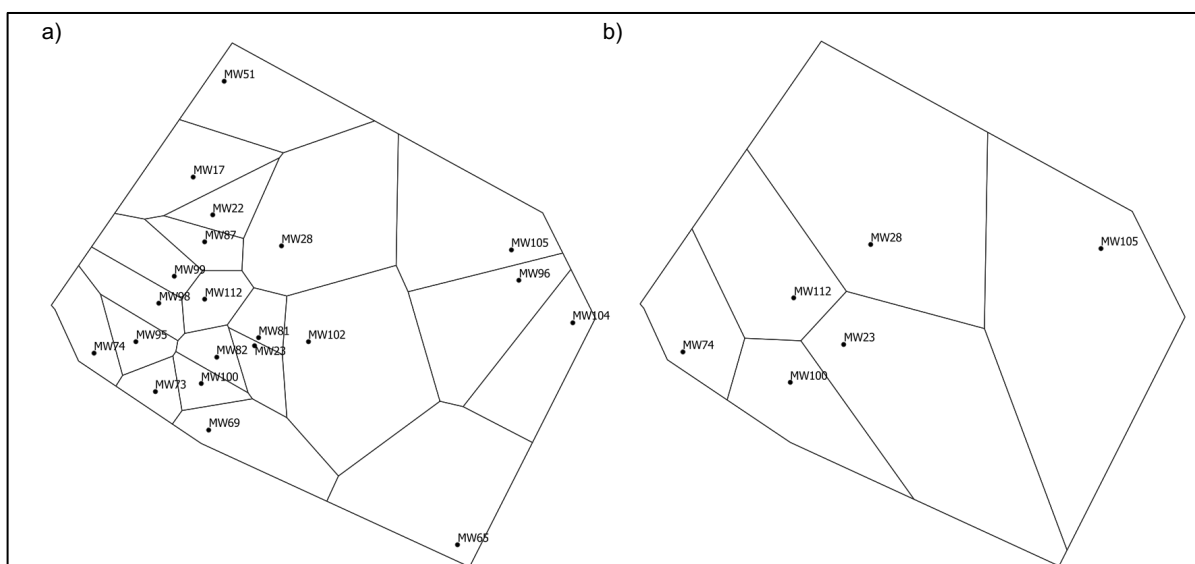


**Figure 61. Voronoi polygon areas constructed using QGIS for thermistor measurement locations for site F in (a) May 2019 and (b) September 2019**

## Gas sampling results

Gas sampling results for the gas analyser and laboratory analysis produced similar results, thus for the May 2019 data these datasets were combined and averaged for the purpose of this study. The May and September data were analysed separately as several factors influence the gas concentrations including seasonal variability, falling groundwater levels and in-well infrastructure changes (MPE straws in place in May were removed until the September sampling campaign). In particular wells with MPE straws deployed in May (MW83, MW98 and MW99), had substantially lower  $O_2$  and  $CO_2$  concentrations (higher NSZD rates) in September than recorded in May.

Independent of analysis method and sampling time  $CO_2$  concentrations measured were stoichiometrically less than the depletion in  $O_2$  concentrations associated with hydrocarbon degradation. This discrepancy between the  $O_2$  and  $CO_2$  concentrations could not be satisfactorily explained by the investigators. Thus, NSZD rates were only calculated using the measured  $O_2$  concentrations as subsurface concentrations are related to diffusion of atmospheric oxygen into the subsurface and subsequent hydrocarbon degradation processes.

Based on interpretation of the data by CSIRO (this study), the in-well measurements of  $O_2$  yielded NSZD rates that range from 0 to 1,586 L LNAPL  $ha^{-1} yr^{-1}$  and 401 to 1600 L LNAPL  $ha^{-1} yr^{-1}$  for May and September, respectively (Table 56).

The polygon areas used to compute site-wide total NSZD rates for the gas in-well sampling results are shown in Figure 62. The site-wide total NSZD rates for the gas in-well ( $O_2$ ) are 0.40 and 0.68 t  $yr^{-1}$  for May and September, respectively.

**Table 56. Summary of results for NSZD based on in-well gas data (O<sub>2</sub>)**

Location	Date/time	NSZD (L LNAPL ha <sup>-1</sup> yr <sup>-1</sup> )
MW02	27 May 2019	683
MW100	28 May 2019	1586
MW100	12 Sept 2019	1608
MW102	28 May 2019	541
MW104	27 May 2019	860
MW105	28 May 2019	857
MW105	12 Sept 2019	890
MW112	28 May 2019	1483
MW112	12 Sept 2019	409
MW113	29 May 2019	49
MW17	28 May 2019	833
MW22	28 May 2019	627
MW23	28 May 2019	904
MW23	12 Sept 2019	1189
MW28	12 Sept 2019	447
MW51	27 May 2019	445
MW65	27 May 2019	0
MW69	27 May 2019	98
MW74	28 May 2019	1004
MW74	12 Sept 2019	850
MW81	28 May 2019	752
MW82	28 May 2019	0
MW83	28 May 2019	0
MW83	12 Sept 2019	1450
MW87	28 May 2019	0
MW93	27 May 2019	239
MW95	28 May 2019	265
MW96	28 May 2019	872
MW98	29 May 2019	303
MW98	12 Sept 2019	1092
MW99	28 May 2019	14
MW99	12 Sept 2019	401

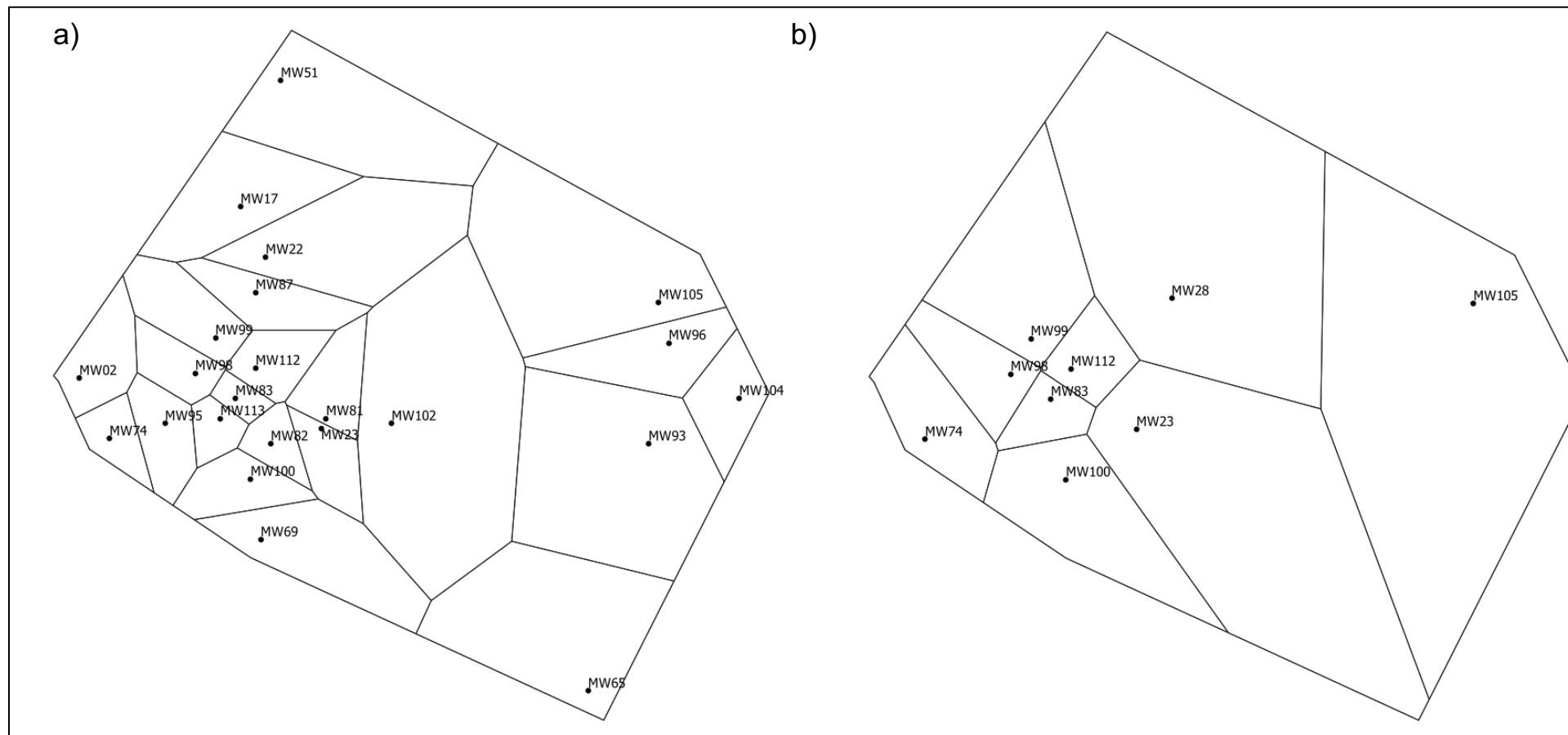


**Figure 62. Voronoi polygon areas constructed using QGIS for gas in-well measurement locations for site F in (a) May 2019, and (b) September 2019.**

### 8.5.3 NSZD results: LNAPL composition

Recovered LNAPL samples from 2008 contained predominately gasoline range product consistent with unleaded gasoline (based on the presence of isooctane and high refining of the product) and were affected by weathering except for LNAPL sample MW60 which showed no significant effects from weathering. All of the 2008 samples also contained a minor proportion of light diesel range product (similar to a winter diesel) and likely associated with the presence of an underlying leaded gasoline at the site. The unleaded gasoline in the LNAPL samples from the site had benzene concentrations ranging from 1.82% to 3.58% (w/w) and was therefore likely related to a spill that occurred prior to 2006 when the *Australian National Fuel Quality Standards Act 2000* required gasoline to contain less than 1% (v/v) benzene by 2006 (previously gasoline was required to contain <5 % (v/v) benzene). Estimated losses due to weathering of the 2008 LNAPL samples (assuming no losses for sample MW60) ranged from 0% to 35% (Appendix Table F.2-1.)

Most of the 2019 samples now comprise of light diesel range product (or winter diesel) similar to that observed as a minor component in the 2008 samples (MW69 from 2019 contained a mixture of weathered gasoline and diesel range products; MW96 from 2019 contained weathered unleaded gasoline with estimated mass losses of 28%). Comparison of the GC-FID chromatograms (and isoprenoid ratios) for the 2008 and 2019 LNAPL samples suggests the diesel range product present in the 2019 samples was present as a minor contaminant (~1–3%) in the gasoline range product in the 2008 samples. The concentrated diesel range product present in the 2019 samples was likely due to the removal of the gasoline range product as a result of MPE carried out at the site. Comparison of the isoprenoid ratios (pristane/phytane, Pr/Ph) shows both the 2008 and 2019 LNAPL samples have similar and not commonly observed values due to the high relative abundance of pristane than usually observed as well as the C15 to C27 carbon range present in the 2008 samples matches well with the least biodegraded sample from 2019 (MW98, Appendix Figures F.2-1 to F.2-4). GC-MS analyses of the samples showed the presence of tetraethylleads in some samples (MW23, MW69, MW81, MW83, MW112) suggesting the presence of leaded gasoline and the presence of isooctane in the samples suggests the presence of unleaded gasoline, therefore the LNAPL at the site is likely a result of multiple spills including leaded and unleaded gasoline with the winter diesel range product present in the samples possibly from the leaded gasoline (leaded gasoline is a less refined product). Therefore, the pristane concentration in the least weathered 2008 LNAPL sample (MW60) was used to calculate mass losses from 2008 to 2019 which ranged from 98% to 99% (Appendix Table F.2-1), excluding sample MW96 from 2019 which contained no diesel range product.

## 8.6 Overview of hydrocarbon mass removal – recovery and NSZD

As discussed in Section 8.5.1 (Table 54), the most recent LNAPL recovery rate in 2018 was about 1.7 t yr<sup>-1</sup>. In comparison, the range of NSZD rates are provided in Table 57. In addition, NSZD rates for the iButton results (not spatially weighted) are 4315 L LNAPL ha<sup>-1</sup> yr<sup>-1</sup> (average for May 2019) and 7580 L LNAPL ha<sup>-1</sup> yr<sup>-1</sup> (September 2019). These correspond to 3.3 and 5.9 t yr<sup>-1</sup> for May and September 2019, respectively (based on 1.1 ha area and 703 kg m<sup>-3</sup>).

**Table 57. Tabulation of NSZD rates across methods used and total site-wide mass losses per time**

NSZD methods	Intrinsic rate estimates (L LNAPL ha <sup>-1</sup> yr <sup>-1</sup> )*	Rate mass/time (t yr <sup>-1</sup> )**
Temperature (thermistors)	May 2019: 0 to 15,000 Sept. 2019: 0 to 8,700	May 2019: 3.4 Sept. 2019: 4.3
Gas sampling (in-well)	May 2019: 0 to 1,600 Sept. 2019: 401 to 1,600	May 2019: 0.40 Sept. 2019: 0.68
iButton	May 2019: 4300 Sept. 2019: 7580	3.3 <sup>†</sup> 5.9 <sup>†</sup>

\* Rates have been determined across a number of locations, the range denotes variability across different locations at the site. Values are rounded to two significant figures. \*\* A polygon areal weighting approach has been adopted to determine these rates, with the polygon areas scaled to the LNAPL plume area at the site (1.1 ha). except where noted (†).

Overall NSZD rates from gas analysis are 2.3–3.9 times lower than LNAPL recovery rates but estimates from temperature data suggest NSZD rates are 2.2–2.8 times higher than LNAPL recovery rates.

## 8.7 Sources of uncertainty in hydrocarbon mass loss estimation

MPE was the main mass removal technique used at this site. Discussions with site operators indicate this was successful with most of the gasoline mass removed through the vapour phase as would be expected. Uncertainty arises from high flow rates and varying VOC concentrations making the sum product of these two measurements problematic.

The stratigraphy at site F is complex with clays and concrete overlying weathered and fractured phyllite. The moisture profiles are also likely to vary spatially due to the surface materials, for example evaporation from bare soil will be different from beneath concrete, and due to the spatial variation in groundwater depth (3 to 14 mbg). Thus, it would be expected that the thermal conductivity and gas diffusion coefficient to vary spatially and vertically across the site.

Representing these soil properties with a single value was a necessary simplification due to the lack of data with which to these parameters. While the best available literature values were used uncertainty is introduced when calculating the NSZD rates from the in-well temperature profiles and in-well gas concentrations.

The single location of sampling for in-well gas methodology may also introduce uncertainty. Should similar gas concentrations be observed at shallower depth then the concentration gradient will be greater resulting in a higher calculated NSZD rates. Using a single measurement point will also result in different gradients if there are fluid level changes between sampling campaigns.

Selection of background location for temperature profile was influenced by shading on soil temperatures. Shading has the effect of reducing heat transfer to the ground surface and reducing soil temperatures (Napoli *et al* 2016). A potential background location at site F was eliminated after it was observed that it had lower temperatures throughout the profile as a result of near permanent shading of a nearby tall building. Use of this background site would have resulted in estimated higher NSZD rates due to the greater temperature difference. The compromise location was closer to the

contaminated area and it is unknown whether this was influenced by biodegradation. This highlights the importance of selecting representative background sites.

While the polygon approach used for the assessment of site-wide NSZD rates was the best available, it still may introduce uncertainties. The distribution of measurement locations within the area of interest could potentially skew the results especially if the distribution of data points poorly represents the area.



## 9. Site-specific considerations for estimating rates of NSZD: observations from this study

---

In general, more complex sites (in terms of subsurface heterogeneity, layering of variably textured sediments, sealed surfaces, varying water table elevation, soil moisture and temporal behaviour) require more rigorous application of NSZD methods and more comprehensive characterisation of subsurface properties.

Sites C and F are examples of this as they demonstrated some large differences in NSZD rates for the same methods at two sampling times potentially reflecting seasonal variability. Sampling times were in May and September 2019. Interpretation of the differences are not straightforward without further measurements and investigation. These sites are complex stratigraphically, exhibiting weathered clay overlying fractured bedrock with large areas that are paved or compacted.

Two of the main seasonal parameters impacting NSZD rates are the fluid elevation and vadose zone moisture content and these may impact NSZD rates in different ways. An increase in the fluid elevation can move the aerobic/anaerobic zone higher in the profile, closer to the ground surface, thereby increasing the major gas gradients. Similarly, increased soil moisture contents in the vadose zone can lead to a decrease in oxygen diffusion into the profile and CO<sub>2</sub> fluxes exiting the subsurface which can also move the biodegradation reactive zone higher in the profile. In the absence of additional data regarding the profile physical properties (i.e. the change to gas diffusion coefficients from increased soil moisture), this may result in higher calculated NSZD rates for gas gradient methods, and lower calculated results from surface CO<sub>2</sub> flux methods. Such seasonal features due to soil moisture changes was previously reported in Davis *et al* 2005.

At site C, the additional soil moisture also had the effect of doubling the background CO<sub>2</sub> flux rate, and the underlying assumption is that this background increase is uniform across the LNAPL source zone. If this assumption does not hold, NSZD rates will be underestimated due to overcompensation of the background fluxes.

For reasons like these, assessment of the temporal variability in NSZD rates needs to be incorporated into monitoring programs with repeated measurements required for the same methodology at the same locations. Where estimated rates from different methods are contradictory at a significant level, further measurements should be conducted to determine the source of the discrepancies.

E-Flux traps are prone to the same variability as other surface flux methods. However, they also have a longer deployment time (7 to 20 days) which can reduce errors from diurnal or other temporal fluctuations when compared with methods such as LI-COR. They will not however account for seasonal or local short-term variations without additional sampling events. Site D is an example of this where three repeated E-Flux sampling events at 4 sampling locations recorded an average relative standard deviation of 75%. The main difference in results between readings was caused by increased soil moisture resulting from a large rainfall event. Since rainfall events are not predictable and given the relatively long deployment time for E-Flux traps, potential impacts of such events should be considered when interpreting results especially in finer textured soils. The main advantage of E-Flux traps is distinguishing between

modern (<50,000 years) and petrogenic carbon so they are not subject to errors associated with correction using a background location. This is extremely important as five out of six sites reviewed in this study (including sites A, C, D, E and F) had difficulty establishing representative background locations that presented similar surface and subsurface properties to the average conditions across the site, but with the absence of LNAPL contamination. Currently, the other main consideration of the E-Flux trap method is the relatively high cost compared with other methods, which potentially leads to less spatial and temporal coverage and hence higher variability in site-wide estimates.

LNAPL compositional analysis provides a good estimate of relative mass loss between two sampling periods (generally > 1 year in duration depending on the degradation rate) provided the source zone is stable and there are no unknown contributions of LNAPL. Like all the other subsurface methods, it also relies on a good connection between the well or sampling point and the formation, but it has the great advantage that it directly targets the LNAPL itself and can provide estimates at locations wherever LNAPL is present in a well. At 5 out of 6 sites, relative mass losses of LNAPL were estimated by this method, and in most cases, there was a large range of estimated relative losses (-1 to 99% of initial or changes over a time period for the spilled mass) reflecting the large variability of degradation rates across the sites and LNAPL types. Coupled with a mass estimate of the initial spill release or subsequently measured specific mass, an estimate of absolute mass loss can be calculated. Generally, in this study the absolute mass losses could not be calculated as the mass of the initial spill or specific mass estimates in the subsurface were not known.

Major gas and thermal gradient methods have the advantage in that they are relatively rapid (c. 15 min and 60 min respectively) and can be used in existing subsurface infrastructure provided the well construction is known and conditions met. In some cases in this study, construction was not known prior to sampling and samples were taken in the field where the screen interval was submerged making the readings for major gas gradients invalid. For the major gas method, this was evident by either fluid levels rising in the well as vacuum was increased, or by gas concentrations remaining relatively constant during measurement. Therefore, well construction information and groundwater elevation data are critical in developing a NSZD monitoring program. This is particularly the case in determining background locations as inappropriate well construction could potentially render an entire method invalid. In addition, some sites had very promising thermal background locations that were continually shaded at the surface by buildings, which results in thermal differences in the profile compared to a non-shaded site.

One of the main considerations in determining NSZD rates from gradient methods is the application of correct soil thermal conductivity and gas diffusion values. In this study no measured data was available, hence the most appropriate literature values were used. These values are also highly dependent on the water content and no allowance was made here for either temporal or spatial variations as no data was available.

Gradient methods by definition are also reliant on determining the depth at which the temperature or gas concentration is measured. In the case of in-well major gas sampling, the measurement depth is predetermined to be 300 mm above the fluid interface. However, if the same or higher O<sub>2</sub> or CO<sub>2</sub> concentration occurs higher in the

profile, then the gradient and therefore the NSZD rate will be higher (assuming gas diffusion properties are the same). In this way NSZD rates determined from major gas concentrations are likely to be conservative estimates. The installation of multiport vapour sampling strings is a way to overcome this in-well limitation, however such installations were only available at sites A and B and in both cases recorded higher NSZD rates than in-well based estimates. Comparison of NSZD rates from major gases sampled from in-well or in-ground multiport is the subject of ongoing research.

In summary, all methods employed here had advantages and disadvantages that were specific to each site, and in some cases with a level of specificity to the LNAPL type. Fundamentally all sites should have LNAPL samples collected periodically to provide an understanding of compositional changes over time as this is core information describing all the subsurface processes impacting LNAPL source zones. It also provides relative mass loss estimates. In addition to LNAPL composition, the application of appropriate NSZD gradient and surface CO<sub>2</sub> flux measurement methods, following a multiple lines of evidence approach, gives confidence in the determination of representative NSZD rates.

## 10. Conclusion

---

Six LNAPL contaminated sites documented in this study provide comparative example estimates of LNAPL recovery and NSZD rates across Australian climatic and hydrogeological environments. The sites have different LNAPLs (crude oil, gas condensate, diesel, gasoline and jet fuel), and different soil/aquifer types (limestone, sand, fluvial, fractured rock). Water tables reside at depths below ground surface ranging from around 2 m to 20 m and in some cases seasonal fluctuations were very little (<0.5 m) or very substantial (>4 m). In the case of site A the water table had daily fluctuations of about 1 m.

Site remedial efforts have involved conventional skimming, with and without drawdown, and multi-phase extraction, with some LNAPL recovery programs extending from months to decades. LNAPL recovery rates varied from less than a litre a day to perhaps greater than 100 L day<sup>-1</sup>.

NSZD rate estimation methods included carbon dioxide surface fluxes, subsurface temperature and soil gas, and LNAPL composition. Not all methods were undertaken at all sites, and in some instances, data was collected but deemed invalid because of adverse conditions, such as seasonally high water table elevations or inappropriate well construction. The average range across the six sites was around 2250 to 88,400 L LNAPL ha<sup>-1</sup> yr<sup>-1</sup>, with the upper end of the range measured by surface flux methods at Site E.

Across the six sites NSZD rate estimates were highly spatially variable. There are several factors. One factor is the distribution of existing monitoring well locations that were available to conduct gas and thermal gradient techniques as well as LNAPL composition assessments. The well distributions and density were not optimised for NSZD assessment nor LNAPL collection, thus may not provide ideal coverage within a source area or background locations. Surface flux methods may also provide limited coverage possible due to infrastructure (concrete covers, buildings), locations suitable for background correction (LI-COR) or due to budget constraints (E-Flux). Aside from spatially variable subsurface LNAPL distributions, inherent heterogeneity in subsurface properties (e.g. thermal conductivity and gas diffusion properties) also plays a role in the spatial variability of NSZD rate estimates and is exacerbated by the lack of site-specific measurements of key properties.

For lower NSZD rates, less heat would be produced, and lower consumption of oxygen and production of carbon dioxide would occur. This may lead to subdued changes in temperature, and oxygen and carbon dioxide concentrations that are more difficult to measure and may require longer time series of data or a greater intensity of data to gain greater surety and consistency of changes imposed by NSZD processes. This variability at lower rates creates challenges in then interpolating data spatially from point and local estimates across larger areas.

Temporal changes in NSZD rates are likely to be induced by seasonal variability in temperature, water table dynamics, soil moisture and microbial activity, for example. While this was observed at two sites and is not unexpected, the magnitude of the temporal variation and the impacts on annual rates is difficult to assess based on the data available in these six case studies. To assess the impacts of temporal variability on annual NSZD rates more frequent measurement are required over a longer

timeframe (2 to 3 years) with consideration given to climatic and weather factors that may influence measurements. In addition, utilising online monitoring of parameters (e.g. temperature, gas composition, VOCs, soil moisture) will add insight into the main sources of variability.

Based on mixed results across the sites there appears to be no one NSZD rate estimation method that is suitable for all sites or even for a particular site (due to spatial variability). This may reflect the differences between geology/hydrogeology, LNAPL type and age, season and antecedent conditions encountered during sampling campaigns. A multiple lines of evidence approach utilising multiple methods that cover different timescales may be warranted with different methods providing understanding of different aspects. For example, compositional analysis provides a time-integrated analysis of LNAPL changes but may be difficult to quantify, while thermal and gas gradient methods provide instantaneous rates based on vadose zone processes, and the different surface flux methods can provide rates over different timescales. Critical to all techniques except E-Flux is reference information, i.e. composition of LNAPL at the time of the spill (or early in the spill life) for comparison, or background reference locations for LI-COR and thermal/gas gradient methods.

Despite the variability induced by spatial, temporal and methodological factors NSZD rates for mature LNAPL sites or where recovery is limited by other factors (e.g. fractured rock) was generally shown to be equivalent to or indeed higher (up to 20 times) than recovery efforts at the six case study sites.

As the inclusion of NSZD assessment in LNAPL site management increases, additional case studies across an expanded combination of LNAPL types and geologies will provide greater certainty around rates and provide direction as to the best methods to use to estimate them.

## 11. References

---

- Alexander, R, Kagi, RI, Nobel, R & Volkman, JK 1984, 'Identification of some bicyclic alkanes in petroleum', *Organic Chemistry*, vol. 6, pp. 63–70.
- AS:2520-1981 1981, *Petroleum measurement tables*, Standards Australia.
- ASTM:D1655-18a 2018, *Standard specification for aviation turbine fuels*, ASTM International, West Conshohocken, Pennsylvania, United States.
- Baedecker, M, Eganhouse, R, Qi, H, Cozzarelli, I, Trost, J & Bekins, B 2018, 'Weathering of oil in a Surficial Aquifer', *Groundwater*, vol. 56, no. 5, pp. 797–809.
- Braissant, O, Wirz, D, Gopfert, B & Daniels, A 2010, 'Use of isothermal microcalorimetry to monitor microbial activities', *Fems Microbiology Letters*, vol. 303, no. 1, pp. 1–8.
- Brauner, JS, Downey, DC, Hicks, JR, Henry, BM & Hansen, JE, 2004, *Implementing monitored natural attenuation and expediting closure at fuel-release sites*, Technical report prepared for the Air Force Centre for Environmental Excellence and Defense Logistics Agency, Contract No. F41624-00-D-8024.
- Christensen, LB & Larsen, TE 1993, 'Method for determining the age of diesel oil spills in the soil', *Ground Water Monitoring and Remediation*, vol. 13, no. 4, pp. 142–149.
- CL:AIRE 2014, *An illustrated handbook of LNAPL transport and fate in the subsurface*, Contaminated Land: Applications in Real Environments, London, UK, available online at [www.claire.co.uk/LNAPL](http://www.claire.co.uk/LNAPL) (accessed February 22, 2018).
- CRC CARE 2018, *Technical measurement guidance for LNAPL natural source zone depletion*, CRC CARE Technical Report no. 44, CRC for Contamination Assessment and Remediation of the Environment, Newcastle, Australia.
- CRC CARE 2020, *The role of natural source zone depletion in the management of light non-aqueous phase liquid (LNAPL) contaminated sites*, CRC CARE Technical Report no. 46, CRC for Contamination Assessment and Remediation of the Environment, Newcastle, Australia.
- CSIRO 2019, *Database of corrected groundwater levels for Site D* (data extracted October 2019), Commonwealth Scientific and Industrial Research Organisation, Canberra, Australia.
- CSIRO 2019b, *Database of fluid levels for Site D* (data extracted October 2019), Commonwealth Scientific and Industrial Research Organisation, Canberra, Australia.
- Davis, GB, Barber, C, Power, TR, Thierrin, J, Patterson, BM, Rayner, JL & Wu, QL 1999, 'The variability and intrinsic remediation of a BTEX plume in anaerobic sulphate-rich groundwater', *Journal of Contaminant Hydrology*, vol. 36, no. 3–4, pp. 265–290.
- Davis, GB, Rayner, JL, Trefry, MG, Fisher, SJ & Patterson, BM 2005, 'Measurement and modeling of temporal variations in hydrocarbon vapor behavior in a layered soil profile', *Vadose Zone J.*, vol. 4, no. 2, pp. 225–239.
- Dobson, R, Schroth, M & Zeyer, J 2007, 'Effect of water-table fluctuation on dissolution and biodegradation of a multi-component, light nonaqueous-phase liquid', *Journal of Contaminant Hydrology*, vol. 94, no. 3–4, pp. 235–248.
- Domenico, PA & Schwartz, FW 1998, *Physical and chemical hydrogeology*. John Wiley & Sons, New York, USA.

Donn, M, Rayner, JL & Davis, GB 2017, *List of items/data and measurements required from industry for the SZND National Guidance Project*, CSIRO Land and Water Report to CRC CARE (Confidential).

Douglas, G, Bence, A, Prince, R, McMillen, S & Butler, E 1996, 'Environmental stability of selected petroleum hydrocarbon source and weathering ratios', *Environmental Science & Technology*, vol. 30, no. 7, pp. 2332–2339.

Douglas, G, Hardenstine, J, Liu, B & Uhler, A 2012, 'Laboratory and field verification of a method to estimate the extent of petroleum biodegradation in soil', *Environmental Science & Technology*, vol. 46, no. 15, pp. 8279–8287.

Eichert, J, McAlexander, B, Lyverse, M, Michalski, P & Sihota, N 2017, 'Spatial and temporal variation in natural source zone depletion rates at a former oil refinery', *Vadose Zone Journal*, vol. 16, no. 10.

Fiorenza, S & Ward, C 1997, 'Microbial adaptation to hydrogen peroxide and biodegradation of aromatic hydrocarbons', *Journal of Industrial Microbiology & Biotechnology*, vol. 18, no. 2–3, pp. 140–151.

Fisher, S, Alexander, R & Kagi, R 1996, 'Biodegradation of alkyl-naphthalenes in sediments adjacent to an off-shore petroleum production platform', *Polycyclic Aromatic Compounds*, vol. 11, no. 1–4, pp. 35–42.

Franzmann, PD, Zappia, LR, Power, TR, Davis, GB & Patterson, BM 1999, 'Microbial mineralisation of benzene and characterisation of microbial biomass in soil above hydrocarbon-contaminated groundwater', *Fems Microbiology Ecology*, vol. 30, no. 1, pp. 67–76.

Garg, S, Newell, C, Kulkarni, P, King, D, Adamson, D, Renno, M & Sale, T 2017, 'Overview of natural source zone depletion: processes, controlling factors, and composition change', *Ground Water Monitoring and Remediation*, vol. 37, no. 3, pp. 62–81.

Geoscience Australia 2015, *Elvis – Elevation and depth foundation spatial data*, available at [elevation.fsdf.org.au](http://elevation.fsdf.org.au).

Hansen, D, van Aarssen, BGK, Bastow, TP, Alexander, R & Kagi, RI, 2002, *Maturation and biodegradation effects on the diastereomers of pristane and phytane*, Poster presentation at Australian Organic Geochemistry Conference, Hobart, Australia, 12–15 February.

Howarth, RJ 2017, *Dictionary of mathematical geosciences: with historical notes*, Springer International Publishing, Cham, Switzerland, pp. 133–175.

Interstate Technology & Regulatory Council (ITRC) 2009a, *Evaluating LNAPL remedial technologies for achieving project goals*, Interstate Technology & Regulatory Council, LNAPLs Team, Washington, DC, available online [www.itrcweb.org/guidance/getdocument?documentid=48](http://www.itrcweb.org/guidance/getdocument?documentid=48) (accessed on February 22, 2018).

ITRC 2009b, *Evaluating natural source zone depletion at sites with LNAPL*, Interstate Technology & Regulatory Council, LNAPLs Team, Washington, DC, available online [www.itrcweb.org/GuidanceDocuments/LNAPL-1.pdf](http://www.itrcweb.org/GuidanceDocuments/LNAPL-1.pdf) (accessed on February 22, 2018).

Johnston, C, Bastow, T & Innes, N 2007, 'The use of biodegradation signatures and biomarkers to differentiate spills of petroleum hydrocarbon liquids in the subsurface and estimate natural mass loss', *European Journal of Soil Biology*, vol. 43, no. 5–6, pp. 328–334.

Johnston, CD, Robertson, BS & Bastow, T, 2008, 'GQ07: Evidence for the success of biosparging LNAPL diesel in the water table zone of a shallow sand aquifer' in *Securing groundwater quality in urban and industrial environments Proceedings of the*

6th International IAHS Groundwater Quality Conference, Fremantle, Western Australia, 2–7 December 2007, pp. 234–241.

Kaplan, I, Galperin, Y, Alimi, H, Lee, R & Lu, S 1996, 'Patterns of chemical changes during environmental alteration of hydrocarbon fuels', *Ground Water Monitoring and Remediation*, vol. 16, no. 4, pp. 113–124.

Kechavarzi, C, Soga, K & Illangasekare, T 2005, 'Two-dimensional laboratory simulation of LNAPL infiltration and redistribution in the vadose zone', *Journal of Contaminant Hydrology*, vol. 76, no. 3–4, pp. 211–233.

Kulkarni, PR, King, DC, McHugh, TE, Adamson, DT & Newell, CJ 2017, 'Impact of temperature on groundwater source attenuation rates at hydrocarbon sites', *Ground Water Monitoring and Remediation*, vol. 37, no. 3, pp. 82–93.

Lenhard, R, Rayner, J & Davis, G 2017, 'A practical tool for estimating subsurface LNAPL distributions and transmissivity using current and historical fluid levels in groundwater wells: effects of entrapped and residual LNAPL', *Journal of Contaminant Hydrology*, vol. 205, pp. 1–11.

Napoli, M, Massetti, L, Brandani, G, Petralli, M & Orlandini, S 2016, 'Modeling tree shade effect on urban ground surface temperature', *Journal of Environmental Quality*, vol. 45, no. 1, pp. 146–156.

Newell, CJ, Acree, SD, Ross, RR & Huling, SG, 1995, *Light nonaqueous phase liquids*, EPA Ground Water Issue EPA/540/S-95/500, United States Environmental Protection Agency, Washington DC, USA.

Palaia, T 2016, 'Natural source zone depletion rate assessment', *Applied NAPL Science Review* 6

Pandey, J, Chauhan, A & Jain, RK 2009, 'Integrative approaches for assessing the ecological sustainability of in situ bioremediation', *Fems Microbiology Reviews*, vol. 33, no. 2, pp. 324–375.

Patterson, B & Davis, G 2008, 'An in situ device to measure oxygen in the vadose zone and in ground water: Laboratory testing and field evaluation', *Ground Water Monitoring and Remediation*, vol. 28, no. 2, pp. 68–74.

Patterson, B, Furness, A & Bastow, T 2013, 'Soil gas carbon dioxide probe: laboratory testing and field evaluation', *Environmental Science-Processes & Impacts*, vol. 15, no. 5, pp. 1062–1069.

Patterson, BM, Davis, GB & McKinley, AJ 2000, 'Volatile organic compounds in groundwater, probes for the analysis of' in Meyers, RA (Ed.), *Encyclopedia of analytical chemistry: instrumentation and application*, John Wiley & Sons Ltd., New Jersey, USA, pp. 3515–3526.

Peters, KE & Moldowan, JM 1993, *The biomarker guide. Interpreting molecular fossils in petroleum and ancient sediments*, Prentice-Hall Inc., Englewood Cliffs, New Jersey, USA.

QGIS Development Team 2019, *QGIS Geographic Information System*, Open Source Geospatial Foundation Project, [qgis.osgeo.org](http://qgis.osgeo.org).

Queensland Government 2019, *SILO – Australian climate data from 1889 to yesterday*, Department of Environmental Science, Brisbane, QLD, Australia, available at [www.longpaddock.qld.gov.au/silo/](http://www.longpaddock.qld.gov.au/silo/).

Sookhak Lari, K, Rayner, JL & Davis, GB 2018, 'Towards characterizing LNAPL remediation endpoints', *Journal of Environmental Management*, vol. 224, pp. 97–105.



Suthersan, SS, Horst, J, Schnobrich, M, Welty, N & McDonough, J 2017, *Remediation engineering: design concepts*, Second edition, Taylor & Francis, CRC Press, Boca Raton, USA.

Sweeney, R & Ririe, G 2014, 'Temperature as a tool to evaluate aerobic biodegradation in hydrocarbon contaminated soil', *Ground Water Monitoring and Remediation*, vol. 34, no. 3, pp. 41–50.

Teramoto, EH & Chang, HK 2017, 'Field data and numerical simulation of btex concentration trends under water table fluctuations: example of a jet fuel-contaminated site in Brazil', *Journal of Contaminant Hydrology*, vol. 198, pp. 37–47.

van Aarssen, BGK, Cox, HC, Hoogendoorn, P & de Leeuw, JW 1990, 'A cadinene biopolymer in fossil and extant dammar resins as a source for cadinanes and bicadinanes in crude oils from South East Asia'. *Geochimica Et Cosmochimica Acta*, vol. 54, no.11, pp. 3021-3031. DOI:10.1016/0016-7037(90)90119-6

Vasudevan, M, Johnston, CD, Bastow, TP, Lekmine, G, Rayner, JL, Nambi, IM, Kumar, GS, Krishna, RR & Davis, GB 2016, 'Effect of compositional heterogeneity on dissolution of non-ideal LNAPL mixtures'. *Journal of Contaminant Hydrology*, vol. 194, pp. 10-16. DOI:10.1016/j.jconhyd.2016.09.006

Volkman, JK, Alexander, R, Kagi, RI, Rowland, SJ & Sheppard, PN 1984, 'Biodegradation of aromatic hydrocarbons in crude oils from the Barrow Sub-basin of Western Australia', *Organic Geochemistry*, vol. 6, pp. 619–632.

Volkman, JK, Alexander, R, Kagi, RI & Woodhouse, GW 1983, 'Demethylated hopanes in crude oils and their applications in petroleum geochemistry', *Geochimica et Cosmochimica Acta*, vol. 47, no. 4, pp. 785–794.

Wade, M 2001, 'Age-dating diesel fuel spills: using the European empirical time-based model in the USA', *Environmental Forensics*, vol. 2, no. 4, pp. 347–358.

Warren, E & Bekins, B 2015, 'Relating subsurface temperature changes to microbial activity at a crude oil-contaminated site', *Journal of Contaminant Hydrology*, vol. 182, pp. 183–193.

Wiedemeier, TH, Rifai, HS, Newell, CJ & Wilson, JT 1999, *Natural attenuation of fuels and chlorinated solvents in the subsurface*, John Wiley & Sons Inc, New Jersey, USA.

Yadav, B & Hassanizadeh, S 2011, 'An overview of biodegradation of LNAPLs in coastal (semi)-arid environment', *Water Air and Soil Pollution*, vol. 220, no. 1–4, pp. 225–239.

Yang, X, Erickson, L & Fan, L 1995, 'A study of the dissolution rate-limited bioremediation of soils contaminated by residual hydrocarbons', *Journal of Hazardous Materials*, vol. 41, no. 2–3, pp. 299–313.

## 12. Coded references to confidential reports and files

### 12.1 Site A

ID	File name	Date
SiteA_Ref1	10-RG-10009_Rev A.pdf	5/01/2016
SiteA_Ref2	10-RG-10014_Rev 0.pdf	13/05/2016
SiteA_Ref3	10-RG-10015_Rev 0.pdf	13/05/2016
SiteA_Ref4	10-RG-10018_Rev 0.pdf	12/05/2016
SiteA_Ref5	10-RG-10019_Rev 0.pdf	9/05/2016
SiteA_Ref6	10-RG-10023_Rev 0.pdf	26/04/2016
SiteA_Ref7	10-RG-10033_Rev A_review.pdf	30/09/2016
SiteA_Ref8	10-RI-10035_Rev 0.pdf	23/05/2016
SiteA_Ref9	10-RI-10058_Rev 0.pdf	6/06/2017
SiteA_Ref10	10-RI-10059_Rev 0.pdf	23/05/2017
SiteA_Ref11	10-RI-10064_Rev 1_review.pdf	26/06/2017
SiteA_Ref12	10-RI-10079_Rev 0.pdf	29/06/2017
SiteA_Ref13	10-RI-10091.0.IFA.pdf	23/04/2018
SiteA_Ref14	14C Results Report XXXAU 2-9-2018.pdf	December 2017
SiteA_Ref15	Figures from XXX-10-RI-10078_Rev A.pdf	18/7/2017
SiteA_Ref16	XXX_LNAPL_Cumulative_recovery.xlsx	October 2018

XXX = location name omitted to maintain confidentiality

### 12.2 Site B

ID	File name	Date
SiteB_Ref1	JA1376 [A PowerPoint presentation on "Vacuum Enhanced Pumping (VEP): Specifications and Operating Procedures"]	Oct-04
SiteB_Ref2	Recoverability.ppt [A PowerPoint presentation on 'Practical Approach to Prioritising and Optimising Product Recovery']	Oct-05
SiteB_Ref3	Monitoring and Recovery of Separate Phase Hydrocarbon, Jan 2005 – Dec 2005	Feb-06
SiteB_Ref4	XXX_PER_2003-2006_V2.pdf	Dec-06
SiteB_Ref5	Subsurface Temperature Investigation Report.pdf	Mar-10
SiteB_Ref6	Plume area 2013.pdf	2013
SiteB_Ref7	XXX_SZNA Site Selection Report – 29Jan16 – Draft.docx	Jan-16
SiteB_Ref8	XXX_LNAPL Recovery_Site_Selection Phase 1_supplementary.pdf	Mar-16
SiteB_Ref9	XXX_LNAPL Recovery_Site_Section-23Mar16.docx	Mar-16
SiteB_Ref10	CSIRO XXX NSZD Project – Phase 2 report draft.pdf	Oct-16
SiteB_Ref11	2016 LNAPL Contour Maps_V01.pdf	Feb-16

XXX = location name omitted to maintain confidentiality

## 12.3 Site C

ID	File name	Date
SiteC_Ref1	XXX-HSE-0201494.pdf	25-Oct-13
SiteC_Ref2	XXX_2013_GME_Final_Report.pdf	01-Apr-14
SiteC_Ref3	CRC CARE Technical Report Remediation in Fractured Rock Draft April 2014.pdf	10-Apr-14
SiteC_Ref4	XXX_T0267_G0740_B.PDF	26-Jun-14
SiteC_Ref5	XXX_T0267_G0741_B.PDF	30-Jun-14
SiteC_Ref6	XXX_monitoring_logs_20150528_DRAFT.PDF	22-May-15
SiteC_Ref7	Bore installation report-ERB.pdf	04-Jun-15
SiteC_Ref8	XXX_GME_October_2015-Final.pdf	10-Mar-16
SiteC_Ref9	XXX_Oct_2016_GME_Rev 0.pdf	22-Dec-16
SiteC_Ref10	60550172_XXX6Oct 2017_DSIGME.pdf	27-Mar-18
SiteC_Ref11	60579998_XXX21Dec 2018_GME_0.pdf	21-Dec-18
SiteC_Ref12	XXXWell locations 2014.xlsx	July 2019
SiteC_Ref13	XX_Project Exit Report_140410.docx	14-Apr-14

XXX = location name omitted to maintain confidentiality

## 12.4 Site D

ID	File name	Date
SiteD_Ref1	AJL_University_Honours_thesis_Potential_for_NaturalAttenuation_atXXX.pdf	26-Oct-00
SiteD_Ref2	Nov2011 Updated CleanUp Plan_Final.pdf	17-Nov-11
SiteD_Ref3	0182278 Monthly PSH Gauging Data 2013 Dec2012 to May2013.xls	14-May-13
SiteD_Ref4	43295485 XXX GME May13_Final.pdf	09-Sept-13
SiteD_Ref5	Methods and observations during sampling from XXX.docs	15-May-14
SiteD_Ref6	Well logs MPV01 to MPV12.pdf	19-May-14
SiteD_Ref7	XXX Review Ver 2014-1-2.docx	July 2014
SiteD_Ref8	Aquifer pump test well NP51 24 August 2014 – Report Dec 2014 v1.docx	Dec 2014
SiteD_Ref9	XXX Drilling Logs.pdf	16-Jan-17
SiteD_Ref10	XXX MPVE Data & Graphs.xlsx	16-Jan-17
SiteD_Ref11	XXX GME October 2018_Draft RO Comments 21Dec.pdf	7-Dec-18

XXX = location name omitted to maintain confidentiality

## 12.5 Site E

ID	File name	Date
SiteE_Ref1	2017_05_11_1158-XXX -Natural Source Zone Depletion Assessment.pdf	May 2017
SiteE_Ref2	PSI_Proposed_Apartment_Development_XXX.pdf	September 2017
SiteE_Ref3	XXX Pollution Incident Response Management Plan.pdf	April 2015
SiteE_Ref4	Geological Survey of XXX	2014
SiteE_Ref5	XXX Coast and Estuary Management Study	2003

XXX = location name omitted to maintain confidentiality

## 12.6 Site F

ID	File name	Date
SiteF_Ref1	R10 (XXX ESA 2019) Rev A reduced size.pdf	18/01/2019
SiteF_Ref2	XXX rev B FIG 5.pdf	25/06/2007
SiteF_Ref3	Historical Tables March 2019 -XXX.xlsx	March 2019

XXX = location name omitted to maintain confidentiality

## Appendices

Appendix	Title	Figures and tables
A.1	Site A methodology for E-Flux	Figure A.1-1 Schematic diagram showing an E-Flux CO <sub>2</sub> trap installation from SiteA_Ref4 (2016) Figure A.1-2 A typical deployment of E-Flux CO <sub>2</sub> trap installations from SiteA_Ref4 (2016)
A.2	Site A methodology for LI-COR	Figure A.2-1 Collar for connection to CO <sub>2</sub> chamber from SiteA_Ref4 (2016)
A.3	Site A well construction logs	Well construction logs for MW35, MW44, MW46a, MW57, MW58, MW60, MW67, MW72, MW73, MW74, MW76, SV1
A.4	Site A time series plots of LNAPL thickness (bn), corrected water table elevation (Zaw), and LNAPL elevation (Zan) for selected wells	Time series plots for MW16, MW40, MW41, MW46a, MW57, MW58, MW58, MW60, MW67, MW69, MW70, MW71, MW72, MW73, MW74
A.5	Site A methodology for in-well temperature monitoring	—
A.6	Site A methodology for sampling soil vapour from soil vapour probes	—
A.7	Site A methodology for in-well gas sampling	—
A.8	Site A density and analytical results for condensate LNAPL samples	Table A.8-1 Density and analytical results for condensate LNAPL samples
A.9	Site A LNAPL percentage loss relationships	Figure A.8-1 Plot of % loss (w/w) versus density for site A samples Figure A.8-2 Plot of % loss (w/w) versus time for site A samples
B.1	Site B methodology for gas sampling and CSIRO analytical methods	Table B.1-1 Results for selected components for samples taken from core C67 for the D6 site Table B.1-2 Results for selected components for samples taken from core C70 for the D10 site Table B.1-3 Results for selected components for samples taken from core C71 for the D10 site
C.1	GC-MS analytical and density results	Figure C.1-1 GC-MS analysis of LNAPL sample CS01 from 2012 and 2019 Figure C.1-2 GC-MS analysis of LNAPL sample CS02 from 2012 and 2019 Figure C.1-3 GC-MS analysis of LNAPL sample CS03 from 2012 and 2019 Figure C.1-4 GC-MS analysis of LNAPL sample MW19 from 2011 and 2019 Figure C.1-5 GC-MS analysis of LNAPL sample MW31 from 2011 and 2019

Appendix	Title	Figures and tables
		<p>Figure C.1-6 GC-MS analysis of LNAPL sample MW125 from 2019</p> <p>Figure C.1-7. GC-MS analysis of LNAPL sample MW157 from 2011 and 2019</p> <p>Figure C.1-8 GC-MS analysis of LNAPL sample MB14CL052 from 2019</p> <p>Table C.1-1 Density and analytical results for site C LNAPL samples</p>
C.2	Site C logs from six wells drilled for a research program conducted by CSIRO (SiteC_Ref3, 2014)	CS01, CS02, CS03, CS04, CS05, and CS06
D.1	Site D GC-FID analytical and density results	<p>Figure D.1-1 GC-FID analysis of LNAPL sample OS08 from 2013 and 2018</p> <p>Figure D.1-2 GC-FID analysis of LNAPL sample OS12 from 2013 and 2018</p> <p>Figure D.1-3 GC-FID analysis of LNAPL sample OS28 from 2013 and 2018</p> <p>Figure D.1-4 GC-FID analysis of LNAPL sample OS41 from 2018</p> <p>Figure D.1-5 GC-FID analysis of LNAPL sample OS70 from 2018</p> <p>Figure D.1-6 GC-FID analysis of LNAPL sample OS63 from 2013 and 2018</p> <p><b>Table D.1-1 Density and analytical results for site D LNAPL samples</b></p>
D.2	Site D well logs	MPVE03, MPVE05, MPVE10, OS08, OS12, OS22, OS41 and OS63
E.1	Site E natural source zone depletion rate estimates	Table E.1-1 NSZD rates from SiteE_Ref1 (2017)
F.1	Site F well logs	BH59, BH60, and BH61
F.2	Site F GC-FID analytical and density results	<p>Figure F.2-1 GC-FID analysis of LNAPL sample MW1 from 2008 as well as comparison of C15-27 components in LNAPL MW98 from 2019 (the least biodegraded 2019 LNAPL sample)</p> <p>Figure F.2-2 GC-FID analysis of LNAPL sample MW22 from 2008 as well as comparison of C15-27 components in LNAPL MW98 from 2019 (the least biodegraded 2019 LNAPL sample)</p> <p>Figure F.2-3 GC-FID analysis of LNAPL sample MW36 from 2008 as well as comparison of C15-27 components in LNAPL MW98 from 2019 (the least biodegraded 2019 LNAPL sample)</p> <p>Figure F.2-4 GC-FID analysis of LNAPL sample MW60 from 2008 as well as comparison of C15-27 components in LNAPL MW98 from 2019 (the least biodegraded 2019 LNAPL sample)</p> <p>Figure F.2-5 GC-FID analysis of LNAPL sample MW9S from 2019 MW9S from 2019</p> <p>Figure F.2-6 GC-FID analysis of LNAPL sample MW22 from 2019</p> <p>Figure F.2-7 GC-FID analysis of LNAPL sample MW23 from 2019</p>

Appendix	Title	Figures and tables
		<p>Figure F.2-8 GC-FID analysis of LNAPL sample MW28 from 2019</p> <p>Figure F.2-9 GC-FID analysis of LNAPL sample MW40 from 2019</p> <p>Figure F.2-10 GC-FID analysis of LNAPL sample MW69 from 2019</p> <p>Figure F.2-11 GC-FID analysis of LNAPL sample MW81 from 2019</p> <p>Figure F.2-12 GC-FID analysis of LNAPL sample MW82 from 2019</p> <p>Figure F.2-13 GC-FID analysis of LNAPL sample MW83 from 2019</p> <p>Figure F.2-14 GC-FID analysis of LNAPL sample MW85 from 2019</p> <p>Figure F.2-15 GC-FID analysis of LNAPL sample MW96 from 2019</p> <p>Figure F.2-16 GC-FID analysis of LNAPL sample MW98 from 2019</p> <p>Figure F.2-17 GC-FID analysis of LNAPL sample MW99 from 2019</p> <p>Figure F.2-18 GC-FID analysis of LNAPL sample MW112 from 2019</p> <p>Figure F.2-19 GC-FID analysis of LNAPL sample MW113 from 2019</p> <p>Table F.2-1 Density and analytical results for site F LNAPL samples</p>

## APPENDIX A.1

### Site A methodology for E-Flux

The E-Flux equipment included a receiver pipe, a CO<sub>2</sub> trap with dual sorbent pucks and a vented protective cover. The installation of the trap into the sub-surface is shown in Figure A.1-1 and Figure A.1-2. The trap was deployed for the period between 29 October 2015 and 3 November 2015 at one sample location (FS5) (SiteA\_Ref4 2016). An additional CO<sub>2</sub> trap was assessed on the site at a background location consistent with location FS7. The trap was retained on site to establish background CO<sub>2</sub>. E-Flux CO<sub>2</sub> traps were sent to the manufacturer (E-Flux LLC) for analysis. The chemical analysis is based on methods ASTM 4373-02 (*Rapid determination of carbonate content in soils* (ASTM 2002)) and ASTM D6686-12 (*Determining the biobased content of solids, liquids and gases using radiocarbon analysis* (ASTM 2012)) as stated in SiteA\_Ref4 (2016).

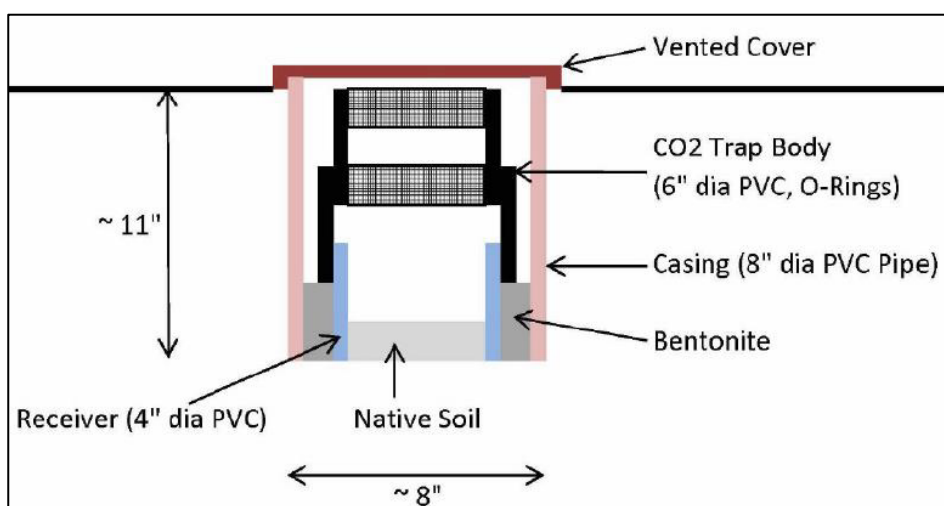


Figure A.1-1 Schematic diagram showing an E-Flux CO<sub>2</sub> trap installation from SiteA\_Ref4 (2016)



Figure A.1-2 A typical deployment of E-Flux CO<sub>2</sub> trap installations from SiteA\_Ref4 (2016)



## APPENDIX A.2

### Site A methodology for LI-COR

---

According to SiteA\_Ref4 (2016), a 10-cm LI-COR chamber was sealed with the ground and the equipment connected consistent with the manufacturer's specification.

Moreover:

'...to ensure connectivity with the ground surface, a collar [Figure A.2-1] having a diameter consistent with the survey chamber, was set into the ground with the chamber then positioned in this collar. The collars were set below the depth of vegetation (approximately 5–8 cm into the ground surface)' (SiteA\_Ref4 2016, p. 4).



**Figure A.2-1 Collar for connection to CO<sub>2</sub> chamber from SiteA\_Ref4 (2016)**

Additional notes on the LI-COR methodology are as follows:

'Measurements of CO<sub>2</sub> concentration versus time were then recorded. The slope of the CO<sub>2</sub> concentration is the efflux of CO<sub>2</sub> from the sub-surface. A minimum of ten sample measurements, of approximately 3 minutes duration each in accordance with the manufacturer's operating instructions, were made at each location. Only data where a stable slope was observed in the measurement was used to assess CO<sub>2</sub> flux.

A total of six sampling locations (FS1 to FS6) were undertaken across the extent of the condensate plume in accessible locations...The precise location of each sample was not critical, instead sampling locations were distributed to include various locations across the extent of impact, including the edge and middle of the Condensate LNAPL Plume. It is noted that the locations chosen for collar placement were devoid of vegetation, although the surrounding ground surface may have included vegetation' (SiteA\_Ref4 2016, p. 4).

## APPENDIX A.3

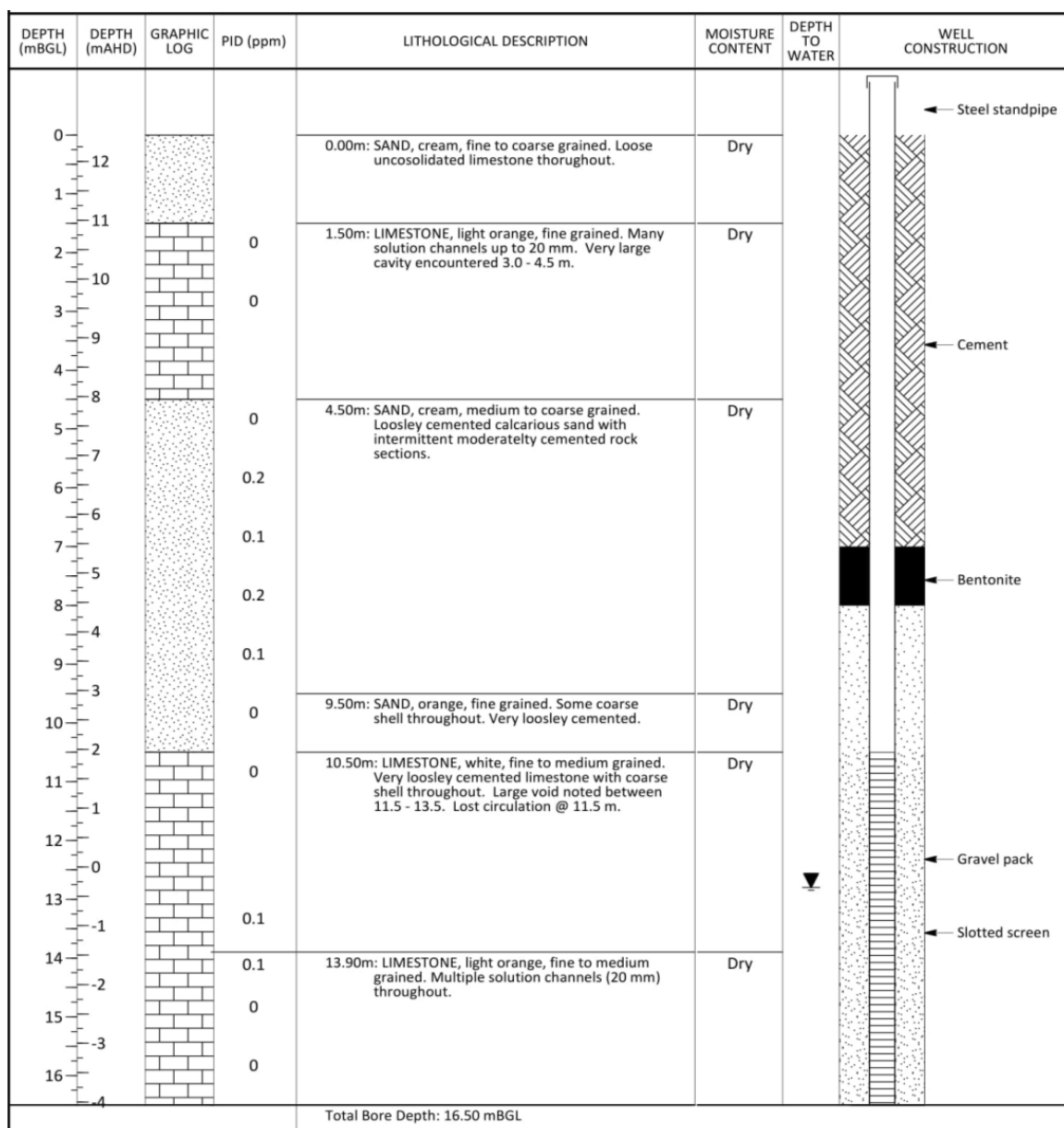
### Site A well construction logs

MW35

Ground level mAHD: 12.56

Drilling method: Diamond Core/Mud Rotary 160 mm

Casing Diameter: 100 mm



MW44

Ground level mAHD: 4.78

SUBSURFACE PROFILE						SAMPLING				
Drilling Method	Water	Depth (m)	Graphic	USCS	Description	Moisture	Recovery	Sampling	Well Construction Details	PID (ppm)
Sonic		-1								
		0								
		1		SW	<b>SAND</b> Pale brown, fine to coarse grained, trace of fine gravels, shell fragments present, roots on top 0.1m.					
		2			<b>LIMESTONE</b> Weathered on surface, hard.					
		3								
		4								
		5								
		6				From 4.5 to 7.2m, black staining (smear zone), slight hydrocarbon odour in black stained areas. More staining / odour in the more porous sectors of the profile and within solution channels. PID readings taken through profile by placing probe tip into solution holes and cavities.				
		7								
		8				Groundwater well terminated at 7.2m.				
		9								
		10								
		11								
		12								
		13								
		14								
		15								
		16								
		17								
		18								
	19									
	20									

Hole diameter 150mm.

PVC Riser

Bentonite

50mm Casing

2.2mbgl.

50mm Screen

Water level at 5.09 mbgl. (14:20/25.08.15)

Sand

End Cap at 7.2mbgl.

2.8

0.6

Legend: D - Dry

SW - Soil/Coarse

SP - Soil/Fine

GW - Gravel/Course

GC - Gravel/Clays

MW46a

Ground level mAHD: 9.57

SUBSURFACE PROFILE						SAMPLING				
Drilling Method	Water	Depth (m)	Graphic	USCS	Description	Moisture	Recovery	Sampling	Well Construction Details	PID (ppm)
Sonic		-1								
		0		SW	<b>FILL</b> Gravelly SAND, red-brown, fine to coarse grained sand, fine to medium gravels.				Hole diameter 150mm.	
		1			<b>LIMESTONE</b> No sample recovery, flat drill bit used.				PVC Riser	
		2							Grout	
		3								
		4								
		5							Bentonite	
		6							80mm Casing	
		7				Pale brown to red-brown, hard, minor solutions cavities throughout.				
		8				Staining from 8.5 to 9.5m. Slight to moderate hydrocarbon odour.				
		9				No sample recovery, flat drill bit used. No notable odours or groundwater colour change.			Water level at 9.60 mbgl. (17:15/17.10.15)	
		10							Sand	
		11							80mm Screen	
		12							End Cap at 13.2mbgl.	
		13			Groundwater well terminated at 13.2m.					
		14								
		15								
		16								
		17								
		18								
		19								
		20								

MW57

Ground level mAHD: 8.13

SUBSURFACE PROFILE						SAMPLING				
Drilling Method	Water	Depth (m)	Graphic	USCS	Description	Moisture	Recovery	Sampling	Well Construction Details	PID (ppm)
Sonic		-1								
		0								
		1		SP	<b>FILL</b> Gravelly SAND, pale brown, fine to coarse grained sand, fine to coarse gravels, trace of silt.	D				
		2			<b>LIMESTONE</b> Pale brown with red-brown mottling. Gravels are fine to coarse. Pores are small and frequent. Rare dissolution cavities to 7.5m.					
		3								
		4								
		5								
		6								
		7								
		8			Pale grey staining from 7.5 to 8.0m.					
		9			Heavy dark staining from 8.0 to 8.9m throughout core profile with moderate hydrocarbon odour.					
		10			Below 8.9m staining is pale grey to predominantly within dissolution channels. Mottled staining all the way to 12.0m.					
		11								
		12			Groundwater well terminated at 12.0m.					
		13								
		14								
		15								
		16								
		17								
		18								
	19									
	20									

							</			

Legend: D - Dry

SW - Soil/Coarse

SP - Soil/Fine

GW - Gravel/Course

GC - Gravel/Clays

MW58

Ground level mAHd: 10.45

SUBSURFACE PROFILE						SAMPLING				
Drilling Method	Water	Depth (m)	Graphic	USCS	Description	Moisture	Recovery	Sampling	Well Construction Details	PID (ppm)
Sonic		-1							Hole diameter 150mm.	
		0		SP	<b>Gravelly SAND</b> Medium brown, fine to coarse grained sand, fine to coarse gravels, trace of silt, gravel content reducing with depth.	D			PVC Riser	0.0
		1		SP	<b>SAND</b> Medium brown, fine to coarse grained, trace of fine gravels and silt.	D			Bentonite	0.1
		2							80mm Casing	0.1
		3								
		4		SP	<b>Gravelly SAND</b> Medium brown, fine to coarse grained sand, fine to coarse gravels.	D				
		5								
		6								
		7							7.3mbgl.	0.1
		8			<b>LIMESTONE</b> Pale brown to red-brown, weathered on top of limestone, hard. Pores are small and in-frequent. Staining with degraded hydrocarbon odour at 8.8m. More pores and larger pores at 9.0m. Black staining and hydrocarbon odour in cavities.					0.1
		9							Water level at 9.02 mbgl. (15:30/02.09.15)	0.1
		10								199
		11							80mm Screen	
		12			Dark black band at 11.5m, mild hydrocarbon odour, weathered.				Sand	2.9
		13			Groundwater well terminated at 13.5m.				End Cap at 13.3mbgl.	
		14								
		15								
		16								
		17								
		18								
	19									
	20									

Legend: D - Dry      SW - Soil/Coarse      SP - Soil/Fine      GW - Gravel/Course      GC - Gravel/Clays

Legend: D - Dry

SW - Soil/Coarse

SP - Soil/Fine

GW - Gravel/Coarse

GC - Gravel/Clays

MW60

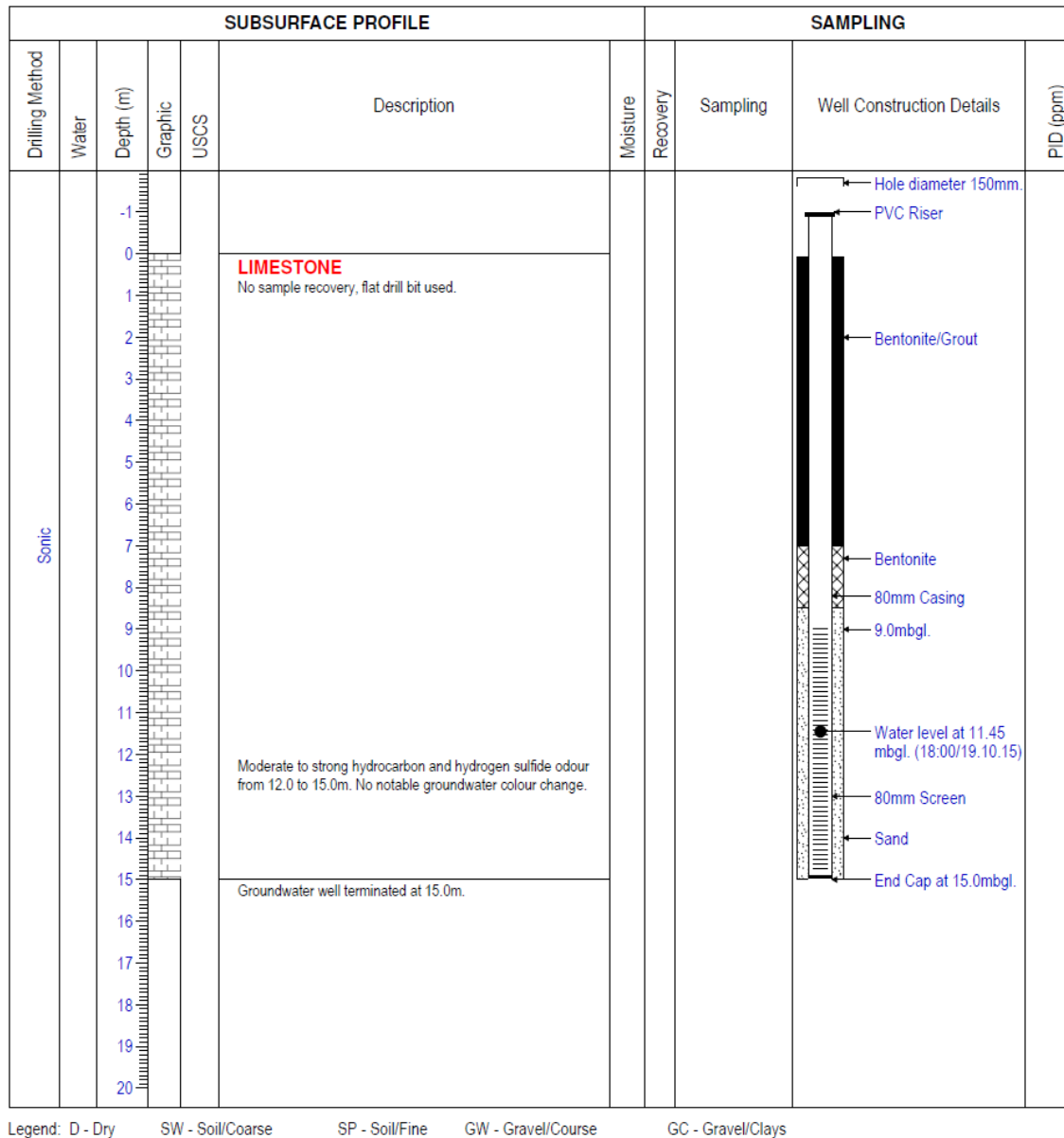
Ground level mAHD: 9.28

SUBSURFACE PROFILE						SAMPLING			
Drilling Method	Water	Depth (m)	Graphic	USCS	Description	Moisture	Recovery	Sampling	Well Construction Details
Sonic		-1							Hole diameter 150mm.
		0			<b>LIMESTONE</b>				PVC Riser
		1			Drilled with flat bit, no sample.				
		2							Bentonite
		3							80mm Casing
		4							
		5							
		6							6.8mbgl.
		7							
		8							Water level at 8.73 mbgl. (17:40/02.09.15)
		9			Grey water returns with hydrocarbon odour at 9.5m.				80mm Screen
		10			Loss of water return at 10.5 to 11.0m.				Sand
		11							
		12							End Cap at 12.8mbgl.
		13			Groundwater well terminated at 13.0m.				
		14							
		15							
		16							
		17							
		18							
		19							
		20							

Legend: D - Dry      SW - Soil/Coarse      SP - Soil/Fine      GW - Gravel/Course      GC - Gravel/Clays

MW67

Ground level mAHD: 11.66





MW72

Ground level mAHD: 8.25

SUBSURFACE PROFILE						SAMPLING				
Drilling Method	Water	Depth (m)	Graphic	USCS	Description	Moisture	Recovery	Sampling	Well Construction Details	PID (ppm)
Sonic		-1							<p>Hole diameter 150mm.</p> <p>PVC Riser</p> <p>Bento/Grout</p> <p>Bentonite</p> <p>100mm Casing</p> <p>6.3mbgl.</p> <p>Water Level at 8.75 mbgl. (16.45/26.09.15)</p> <p>100mm Screen</p> <p>Sand</p> <p>End Cap at 12.3mbgl.</p>	
		0			<b>LIMESTONE</b> No sample returns, flat drill bit used.					
		1								
		2								
		3								
		4								
		5								
		6								
		7								
		8								
		9			Dark grey to black return water at 8.7m with hydrocarbon odour.					
		10								
		11								
		12								
		13			Groundwater well terminated at 12.5m.					
		14								
		15								
		16								
		17								
		18								
		19								
	20									

Legend: D - Dry    SW - Soil/Coarse    SP - Soil/Fine    GW - Gravel/Course    GC - Gravel/Clays

MW73

Ground level mAHD: 8.15

SUBSURFACE PROFILE						SAMPLING			
Drilling Method	Water	Depth (m)	Graphic	USCS	Description	Moisture	Recovery	Sampling	Well Construction Details
Sonic		-1							
		0			<b>LIMESTONE</b> No sample returns, flat drill bit used.				
		1							
		2							
		3							
		4							
		5							
		6							
		7							
		8							
		9			Dark grey to black return water at 8.5m. Strong hydrocarbon odour.				
		10							
		11							
		12			Groundwater well terminated at 12.0m.				
		13							
		14							
		15							
		16							
		17							
		18							
		19							
		20							

Legend: D - Dry

SW - Soil/Coarse

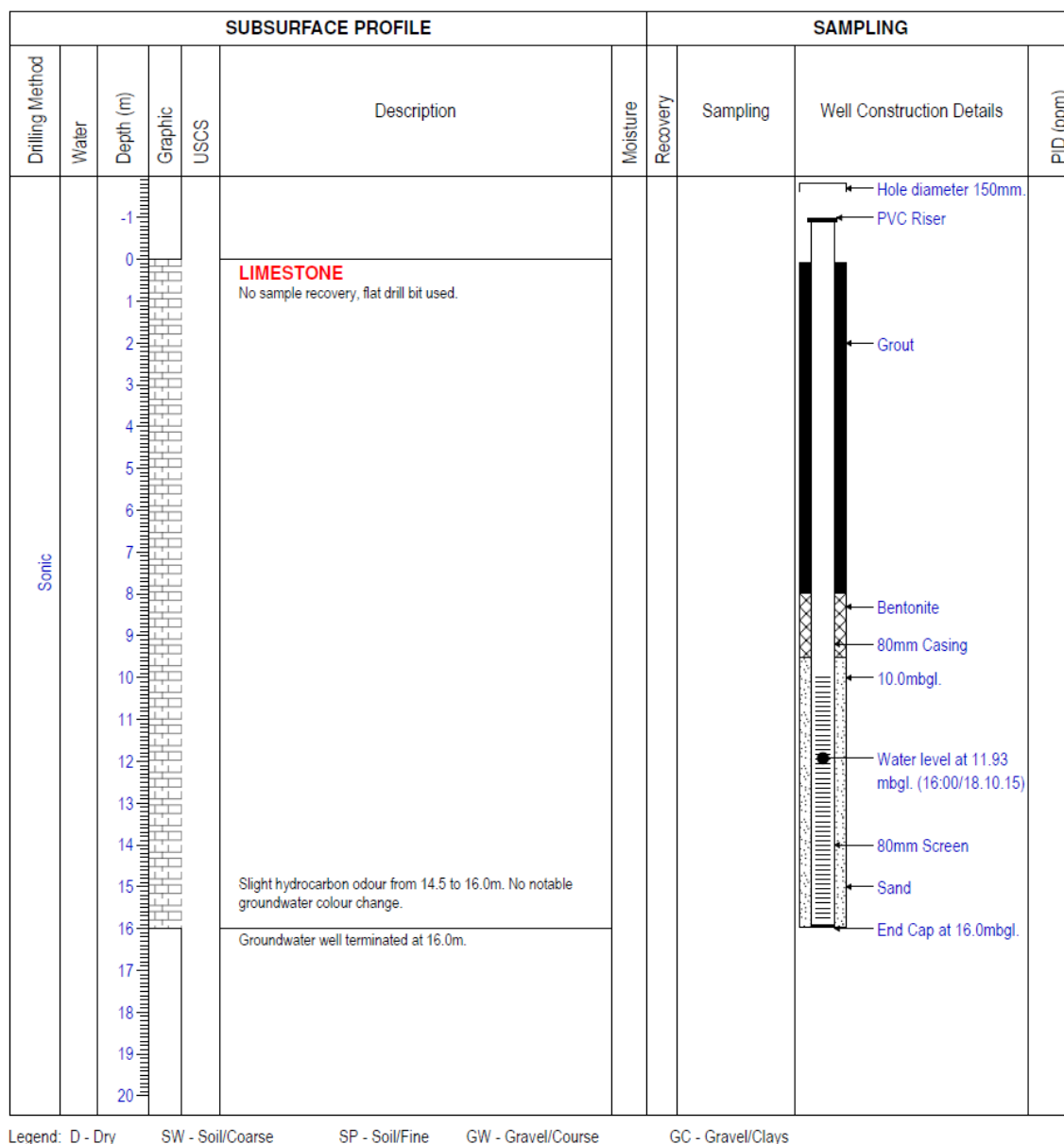
SP - Soil/Fine

GW - Gravel/Coarse

GC - Gravel/Clays

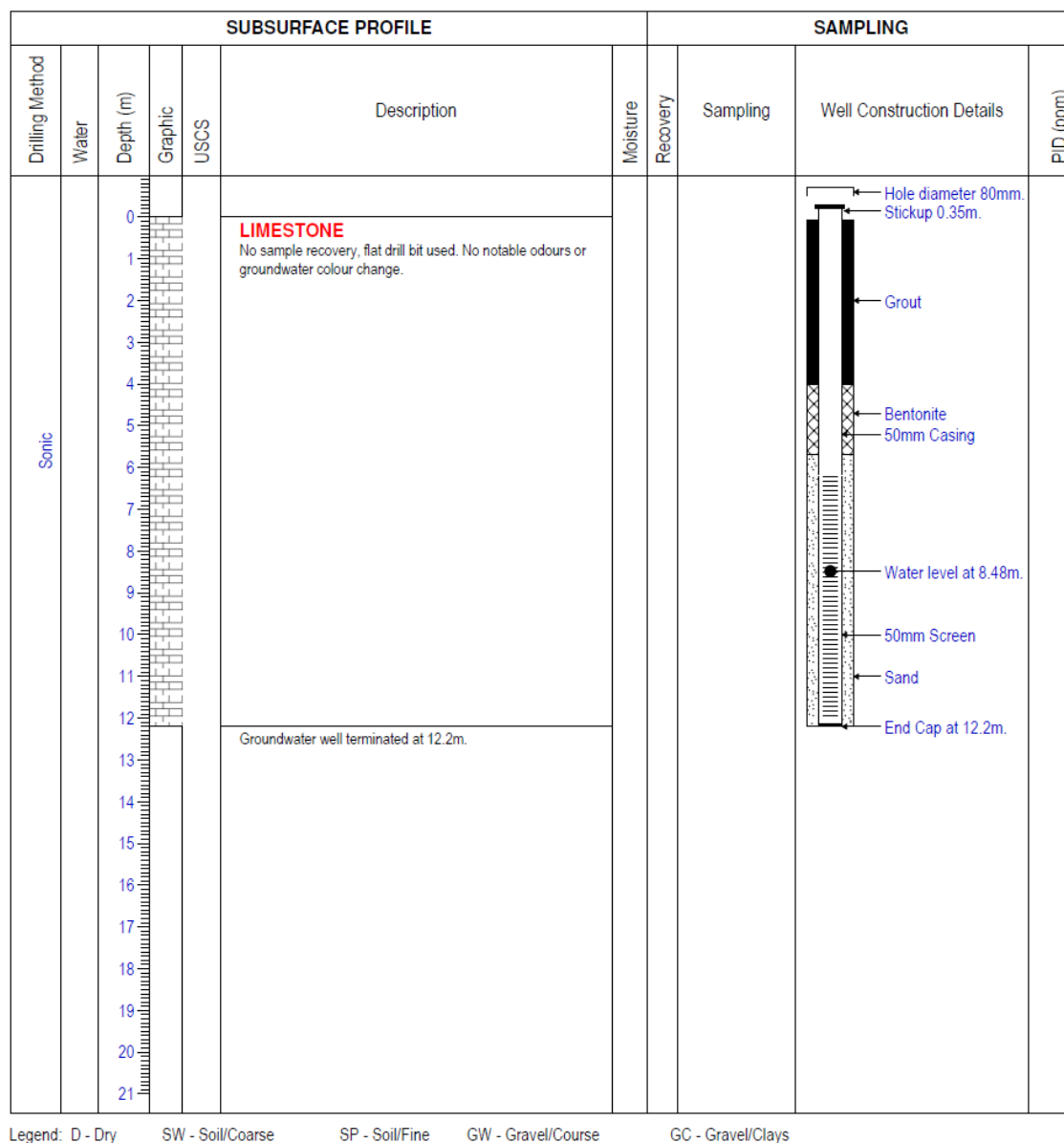
MW74

Ground level mAHD: 12.17



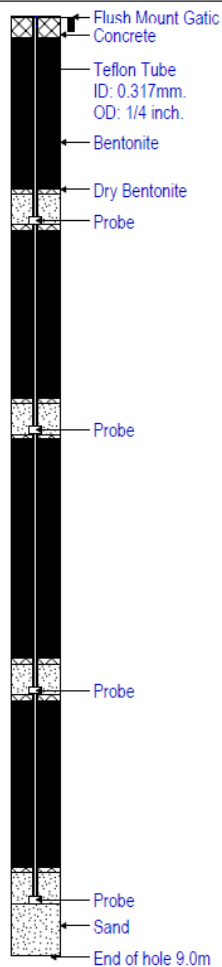
MW76

Ground level mAHD: 7.96



SV1

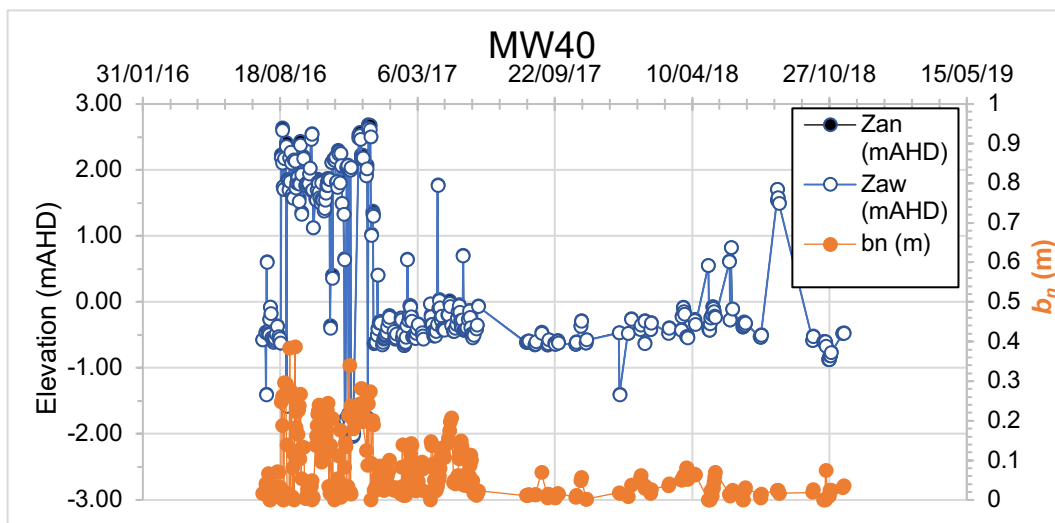
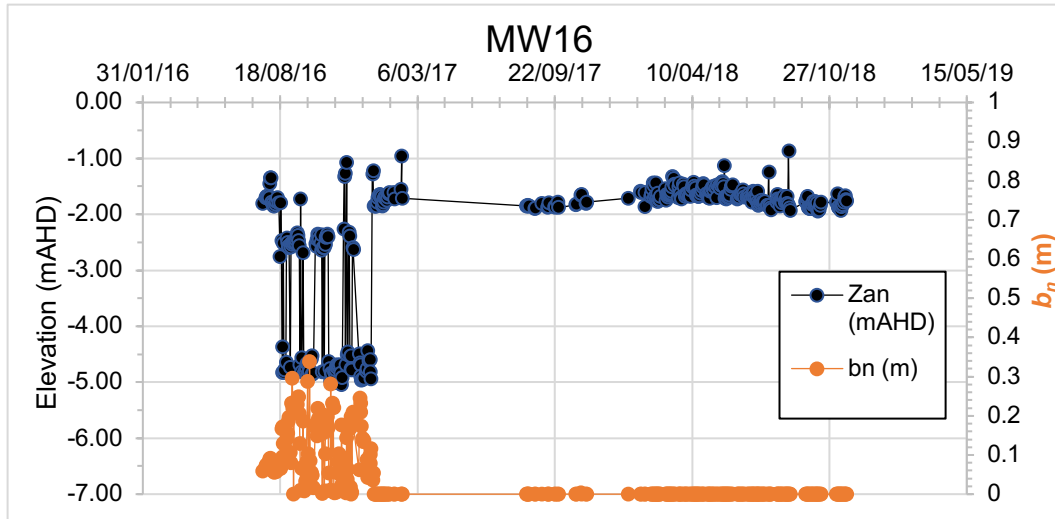
R.L. Top of Casing mAHD: 11.5

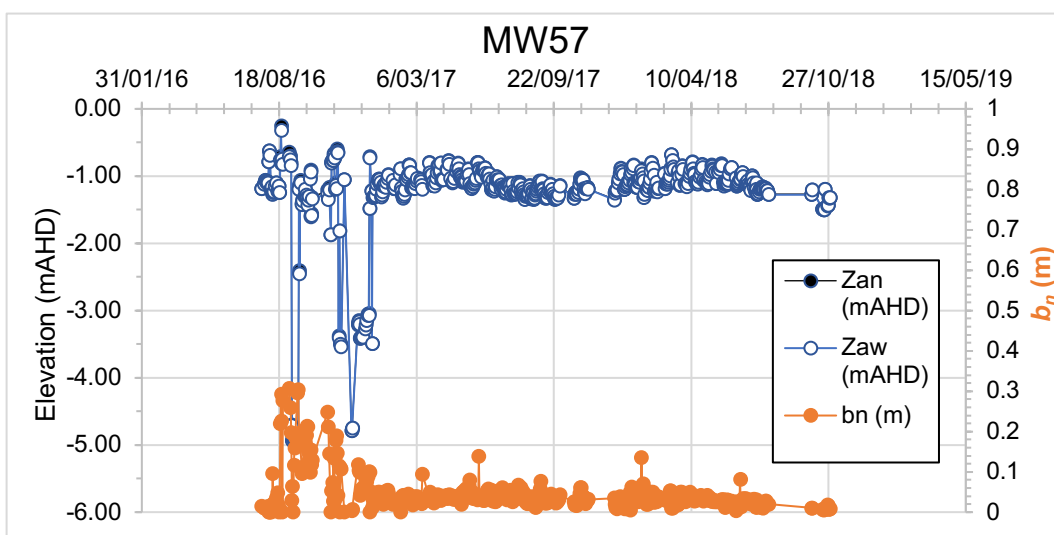
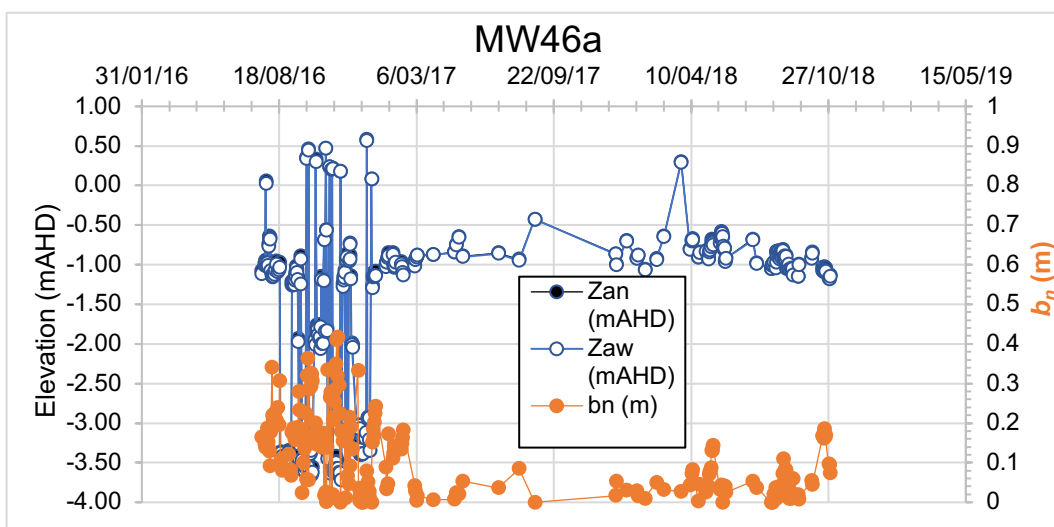
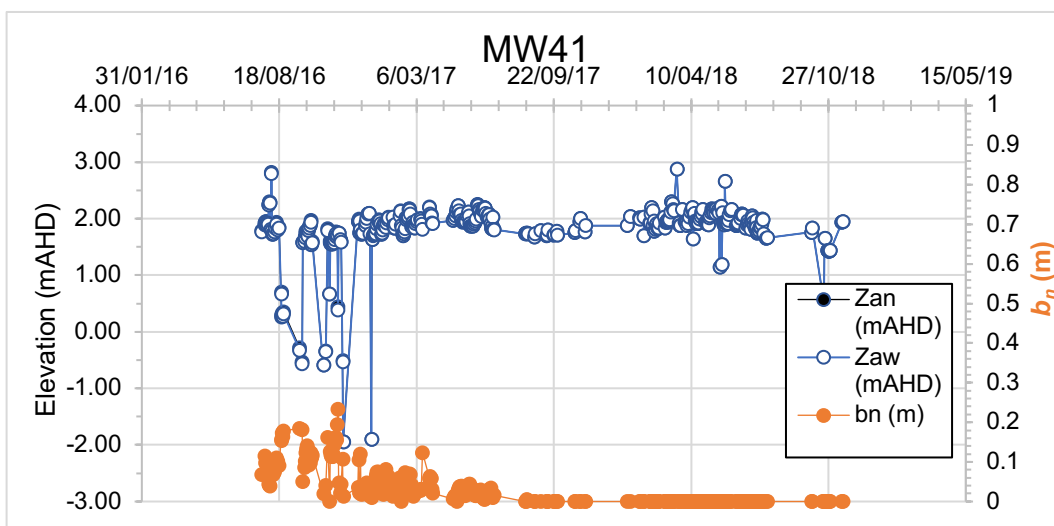
SUBSURFACE PROFILE					SAMPLING					
Drilling Method	Water	Depth (m)	Graphic	USCS	Description	Moisture	Recovery	Sampling	Well Construction Details	PID (ppm)
Auger		1			<b>LIMESTONE</b> No sample recovery, flat drill bit used. No notable odours.	D				0.0
		2								
		3								
		4								
		5								
		6								
		7								
		8								
		9								
					Vapour probe terminated at 9.0m.					

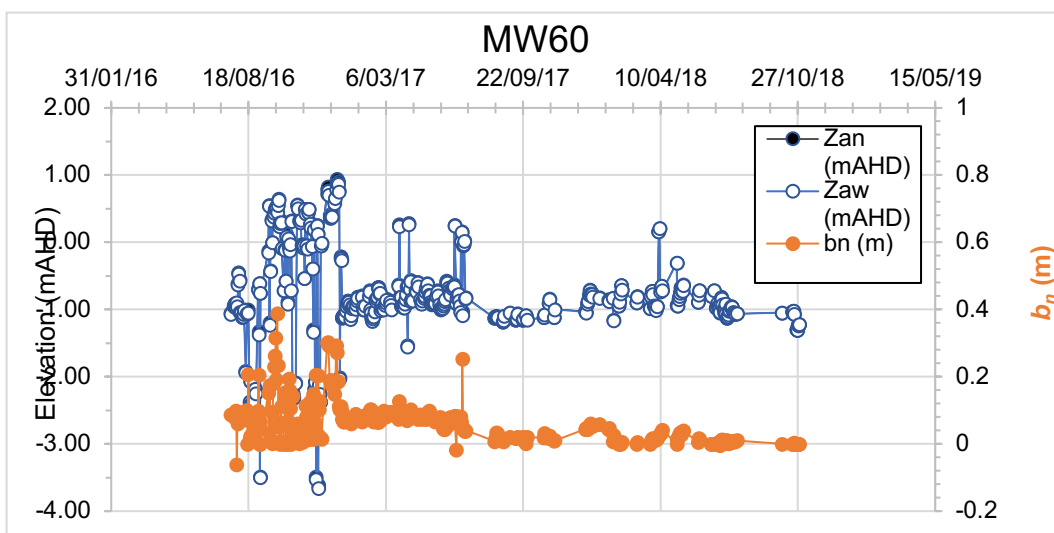
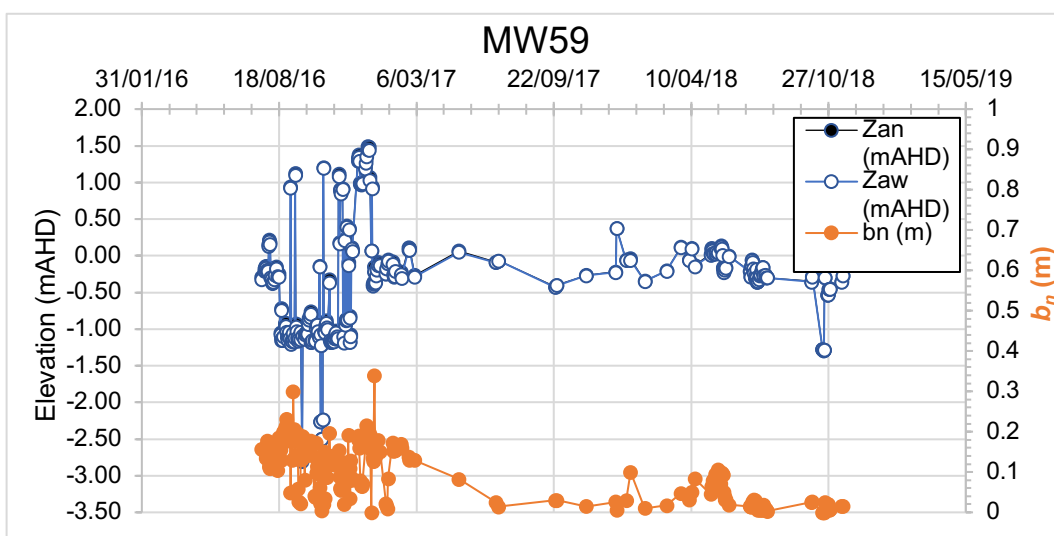
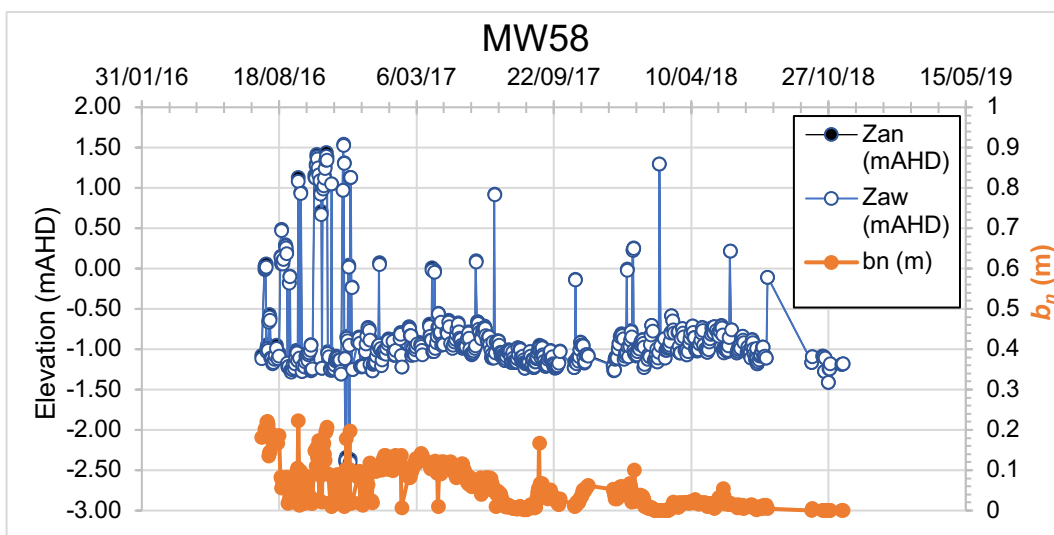
Legend: VD - Very Dry   D - Dry   M - Moist   ID - Inner Daimeter   OD - Outer Daimeter   SW - Soil/Coarse

## APPENDIX A.4

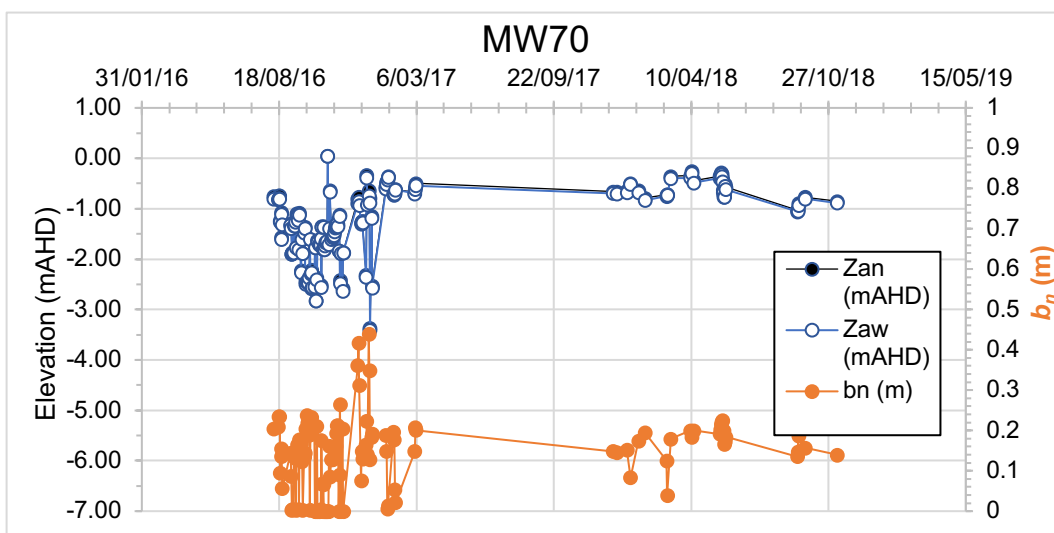
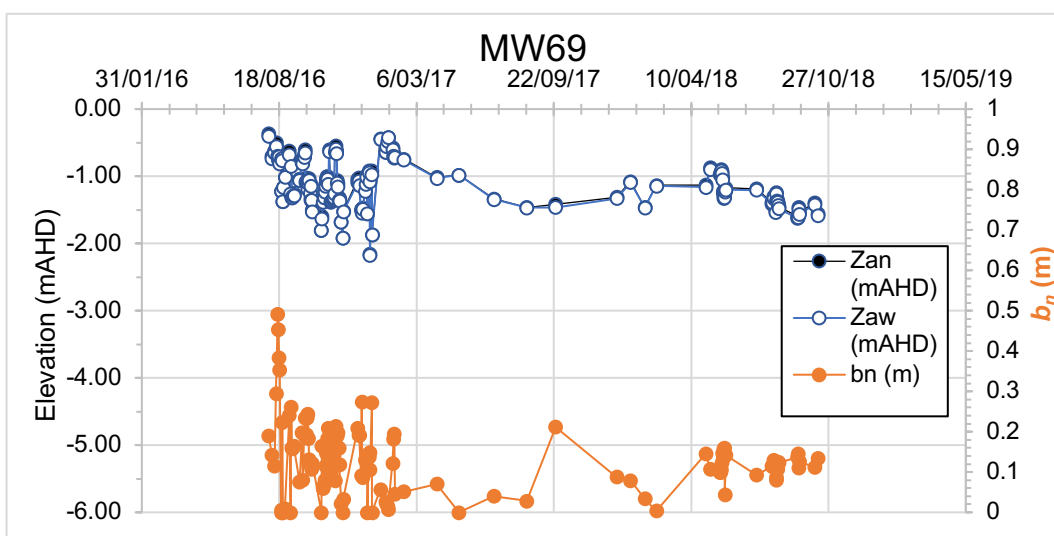
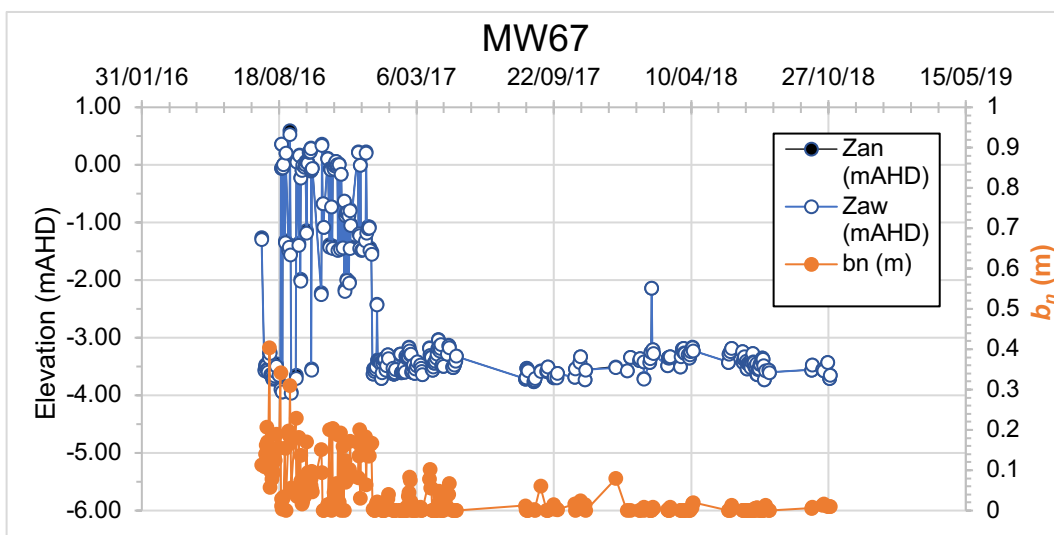
Site A time series plots of LNAPL thickness ( $b_n$ ), corrected water table elevation ( $Z_{aw}$ ), and LNAPL elevation ( $Z_{an}$ ) for selected wells

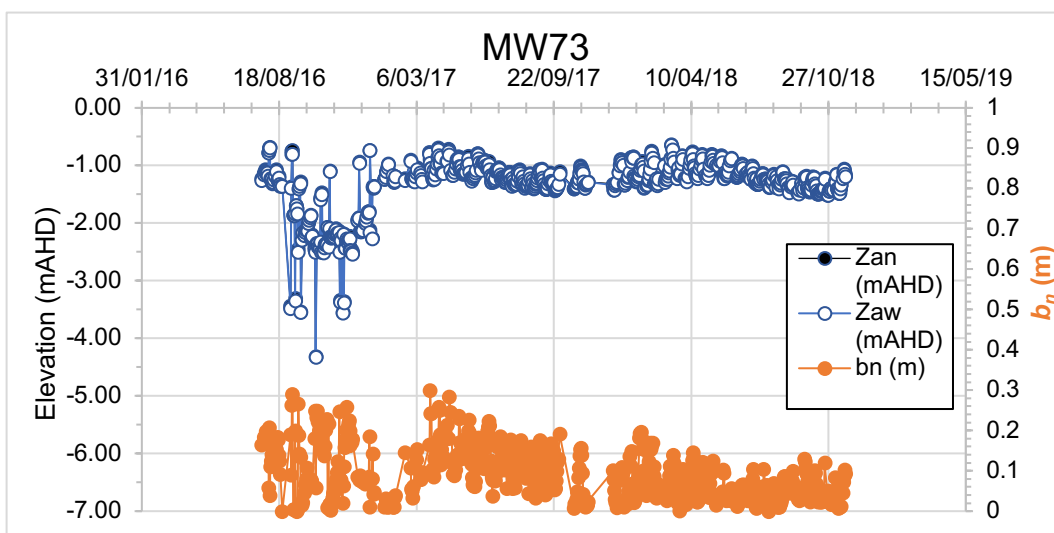
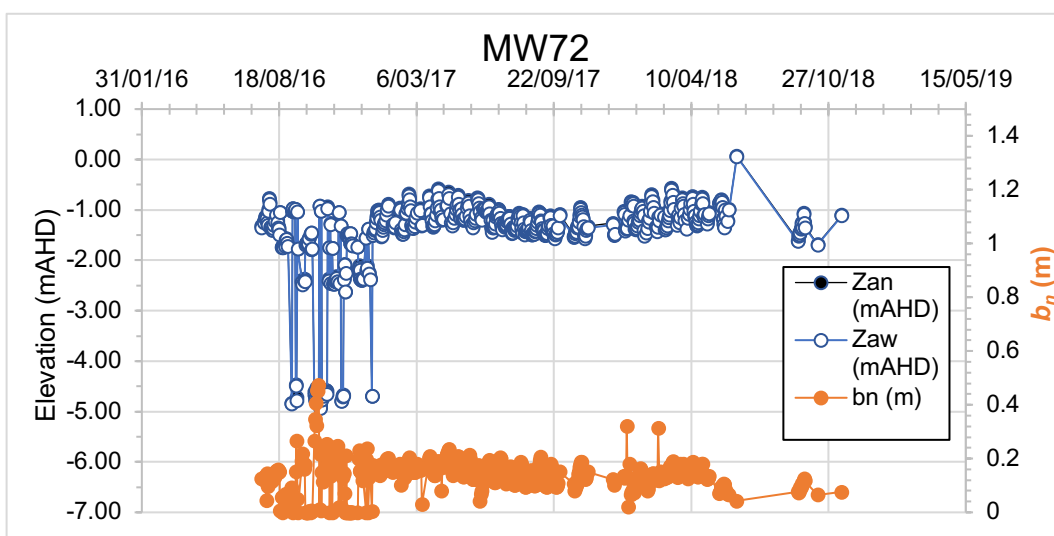
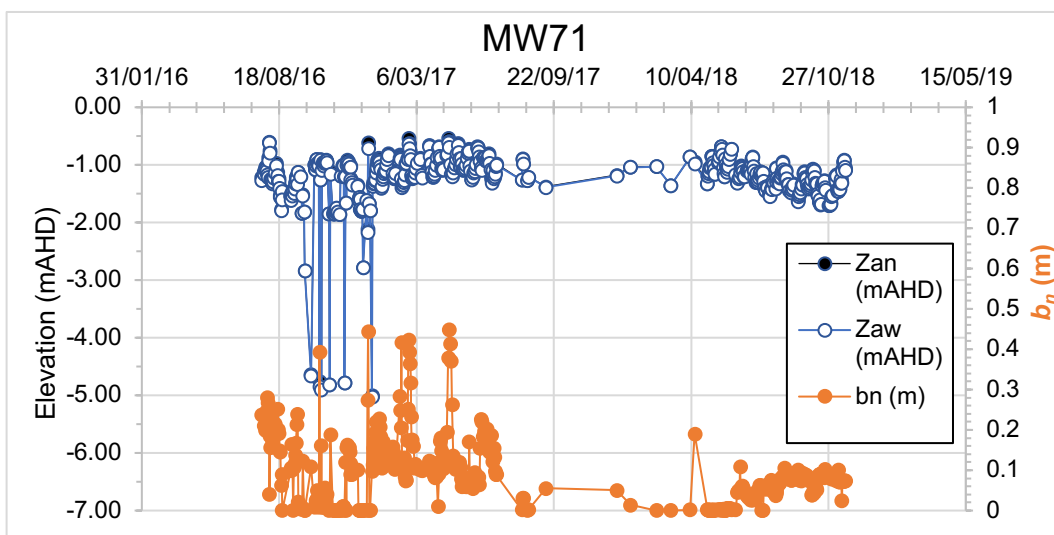


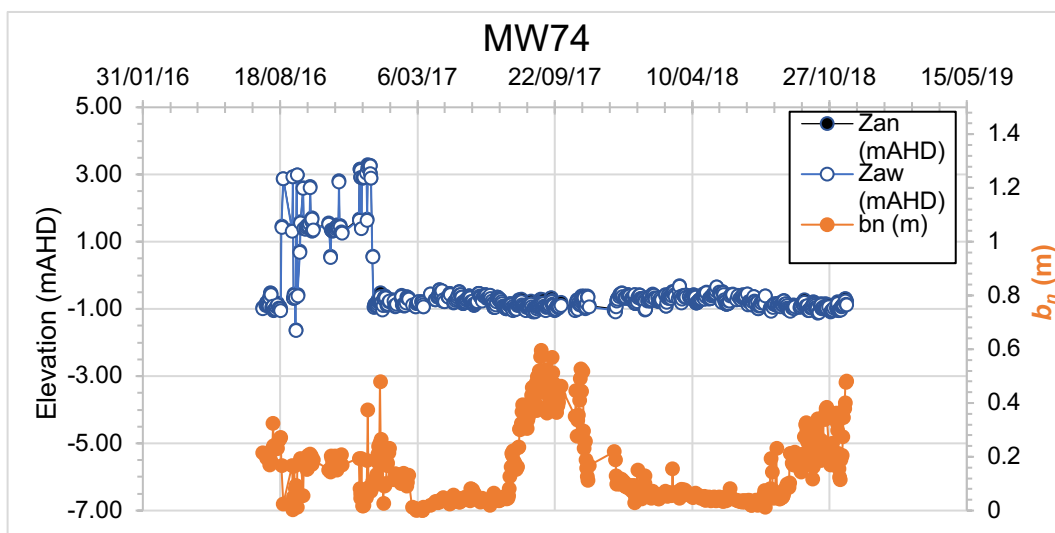












## APPENDIX A.5

---

### Site A methodology for in-well temperature monitoring

According to SiteA\_Ref13 (2018), the temperature profiling was undertaken according to the following procedure:

- 'The thermistor was lowered to less than 0.5 m above the SWL. The foam plug was replaced into the top of the well to create a seal.
- Resistance measurements used to calculate temperature were taken near the SWL, and then at discrete intervals progressively up the well. The distance between the ToC and SWL was measured, and measurements were recorded at every 0.5 m interval for the lower half of the sample column, and 1.0 m for the upper portion of the sample column. The thermistor was allowed to stabilise for approximately two minutes at each depth, before moving the probe to the next depth.
- The time, depth (in relation to the ToC) and resistance was recorded for each reading' (SiteA\_Ref13 2018, p. 19).

## APPENDIX A.6

### Site A methodology for sampling soil vapour from soil vapour probes

---

According to SiteA\_Ref11 (2017):

‘Sample collection via Summa canister was generally undertaken in accordance with the Cooperative Research Centre for Contamination Assessment and Remediation of the Environment (2013) document<sup>1</sup>:

A flow restrictor with a flow rate of 13.3 mL/minute was utilised for a sample collection period of one hour. The sample train comprised 0.25 inch teflon tubing and swagelock stainless steel or brass fittings. Prior to sample collection the vacuum in each canister was assessed with a pressure gauge to confirm there had been no vacuum loss during transport. The pre-sample canister pressure was recorded on the sample collection log.

The sample collection methodology involved:

- Shut-in test:
  - The flow restrictor, teflon tubing and Swagelok fittings were all connected to the canister.
  - The sample inlet tube was sealed and a shut in test array comprising a pressure gauge, ball valve and syringe was connected to the ‘T’ piece on top of the flow restrictor.
  - The syringe was pulled to create a vacuum, the ball valve closed and the pressure monitored for 30 seconds.
  - If the vacuum remained unchanged, the system was considered to be free of leaks. If the vacuum decreased, the fittings were tightened or adjusted and the test repeated until the vacuum held steady.
- Purging:
  - The soil vapour probe was purged using a GA5000 portable landfill gas analyser (LGA) with a flow rate of 550 ml/min.
  - A H<sub>2</sub>S/VOC filter was fitted to the LGA and field gas parameters including CH<sub>4</sub>, CO<sub>2</sub>, O<sub>2</sub>, H<sub>2</sub>S and CO results were recorded at two minute intervals until they had stabilised within 10% of the previous reading.
- Sample collection:
  - The Summa canister was connected to the soil vapour probe after the completion of a successful shut in test and purging.
  - A 20 mL portion of 100% isopropanol was poured onto a rag and placed around the Teflon tubing where it protruded from the ground surface.

---

<sup>1</sup> CRC CARE 2013, *Petroleum hydrocarbon vapour intrusion assessment: Australian guidance*, Technical Report no. 23, Cooperative Research Centre for Contamination Assessment and Remediation of the Environment. Adelaide, Australia.

- A shroud was placed over the soil vapour probe and isopropanol rag.
- The Summa canister was placed outside of the shroud and opened for sampling.
- After one hour, the canister pressure was recorded from the flow restrictor and the canister closed.
- Following sample collection, an additional set of field gas readings was collected with the LGA' (SiteA\_Ref11 2017, p. 20).

## APPENDIX A.7

---

### Site A methodology for in-well gas sampling

---

SiteA\_Ref13 (2018) provides the following sampling methodology for in-well soil vapour sampling:

- 'The depth to groundwater in relation to the well top of casing (ToC) was gauged using an interface probe, and the presence and thickness of LNAPL (if any) was recorded.
- A stainless steel weight was attached to the end of the sample tube to ensure that the sample tube was positioned correctly within the well.
- The sample tubing was lowered into the well until the end of the tubing was less than 0.5 m above the SWL, but ensuring that the tubing did not come into contact with groundwater. Once this position was achieved, the tubing was secured to maintain the position and a foam plug was inserted into the top of the well to create a seal.
- The tubing was connected to the landfill gas analyser (LFGA).
- The LFGA was turned on and vapour purging from the well commenced. The LFGA was set to run for approximately five minutes, or until the field readings stabilised, and the final vapour measurements were recorded.
- The LFGA was disconnected from the tubing and a three-way tap was connected to the tubing. A 60 mL plastic syringe was connected to the second port of the tap, and a foil sampling bag (with the valve open) was connected to the third port of the tap.
- The tap was set to allow flow between the tubing and the syringe. The syringe was used to purge any fresh air that may have entered the tubing between disconnecting the LFGA and connecting the tap.
- Once the tubing had been purged of fresh air, vapour was collected in the syringe. The tap was set to allow flow between the syringe and the sample bag, and the contents of the syringe were discharged into the sample bag. The tap was immediately set back to its original position and this process was repeated until the sample bag was approximately 80% full.
- The valve on the foil vapour sample bag was closed after the completion of sample collection, and the sample cap also replaced.
- This process was repeated for a second vapour sample bag.
- The sample bags were placed in an esky with no preservation required' (SiteA\_Ref13 2018, p. 18).

## APPENDIX A.8

---

### Site A density and analytical results for condensate LNAPL samples



**Table A.8-1. Density and analytical results for site A condensate LNAPL samples**

Sample name	Date	Density at 20 °C	%w/w loss*	Evidence of biodeg.	Pr/nC17	nC6	Benzene	Toluene	Ethyl Benzene	m/p-Xylene	o-Xylene	135-TMB	124-TMB	123-TMB	Naph	Pristane
		g mL <sup>-1</sup>			Ratio	%(w/w)	%(w/w)	%(w/w)	%(w/w)	%(w/w)	%(w/w)	%(w/w)	%(w/w)	%(w/w)	%(w/w)	%(w/w)
Source condensate	Apr-15	0.784	0		0.35	1.90	1.34	6.37	0.66	5.96	1.63	0.87	1.70	0.37	0.40	0.08
MW40	Jan-18	0.798	50		0.33	0.50	0.02	0.03	0.08	2.22	0.31	0.87	1.59	0.37	0.12	0.16
MW40	Mar-19	0.823	73		0.31	0.04	<0.01	<0.01	0.03	0.80	0.07	0.65	1.13	0.28	0.08	0.31
MW40	Apr-19	0.811	71		0.32	0.15	<0.01	<0.01	0.06	1.26	0.13	0.93	1.54	0.39	0.09	0.29
MW46a	Oct-15	0.777	3		0.31	2.40	0.46	3.11	0.53	4.70	1.24	0.78	1.49	0.32	0.29	0.09
MW46a	Jan-18	0.807	60		0.34	0.20	0.01	0.05	0.05	2.06	0.64	0.82	1.32	0.36	0.14	0.21
MW46a	Oct-18	0.803	55		0.32	0.18	<0.01	0.13	0.13	2.49	0.68	0.88	1.36	0.34	0.17	0.19
MW46a	Mar-19	0.810	62		0.31	0.16	<0.01	0.03	0.06	2.15	0.57	0.92	1.31	0.36	0.13	0.22
MW46a	Apr-19	0.808	65		0.31	0.18	<0.01	0.03	0.09	2.47	0.66	1.09	1.51	0.42	0.14	0.24
MW57	Jan-18	0.818	64		0.31	<0.01	<0.01	<0.01	<0.01	0.19	0.01	0.04	1.06	0.27	0.01	0.23
MW58	Oct-15	0.780	15		0.32	2.20	0.20	1.52	0.47	4.09	1.05	0.80	1.54	0.33	0.28	0.10
MW58	Jan-18	0.794	38		0.33	0.60	<0.01	0.27	0.39	3.94	0.94	0.92	1.79	0.38	0.30	0.13
MW58	Apr-19	0.813	75	Y	0.32	0.02	<0.01	0.02	0.11	1.59	0.32	0.71	1.32	0.31	0.18	0.33
MW59	Oct-15	0.782	16		0.31	1.80	0.13	0.97	0.44	4.14	1.01	0.82	1.59	0.34	0.28	0.10
MW59	Jan-18	0.799	44		0.33	0.20	<0.01	0.01	0.16	2.47	0.47	1.00	1.80	0.40	0.23	0.15
MW59	Mar-19	0.826	75	Y	0.32	<0.01	<0.01	<0.01	0.04	0.42	0.07	0.82	1.15	0.34	0.12	0.33
MW59	Apr-19	0.822	73	Y	0.32	<0.01	<0.01	<0.01	0.01	0.42	0.09	0.93	1.14	0.38	0.11	0.31
MW60	Oct-15	0.784	24		0.32	1.70	0.05	0.45	0.33	3.88	0.89	0.85	1.59	0.34	0.28	0.11
MW60	Jan-18	0.808	54		0.32	<0.01	<0.01	<0.01	0.01	0.99	0.15	0.97	1.46	0.38	0.18	0.18
MW60	Mar-19	0.822	74	Y	0.32	0.06	<0.01	0.01	0.03	1.02	0.28	0.72	0.88	0.31	0.11	0.31
MW60	Apr-19	0.822	79	Y	0.33	<0.01	<0.01	<0.01	<0.01	0.15	0.04	0.75	0.54	0.32	0.07	0.39
MW67	Mar-19	0.822	77	Y	0.33	<0.01	<0.01	<0.01	0.04	0.60	0.13	0.67	1.19	0.32	0.15	0.36
MW67	Apr-19	0.813	63		0.31	0.17	<0.01	0.09	0.23	3.08	0.66	0.88	1.61	0.36	0.23	0.23

Sample name	Date	Density at 20 °C	%w/w loss*	Evidence of biodeg.	Pr/nC17	nC6	Benzene	Toluene	Ethyl Benzene	m/p-Xylene	o-Xylene	135-TMB	124-TMB	123-TMB	Naph	Pristane
		g mL <sup>-1</sup>			Ratio	%(w/w)	%(w/w)	%(w/w)	%(w/w)	%(w/w)	%(w/w)	%(w/w)	%(w/w)	%(w/w)	%(w/w)	%(w/w)
MW69	Oct-15	0.783	23		0.32	1.90	0.05	0.02	0.31	3.23	0.56	0.86	1.58	0.33	0.28	0.11
MW69	Jan-18	0.806	51		0.29	<0.01	<0.01	<0.01	0.07	0.74	0.21	0.91	1.42	0.41	0.11	0.17
MW69	Oct-18	0.818	66	Y	0.32	<0.01	<0.01	<0.01	0.06	0.41	0.11	0.72	1.28	0.35	0.08	0.24
MW69	Mar-19	0.822	71	Y	0.32	<0.01	<0.01	<0.01	0.03	0.20	0.05	0.58	1.23	0.34	0.07	0.29
MW69	Apr-19	0.821	73	Y	0.33	<0.01	<0.01	<0.01	0.03	0.18	0.04	0.65	1.13	0.36	0.07	0.31
MW70	Oct-15	0.781	23		0.32	2.10	0.04	0.02	0.36	2.90	0.70	0.80	1.57	0.32	0.25	0.11
MW70	Jan-18	0.796	47		0.32	0.30	<0.01	<0.01	0.11	1.03	0.27	0.61	1.69	0.35	0.11	0.15
MW70	Oct-18	0.814	65		0.32	0.03	<0.01	<0.01	0.04	0.42	0.10	0.36	1.36	0.30	0.04	0.24
MW70	Mar-19	0.817	69		0.31	0.01	<0.01	<0.01	0.02	0.30	0.07	0.27	1.23	0.28	0.03	0.27
MW70	Apr-19	0.814	70		0.32	0.01	<0.01	<0.01	0.02	0.29	0.07	0.28	1.25	0.29	0.02	0.27
MW71	Oct-18	0.802	55		0.31	0.36	<0.01	<0.01	0.09	1.07	0.22	0.59	1.47	0.32	0.08	0.18
MW71	Mar-19	0.813	67		0.32	0.06	<0.01	<0.01	0.04	0.71	0.06	0.56	1.48	0.33	0.10	0.25
MW71	Apr-19	0.808	66		0.31	0.13	<0.01	<0.01	0.05	0.77	0.08	0.56	1.45	0.33	0.10	0.24
MW72	Jan-18	0.786	29		0.33	1.20	0.03	0.01	0.37	3.31	0.82	0.83	1.66	0.34	0.25	0.12
MW72	Oct-18	0.797	46		0.30	0.83	<0.01	<0.01	0.19	2.61	0.65	0.79	1.54	0.33	0.21	0.16
MW72	Mar-19	0.805	56		0.30	0.46	<0.01	<0.01	0.23	2.32	0.58	0.76	1.51	0.33	0.20	0.19
MW72	Apr-19	0.800	54		0.31	0.55	<0.01	<0.01	0.18	2.45	0.61	0.80	1.51	0.33	0.20	0.18
MW73	Jan-18	0.798	38		0.31	0.40	0.01	0.01	0.18	2.43	0.71	0.89	1.79	0.40	0.20	0.13
MW73	Mar-19	0.822	71		0.31	0.05	<0.01	<0.01	0.06	0.89	0.30	0.79	1.53	0.38	0.15	0.29
MW73	Apr-19	0.822	79	Y	0.34	<0.01	<0.01	<0.01	0.02	0.28	0.10	0.63	1.14	0.34	0.09	0.39
MW74	Jan-18	0.784	26		0.32	1.50	0.04	0.30	0.33	4.01	0.96	0.83	1.64	0.35	0.29	0.11
MW74	Oct-18	0.790	36		0.34	1.46	0.02	0.21	0.35	3.45	0.82	0.79	1.57	0.34	0.23	0.13
MW74	Mar-19	0.799	50		0.30	0.58	0.02	0.15	0.31	3.52	0.76	0.86	1.61	0.35	0.20	0.17
MW74	Apr-19	0.796	52		0.31	0.67	0.02	0.15	0.27	3.43	0.71	0.84	1.52	0.33	0.20	0.17

\* % Loss (w/w) relative to source based on pristane, Pr/nC17: ratio of pristane/n-heptadecane, Naph: naphthalene, nC6: n-hexane, TMB: trimethylbenzene.

## APPENDIX A.9

### Site A LNAPL percentage loss relationships

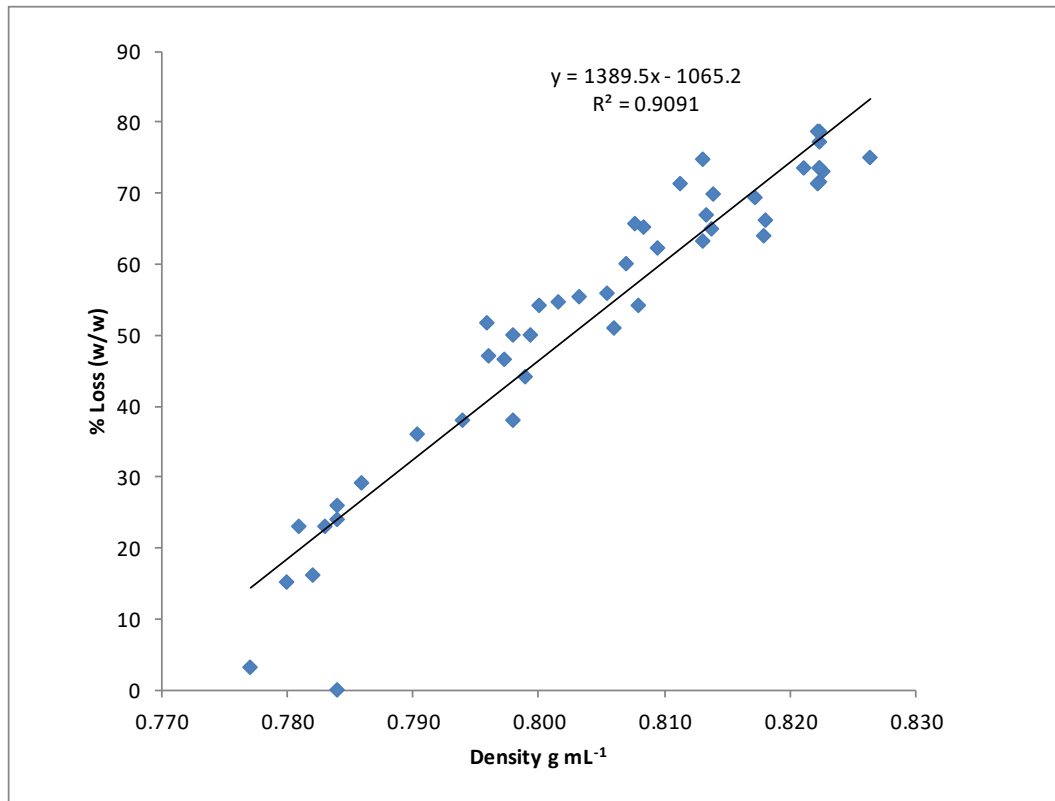


Figure A.8-1 Plot of % loss (w/w) versus density for site A samples

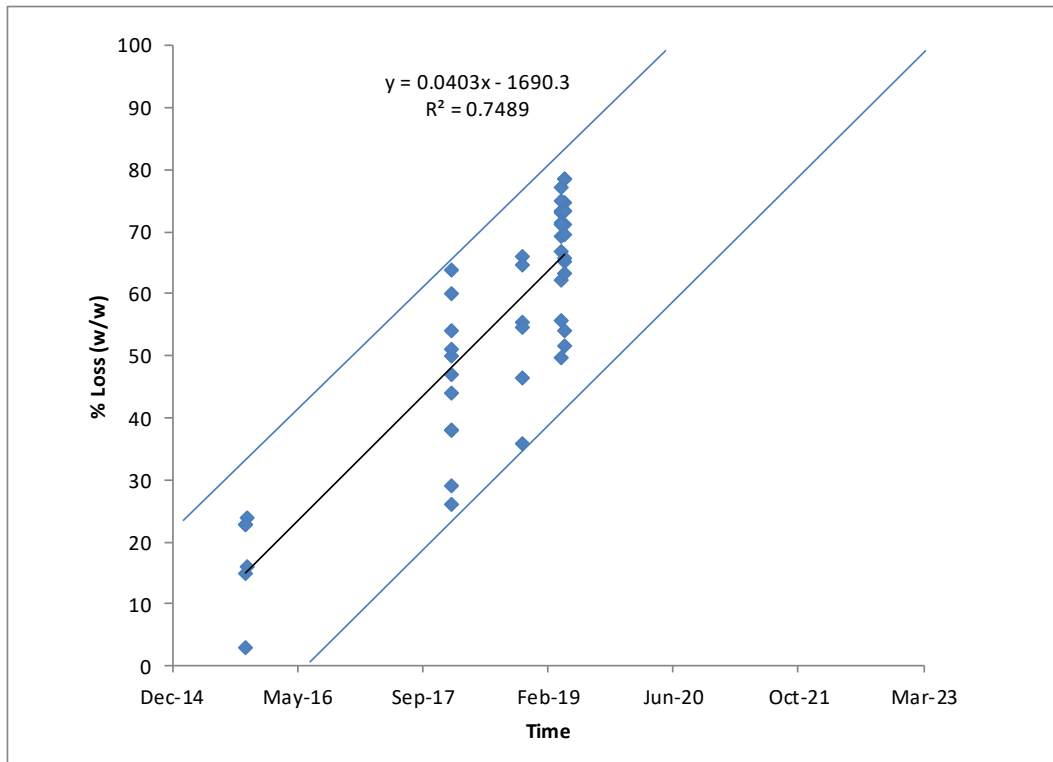


Figure A.8-2 Plot of % loss (w/w) versus time for site A samples

## APPENDIX B.1

---

### Site B methodology for gas sampling and CSIRO analytical methods

#### *Major Gas Analysis*

Analyses were carried out using an Agilent 7890 gas chromatograph (GC) fitted with a 10 port sampling valve, thermal conductivity detector (TCD), a flame ionising detector (FID), an air actuated heated (75 °C) valve box (containing a gas sampling loops, 2 x 0.25 mL), a packed column (60/80 Carboxen-1000 Supleco, 15' x 1/8" SS) connected to the TCD a capillary column (0.53mm ID) connected to FID. Helium was used as carrier gas at a constant pressure of 40 psi and the GC oven was initially held isothermal at 35 °C for 5 minutes, heated to 225 °C at 6 °C min<sup>-1</sup> and then held at 225 °C for 5 minutes. Samples were injected to the GC sample port via an Agilent 7697A headspace sampler.

**Table B.1-1 Results for selected components of samples taken from core C67 for the D6 site**

Sample #	Depth	Pr/Ph	Benz	Tol	EBenz	m/p-Xyl	o-Xyl	135-TMB	124-TMB	123-TMB	Naph	2-MN	1-MN	Phen	TPH
	(m)	Ratio	mg/kg	mg/kg	mg/kg	mg/kg	mg/kg	mg/kg	mg/kg	mg/kg	mg/kg	mg/kg	mg/kg	mg/kg	g/kg
171	1.1–1.15	-	<1	<1	<1	1	<1	<1	<1	<1	<1	<1	<1	<1	<1
172	1.5–1.55	-	<1	<1	<1	1	<1	<1	<1	<1	<1	<1	<1	<1	<1
173	2–2.05	-	<1	<1	<1	1	<1	<1	<1	<1	<1	<1	<1	<1	<1
174	2.6–2.65	-	<1	<1	<1	1	<1	<1	<1	<1	<1	<1	<1	<1	<1
175	2.95–3	-	<1	<1	<1	1	<1	<1	<1	<1	<1	<1	<1	<1	<1
176	3.2–3.25	1.3	<1	<1	<1	<1	<1	<1	<1	<1	<1	<1	<1	<1	1.1
177	3.35–3.4	1.8	<1	<1	<1	<1	1	<1	<1	<1	<1	<1	<1	<1	4.6
178	3.4–3.45	1.8	<1	<1	<1	1	<1	<1	<1	<1	1	2	2	<1	15
179	3.45–3.8	1.9	<1	<1	<1	<1	<1	<1	<1	<1	2	10	10	<1	31
180	3.8–3.85	1.8	<1	<1	<1	<1	<1	<1	<1	<1	3	14	15	2	41
181	3.85–3.9	1.8	<1	<1	<1	<1	<1	<1	<1	<1	4	16	17	<1	57
182	3.9–3.95	1.9	<1	<1	1	1	<1	<1	<1	<1	14	48	56	9	188
183	3.95–4	1.8	<1	<1	1	1	<1	<1	<1	<1	8	34	45	<1	128
184	4–4.05	1.8	<1	<1	<1	<1	<1	<1	<1	<1	4	17	19	<1	44
185	4.05–4.1	1.9	<1	<1	<1	1	<1	<1	<1	<1	6	26	40	3	48
186	4.1–4.15	1.9	<1	<1	<1	1	<1	<1	<1	<1	7	11	49	10	44
187	4.15–4.2	2.0	<1	<1	<1	1	<1	<1	<1	<1	6	2	29	6	30

Sample #	Depth	Pr/Ph	Benz	Tol	EBenz	m/p-Xyl	o-Xyl	135-TMB	124-TMB	123-TMB	Naph	2-MN	1-MN	Phen	TPH
	(m)	Ratio	mg/kg	mg/kg	mg/kg	mg/kg	mg/kg	mg/kg	mg/kg	mg/kg	mg/kg	mg/kg	mg/kg	mg/kg	g/kg
188	4.2–4.25	1.9	<1	<1	<1	<1	<1	<1	<1	<1	2	<1	10	0	22
189	4.25–4.3	1.9	<1	<1	1	1	<1	<1	<1	<1	2	5	18	9	16
190	4.3–4.35	1.7	<1	<1	<1	<1	<1	<1	<1	<1	4	1	16	8	7.2
191	4.35–4.4	1.8	<1	<1	1	1	<1	<1	<1	<1	12	24	23	9	13
192	4.4–4.45	1.7	<1	<1	1	1	<1	<1	<1	<1	3	25	22	4	11
193	4.45–4.5	1.6	<1	<1	<1	1	<1	<1	<1	<1	12	13	12	3	13
194	4.5–4.55	1.6	<1	<1	<1	2	<1	<1	<1	<1	5	5	10	<1	9.0
195	4.55–4.6	1.5	<1	<1	<1	<1	<1	<1	<1	<1	<1	3	14	4	8.6
196	4.6–4.67	1.4	<1	<1	<1	<1	<1	<1	<1	<1	1	<1	12	5	9.2
197	4.95–5	1.7	<1	<1	<1	<1	<1	<1	<1	<1	<1	1	3	<1	3.4
198	5–5.05	1.8	<1	<1	<1	<1	<1	<1	<1	<1	<1	1	2	<1	3.6
199	5.05–5.1	-	<1	<1	<1	1	<1	<1	<1	<1	<1	<1	<1	<1	<1
200	5.1–5.15	-	<1	<1	<1	1	<1	<1	<1	<1	<1	<1	<1	<1	<1
201	5.15–5.2	-	<1	<1	<1	1	<1	<1	<1	<1	<1	<1	<1	<1	<1
202	5.4–5.45	-	<1	<1	<1	1	<1	<1	<1	<1	<1	<1	<1	<1	<1
203	5.6–6.65	-	<1	<1	<1	1	<1	<1	<1	<1	<1	<1	<1	<1	<1

Benz: benzene, E: ethyl, MN: methylnaphthalene, Naph: naphthalene TMB: trimethylbenzene, Tol: toluene, Xyl: xylene, Phen: phenanthrene

**Table B.1-2 Results for selected components of samples taken from core C70 for the D10 site**

Sample #	Depth	Pr/Ph	Benz	Tol	EBenz	m/p-Xyl	o-Xyl	135-TMB	124-TMB	123-TMB	Naph	2-MN	1-MN	Phen	TPH
	(m)	Ratio	mg/kg	mg/kg	mg/kg	mg/kg	mg/kg	mg/kg	mg/kg	mg/kg	mg/kg	mg/kg	mg/kg	mg/kg	g/kg
261	1.2–1.25	-	<1	<1	<1	1	<1	<1	<1	<1	<1	<1	<1	<1	<1
262	1.5–1.55	-	<1	<1	<1	1	<1	<1	<1	<1	<1	<1	<1	<1	<1
263	2–2.05	-	<1	<1	<1	1	<1	<1	<1	<1	<1	<1	<1	<1	<1
264	2.65–2.7	-	<1	<1	<1	1	<1	<1	<1	<1	<1	<1	<1	<1	<1
265	3–3.05	-	<1	<1	<1	1	<1	<1	<1	<1	<1	<1	<1	<1	<1
266	3.05–3.1	-	<1	<1	<1	1	<1	<1	<1	<1	<1	<1	<1	<1	<1
267	3.1–3.15	-	<1	<1	<1	2	1	<1	<1	<1	<1	<1	<1	<1	1.14
268	3.15–3.2	-	<1	<1	<1	<1	<1	<1	<1	<1	<1	<1	<1	<1	3.9
269	3.2–3.25	-	<1	<1	<1	<1	<1	<1	<1	<1	<1	<1	<1	<1	2.28
270	3.25–3.3	-	<1	<1	<1	<1	1	<1	<1	<1	<1	<1	<1	<1	4.14
271	3.3–3.35	2.8	<1	<1	<1	1	<1	<1	<1	<1	6	28	19	4	17.31
272	3.35–3.4	3.3	<1	<1	<1	1	<1	<1	<1	<1	14	78	43	9	24.57
273	3.4–3.45	3.4	<1	<1	2	<1	<1	<1	<1	<1	8	46	27	5	13.36
274	3.45–3.49	3.3	<1	<1	1	1	<1	<1	<1	<1	6	35	22	3	8.69
275	3.7–3.75	3.4	<1	<1	2	<1	<1	<1	<1	<1	18	77	49	10	21.11
276	3.75–3.8	3.6	<1	<1	12	<1	<1	<1	1	<1	40	167	94	17	47.01
277	3.8–3.85	3.4	<1	<1	18	<1	<1	<1	<1	<1	54	199	114	23	56.35
278	3.85–3.9	3.5	<1	1	1	<1	<1	<1	<1	<1	19	78	44	8	20.3
279	3.9–3.95	3.7	<1	<1	4	1	<1	<1	<1	<1	13	66	42	8	15.95

Sample #	Depth	Pr/Ph	Benz	Tol	EBenz	m/p-Xyl	o-Xyl	135-TMB	124-TMB	123-TMB	Naph	2-MN	1-MN	Phen	TPH
	(m)	Ratio	mg/kg	mg/kg	mg/kg	mg/kg	mg/kg	mg/kg	mg/kg	mg/kg	mg/kg	mg/kg	mg/kg	mg/kg	g/kg
280	3.95–4	3.5	<1	<1	9	<1	<1	<1	<1	<1	15	77	42	9	21.75
281	4–4.05	3.9	<1	<1	4	1	<1	<1	<1	<1	7	38	21	5	8.74
282	4.05–4.1	3.8	<1	<1	1	2	<1	<1	<1	<1	<1	7	4	1	2.31
283	4.1–4.15	-	<1	<1	<1	1	<1	<1	<1	<1	<1	<1	<1	<1	<1
284	4.15–4.2	-	<1	<1	<1	1	<1	<1	<1	<1	<1	<1	<1	<1	<1
285	4.2–4.25	-	<1	<1	<1	1	<1	<1	<1	<1	<1	<1	<1	<1	<1
286	4.25–4.3	-	<1	<1	<1	1	<1	<1	<1	<1	<1	<1	<1	<1	<1
287	4.3–4.35	-	<1	<1	<1	1	<1	<1	<1	<1	<1	<1	<1	<1	<1
288	4.35–4.4	-	<1	<1	<1	1	<1	<1	<1	<1	<1	<1	<1	<1	<1
289	4.4–4.45	-	<1	<1	<1	1	<1	<1	<1	<1	<1	<1	<1	<1	<1
290	4.45–4.5	-	<1	<1	<1	1	<1	<1	<1	<1	<1	<1	<1	<1	<1
291	4.65–4.71	-	<1	<1	<1	1	<1	<1	<1	<1	<1	<1	<1	<1	<1
292	5.1–5.15	-	<1	<1	<1	1	<1	<1	<1	<1	<1	<1	<1	<1	<1
293	5.6–5.65	-	<1	<1	<1	1	<1	<1	<1	<1	<1	<1	<1	<1	<1

Benz: benzene, E: ethyl, MN: methylnaphthalene, Naph: naphthalene TMB: trimethylbenzene, Tol: toluene, Xyl: xylene, Phen: phenanthrene



**Table B.1-3 Results for selected components for samples taken from core C71 for the D10 site**

Sample #	Depth	Pr/Ph	Benz	Tol	EBenz	m/p-Xyl	o-Xyl	135-TMB	124-TMB	123-TMB	Naph	2-MN	1-MN	Phen	TPH
	(m)	Ratio	mg/kg	mg/kg	mg/kg	mg/kg	mg/kg	mg/kg	mg/kg	mg/kg	mg/kg	mg/kg	mg/kg	mg/kg	g/kg
294	1.3–1.35	-	<1	<1	<1	1	<1	<1	<1	<1	<1	<1	<1	<1	<1
295	1.7–1.75	-	<1	<1	<1	1	<1	<1	<1	<1	<1	<1	<1	<1	<1
296	2.05–2.1	-	<1	<1	<1	1	<1	<1	<1	<1	<1	<1	<1	<1	<1
297	2.6–2.65	-	<1	<1	<1	1	<1	<1	<1	<1	<1	<1	<1	<1	<1
298	2.9–2.95	-	<1	<1	<1	1	<1	<1	<1	<1	<1	<1	<1	<1	<1
299	2.95–3	-	<1	<1	<1	1	<1	<1	<1	<1	<1	<1	<1	<1	<1
300	3–3.05	-	<1	<1	<1	1	<1	<1	<1	<1	<1	<1	<1	<1	<1
301	3.05–3.1	-	<1	<1	<1	1	<1	<1	<1	<1	<1	<1	<1	<1	<1
302	3.1–3.15	-	<1	<1	<1	1	<1	<1	<1	<1	<1	<1	<1	<1	<1
303	3.15–3.2	-	<1	<1	<1	1	<1	<1	<1	<1	<1	<1	<1	<1	<1
304	3.2–3.25	-	<1	<1	<1	1	<1	<1	<1	<1	<1	<1	<1	<1	3.61
305	3.25–3.3	2.4	<1	<1	<1	<1	<1	<1	<1	<1	<1	<1	1	<1	21.34
306	3.3–3.35	3.3	<1	<1	<1	1	1	<1	<1	<1	5	38	25	7	41.18
307	3.35–3.4	3.7	<1	<1	<1	1	<1	<1	<1	<1	11	70	47	11	55.92
308	3.4–3.45	3.9	<1	<1	1	1	<1	<1	<1	<1	2	17	11	4	11.64
309	3.45–3.5	3.9	<1	<1	<1	<1	<1	<1	<1	<1	2	15	12	3	15.96
310	3.7–3.75	3.9	<1	<1	<1	<1	<1	<1	<1	<1	1	7	6	1	7.07
311	3.75–3.8	3.9	<1	<1	1	1	<1	<1	<1	<1	4	22	14	2	17.39
312	3.8–3.85	3.8	<1	<1	1	1	1	<1	<1	<1	5	25	17	3	21.48

Sample #	Depth	Pr/Ph	Benz	Tol	EBenz	m/p-Xyl	o-Xyl	135-TMB	124-TMB	123-TMB	Naph	2-MN	1-MN	Phen	TPH
	(m)	Ratio	mg/kg	mg/kg	mg/kg	mg/kg	mg/kg	mg/kg	mg/kg	mg/kg	mg/kg	mg/kg	mg/kg	mg/kg	g/kg
313	3.85–3.9	3.8	<1	<1	<1	1	<1	<1	<1	<1	5	31	21	4	27.15
314	3.9–3.95	-	<1	<1	<1	1	<1	<1	<1	<1	<1	<1	<1	<1	<1
315	3.95–4	-	<1	<1	<1	1	<1	<1	<1	<1	<1	<1	<1	<1	<1
316	4–4.05	-	<1	<1	<1	1	<1	<1	<1	<1	<1	<1	<1	<1	<1
317	4.05–4.1	-	<1	<1	<1	1	<1	<1	<1	<1	<1	<1	<1	<1	<1
318	4.1–4.55	-	<1	<1	<1	1	<1	<1	<1	<1	<1	<1	<1	<1	<1

*Benz: benzene, E: ethyl, MN: methylnaphthalene, Naph: naphthalene TMB: trimethylbenzene, Tol: toluene, Xyl: xylene, Phen: phenanthrene*

## APPENDIX C.1.

### Site C GC-MS analytical and density results

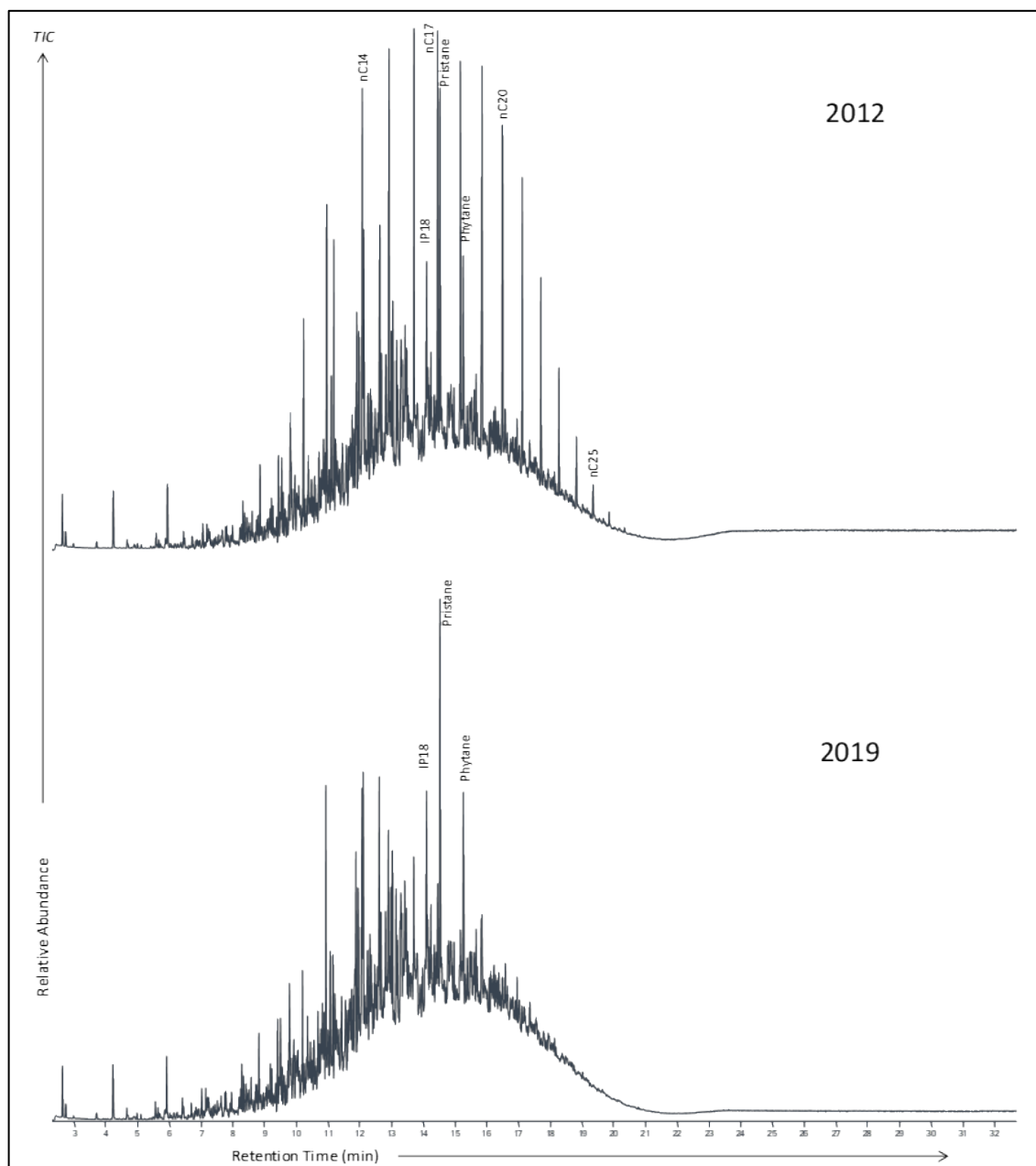
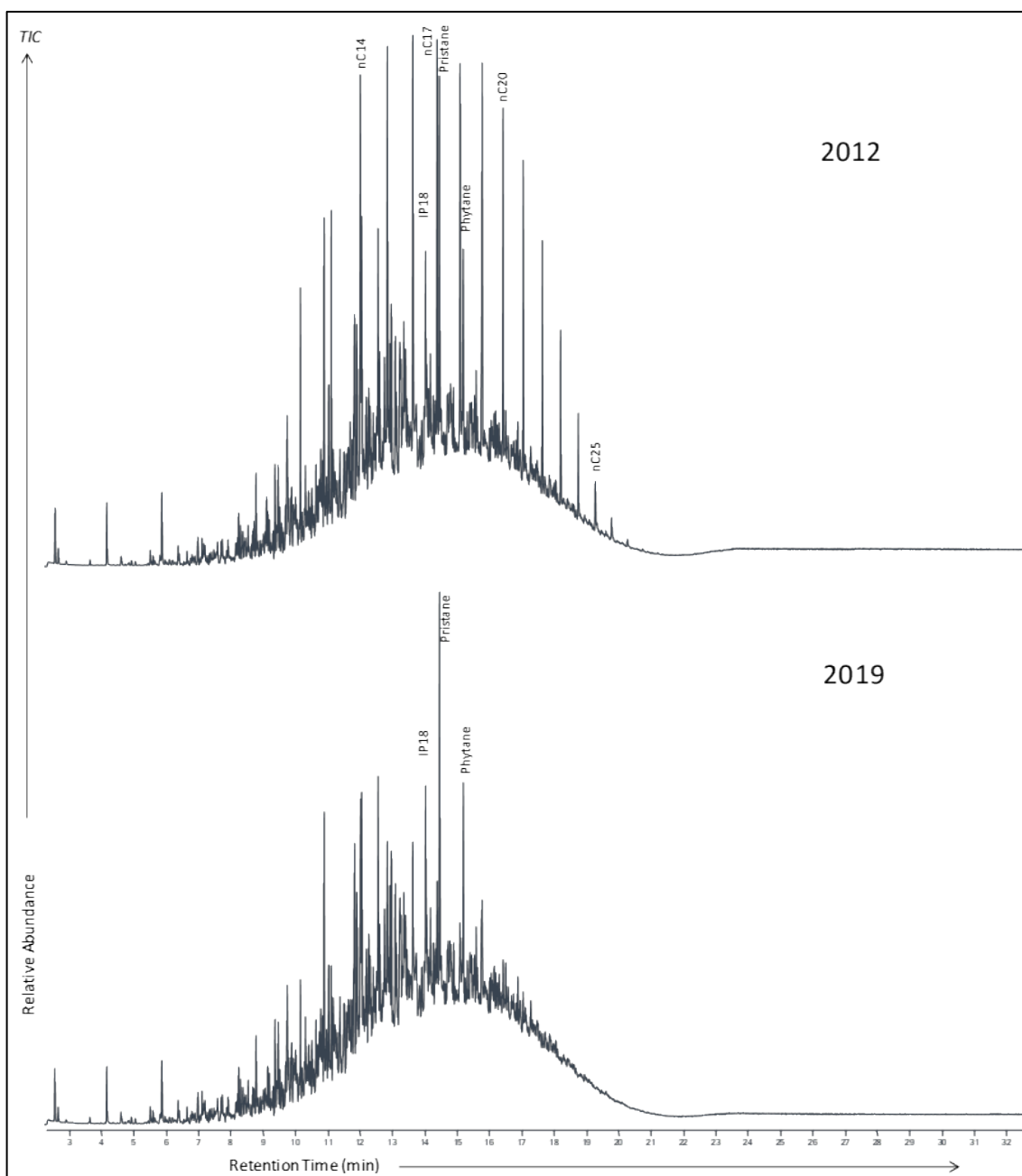
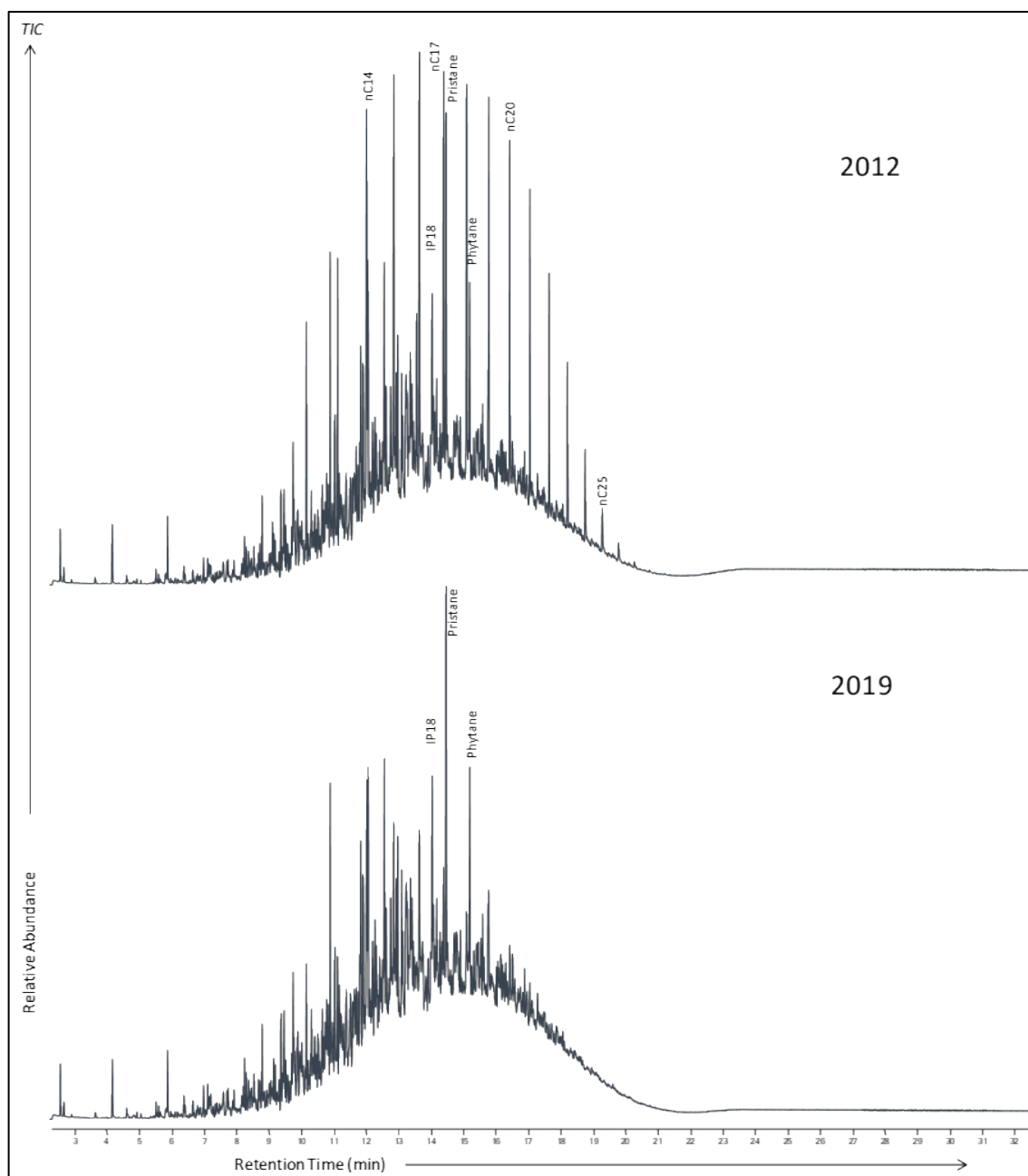


Figure C.1-1 GC-MS analysis of LNAPL sample CS01 from 2012 and 2019. Benz: benzene, CHX: cyclohexane, Cx: straight or branched alkane containing x carbons, D: di, E: ethyl, i: iso, IP: isoprenoid, M: methyl, n: normal, Naph: naphthalene, P: pentane, TMB: trimethylbenzene, Tol: toluene, Xyl: xylene



**Figure C.1-2 GC-MS analysis of LNAPL sample CS02 from 2012 and 2019. Benz: benzene, CHX: cyclohexane, Cx: straight or branched alkane containing x carbons, D: di, E: ethyl, i: iso, IP: isoprenoid, M: methyl, n: normal, Naph: naphthalene, P: pentane, TMB: trimethylbenzene, Tol: toluene, Xyl: xylene**



**Figure C.1-3 GC-MS analysis of LNAPL sample CS03 from 2012 and 2019. Benz: benzene, CHX: cyclohexane, Cx: straight or branched alkane containing x carbons, D: di, E: ethyl, i: iso, IP: isoprenoid, M: methyl, n: normal, Naph: naphthalene, P: pentane, TMB: trimethylbenzene, Tol: toluene, Xyl: xylene**

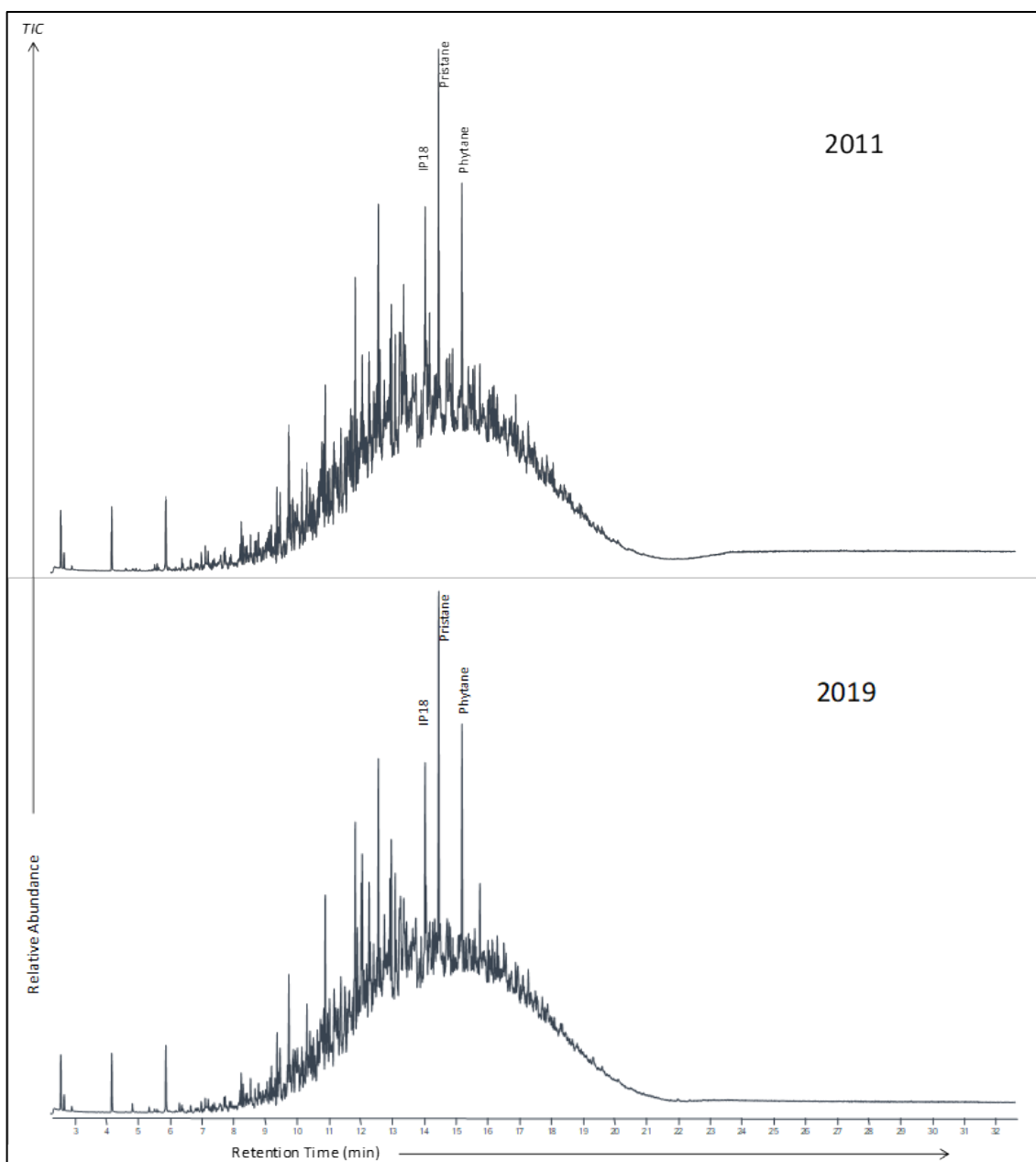


**Figure C.1-4 GC-MS analysis of LNAPL sample MW19 from 2011 and 2019. Benz: benzene, CHX: cyclohexane, Cx: straight or branched alkane containing x carbons, D: di, E: ethyl, i: iso, IP: isoprenoid, M: methyl, n: normal, Naph: naphthalene, P: pentane, TMB: trimethylbenzene, Tol: toluene, Xyl: xylene**

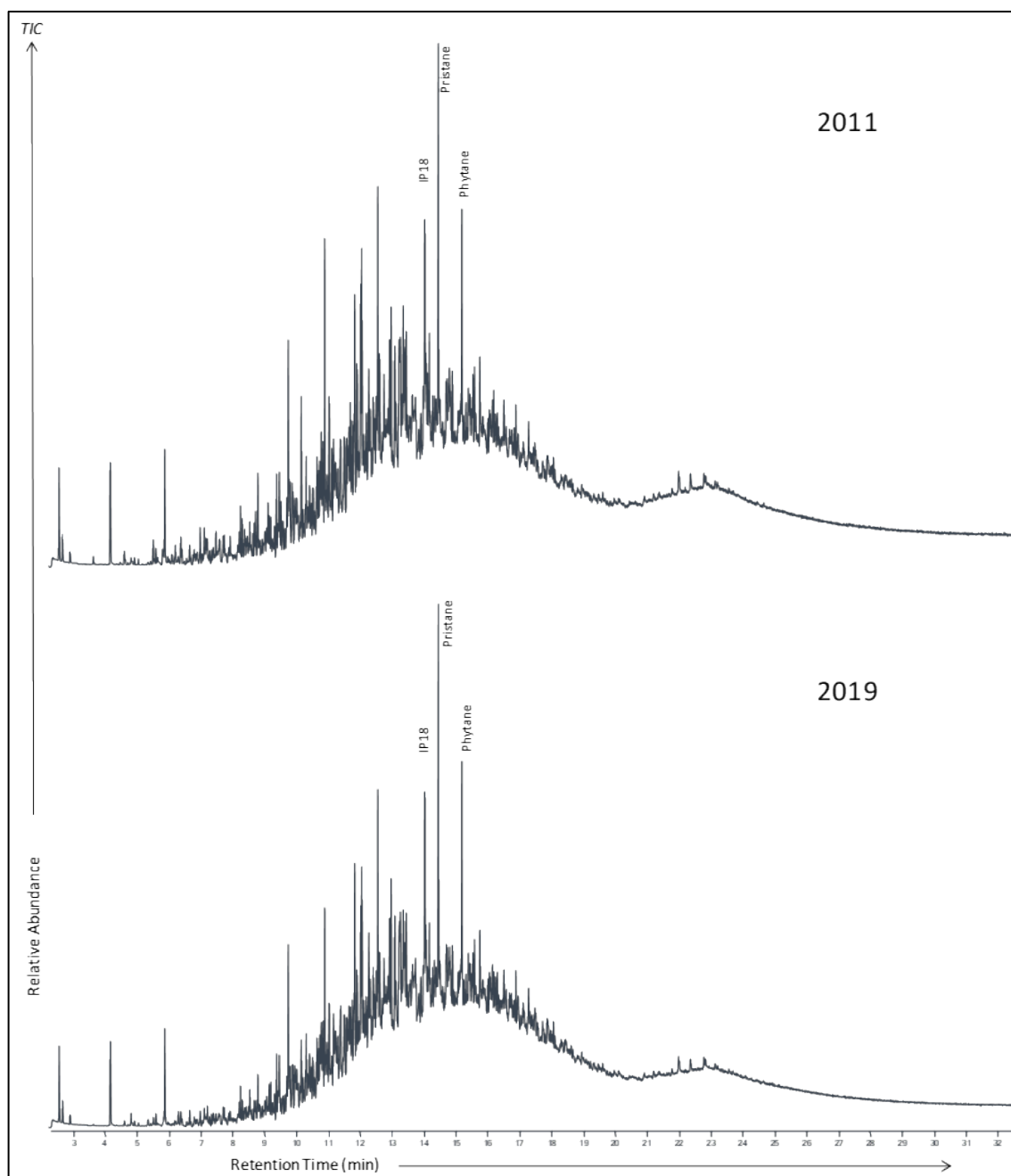


**Figure C.1-5 GC-MS analysis of LNAPL sample MW31 from 2011 and 2019. Benz: benzene, CHX: cyclohexane, Cx: straight or branched alkane containing x carbons, D: di, E: ethyl, i: iso, IP: isoprenoid, M: methyl, n: normal, Naph: naphthalene, P: pentane, TMB: trimethylbenzene, Tol: toluene, Xyl: xylene**

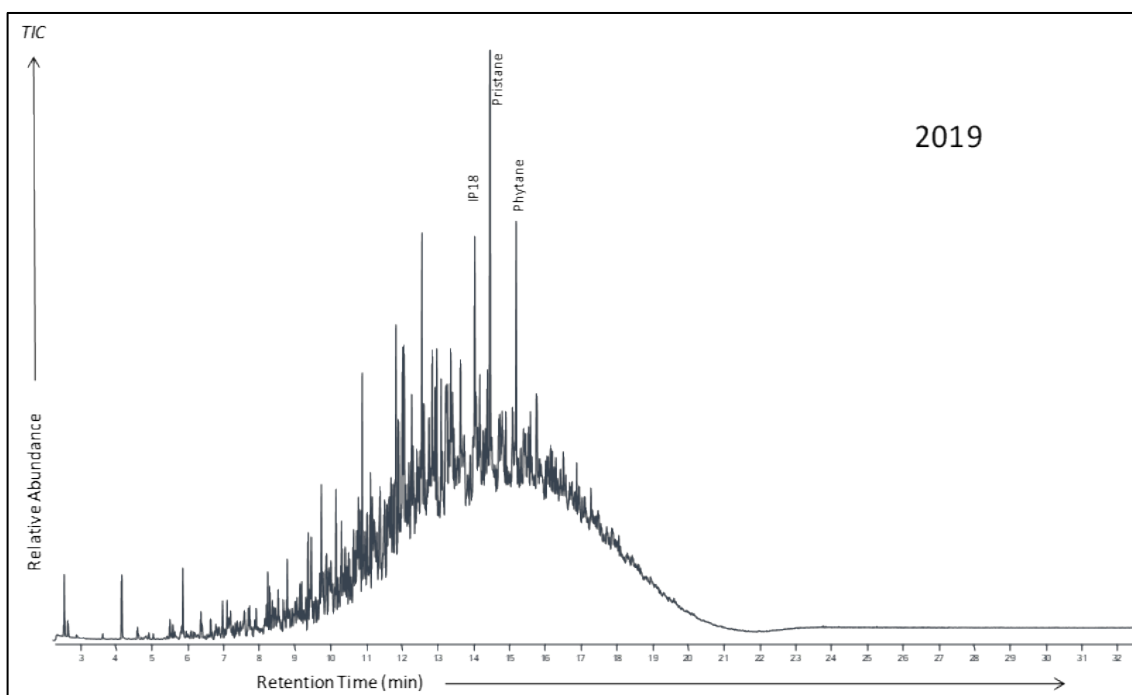


**Figure C.1-6 GC-MS analysis of LNAPL sample MW125 from 2019. Benz: benzene, CHX: cyclohexane, Cx: straight or branched alkane containing x carbons, D: di, E: ethyl, i: iso, IP: isoprenoid, M: methyl, n: normal, Naph: naphthalene, P: pentane, TMB: trimethylbenzene, Tol: toluene, Xyl: xylene**



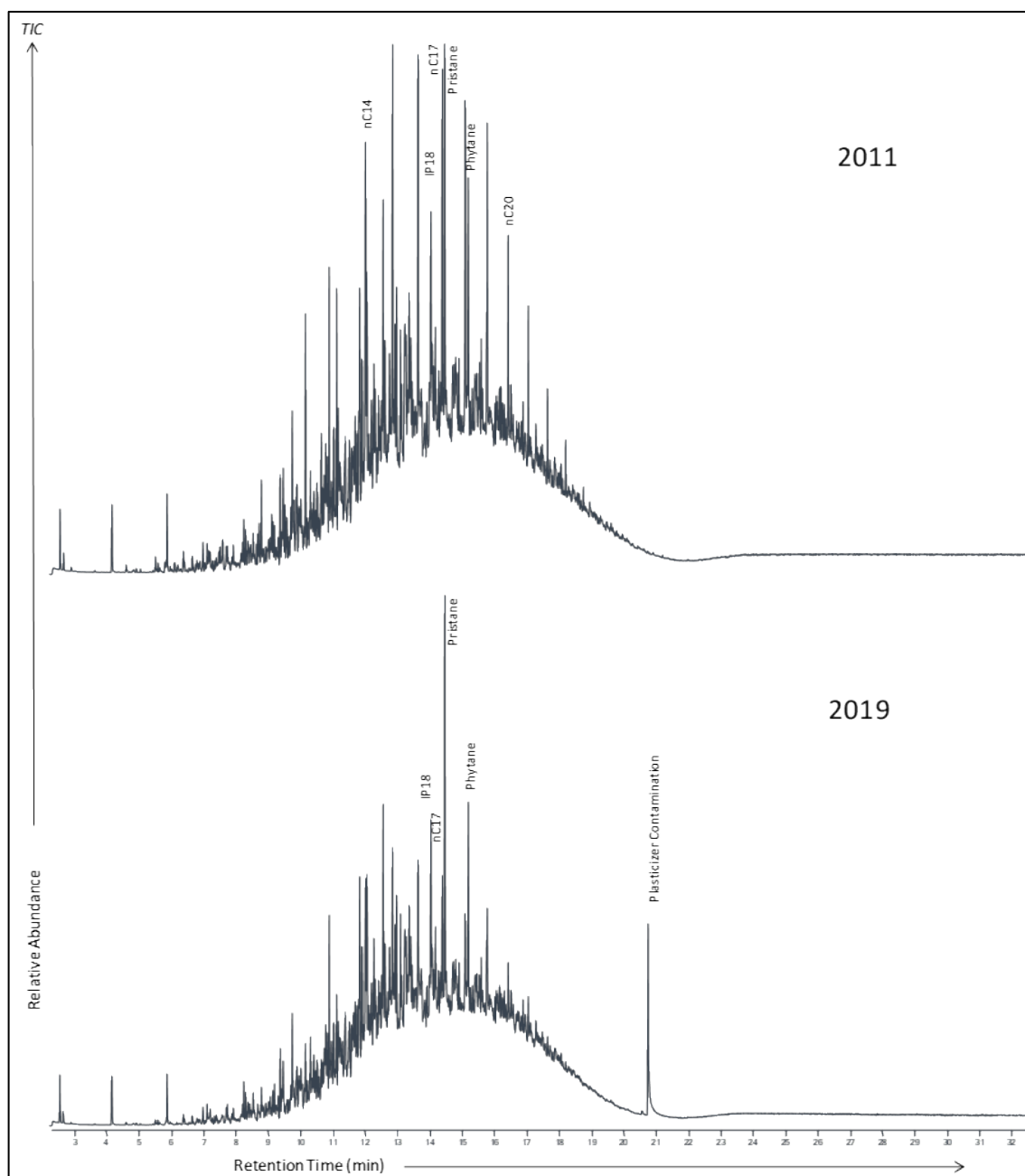


**Figure C.1-7. GC-MS analysis of LNAPL sample MW157 from 2011 and 2019. Benz: benzene, CHX: cyclohexane, Cx: straight or branched alkane containing x carbons, D: di, E: ethyl, i: iso, IP: isoprenoid, M: methyl, n: normal, Naph: naphthalene, P: pentane, TMB: trimethylbenzene, Tol: toluene, Xyl: xylene**

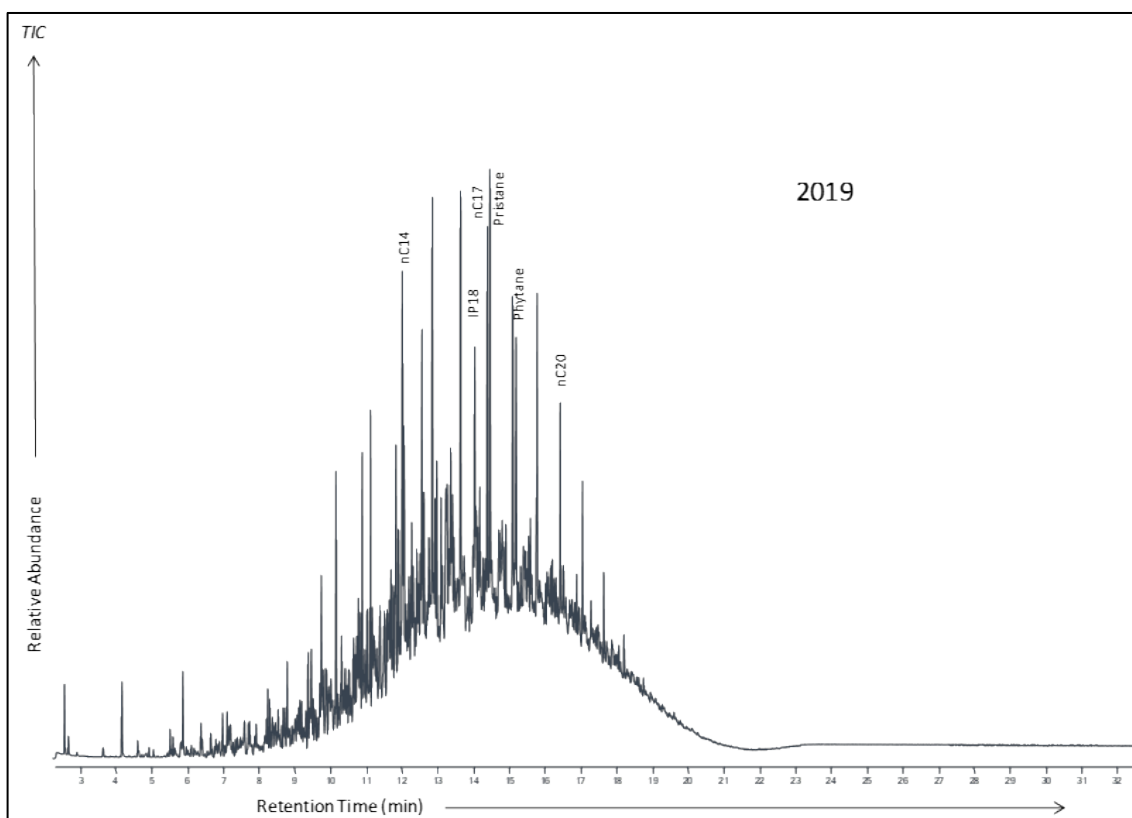


**Figure C.1-8 GC-MS analysis of LNAPL sample MB14CL052 from 2019. Benz: benzene, CHX: cyclohexane, Cx: straight or branched alkane containing x carbons, D: di, E: ethyl, i: iso, IP: isoprenoid, M: methyl, n: normal, Naph: naphthalene, P: pentane, TMB: trimethylbenzene, Tol: toluene, Xyl: xylene**

**Table C.1-1 Density and analytical results for site C LNAPL samples**

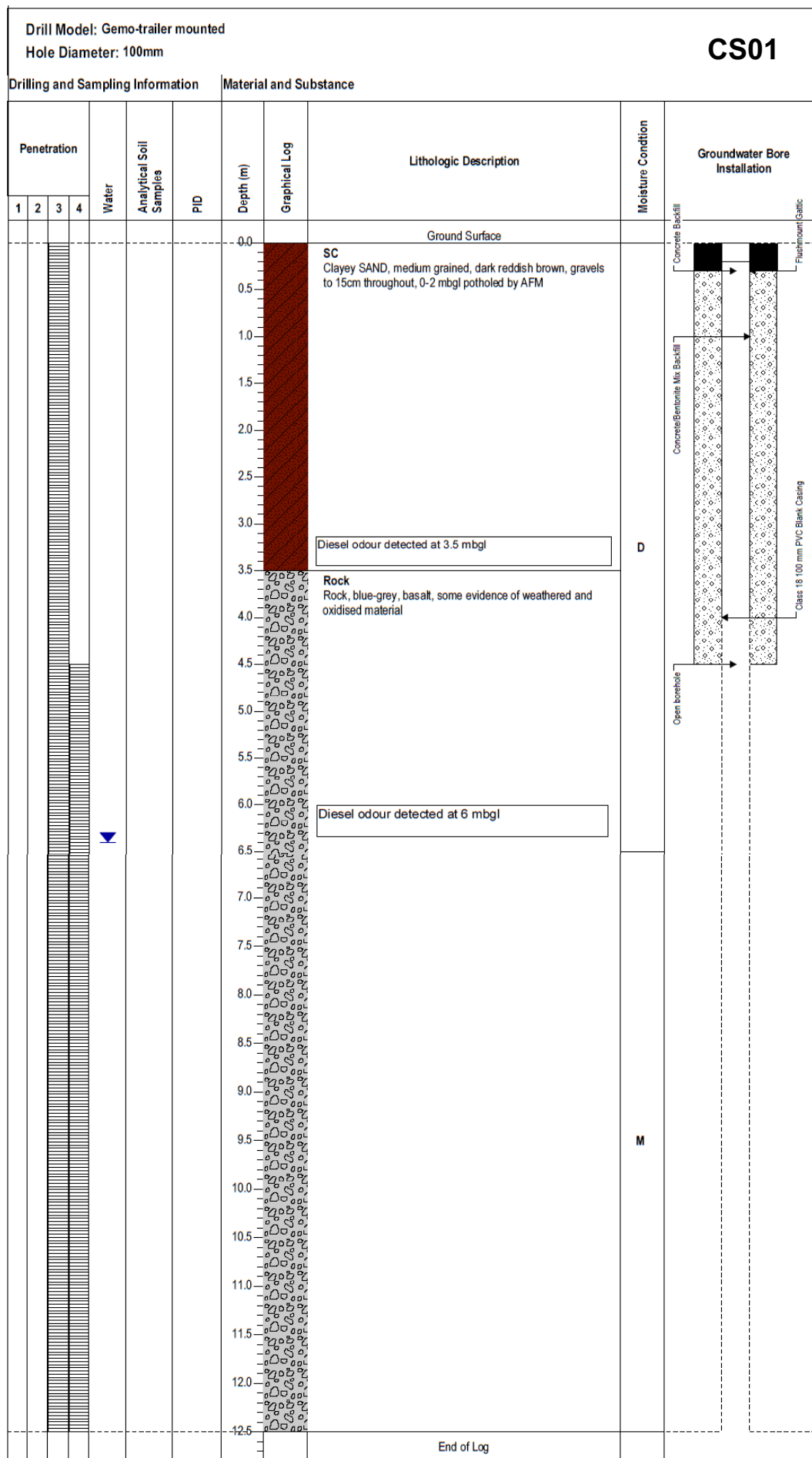
Sample name	Year	Density at 20 °C	Rel. %w/w loss*	Pr/nC17	Pr/Ph	Benzene	Toluene	Ethyl Benzene	m/p-Xylene	o-Xylene	135-TMB	124-TMB	123-TMB	Naph	nC17	Pristane
		g mL <sup>-1</sup>		Ratio	Ratio	%(w/w)	%(w/w)	%(w/w)	%(w/w)	%(w/w)	%(w/w)	%(w/w)	%(w/w)	%(w/w)	%(w/w)	%(w/w)
CS01	2012	0.849	0	0.85	2.7	<0.01	<0.01	0.02	<0.01	<0.01	<0.01	<0.01	<0.01	0.07	1.15	0.98
CS01	2013	0.856	12	0.91	2.6	<0.01	<0.01	<0.01	<0.01	<0.01	<0.01	<0.01	<0.01	0.02	1.21	1.11
CS01	2019	0.865	8	4.48	2.5	<0.01	<0.01	0.02	<0.01	<0.01	<0.01	<0.01	<0.01	0.05	0.24	1.07
CS02	2015	0.850	0	0.81	2.6	<0.01	<0.01	0.02	<0.01	<0.01	<0.01	<0.01	<0.01	0.06	1.21	0.98
CS02	2012	0.850	2	0.82	2.7	<0.01	<0.01	0.02	<0.01	<0.01	<0.01	<0.01	<0.01	0.05	1.22	1.01
CS02	2012	0.851	2	0.83	2.7	<0.01	<0.01	0.02	<0.01	<0.01	<0.01	<0.01	<0.01	0.06	1.21	1.00
CS02	2013	0.859	19	0.91	2.6	<0.01	<0.01	<0.01	<0.01	<0.01	<0.01	<0.01	<0.01	<0.01	1.34	1.22
CS02	2019	0.864	6	4.22	2.6	<0.01	<0.01	0.02	<0.01	<0.01	<0.01	<0.01	<0.01	0.04	0.25	1.04
CS03	2012	0.851	0	0.80	2.7	<0.01	<0.01	0.02	<0.01	<0.01	<0.01	<0.01	<0.01	0.06	1.25	0.99
CS03	2013	0.854	8	0.84	2.6	<0.01	<0.01	<0.01	<0.01	<0.01	<0.01	<0.01	<0.01	0.03	1.28	1.08
CS03	2019	0.863	8	4.28	2.6	<0.01	<0.01	0.02	<0.01	<0.01	<0.01	<0.01	<0.01	0.04	0.25	1.08
MW19	2011	0.860	0	13	2.1	<0.01	<0.01	<0.01	<0.01	<0.01	<0.01	<0.01	<0.01	<0.01	0.07	0.98
MW19	2015	0.862	-5	17	2.1	<0.01	<0.01	0.01	<0.01	<0.01	<0.01	<0.01	<0.01	0.02	0.05	0.93
MW19	2012	0.862	-4	20	2.1	<0.01	<0.01	0.01	<0.01	<0.01	<0.01	<0.01	<0.01	0.02	0.05	0.94
MW19	2019	0.872	3	33	2.1	<0.01	<0.01	<0.01	<0.01	<0.01	<0.01	<0.01	<0.01	0.01	0.03	1.01
MW31	2011	0.871	0	20	1.9	<0.01	<0.01	0.02	<0.01	<0.01	<0.01	<0.01	<0.01	0.03	0.03	0.52
MW31	2011	0.874	-3	20	2.1	<0.01	<0.01	0.02	<0.01	<0.01	<0.01	<0.01	<0.01	0.03	0.02	0.50
MW31	2015	0.873	9	24	2.1	<0.01	<0.01	0.01	<0.01	<0.01	<0.01	<0.01	<0.01	0.02	0.02	0.57
MW31	2019	0.874	16	25	2.1	<0.01	<0.01	<0.01	<0.01	<0.01	<0.01	<0.01	<0.01	0.02	0.03	0.61
MW125	2019	0.865	0	4.56	2.2	<0.01	<0.01	0.01	<0.01	<0.01	<0.01	<0.01	<0.01	0.01	0.20	0.91
MW157	2011	0.861	0	1.06	2.1	<0.01	<0.01	0.02	<0.01	<0.01	<0.01	<0.01	<0.01	0.02	0.82	0.87
MW157	2015	0.862	22	3.66	2.5	<0.01	<0.01	<0.01	<0.01	<0.01	<0.01	<0.01	<0.01	0.03	0.31	1.12
MW157	2019	0.874	21	3.51	2.4	<0.01	<0.01	<0.01	<0.01	<0.01	<0.01	<0.01	<0.01	0.01	0.32	1.11
MB14CL052	2019	0.854	0	1.15	2.0	<0.01	<0.01	0.02	<0.01	<0.01	<0.01	<0.01	<0.01	0.02	0.67	0.77

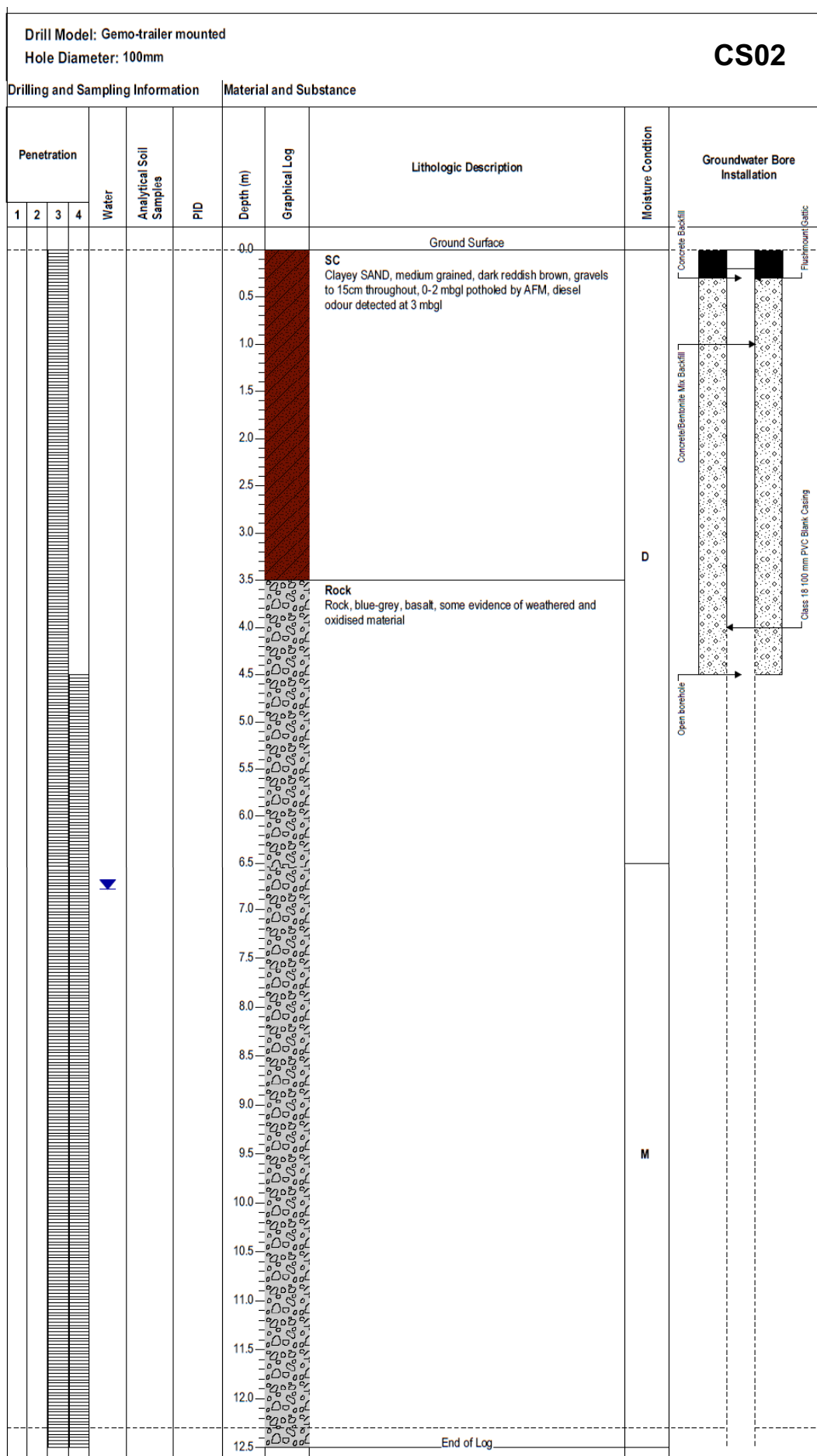
\*%w/w losses relative to source based on pristane; Pr/nC17: ratio of pristane/n-heptadecane; Pr/Ph: ratio of pristane/phytane; Naph: naphthalene; TMB: trimethylbenzene.

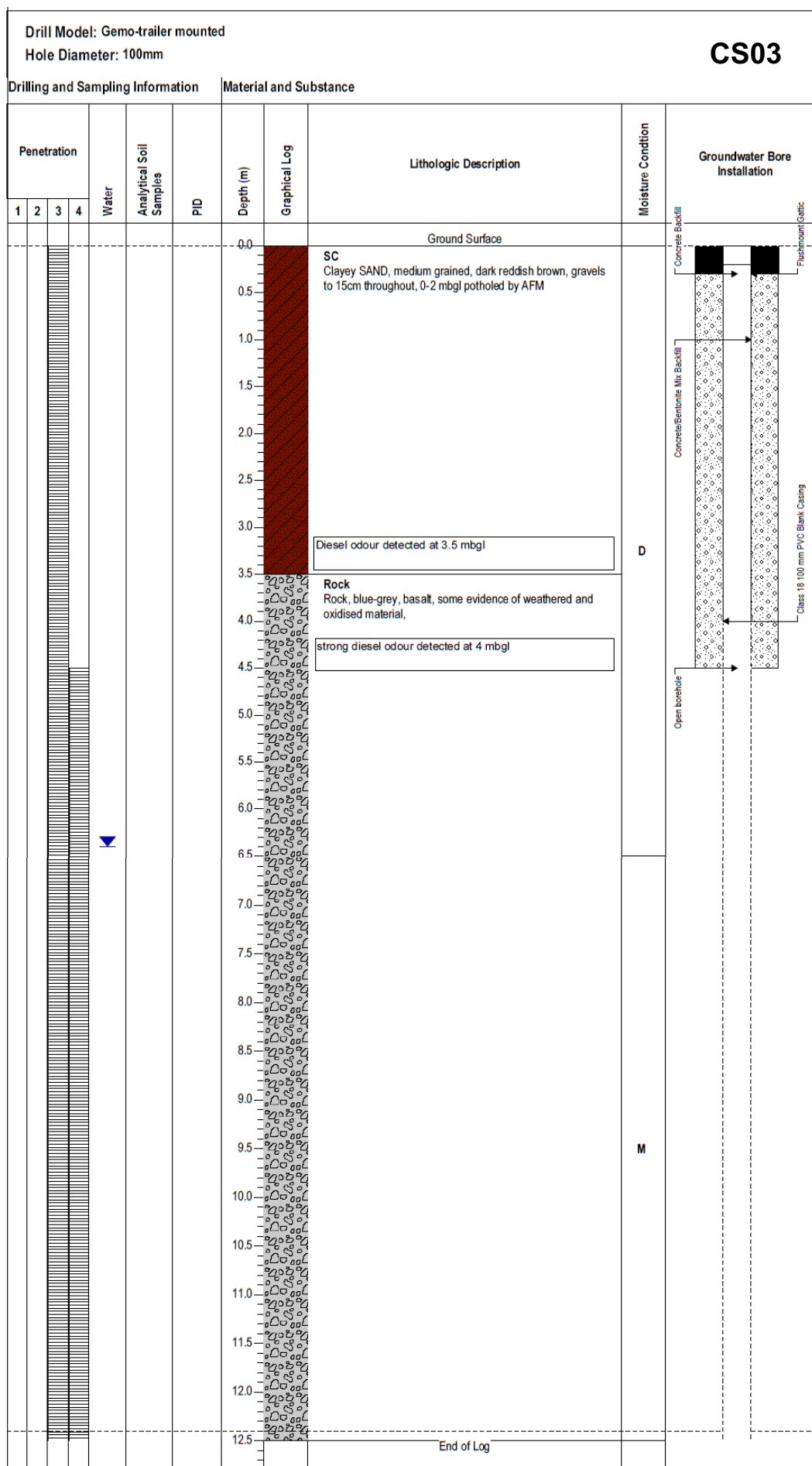
## APPENDIX C.2

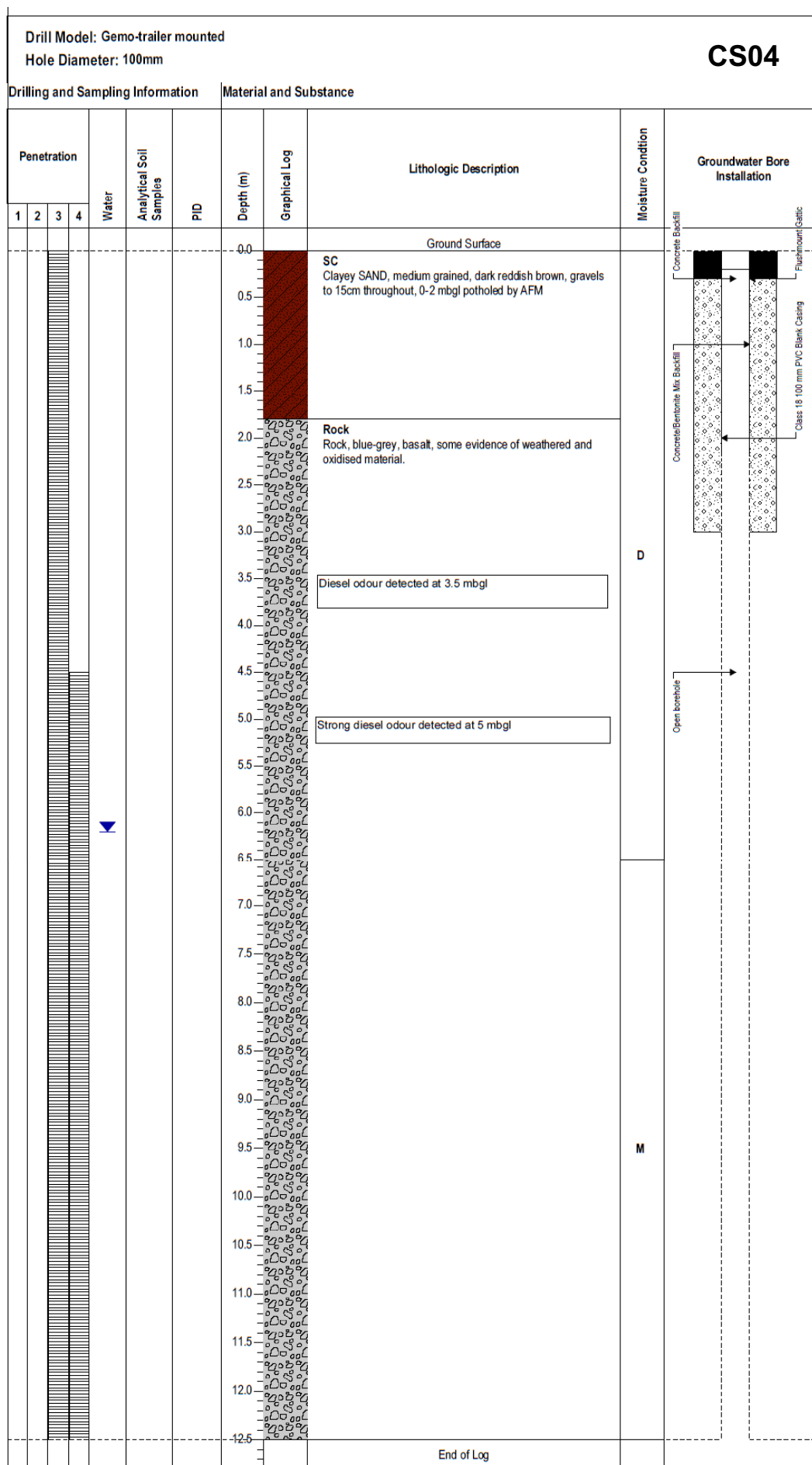
---

Site C logs from six wells drilled for a research program  
conducted by CSIRO (SiteC\_Ref3 2014)

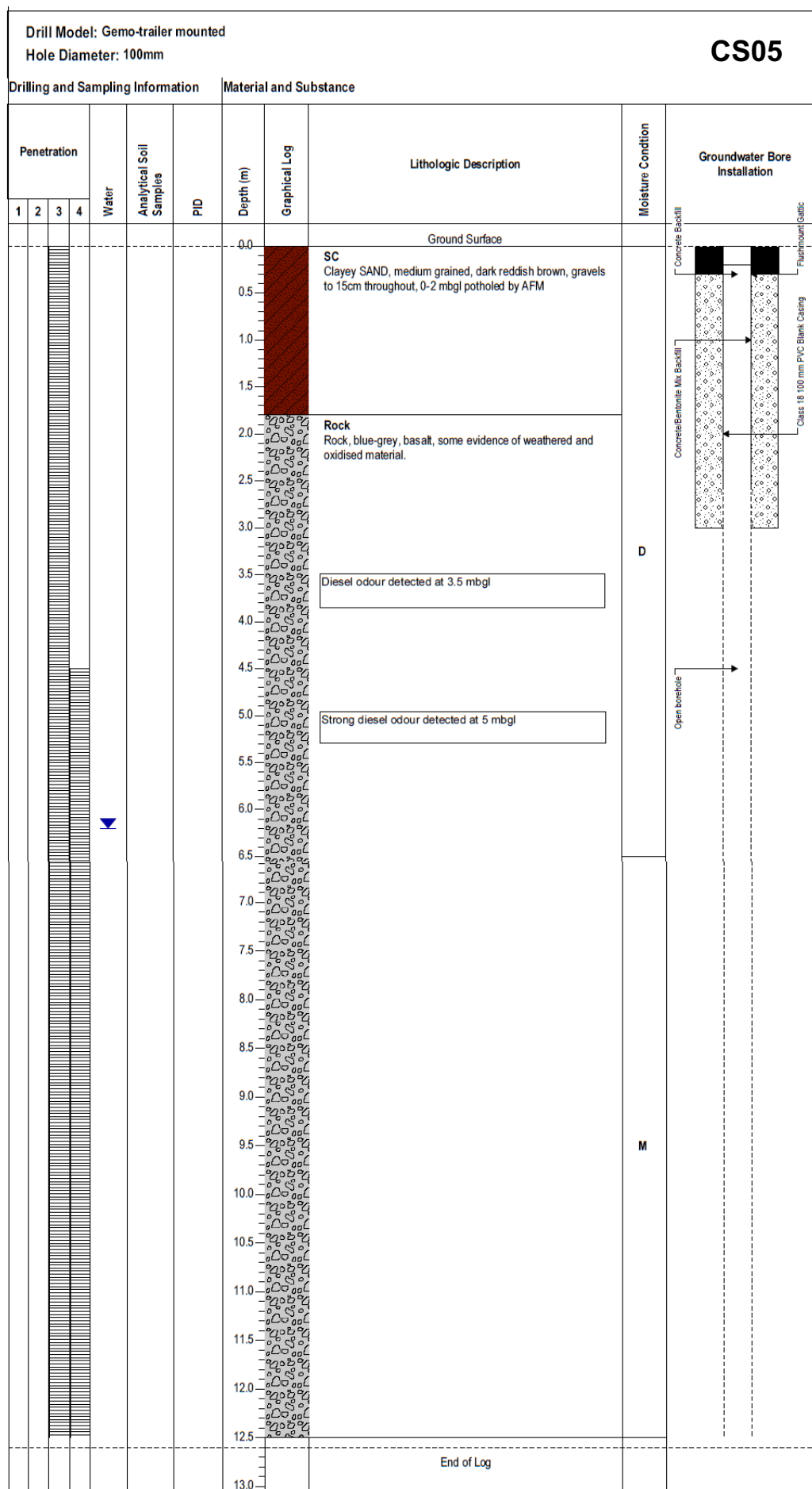


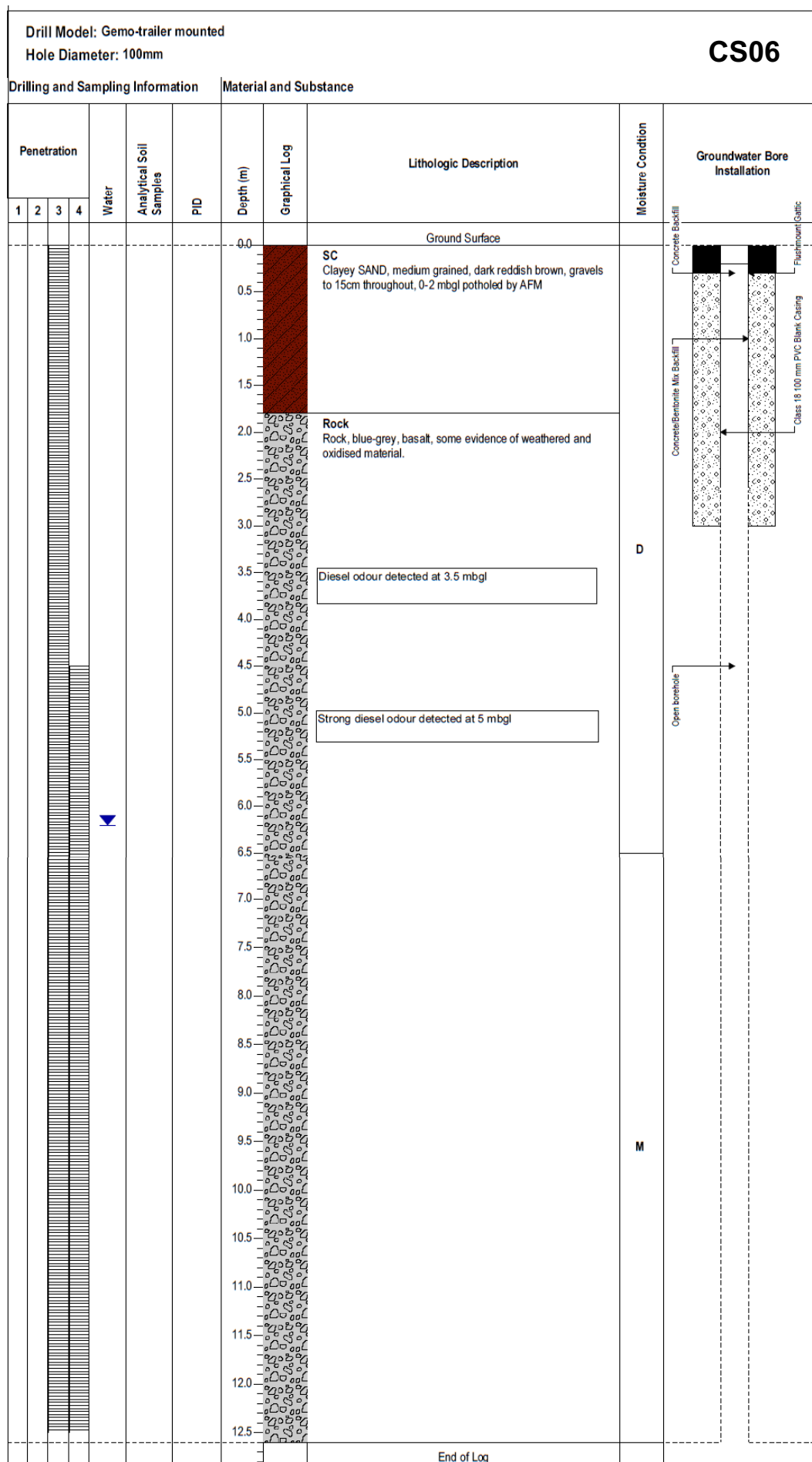












## APPENDIX D.1

### Site D GC-FID analytical and density results

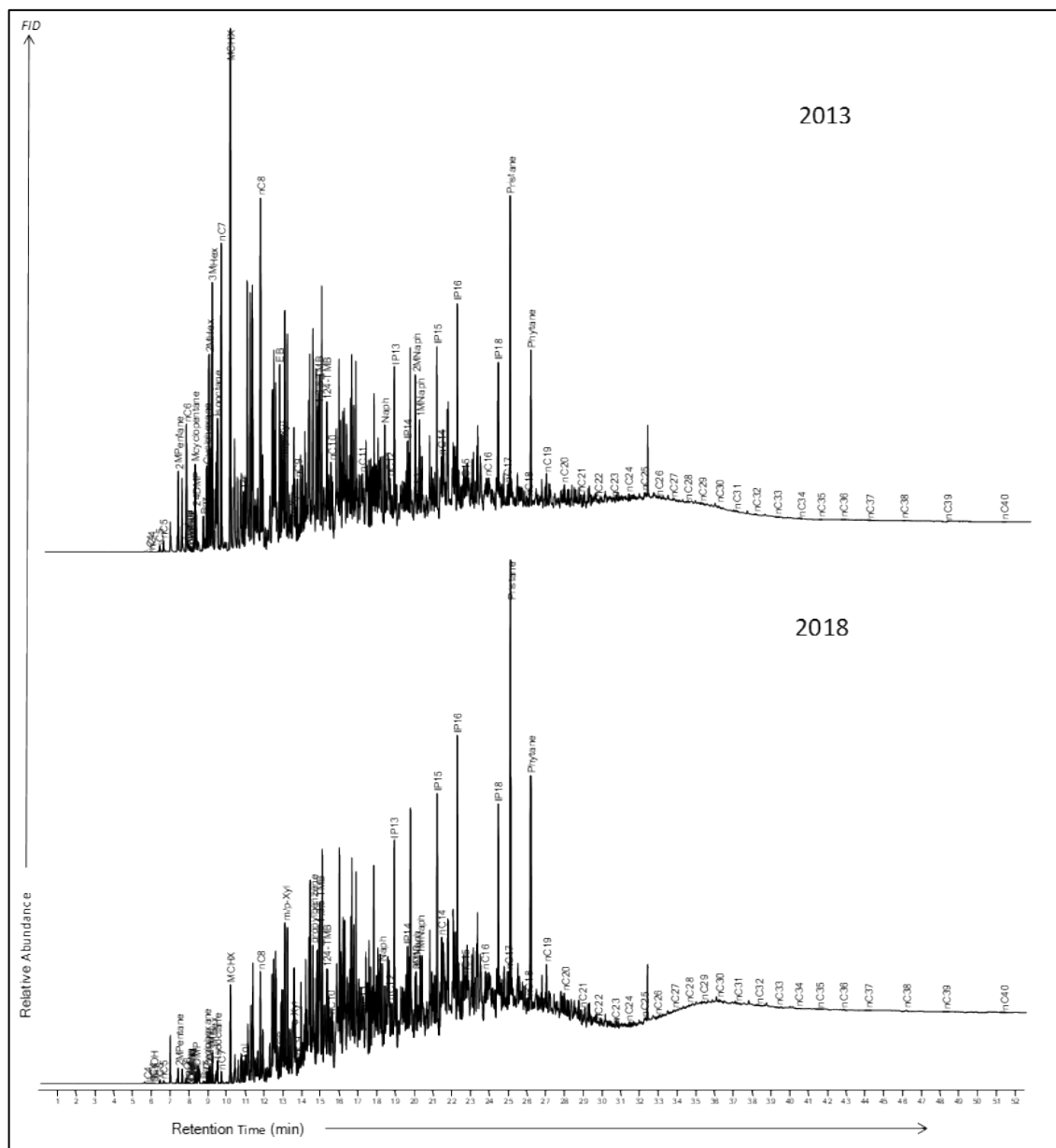
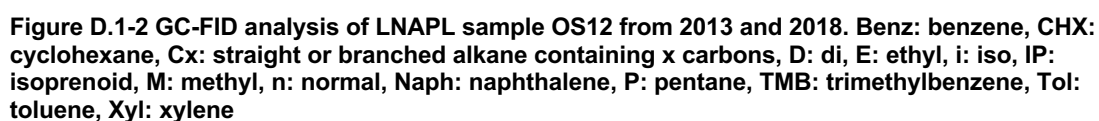
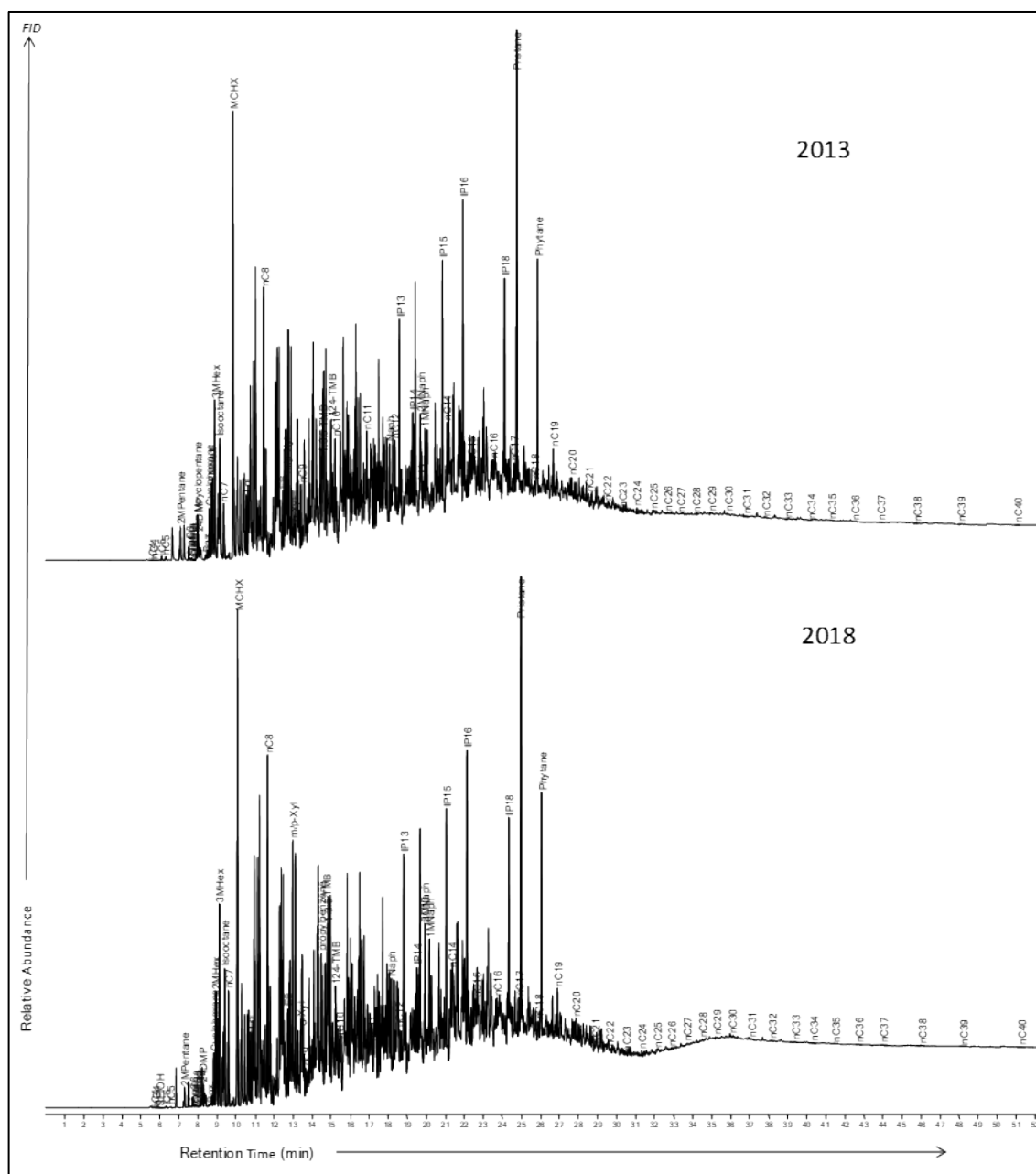
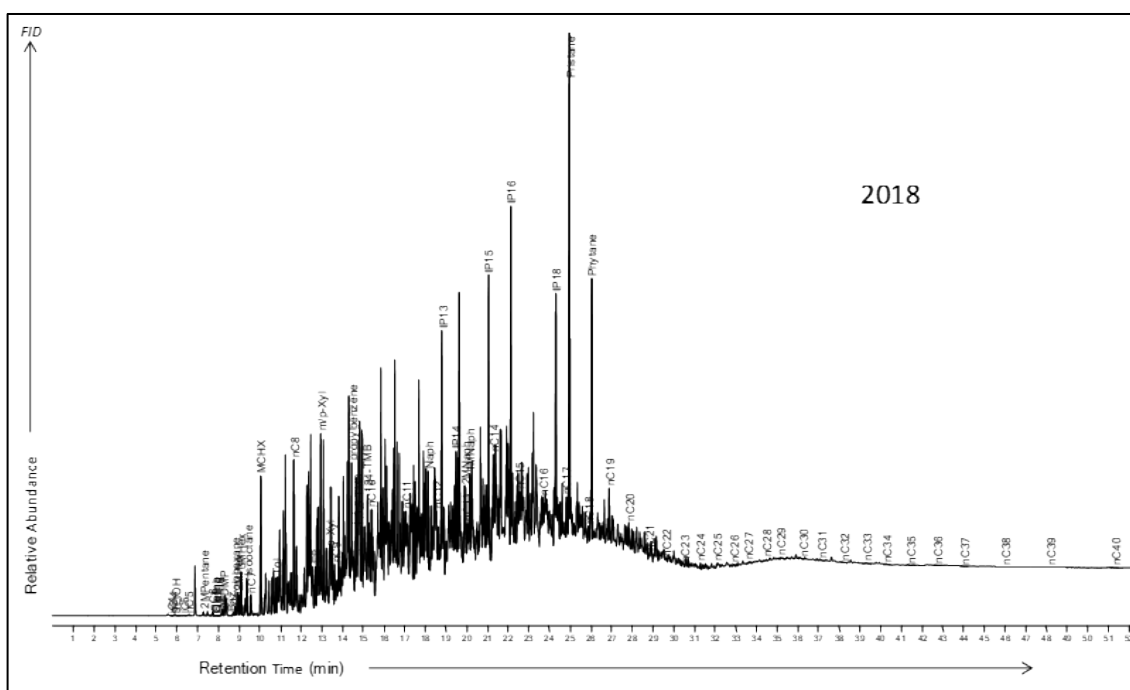
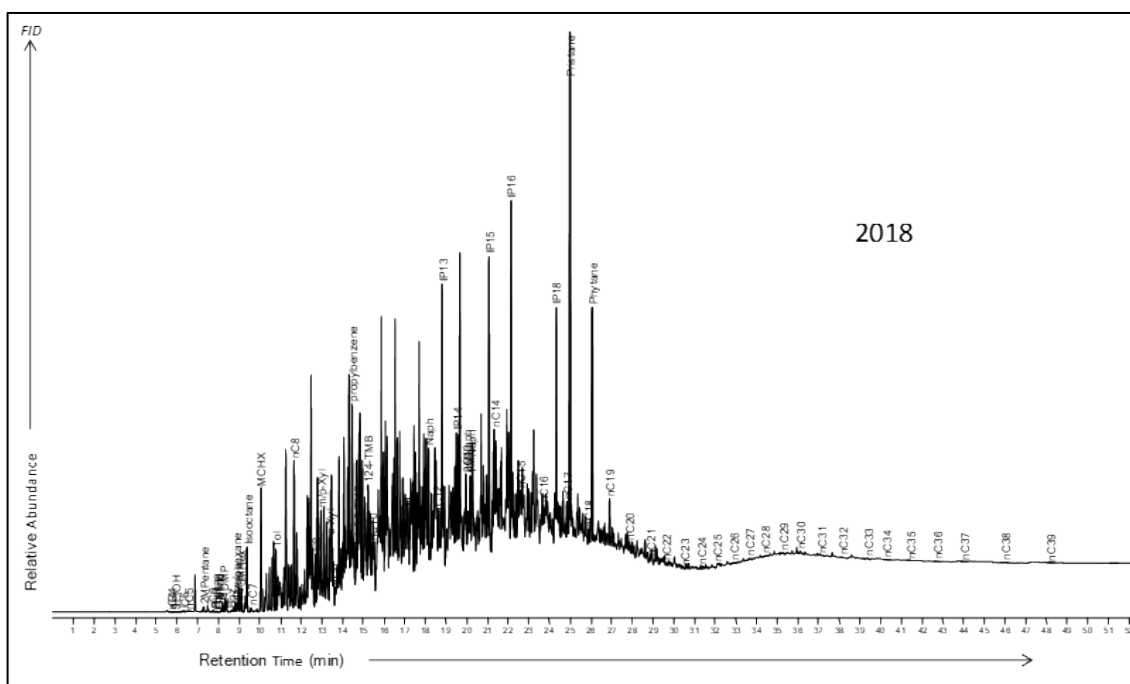


Figure D.1-1 GC-FID analysis of LNAPL sample OS08 from 2013 and 2018. Benz: benzene, CHX: cyclohexane, Cx: straight or branched alkane containing x carbons, D: di, E: ethyl, i: iso, IP: isoprenoid, M: methyl, n: normal, Naph: naphthalene, P: pentane, TMB: trimethylbenzene, Tol: toluene, Xyl: xylene





**Figure D.1-3 GC-FID analysis of LNAPL sample OS28 from 2013 and 2018. Benz: benzene, CHX: cyclohexane, Cx: straight or branched alkane containing x carbons, D: di, E: ethyl, i: iso, IP: isoprenoid, M: methyl, n: normal, Naph: naphthalene, P: pentane, TMB: trimethylbenzene, Tol: toluene, Xyl: xylene**



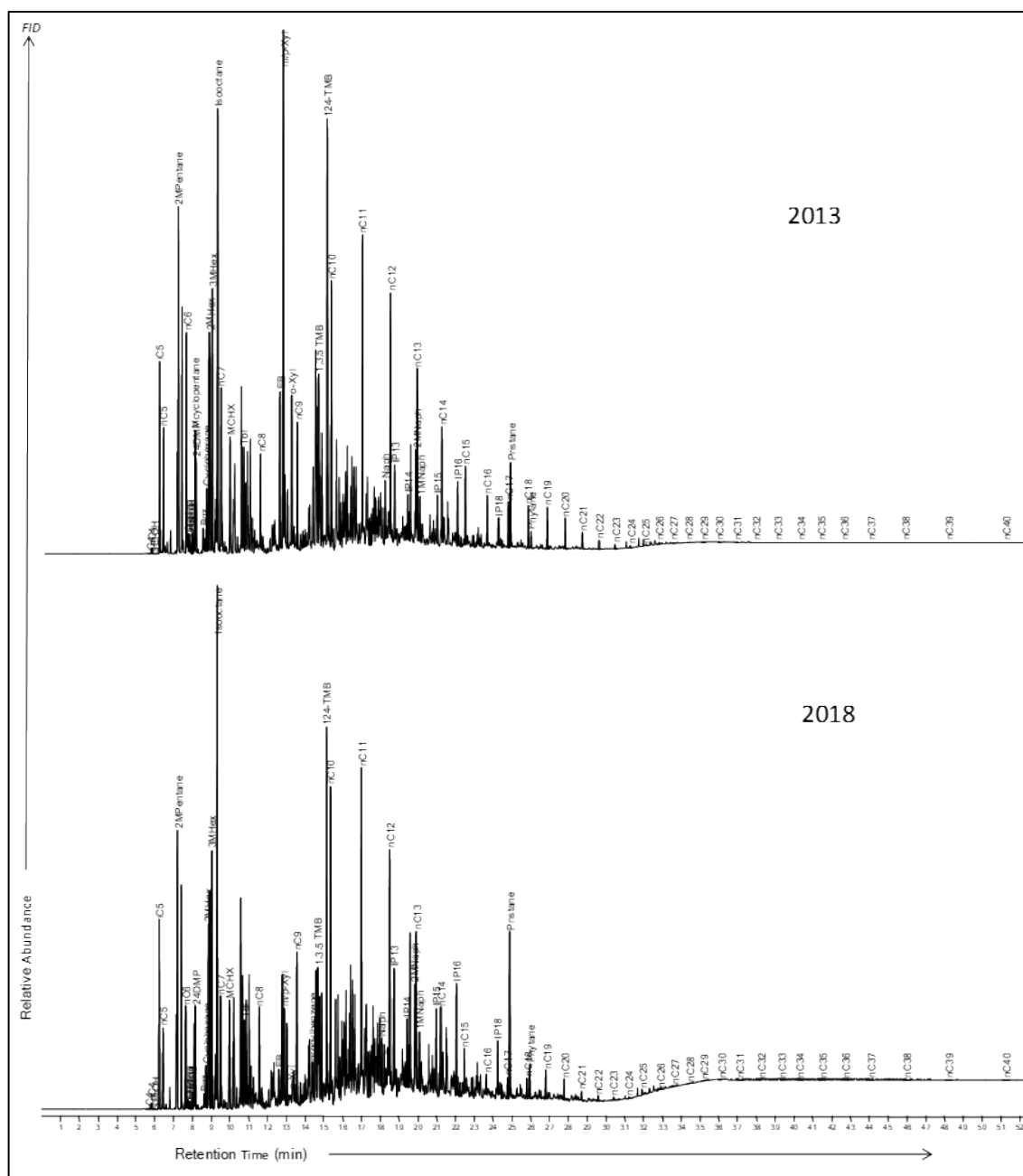


Figure D.1-6 GC-FID analysis of LNAPL sample OS63 from 2013 and 2018. Benz: benzene, CHX: cyclohexane, Cx: straight or branched alkane containing x carbons, D: di, E: ethyl, i: iso, IP: isoprenoid, M: methyl, n: normal, Naph: naphthalene, P: pentane, TMB: trimethylbenzene, Tol: toluene, Xyl: xylene

Table D.1-1 Density and analytical results for Site D LNAPL samples

Sample name	Year	Density at 20 °C	Rel. %w/w loss*	Pr/nC17	Pr/Ph	Benzene	Toluene	Ethyl Benzene	m/p-Xylene	o-Xylene	135-TMB	124-TMB	123-TMB	Naph	nC17	Pristane
		g mL <sup>-1</sup>		Ratio	Ratio	%(w/w)	%(w/w)	%(w/w)	%(w/w)	%(w/w)	%(w/w)	%(w/w)	%(w/w)	%(w/w)	%(w/w)	%(w/w)
OS08	2013	0.837	0	30	2.2	0.08	<0.01	0.30	0.13	0.02	0.18	0.22	0.12	0.14	0.02	0.71
OS08	2017	0.858	11	29	2.2	<0.01	<0.01	0.03	0.02	0.01	0.07	0.06	0.08	0.08	0.03	0.80
OS08	2018	0.862	14	40	2.2	<0.01	<0.01	<0.01	<0.01	<0.01	0.05	0.01	0.05	0.01	0.02	0.82
OS12	2013	0.834	0	31	2.1	0.06	0.01	0.29	0.40	0.06	0.14	0.48	0.18	0.12	0.02	0.65
OS12	2017	0.836	4	26	0.0	0.02	<0.01	0.09	0.15	0.02	0.08	0.20	0.11	0.10	0.03	0.68
OS12	2018	0.842	2	27	2.0	0.05	<0.01	0.20	0.24	0.04	0.12	0.30	0.15	0.12	0.02	0.67
OS70	2018	0.857	0	31	2.2	<0.01	<0.01	<0.01	0.01	<0.01	0.03	0.02	0.03	0.01	0.03	0.88
OS28	2013	0.846	0	37	2.1	0.01	<0.01	0.02	0.08	0.01	0.06	0.14	0.08	0.06	0.02	0.78
OS28	2018	0.848	-1	36	2.2	<0.01	<0.01	0.07	0.02	<0.01	0.02	0.02	0.03	0.06	0.02	0.78
OS41	2018	0.850	0	47	2.5	<0.01	<0.01	<0.01	<0.01	<0.01	<0.01	<0.01	0.01	0.01	0.02	0.88
OS63	2013	0.784	0	2.4	6.7	0.14	0.03	0.80	3.57	0.87	0.89	2.04	0.53	0.28	0.23	0.54
OS63	2017	0.780	-1	6.3	7.0	0.16	0.02	1.08	3.21	0.24	0.87	2.02	0.52	0.31	0.08	0.53
OS63	2018	0.789	24	13	6.7	0.01	<0.01	0.14	0.80	0.03	0.55	1.64	0.39	0.13	0.05	0.71

\*%w/w losses relative to source based on pristane; Pr/nC17: ratio of pristane/n-heptadecane; Pr/Ph: ratio of pristane/phytane; Naph: naphthalene; TMB: trimethylbenzene.



## APPENDIX D.2

### Site D well logs for MPVE03, MPVE05, MPVE10, OS08, OS12, OS22, OS41 and OS63

#### MPVE03

Drill Start Date: 06/12/08	Total Depth (m): 15.0	Water Level (Final): -
Drill Finish Date: 06/12/08	Hole Diam. / Width (mm): 200	RL Ground: 7.85
	Casing Type: PVC	RL Case: 7.73
	Casing Diam. (mm): 100	
Drill Method: AK 0-2, SA 2-4, DHH 4-15	Surface Completion: Gatic	
Hole Type: MPVE Bore	Water Strike: 7.0mbgl	
ERM Australia Pty Ltd		

Lithology	Symbol	Well	Depth (m)	Recovery	Sample Type	PPT (kPa)	PID (ppm)	Sample Details	Remarks
Ground Surface			0						
Grass					AK		0.9	0.2	
CLAY					AK		3.2	0.5	
Sandy gravely silt, brown, dry, no plasticity, gravel to 10mm inclusions (root)			1		AK		4.2	1.0	
CLAY									
grey/brown, dry, very stiff, no plasticity, moist for 1.3mbgl, with moderate plasticity			2		SA		4.0	2.2	
			3						
			4						
BASALT									
Grey, weathered, highly fractured			5						
			6						
some red and grey clay deposits within basalt			7						
			8						
			9						
			10						
			11						
			12						
			13						
			14						
Borehole Terminated at 15mbgl			15						
End of Log			16						

## MPVE05

Drill Start Date: 06/12/07	Total Depth (m): 14.5	Water Level (Final): -
Drill Finish Date: 19/12/07	Hole Diam. / Width (mm): 200	RL Ground: -
	Casing Type: PVC	RL Case: -
	Casing Diam. (mm): 100	
Drill Method: AK 0-2, SA 2-4.8, DHH 4.8-15	Surface Completion: Gatic	
Hole Type: MPVE Bore	Water Strike: 7.5mbgl	

Lithology	Symbol	Well	Depth (m)	Recovery	Sample Type	PPT (kPa)	PID (ppm)	Sample Details	Remarks
Ground Surface			0						
Grass									
Sandy CLAY Sandy silty CLAY, brown, dry, very stiff, low plasticity, some root inclusions					AK		4.5	0.2	
					AK		2.4	0.5	
			1		AK		3.2	1.0	
			2		AK		3.8	2.0	
becoming orange/light brown at 3.0mbgl									
becoming moist with high plasticity at 4.0mbgl			3						
some minor basalt fragments at 4.5mbgl			4						
BASALT Grey					SA		0.5	4.5	
			5						
			6						
			7						
			8						
			9						
			10						
			11						
			12						
			13						
			14						
			15						
Borehole terminated at 14.5mbgl									sand collapsed into well thus bringing the well depth to 14.5mbgl
End of Log			16						

# MPVE10

Drill Start Date: 07/12/07	Total Depth (m): 15.0	Water Level (Final): -
Drill Finish Date: 07/12/07	Hole Diam. / Width (mm): 200	RL Ground: 7.92
	Casing Type: PVC	RL Case: 7.835
	Casing Diam. (mm): 100	
Drill Method: HA 0-2, SA 2-4.8, DHH 4.8-15	Surface Completion: Gatic	
Hole Type: MPVE Bore	Water Strike: 7.5mbgl	

Lithology	Symbol	Well	Depth (m)	Recovery	Sample Type	PPT (kPa)	PID (ppm)	Sample Details	Remarks
Ground Surface			0						
GRASS					HA		4.0	0.2	
Silty CLAY					HA		2.4	0.5	
Silty, brown, dry, stiff, low plasticity, minor organic matter			1		HA		3.6	1.0	
CLAY									
Brown/grey, very stiff, damp			2		HA		4.2	2.0	
CLAY									
Grey/orange/red mottled, damp, high plasticity, moderately dense, no inclusions			3						
			4		SA		3.0	3.5	
			5		SA		2.0	4.5	
			6		SA		2.9	4.8	
BASALT									
Grey, weathered			7						
			8						
			9						
			10						
			11						
			12						
becoming highly weathered at 13mbgl			13						
			14						
Borehole terminated at 15mbgl			15						
End of Log			16						

# OS08

Surface Elev. \_\_\_\_\_ Total Hole Depth 9.5 m Diameter \_\_\_\_\_  
 Top of Casing \_\_\_\_\_ Water Level Initial 8.0 m Static \_\_\_\_\_  
 Screen: Dia 50 mm Length 3.0 m Type/Size \_\_\_\_\_  
 Casing: Dia \_\_\_\_\_ Length 6.0 m Type \_\_\_\_\_  
 Rig/Core \_\_\_\_\_  
 Method Solid Auger/Air Hammer  
 Date 27/04/98 Permit # \_\_\_\_\_

## COMMENTS:

Logs are based on observations of drill cuttings. Finished below surface. Covered with soil.

Depth (m)	Well Completion	PID (ppm)	Sample ID	Blow Count/ % Recovery	Graphic Log	USCS Class.	Description (Color, Texture, Structure) Trace < 10%, Little 10% to 20%, Some 20% to 35%, And 35% to 50%
-1							
0							GRASS/TOPSOIL
1		20.5	1.0				CLAY: brown; hard; stiff; MC<PL; dry. As above.
2		12.5	2.0				As above: some fine gravel.
3		14.2	3.0			CL	As above: some red/brown and yellow bands; very stiff; layering evident; damp.
4		12.4	4.0				As above: red/brown to brown; layering evident.
5		18.0 10.8	4.8 5.0			CL/BAS	CLAY: weathered Basalt. BASALT: grey; fine dust to small chips; hard; dry.
6		29.7	6.0				As above: slight hydrocarbon odour; moist.
7		94.0	7.0			BAS	As above: slight hydrocarbon odour; becoming moist.
8		25.8	8.0				As above: moist to wet.
9		24.0	8.0				
10							Monitoring Well OSB terminated at 9.5 metres, as required.
11							
12							

# OS12

Surface Elev. \_\_\_\_\_ Total Hole Depth 9.0 m Diameter \_\_\_\_\_  
 Top of Casing \_\_\_\_\_ Water Level Initial 7.5 m Static \_\_\_\_\_  
 Screen: Dia 50 mm Length 3.0 m Type/Size \_\_\_\_\_  
 Casing: Dia 50 mm Length 5.5 m Type Class 1B PVC

Rig/Core \_\_\_\_\_  
 Method Solid Auger/Air Hammer  
 Date 27/04/98 Permit # \_\_\_\_\_

## COMMENTS:

Logs are based on observations of drill cuttings. Finished below ground.

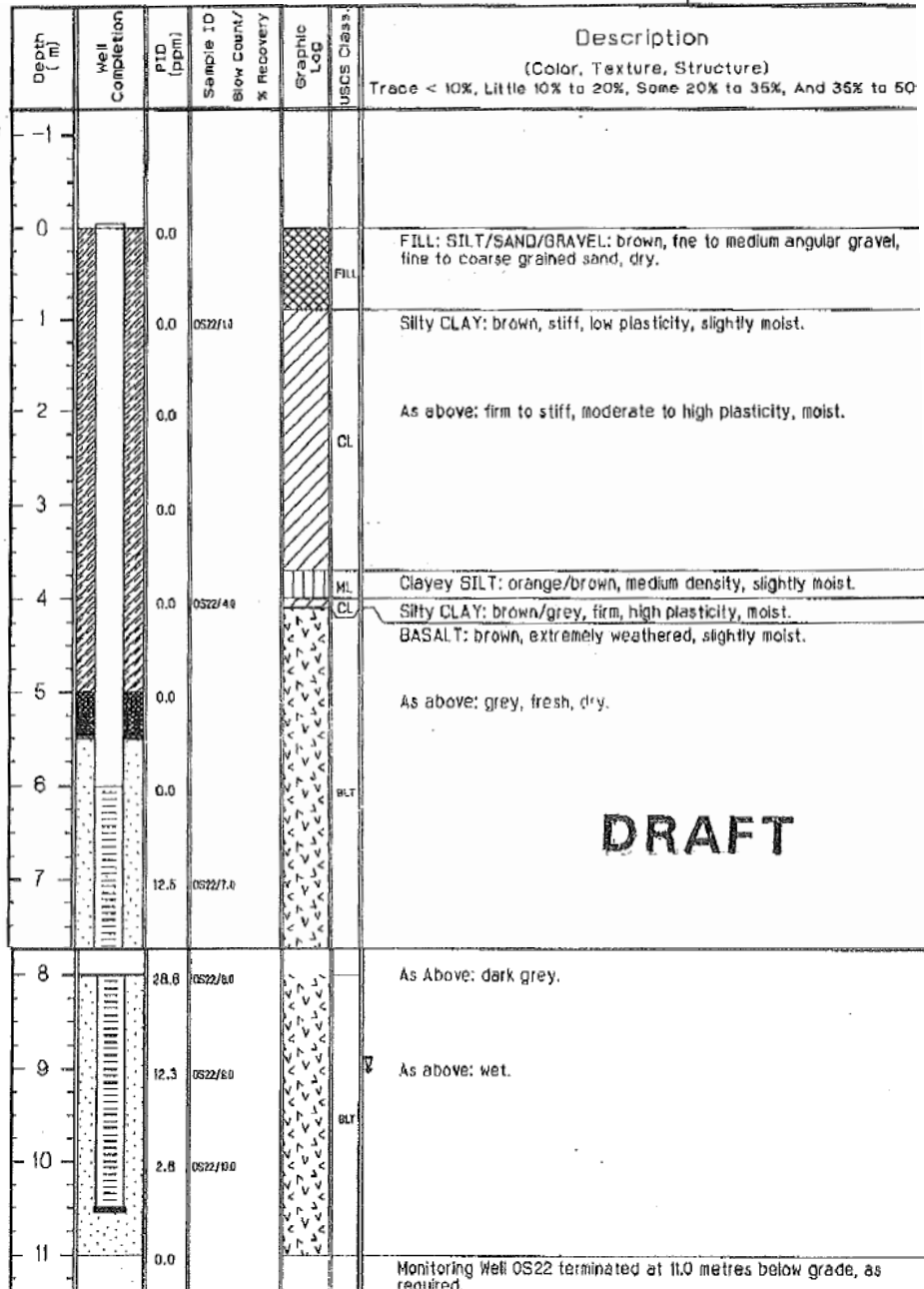
Depth (m)	Well Completion	PTD (ppm)	Sample ID Blow Count/ X Recovery	Graphic Log	USCS Class.	Description (Color, Texture, Structure) Trace < 10%, Little 10% to 20%, Some 20% to 35%, And 35% to 50%
-1						
0						GRASS/TOPSOIL
1		0.0	1.0		CL	CLAY: brown hard; stiff; MC<PL; dry.
2		0.0	2.0			CLAY: brown some red/brown and yellow bands; very stiff; damp. Calcitic CLAY: light grey; friable; MC<PL; dry.
3		0.0	3.0			BASALT: grey; fine dust; small particles; dry.
4		12.8	4.0			As above: minor clay bands.
5		16.4	5.0			As above.
6		12.3	6.0		BAS	As above: hydrocarbon odour.
7		26.2	7.0			As above: hydrocarbon odour; moist.
8		41.8	8.0			As above: moist.
9						Monitoring Well OS12 terminated at 9.0 metres, as required.

# OS22

Surface Elev. \_\_\_\_\_ Total Hole Depth 11.0 m Diameter 150 mm  
 Top of Casing \_\_\_\_\_ Water Level Initial 9.0 m Static \_\_\_\_\_  
 Screen: Dia 50 mm Length 4.5 m Type/Size 0.5 mm  
 Casing: Dia 50 mm Length 6.5 m Type Class 18 PVC  
 Rig/Core Fox Mobile  
 Method Hand Auger/Hollow Rotary Hammer  
 Date 28/01/99 Permit # \_\_\_\_\_

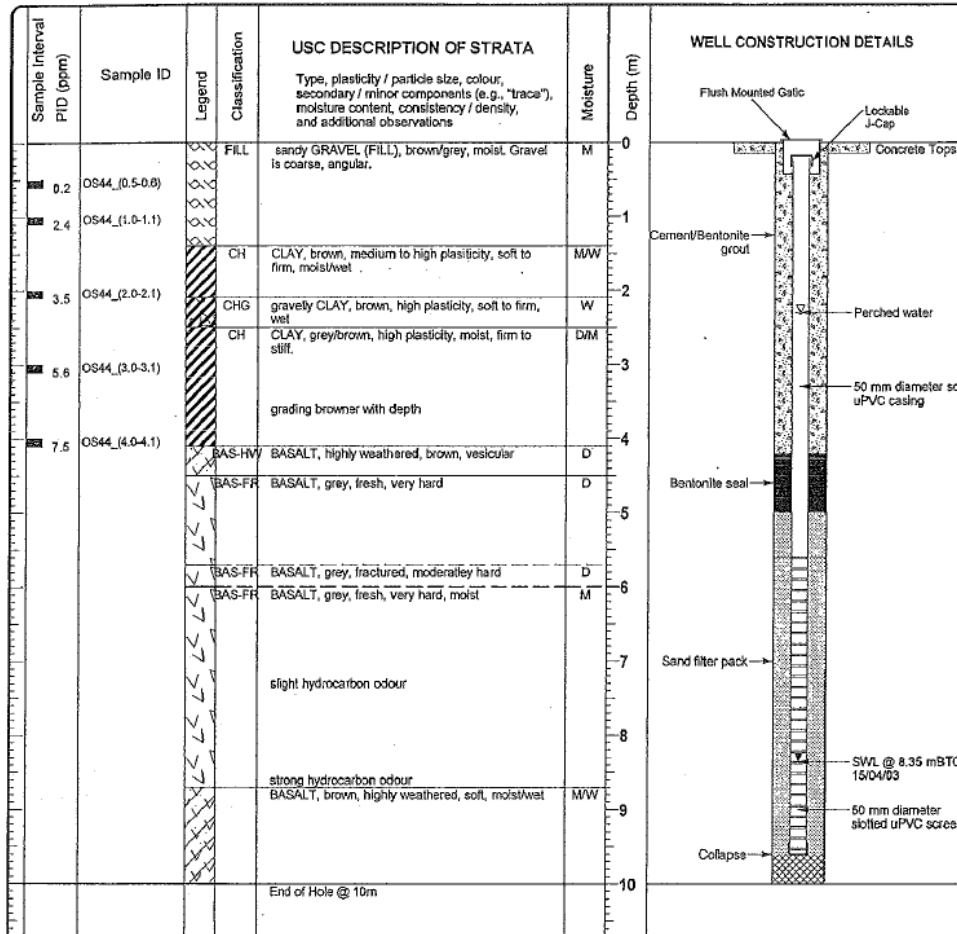
## COMMENTS:

Samples taken with split spoon sampler  
 Basalt taken as grab samples. BLT denotes Basalt.



# OS41

Date Started: 07-04-03	Bore Size: 100 mm Total Depth: 10.00 m Casing Size: 60 mm	Relative Level: mRL Coordinates: mN mE	Drill Type: Push Tube/Solid Stem Auger/Air Hammer Drill Model: Jaco Drill Fluid: Envirotube
Date Finished: 07-04-03			



# OS63

Drill Start Date: 28/08/09		Total Depth (m): 11.5		Final Water Level (m bgl): 9.868	
Drill Finish Date: 28/08/09		Hole Diam. / Width (mm): 150		Elevation (Ground): n/a	
		Casing Type: PVC		Elevation (Case): n/a	
		Casing Diam. (mm): 50			
Drill Method: NDD (1.3 m), DC (11.5 m)		Surface Completion: Gatic cover			
Hole Type: Monitoring well		Water Strike (m bgl): n/a			

Lithology	Symbol	Well	Depth (m)	Recovery	Sample Type	Analysed PPT (kPa)	PID (ppm)	Sample Details	Remarks
Ground Surface			0						
<b>Sandy SILT</b> Brown, dry, loose, sand; fine to medium grained, poorly sorted, fine root inclusions.					HA	0.0	OS63_0.2		PID readings possibly faulty. NDD refusal at 0.3 mbgs.
<b>CLAY</b> Black with orange mottling, dry, very stiff.					HA	0.0	OS63_0.5		
<b>Sandy CLAY</b> Grey with hard black lumps, dry, dense, sand; loose, fine grained, well sorted.			1		HA	0.0	OS63_1.0		
<b>Slightly weathered BASALT</b> Light bluish grey, hard, many vesicles 2 - 3 mm, few vesicles 4 mm, some vesicles 1 mm, trace calcite deposits in vesicles.  Fracture from 1.22 - 1.34 m, 70 degrees, narrow to wide, rough, clay; brown, soft, high plasticity.									Hand auger refusal at 1.0 mbgl.
<b>Moderately weathered BASALT</b> Light bluish grey, hard, many vesicles 2 - 3 mm, few vesicles 4 mm, some vesicles 1 mm, red/orange staining.  Fracture from 1.62 - 1.74 m, very wide (20 mm), medium rough, clay; brown, moist, soft, high plasticity, contains fine roots.			2						
Fracture from 1.74 - 1.76 m, very wide (20 mm), medium rough, clay; brown, moist, soft, high plasticity, contains fine basaltic gravel.									
									Moderate hydrocarbon odour

continued



[illegible]

continued

Lithology	Symbol	Well	Depth (m)	Recovery	Sample Type	Analysed	PPT (kPa)	PID (ppm)	Sample Details	Remarks
Few vesicles 3 - 4 mm from 4.65 - 4.90 m. Calcite at 4.87 m.			5							
Fracture from 5.15 - 5.24 m, 70 degrees, narrow, medium rough, orange staining.										
Fracture from 5.31 - 5.68 m, 80 degrees, wide (2 - 3 mm), medium rough, clay, light brown, soft, high plasticity, orange staining.										
Many vesicles < 1 mm from 5.8 m, black staining, trace orange staining.										
Fracture from 5.90 - 5.92 m, 10 degrees, narrow, medium rough, orange, red, black staining.			6							
Few vesicles 3 - 4 mm from 6.04 - 6.42 m.										
Trace calcite from 6.30 - 6.42 m.										
Fracture zone from 6.70 - 6.95 m.										
No black staining from 6.95 m.			7							

continued

Lithology	Symbol	Well	Depth (m)	Recovery	Sample Type	Analysed	PPT (kPa)	PID (ppm)	Sample Details	Remarks
<b>Moderately weathered BASALT</b> Light bluish grey, hard, few vesicles < 1 mm.  Fracture zone from 7.17 - 8.0 m, narrow, orange, white and black staining.										Moderate hydrocarbon odour
<b>Slightly weathered BASALT</b> Light bluish grey, hard, many vesicles < 1 mm, trace orange staining.  Fracture zone from 7.8 - 8.2 m, flat, narrow, medium rough, orange and green staining.  Fracture at 8.37 m, flat, narrow, medium rough, dark red, white and black staining.  Fracture from 8.5 - 8.52 m, flat, narrow, rough, black staining.			8							Strong hydrocarbon odour
<b>Highly weathered BASALT</b> Dark brown, hard, no vesicles, horizontal layers, trace orange staining.										
<b>Moderately weathered BASALT</b> Light bluish grey, hard, trace vesicles 1 mm, trace orange staining, highly fractured, flat, narrow, medium rough, green and white staining.										
<b>Slightly weathered BASALT</b> Light bluish grey, hard, some vesicles 1 mm, some orange staining.  Fracture at 8.98 m, flat, wide (2 - 5 mm), smooth, green staining.  Fracture at 9.04 m, flat, wide (2 mm), smooth, green staining.			9							Strong hydrocarbon odour

continued

Lithology	Symbol	Well	Depth (m)	Recovery	Sample Type	Analysed PPT (kPa)	PID (ppm)	Sample Details	Remarks
			10						
Moderately weathered BASALT Dark brown, hard, no vesicles, orange staining.  Fracture from 10.65 - 10.70 m, 45 degrees, wide (3 mm), orange staining.									
Highly weathered BASALT Dark brown, hard, no vesicles, orange staining, many very narrow fractures, flat.			11						
Moderately weathered BASALT Light bluish grey, hard, no vesicles, orange staining.									
Highly weathered BASALT Dark brown, hard, no vesicles, orange staining, many very narrow fractures, flat.									
Borehole terminated at 11.50 mbgl.  End of Log									

continued

## APPENDIX E.1

---

### Site E natural source zone depletion rate estimates

Table E.1-1 NSZD rates provided by industry partner

Location	Flux Chamber Results										CO <sub>2</sub> Trap Results			
	Measured CO <sub>2</sub> Flux (μmol/m <sup>2</sup> /s)				Uncorrected CO <sub>2</sub> Flux (μmol/m <sup>2</sup> /s)	Corrected CO <sub>2</sub> Flux <sup>a</sup> (μmol/m <sup>2</sup> /s)	Corrected CO <sub>2</sub> Flux <sup>b</sup> (μmol/m <sup>2</sup> /s)	Corrected NSZD Rate <sup>c</sup> (gal LNAPL/acre/year)	Corrected NSZD Rate <sup>d</sup> (gal LNAPL/acre/year)	Corrected NSZD Rate <sup>e</sup> (litres LNAPL/year)	Sample ID	Modern Carbon CO <sub>2</sub> Flux (μmol/m <sup>2</sup> /s)	Fossil Fuel CO <sub>2</sub> Flux (μmol/m <sup>2</sup> /s)	Equivalent NSZD Rate (gal LNAPL/acre/year)
	Minimum	Maximum	Mean	Standard Deviation										
A1	4.17	4.90	4.47	0.31	4.47	0.90	2.53	563	1,583	833				
A2	3.27	3.74	3.44	0.21	3.44	0.00	1.50	0	940	0				
A3	2.12	2.48	2.25	0.16	2.25	0.00	0.31	0	196	0				
A4*	34.24	38.73	37.04	2.00	37.04	33.47	35.10	20,919	21,940	1537	T2	1.80	24.9	15,565
A6	26.05	26.94	26.64	0.41	26.64	23.07	24.70	14,419	15,440	1059				
A7	5.75	6.20	5.93	0.19	5.93	2.36	3.99	1,475	2,496	108				
A8	1.72	2.71	2.13	0.44	2.13	0.00	0.19	0	121	0				
A9	20.73	23.50	21.75	1.24	21.75	18.18	19.81	11,363	12,383	835	T6	2.30	21.5	13,424
B1	4.09	4.50	4.35	0.19	4.35	0.78	2.41	488	1,508	36	T1	1.06	3.6	2,266
B3	28.91	35.47	32.53	2.72	32.53	28.96	30.59	18,100	19,121	1330				
B6	1.38	1.92	1.64	0.22	1.64	0.00	0.00	0	0	0				
B7	1.54	2.50	1.91	0.42	1.91	0.00	0.00	0	0	0				
B8	3.69	4.09	3.87	0.16	3.87	0.30	1.93	188	1,208	14	T3	1.53	1.7	1,050
B9	10.97	12.71	12.13	0.82	12.13	8.56	10.19	5,350	6,371	393				
C1	5.77	6.05	5.88	0.12	5.88	2.31	3.94	1,444	2,465	106				
C2	3.69	4.67	4.23	0.41	4.23	0.66	2.29	413	1,433	30				
C3	1.20	1.47	1.33	0.11	1.33	0.00	0.00	0	0	0				
C4	6.57	7.02	6.78	0.19	6.78	3.21	4.84	2,006	3,027	147				
C5	4.58	4.90	4.70	0.14	4.70	1.13	2.76	706	1,727	52				
C6	3.73	4.12	3.91	0.16	3.91	0.34	1.97	213	1,233	16				
C7	4.10	4.33	4.19	0.10	4.19	0.62	2.25	388	1,408	28				
C8	2.00	2.50	2.22	0.21	2.22	0.00	0.28	0	177	0				
C9	15.45	16.44	15.83	0.43	15.83	12.26	13.89	7,663	8,683	563				
D2	1.50	1.75	1.64	0.10	1.64	0.00	0.00	0	0	0				
D3	1.07	1.24	1.16	0.07	1.16	0.00	0.00	0	0	0				
D6	9.93	10.26	10.09	0.14	10.09	6.52	8.15	4,075	5,096	299				
D7	11.50	11.77	11.61	0.12	11.61	8.04	9.67	5,025	6,046	369	T4	1.36	3.3	2,033
D8	4.17	4.40	4.25	0.11	4.25	0.68	2.31	425	1,446	31				
D9	27.50	32.51	30.11	2.05	30.11	26.54	28.17	16,588	17,608	1218				
E3	2.05	4.49	2.87	1.15	2.87	0.00	0.93	0	583	0				
E4	1.36	1.64	1.47	0.12	1.47	0.00	0.00	0	0	0	T5	3.57	12.6	7,852
E5*	2.89	3.17	3.04	0.11	3.04	0.00	1.10	0	690	0				
E6	1.13	1.21	1.17	0.04	1.17	0.00	0.00	0	0	0				
E7	7.49	8.45	8.05	0.41	8.05	4.48	6.11	2,800	3,821	206				
E8	8.28	8.55	8.39	0.12	8.39	4.82	6.45	3,013	4,033	221				
E9	10.92	12.98	11.67	0.93	11.67	8.10	9.73	5,063	6,083	372				
F5	1.42	1.62	1.52	0.08	1.52	0.00	0.00	0	0	0				
F6	2.08	2.24	2.17	0.07	2.17	0.00	0.23	0	146	0				
F7	2.03	2.14	2.10	0.05	2.10	0.00	0.16	0	102	0				
F8	2.66	2.80	2.71	0.06	2.71	0.00	0.77	0	483	0				
F9	13.26	14.74	13.85	0.64	13.85	10.28	11.91	6,425	7,446	472				
G9	3.18	3.79	3.45	0.25	3.45	0.00	1.51	0	946	0				
Z3	5.11	7.20	5.94	0.90	5.94	2.37	4.00	1,481	2,502	109				
Z4	5.06	8.12	6.61	1.25	6.61	3.04	4.67	1,900	2,921	140				
Z5	16.08	20.64	19.00	2.07	19.00	15.43	17.06	9,644	10,665	708				
Z6	29.05	30.84	29.70	0.81	29.70	26.13	27.76	16,331	17,352	1200				
Z8	5.37	6.44	5.98	0.45	5.98	2.41	4.04	1,506	2,527	111				
Z9	8.06	8.98	8.49	0.38	8.49	4.92	6.55	3,075	4,096	226				

<sup>a</sup> The **maximum** of the modern CO<sub>2</sub> fluxes from the CO<sub>2</sub> trap results is subtracted from the mean reading for each respective Flux Chamber. Where the reading for an impacted zone location is less than the **maximum** background value, the corrected CO<sub>2</sub> flux is reported as zero. <sup>b</sup> The **average** of the modern CO<sub>2</sub> fluxes from the CO<sub>2</sub> trap results is subtracted from the mean reading for each respective Flux Chamber. Where the reading for an impacted zone location is less than the **average** background value, the corrected CO<sub>2</sub> flux is reported as zero. <sup>c</sup> Assumes that  $1\mu\text{mol m}^{-2} \text{s}^{-1}$  CO<sub>2</sub> flux represents approximately 625 gallons of LNAPL naturally degraded per acre per year (gal LNAPL acre<sup>-1</sup>year<sup>-1</sup>), **maximum** background correction. <sup>d</sup> Assumes that  $1\mu\text{mol m}^{-2} \text{s}^{-1}$  CO<sub>2</sub> flux represents approximately 625 gallons of LNAPL naturally degraded per acre per year (gal LNAPL acre<sup>-1</sup>year<sup>-1</sup>), **average** background correction. <sup>e</sup> Assumes the respective NSZD rate applies radially to a distance of 5 metres from each monitoring point. The distance between monitoring points is approximately 10 metres. **Maximum** background correction

## APPENDIX F.1

---

### Site F well logs

BOREHOLE LOG NO: BH59

Office Method and Size				MATERIAL DESCRIPTION			
% Materials Recovery	Fracture Freq	Run Length (Meters)	Depth (Meters)	Fractures			
SOLID FLIGHT AUGER 110mm to 5.7m							
Meters FTEEL, CANBERRA WITH INDEX							
Start Corro at 5.7m							
NO CORRO							
100	0	2	0.2				
			5.9				
NO CORRO							
100	47	7					
NO CORRO							
100	40	10	2.40				
NO CORRO							
100	16	2.45	10.80				
NO CORRO							
100	71	>20	0.55				
NO CORRO							
100	18	2.7	13.0				
NO CORRO							
100	10	8.0	35.0				
NO CORRO							
100	34	15	2.7				
NO CORRO							
88	34	15	2.7				

continued

LEGEND: % Material recovery = percentage of core recovered per core run length.  
RQD% = percentage of core greater than 0.1m long per core run.  
Fracture frequency = number of fractures per meter of length of core.

Continuation of log

Office Method and Size				MATERIAL DESCRIPTION			
% Materials Recovery	Fracture Freq	Run Length (Meters)	Depth (Meters)	Fractures			
SOLID FLIGHT AUGER 110mm to 5.7m							
Meters FTEEL, CANBERRA WITH INDEX							
Start Corro at 5.7m							
NO CORRO							
100	0	2	0.2				
			5.9				
NO CORRO							
100	47	7					
NO CORRO							
100	40	10	2.40				
NO CORRO							
100	16	2.45	10.80				
NO CORRO							
100	71	>20	0.55				
NO CORRO							
100	18	2.7	13.0				
NO CORRO							
100	10	8.0	35.0				
NO CORRO							
100	34	15	2.7				
NO CORRO							
88	34	15	2.7				

continued

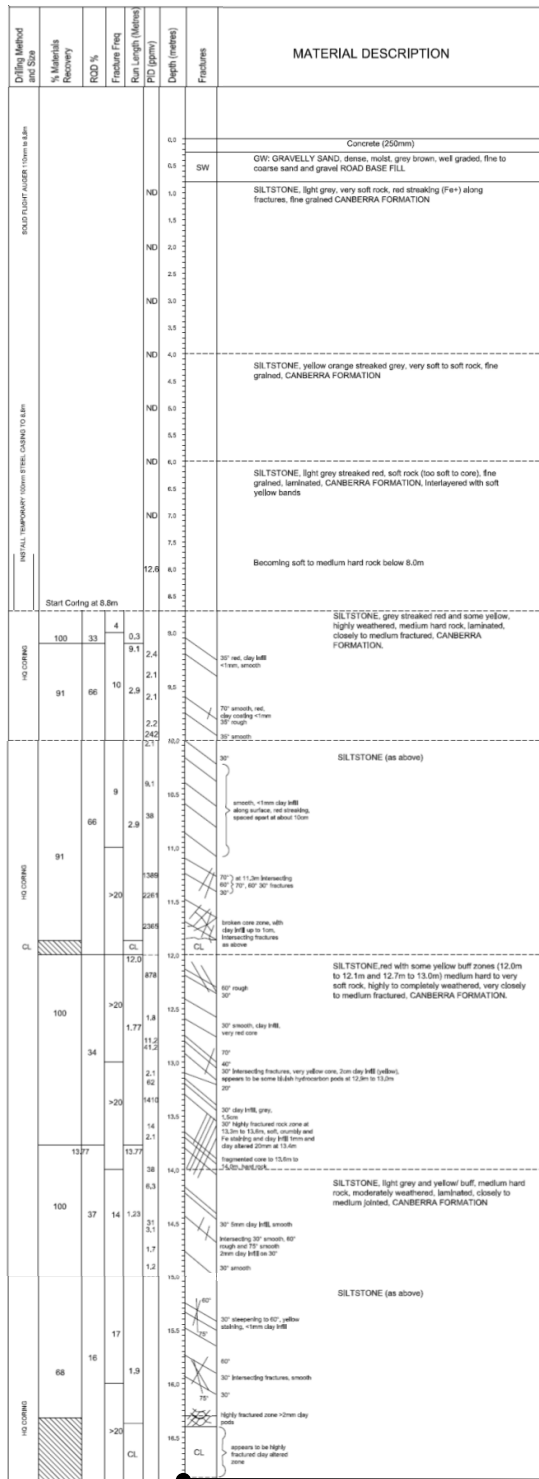
LEGEND: % Material recovery = percentage of core recovered per core run length.  
RQD% = percentage of core greater than 0.1m long per core run.  
Fracture frequency = number of fractures per meter of length of core.

Borehole terminated at 32.9 m

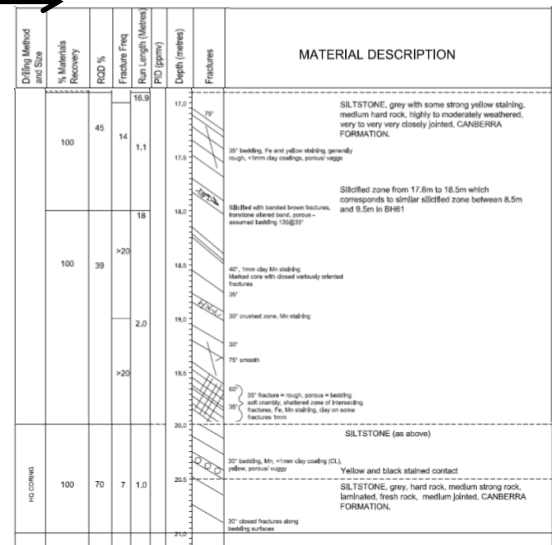


## BOREHOLE LOG NO: BH60

Continuation of log



continued



Borehole terminated at 21.0 m

LEGEND: % Material recovery = percentage of core recovered per core run length.  
 RQD% = percentage of core greater than 0.1m long per core run.  
 Fracture frequency = number of fractures per meter of length of core.

## BOREHOLE LOG NO: BH61

Continuation of log

Drilling Method and Size	% Materials Recovery	RQD %	Fracture Freq. (per meter)	Run Length (meters)	Depth (meters)	Fractures	MATERIAL DESCRIPTION
SOLID FLIGHT AUGER 115mm to 0.3m					0.0		Concrete (200mm)
					0.2	SW	GRAVELLY SAND, grey, fine to coarse sand and fine gravel, well graded, high permeability ROAD BASE FILL
					0.5	CL	SILTY CLAY, low to medium plasticity, yellow brown, low permeability RESIDUAL CLAY
					1.5		
					2.0		
					2.5		
					3.0		SILTSTONE, yellow brown, very soft rock, fractured, laminated, minor red staining and alternating with grey bands
					3.5		
					4.0		
					4.5		
					5.0		
					5.5		
					6.0		
Start Coring at 6.35m					6.35		
	100	76	5	1.72	6.5	30° red, fine, rough	SILTSTONE, light grey streaked red, medium hard rock, highly weathered, closely to medium jointed, laminated, CANBERRA FORMATION
					7.0	30° rough	
					7.5	70° steep and smooth, red Fe	
					8.0	30° clay to 10° from to 1.5m with intersecting steep 70° fractures	
	100	91	5	0.93	8.5	30° smooth, Fe red	
					9.0	30° rough, Fe red	
	100	85	2	3	9.5	30° rough, coarse	
					10.0	30° rough, coarse	
	100	85	9	0.3	10.5	30° rough, coarse, numerous steep 70° + 40° fractures, coarse, mylonitic, closely folded	
					11.0	30° green clay silt, red	SILTSTONE, grey and buff yellow and red streaking, highly weathered, laminated, medium hard rock, CANBERRA FORMATION
					11.5	30° green clay silt, red	
					12.0	30° green clay silt, red	
					12.5	30° green clay silt, red	
					13.0	30° green clay silt, red	
					13.5	30° green clay silt, red	
					14.0	30° green clay silt, red	
					14.5	30° green clay silt, red	
					15.0	30° green clay silt, red	
					15.5	30° green clay silt, red	
					16.0	30° green clay silt, red	
					16.5	30° green clay silt, red	
					17.0	30° green clay silt, red	
					17.5	30° green clay silt, red	
					18.0	30° green clay silt, red	
					18.5	30° green clay silt, red	
					19.0	30° green clay silt, red	
					19.5	30° green clay silt, red	
					20.0	30° green clay silt, red	

continued

LEGEND: % Material recovery = percentage of core recovered per core run length.  
 RQD % = percentage of core greater than 0.1m long per core run.  
 Fracture frequency = number of fractures per meter of length of core.

Drilling Method and Size	% Materials Recovery	RQD %	Fracture Freq. (per meter)	Run Length (meters)	Depth (meters)	Fractures	MATERIAL DESCRIPTION
					15.0		SILTSTONE (see above)
	100	30	8	1.97	15.5	30° rough, generally closed and 70° smooth dark tan	
					16.0	40° smooth clay silt + 10mm	
					16.5	30° clay silt, tan, wavy	
					17.0	30° to 40° smooth	
					17.5	20° and 30° intersecting, highly fractured zone, clay alteration to tan zone at 16.0m to 16.5m, with clay is yellow	
	100	53	12	1.03	18.0	30° rough, rough	
					18.5	70° smooth	
					19.0	30° rough, rough	
					19.5	30° rough, rough	
					20.0	30° rough, rough	
					20.5	30° rough, rough	
					21.0	30° rough, rough	
					21.5	30° rough, rough	
					22.0	30° rough, rough	
					22.5	30° rough, rough	
					23.0	30° rough, rough	
					23.5	30° rough, rough	
					24.0	30° rough, rough	
					24.5	30° rough, rough	
					25.0	30° rough, rough	
					25.5	30° rough, rough	
					26.0	30° rough, rough	
					26.5	30° rough, rough	
					27.0	30° rough, rough	
					27.5	30° rough, rough	
					28.0	30° rough, rough	
					28.5	30° rough, rough	
					29.0	30° rough, rough	
					29.5	30° rough, rough	
					30.0	30° rough, rough	

Borehole terminated at 20.0 m

## APPENDIX F.2

### Site F GC-FID analytical and density results

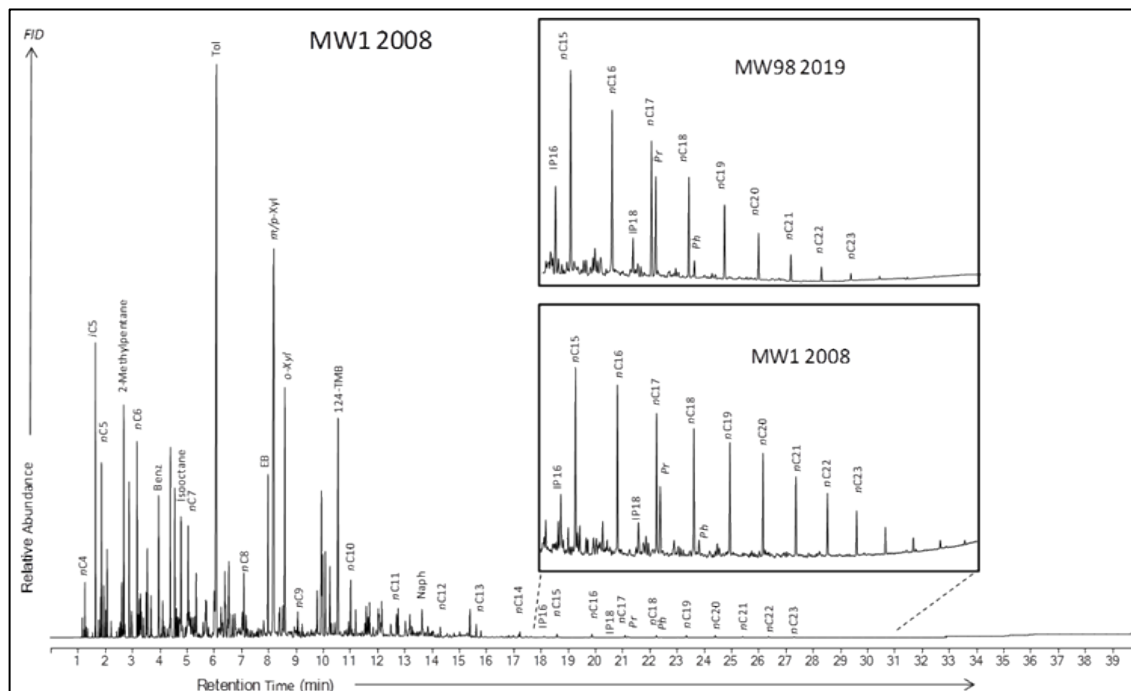


Figure F.2-1 GC-FID analysis of LNAPL sample MW1 from 2008 as well as comparison of C15-27 components in LNAPL MW98 from 2019 (the least biodegraded 2019 LNAPL sample) Benz: benzene, CHX: cyclohexane, Cx: straight or branched alkane containing x carbons, D: di, E: ethyl, i: iso, IP: isoprenoid, M: methyl, n: normal, Naph: naphthalene, P: pentane, TMB: trimethylbenzene, Tol: toluene, Xyl: xylene

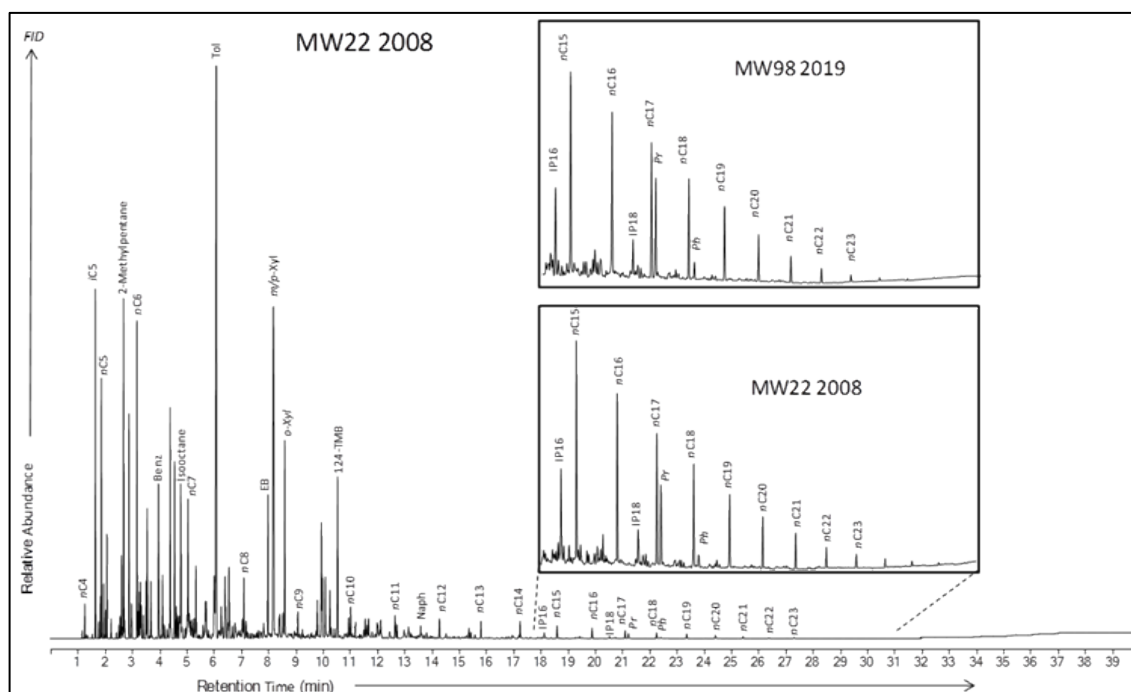
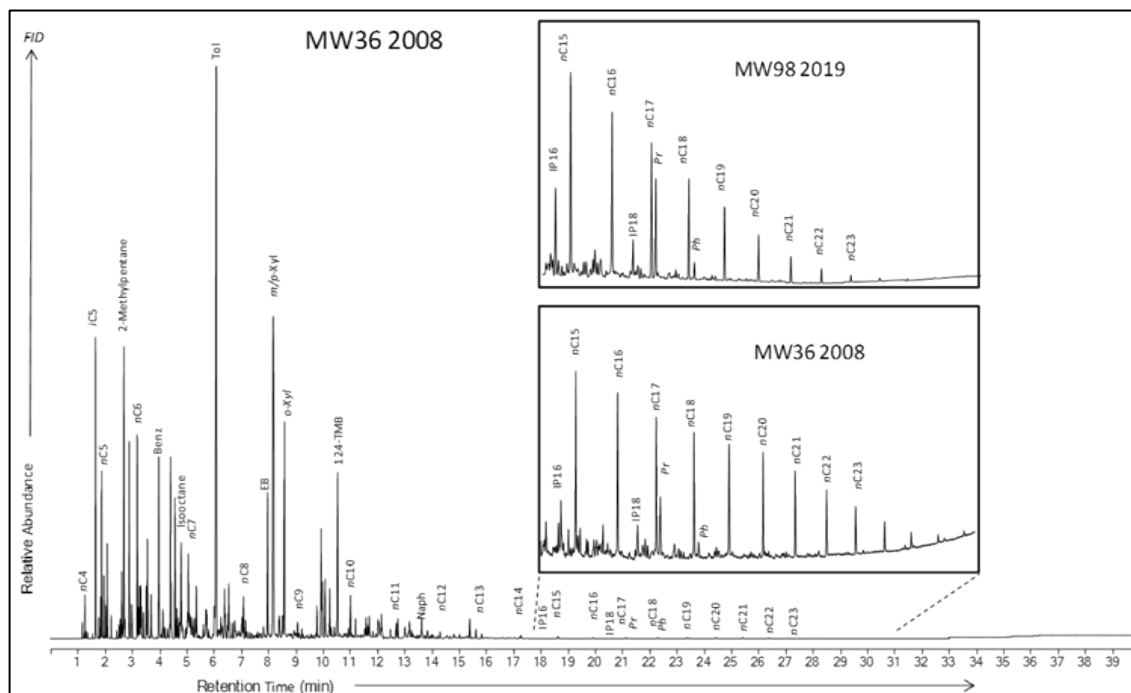
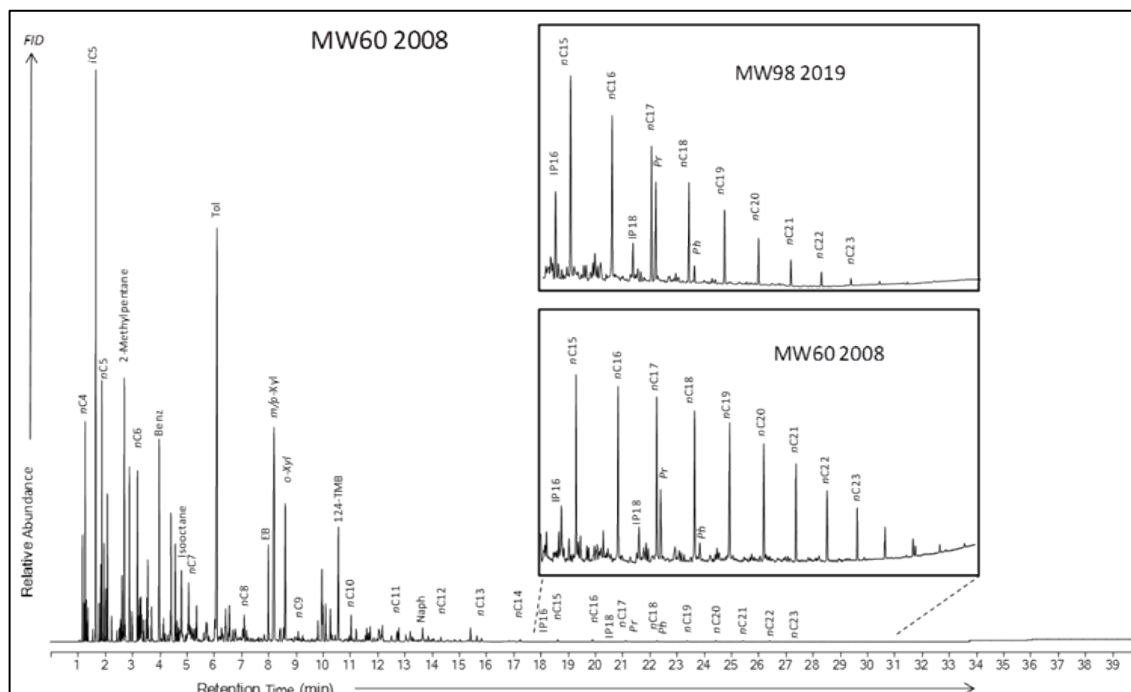


Figure F.2-2 GC-FID analysis of LNAPL sample MW22 from 2008 as well as comparison of C15-27 components in LNAPL MW98 from 2019 (the least biodegraded 2019 LNAPL sample) Benz: benzene, CHX: cyclohexane, Cx: straight or branched alkane containing x carbons, D: di, E: ethyl,

i: iso, IP: isoprenoid, M: methyl, n: normal, Naph: naphthalene, P: pentane, TMB: trimethylbenzene, Tol: toluene, Xyl: xylene



**Figure F.2-3 GC-FID analysis of LNAPL sample MW36 from 2008 as well as comparison of C15-27 components in LNAPL MW98 from 2019 (the least biodegraded 2019 LNAPL sample)** Benz: benzene, CHX: cyclohexane, Cx: straight or branched alkane containing x carbons, D: di, E: ethyl, i: iso, IP: isoprenoid, M: methyl, n: normal, Naph: naphthalene, P: pentane, TMB: trimethylbenzene, Tol: toluene, Xyl: xylene



**Figure F.2-4 GC-FID analysis of LNAPL sample MW60 from 2008 as well as comparison of C15-27 components in LNAPL MW98 from 2019 (the least biodegraded 2019 LNAPL sample)** Benz: benzene, CHX: cyclohexane, Cx: straight or branched alkane containing x carbons, D: di, E: ethyl, i: iso, IP: isoprenoid, M: methyl, n: normal, Naph: naphthalene, P: pentane, TMB: trimethylbenzene, Tol: toluene, Xyl: xylene

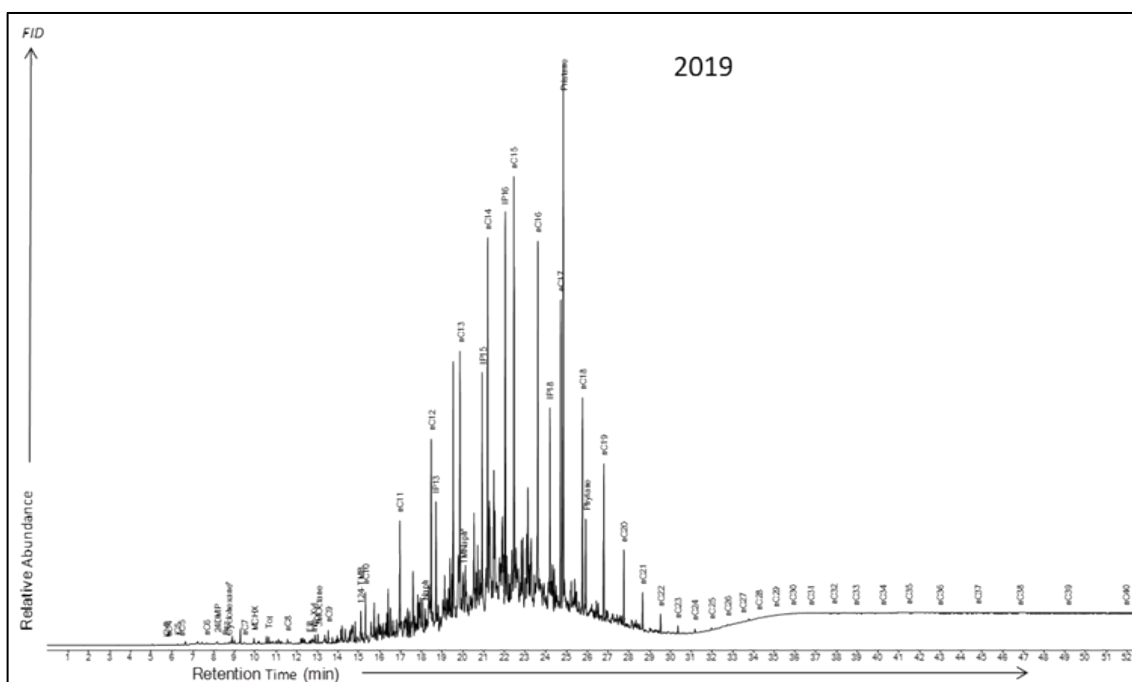


Figure F.2-5 GC-FID analysis of LNAPL sample MW9S from 2019 MW9S from 2019 Benz: benzene, CHX: cyclohexane, Cx: straight or branched alkane containing x carbons, D: di, E: ethyl, i: iso, IP: isoprenoid, M: methyl, n: normal, Naph: naphthalene, P: pentane, TMB: trimethylbenzene, Tol: toluene, Xyl: xylene

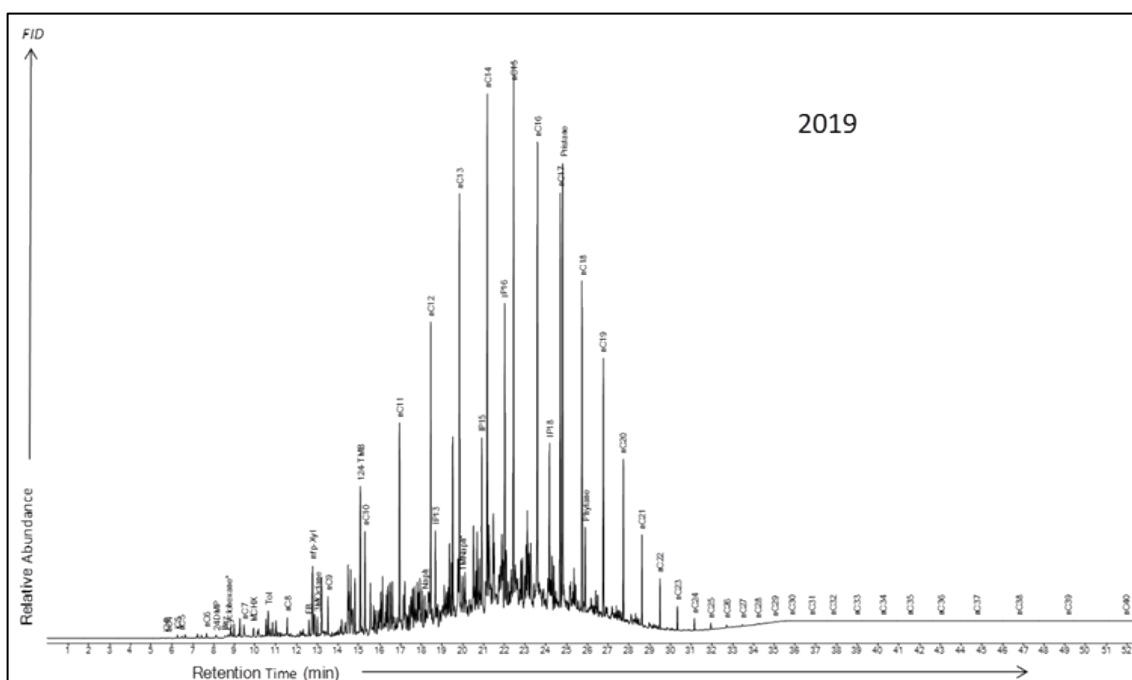
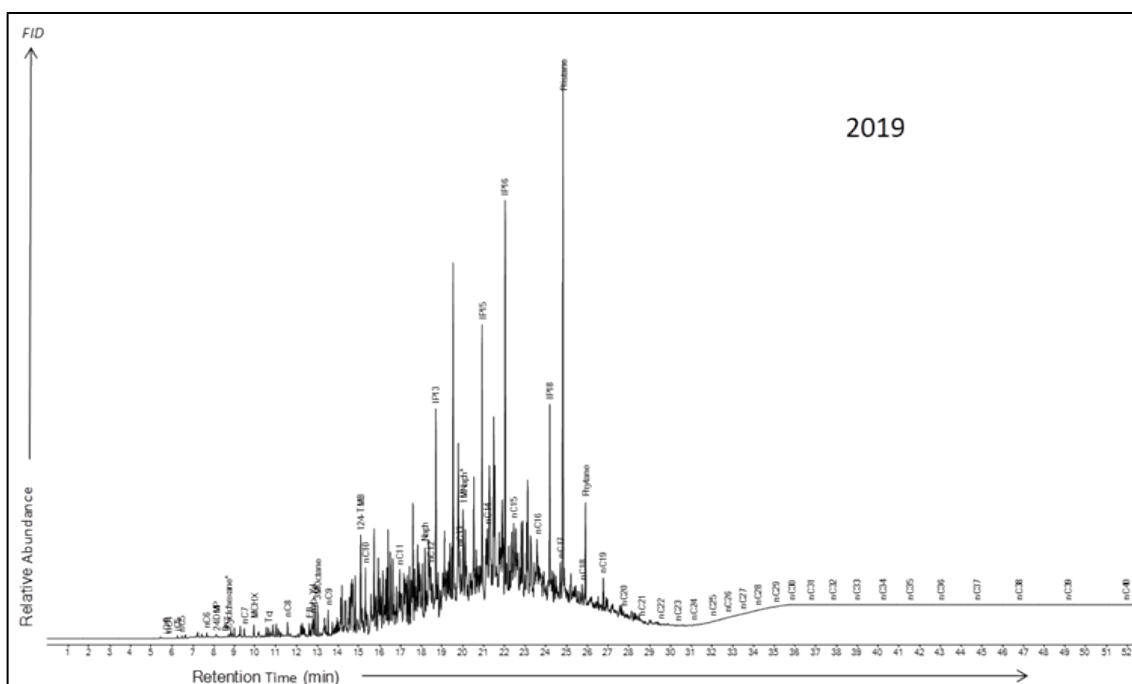
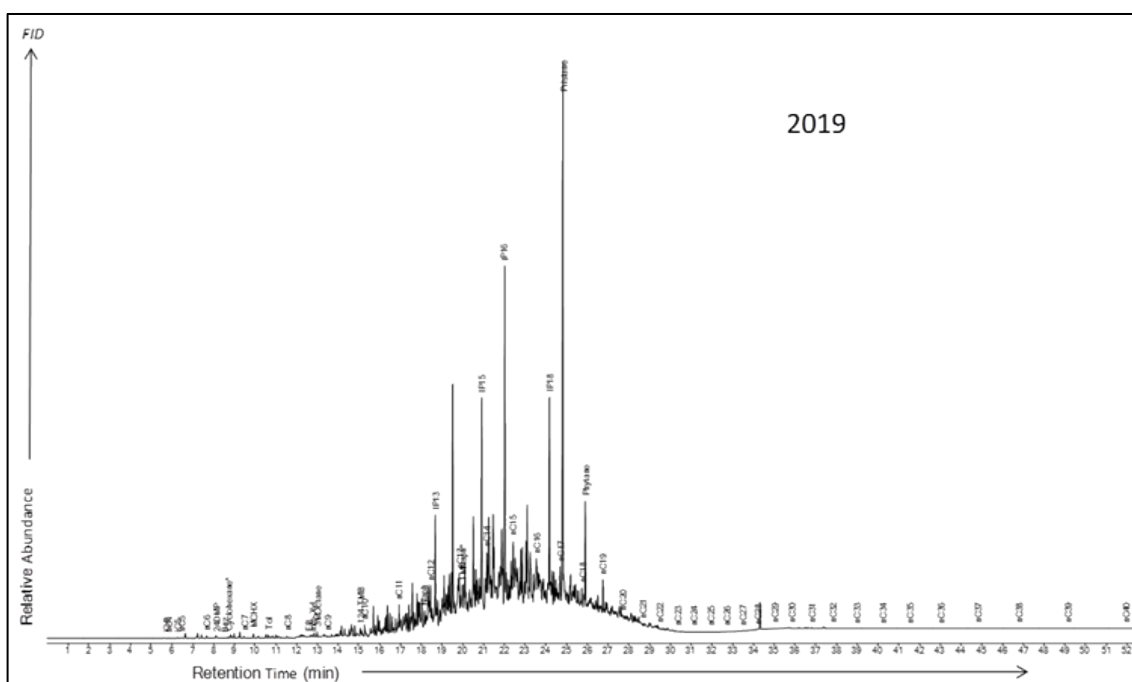


Figure F.2-6 GC-FID analysis of LNAPL sample MW22 from 2019 Benz: benzene, CHX: cyclohexane, Cx: straight or branched alkane containing x carbons, D: di, E: ethyl, i: iso, IP: isoprenoid, M: methyl, n: normal, Naph: naphthalene, P: pentane, TMB: trimethylbenzene, Tol: toluene, Xyl: xylene



**Figure F.2-7 GC-FID analysis of LNAPL sample MW23 from 2019** Benz: benzene, CHX: cyclohexane, Cx: straight or branched alkane containing x carbons, D: di, E: ethyl, i: iso, IP: isoprenoid, M: methyl, n: normal, Naph: naphthalene, P: pentane, TMB: trimethylbenzene, Tol: toluene, Xyl: xylene



**Figure F.2-8 GC-FID analysis of LNAPL sample MW28 from 2019** Benz: benzene, CHX: cyclohexane, Cx: straight or branched alkane containing x carbons, D: di, E: ethyl, i: iso, IP: isoprenoid, M: methyl, n: normal, Naph: naphthalene, P: pentane, TMB: trimethylbenzene, Tol: toluene, Xyl: xylene

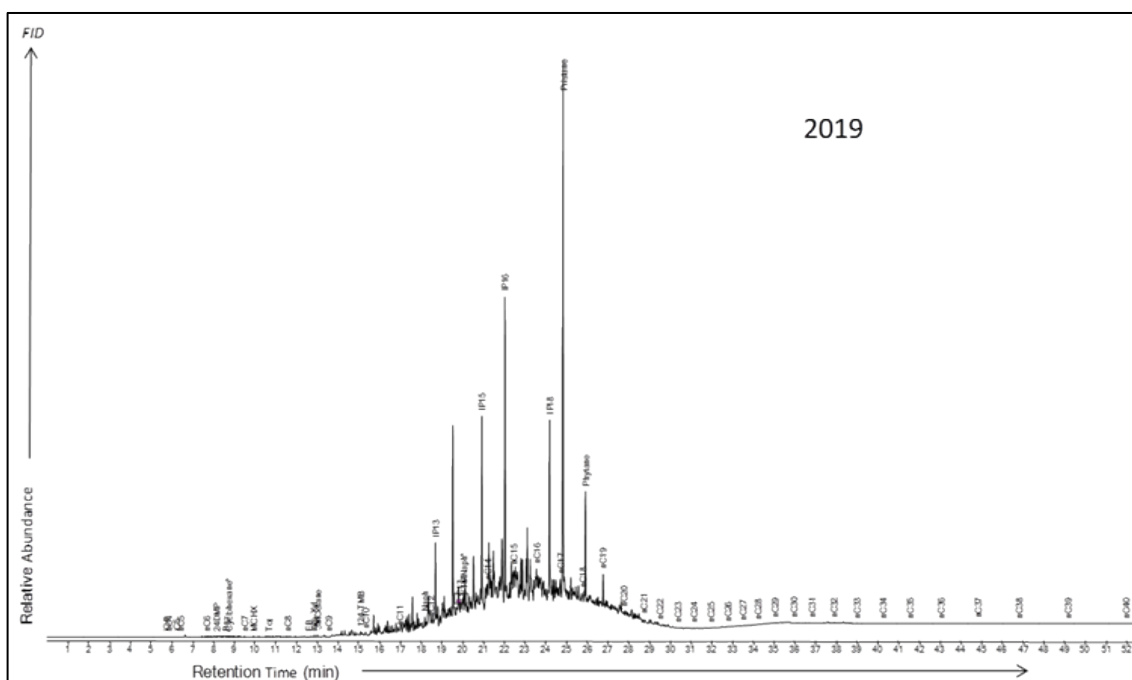


Figure F.2-9 GC-FID analysis of LNAPL sample MW40 from 2019 Benz: benzene, CHX: cyclohexane, Cx: straight or branched alkane containing x carbons, D: di, E: ethyl, i: iso, IP: isoprenoid, M: methyl, n: normal, Naph: naphthalene, P: pentane, TMB: trimethylbenzene, Tol: toluene, Xyl: xylene

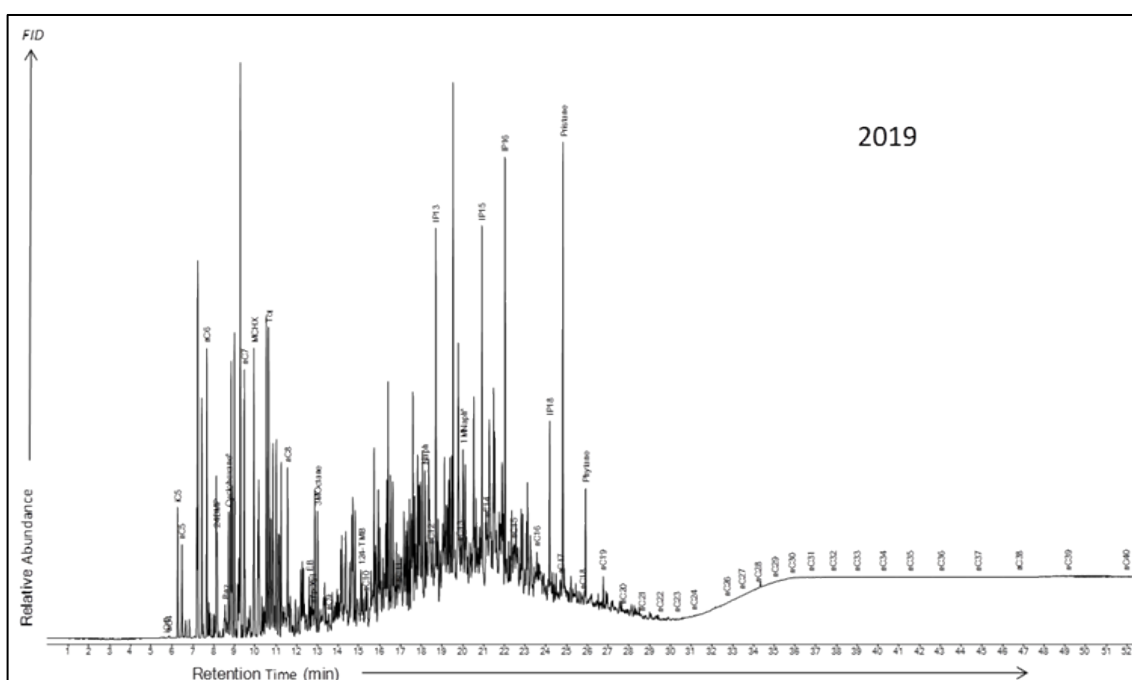


Figure F.2-10 GC-FID analysis of LNAPL sample MW69 from 2019 Benz: benzene, CHX: cyclohexane, Cx: straight or branched alkane containing x carbons, D: di, E: ethyl, i: iso, IP: isoprenoid, M: methyl, n: normal, Naph: naphthalene, P: pentane, TMB: trimethylbenzene, Tol: toluene, Xyl: xylene

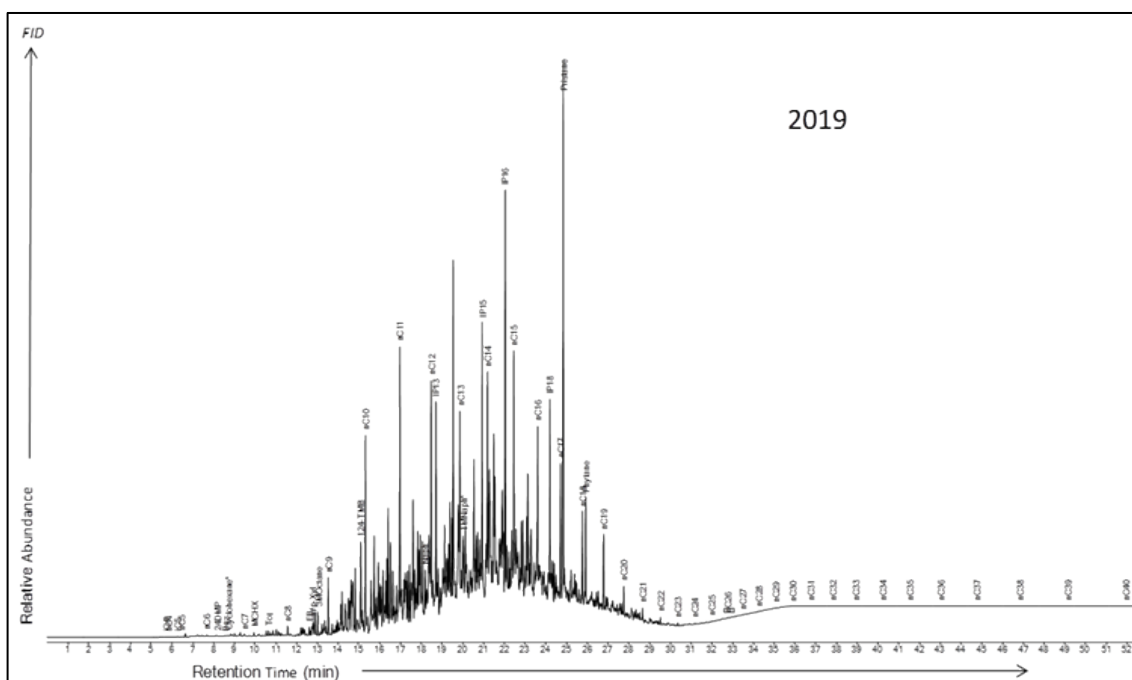


Figure F.2-11 GC-FID analysis of LNAPL sample MW81 from 2019 Benz: benzene, CHX: cyclohexane, Cx: straight or branched alkane containing x carbons, D: di, E: ethyl, i: iso, IP: isoprenoid, M: methyl, n: normal, Naph: naphthalene, P: pentane, TMB: trimethylbenzene, Tol: toluene, Xyl: xylene

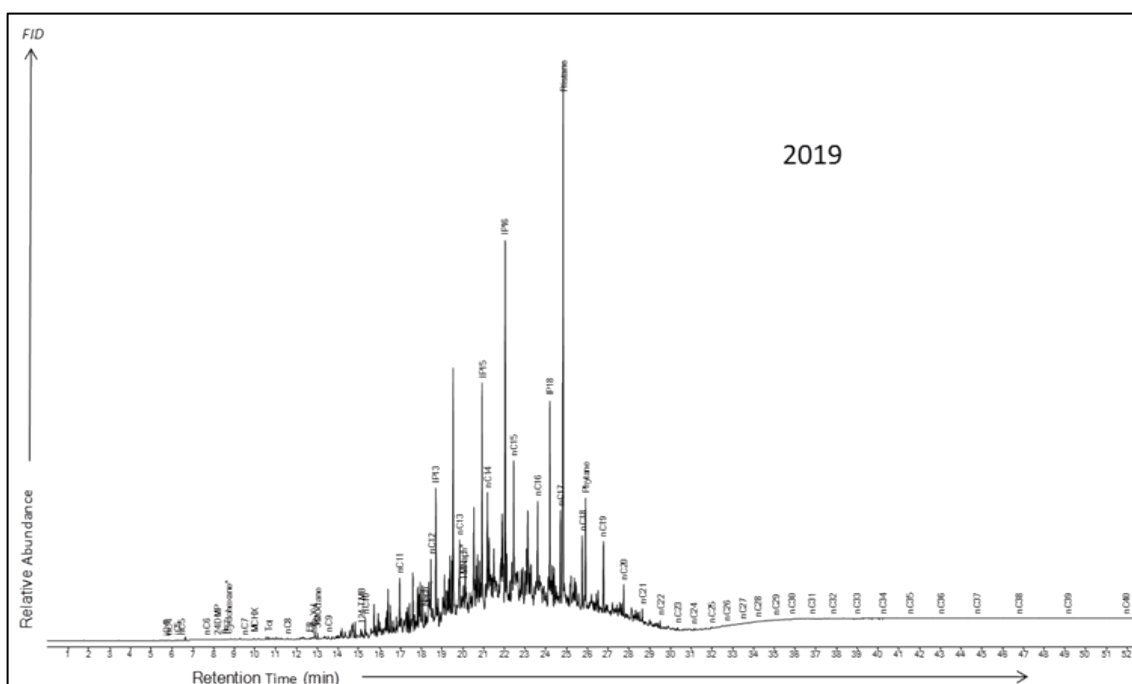


Figure F.2-12 GC-FID analysis of LNAPL sample MW82 from 2019 Benz: benzene, CHX: cyclohexane, Cx: straight or branched alkane containing x carbons, D: di, E: ethyl, i: iso, IP: isoprenoid, M: methyl, n: normal, Naph: naphthalene, P: pentane, TMB: trimethylbenzene, Tol: toluene, Xyl: xylene



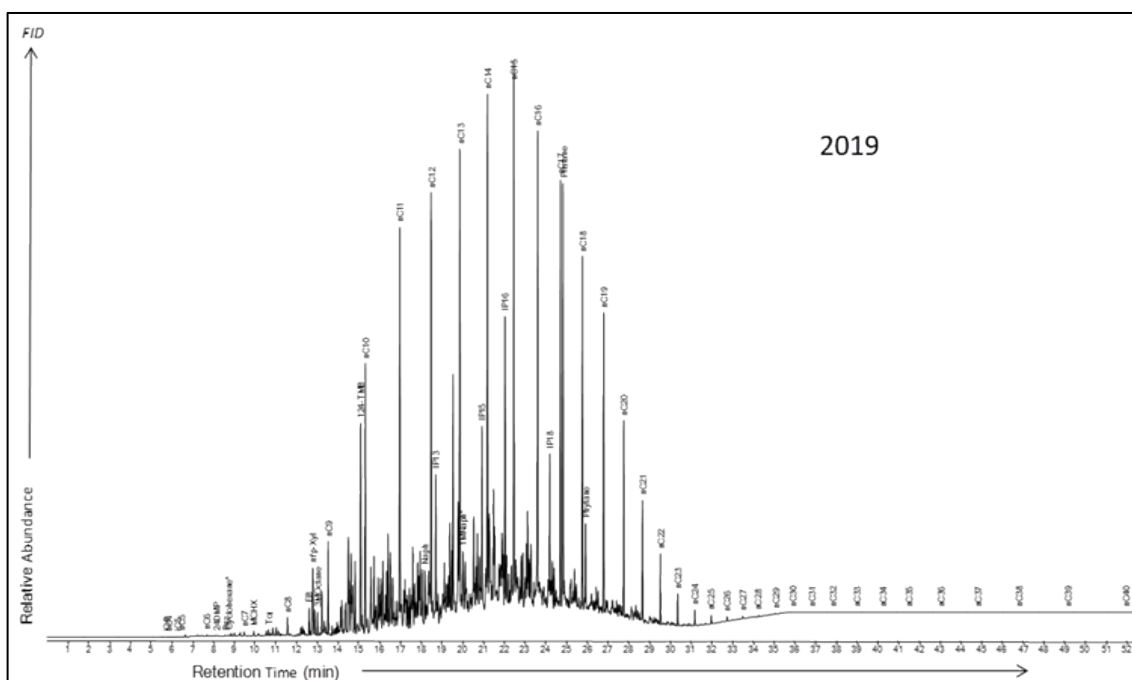


Figure F.2-13 GC-FID analysis of LNAPL sample MW83 from 2019 Benz: benzene, CHX: cyclohexane, Cx: straight or branched alkane containing x carbons, D: di, E: ethyl, i: iso, IP: isoprenoid, M: methyl, n: normal, Naph: naphthalene, P: pentane, TMB: trimethylbenzene, Tol: toluene, Xyl: xylene

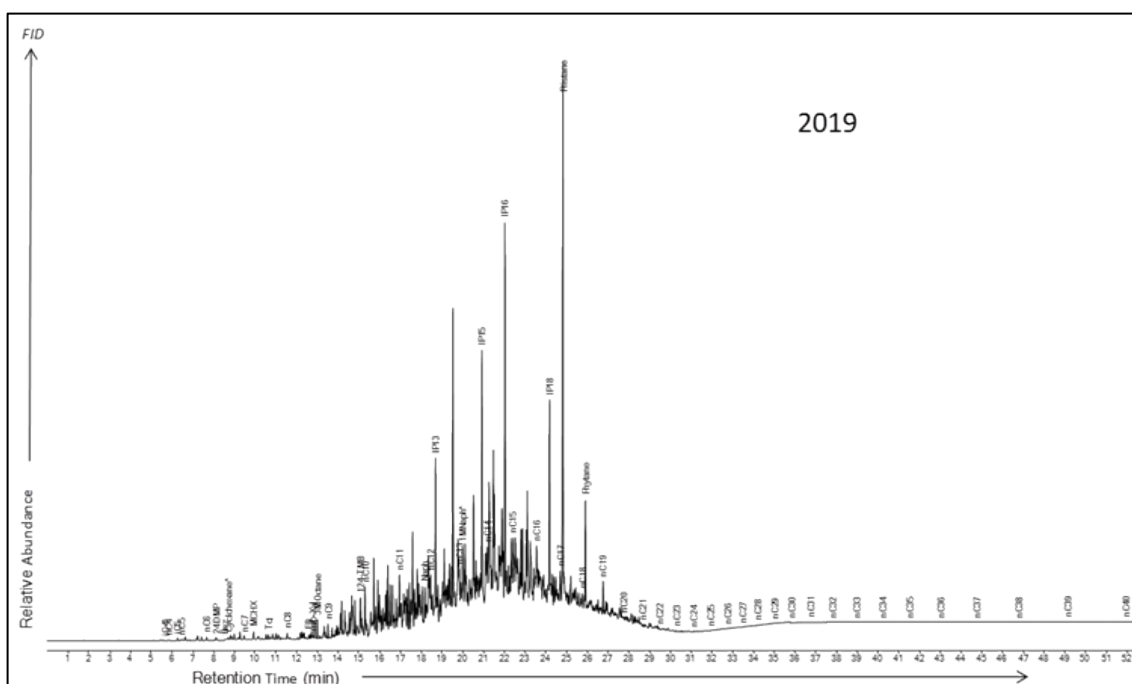


Figure F.2-14 GC-FID analysis of LNAPL sample MW85 from 2019 Benz: benzene, CHX: cyclohexane, Cx: straight or branched alkane containing x carbons, D: di, E: ethyl, i: iso, IP: isoprenoid, M: methyl, n: normal, Naph: naphthalene, P: pentane, TMB: trimethylbenzene, Tol: toluene, Xyl: xylene

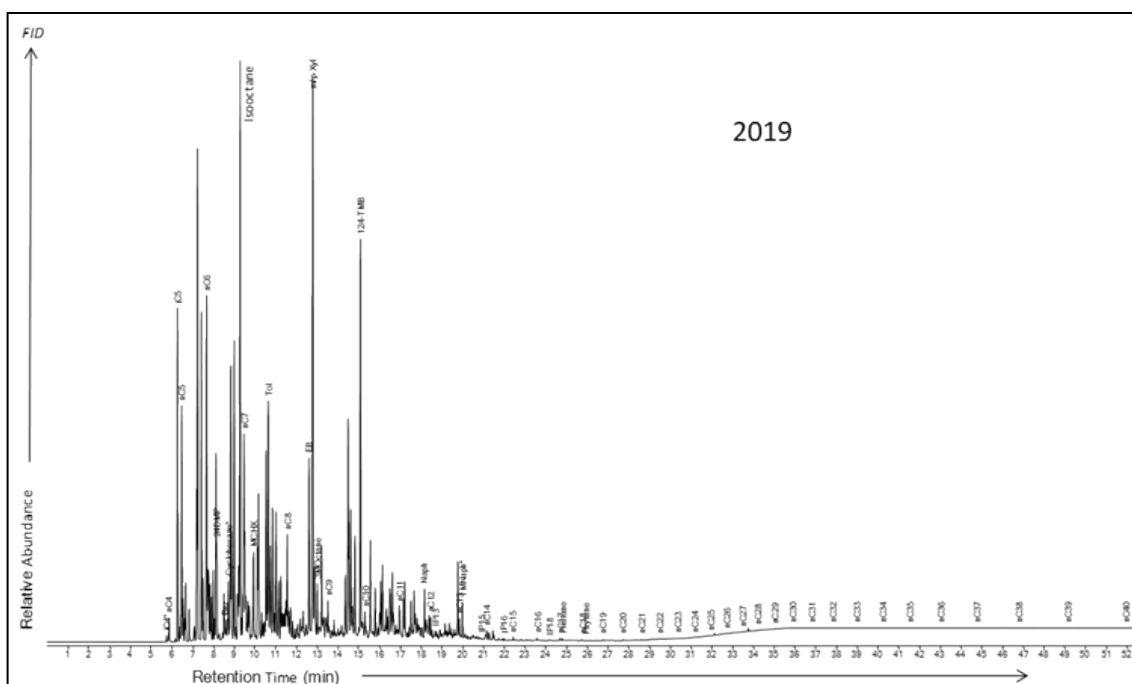


Figure F.2-15 GC-FID analysis of LNAPL sample MW96 from 2019 Benz: benzene, CHX: cyclohexane, Cx: straight or branched alkane containing x carbons, D: di, E: ethyl, i: iso, IP: isoprenoid, M: methyl, n: normal, Naph: naphthalene, P: pentane, TMB: trimethylbenzene, Tol: toluene, Xyl: xylene

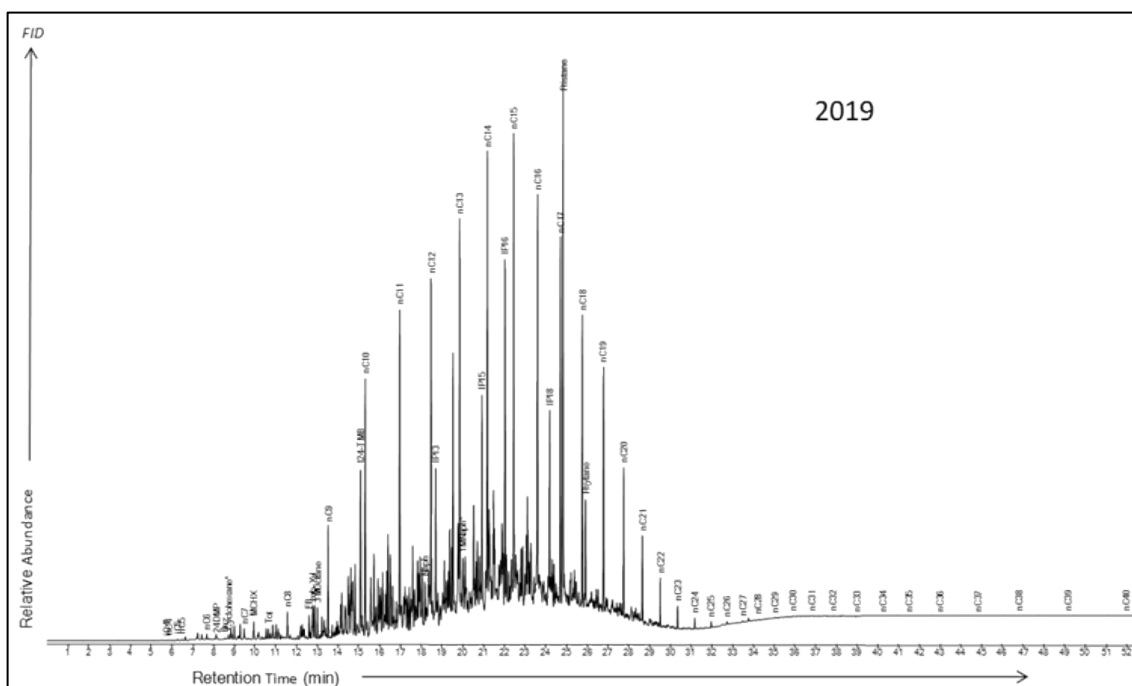


Figure F.2-16 GC-FID analysis of LNAPL sample MW98 from 2019 Benz: benzene, CHX: cyclohexane, Cx: straight or branched alkane containing x carbons, D: di, E: ethyl, i: iso, IP: isoprenoid, M: methyl, n: normal, Naph: naphthalene, P: pentane, TMB: trimethylbenzene, Tol: toluene, Xyl: xylene

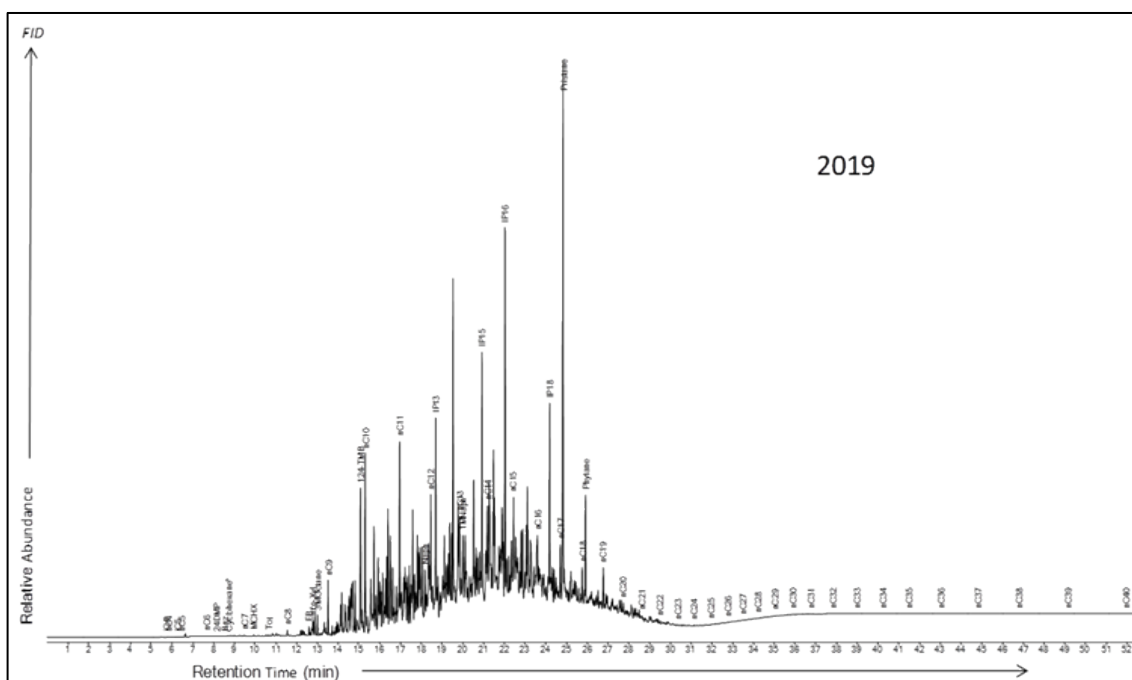


Figure F.2-17 GC-FID analysis of LNAPL sample MW99 from 2019 Benz: benzene, CHX: cyclohexane, Cx: straight or branched alkane containing x carbons, D: di, E: ethyl, i: iso, IP: isoprenoid, M: methyl, n: normal, Naph: naphthalene, P: pentane, TMB: trimethylbenzene, Tol: toluene, Xyl: xylene

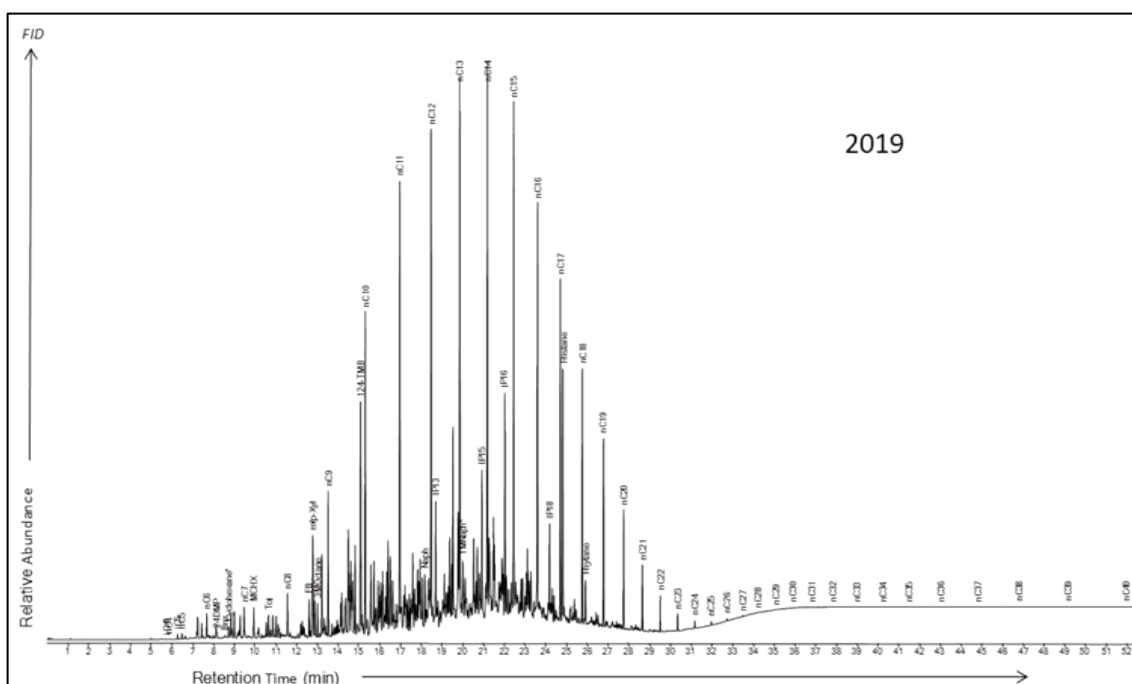


Figure F.2-18 GC-FID analysis of LNAPL sample MW112 from 2019 Benz: benzene, CHX: cyclohexane, Cx: straight or branched alkane containing x carbons, D: di, E: ethyl, i: iso, IP: isoprenoid, M: methyl, n: normal, Naph: naphthalene, P: pentane, TMB: trimethylbenzene, Tol: toluene, Xyl: xylene



**Table F.2-1 Density and analytical results for site F LNAPL samples**

Sample name	Year	Density at 20 °C	%w/w loss	Pr/nC17	Pr/Ph	Benzene	Toluene	Ethyl Benzene	m/p-Xylene	o-Xylene	135-TMB	124-TMB	123-TMB	Naph	nC17	Pristane
		g mL <sup>-1</sup>		Ratio	Ratio	%(w/w)	%(w/w)	%(w/w)	%(w/w)	%(w/w)	%(w/w)	%(w/w)	%(w/w)	%(w/w)	%(w/w)	%(w/w)
Gasoline range product containing minor diesel range product																
Analysis			GCFID*	GCFID	GCFID	GCFID	GCFID	GCFID	GCFID	GCFID	GCFID	GCFID	GCFID	GCFID	GCFID	GCFID
MW1	2008	NR	35	0.59	4.6	1.82	10.7	2.22	11.0	3.93	NR	3.65	NR	0.32	0.04	0.02
MW22	2008	NR	2	0.74	6.4	2.14	9.69	1.97	8.60	2.90	NR	2.41	NR	0.17	0.12	0.09
MW36	2008	NR	20	0.51	4.1	2.64	12.5	2.18	9.95	3.63	NR	2.94	NR	0.26	0.03	0.01
MW60	2008	NR	0	0.51	4.0	3.58	11.4	1.79	8.00	2.92	NR	2.36	NR	0.22	0.04	0.02
Analysis			GCMS*	GCMS	GCMS	GCMS	GCMS	GCMS	GCMS	GCMS	GCMS	GCMS	GCMS	GCMS	GCMS	GCMS
MW96	2019	0.759	28	1.2	6.6	0.05	0.71	1.26	5.51	0.65	0.95	3.25	0.80	0.35	0.01	0.01
Mixture of gasoline and diesel range products																
Analysis			GCMS^	GCMS	GCMS	GCMS	GCMS	GCMS	GCMS	GCMS	GCMS	GCMS	GCMS	GCMS	GCMS	GCMS
MW69	2019	0.816	98	49	4.6	0.07	<0.01	0.07	0.01	<0.01	0.01	0.01	0.04	0.16	0.02	1.10
Diesel range product																
MW9S	2019	0.847	99	2.1	5.8	<0.01	<0.01	0.01	0.02	<0.01	0.04	0.11	0.05	0.03	1.07	2.23
MW22	2019	0.832	99	1.3	5.8	0.01	0.06	0.06	0.46	0.28	0.28	0.72	0.23	0.08	1.46	1.83
MW23	2019	0.850	99	22	5.6	<0.01	<0.01	0.04	0.07	<0.01	0.13	0.33	0.08	0.15	0.09	1.98
MW28	2019	0.853	99	21	5.1	<0.01	<0.01	<0.01	<0.01	<0.01	<0.01	0.01	0.01	0.01	0.11	2.39
MW40	2019	0.853	99	54	4.6	<0.01	<0.01	<0.01	<0.01	<0.01	<0.01	<0.01	<0.01	<0.01	0.05	2.58
MW81	2019	0.842	99	4.8	5.7	<0.01	<0.01	0.02	0.05	0.04	0.15	0.30	0.14	0.06	0.38	1.81
MW82	2019	0.847	99	6.7	5.2	<0.01	<0.01	<0.01	<0.01	<0.01	<0.01	0.01	0.02	<0.01	0.36	2.40
MW83	2019	0.835	99	1.2	5.5	<0.01	0.01	0.10	0.37	0.18	0.28	0.86	0.23	0.13	1.31	1.53

Sample name	Year	Density at 20 °C	%w/w loss	Pr/nC17	Pr/Ph	Benzene	Toluene	Ethyl Benzene	m/p-Xylene	o-Xylene	135-TMB	124-TMB	123-TMB	Naph	nC17	Pristane
MW85	2019	0.853	99	25	5.4	<0.01	<0.01	0.01	0.01	<0.01	0.03	0.12	0.04	0.05	0.09	2.10
MW98	2019	0.838	99	1.7	5.7	<0.01	<0.01	0.07	0.15	0.08	0.21	0.63	0.18	0.09	1.09	1.86
MW99	2019	0.851	99	13	5.4	<0.01	<0.01	0.03	0.06	0.01	0.12	0.54	0.15	0.08	0.15	1.88
MW112	2019	0.825	99	0.9	6.0	0.01	0.04	0.13	0.55	0.33	0.25	0.95	0.25	0.14	1.59	1.45
MW113	2019	0.844	99	2.1	5.6	0.01	0.01	0.18	0.44	0.12	0.35	1.04	0.27	0.18	0.79	1.66

<sup>\*</sup>%w/w losses relative to source based on 1,2,4-trimethylbenzene; <sup>^</sup>%w/w losses relative to source based on pristane; Pr/nC17: ratio of pristane/n-heptadecane; Pr/Ph: ratio of pristane/phytane; Naph: naphthalene; TMB: trimethylbenzene; NR: not reported.

**CRC CARE**

ATC Building  
University of Newcastle  
Callaghan NSW 2308  
Australia

**Postal**

C/- Newcastle University LPO  
PO Box 18  
Callaghan NSW 2308  
Australia

**Contact us**

**P:** +61 2 4985 4941  
**E:** admin@crccare.com

**[www.crccare.com](http://www.crccare.com)**



Australian Government  
Department of Industry, Science,  
Energy and Resources

**Business**  
Cooperative Research  
Centres Program